

Laser probe mass spectrometric study of nitrogen and  
noble gases in individual chondrules from different classes  
of chondrites

**A THESIS**

*submitted for the Award of Ph.D. degree of*

**MOHANLAL SUKHADIA UNIVERSITY**

*in the*

*Faculty of Science*

*by*

*J P Das*



Under the Supervision of

**Prof. S. V. S. Murty**

PLANETARY AND GEOSCIENCE DIVISION  
PHYSICAL RESEARCH LABORATORY, AHMEDABAD

**MOHANLAL SUKHADIA UNIVERSITY**

UDAIPUR

Year of submission: 2007

To  
*My dear wife*

*We are loved beyond our ability to comprehend.*

## **C E R T I F I C A T E**

*I feel great pleasure in certifying that the thesis entitled “Laser probe mass spectrometric study of nitrogen and noble gases in individual chondrules from different classes of chondrites” embodies a record of the results of investigations carried out by Mr. J P Das under my guidance. I am satisfied with the analysis of data, interpretation of results and conclusions drawn.*

*He has completed the residential requirement as per rules.*

*I recommend the submission of thesis.*

Date:

(S V S Murty)

Professor,  
Physical Research Laboratory

## **DECLARATION**

*I hereby declare that the work incorporated in the present thesis entitled “Laser probe mass spectrometric study of nitrogen and noble gases in individual chondrules from different classes of chondrites” is my own work and is original. This work (in part or in full) has not been submitted to any University for the award of a Degree or a Diploma.*

(J P Das)

Signature of the Candidate

# Contents

Acknowledgements	i
Abstract	iii
List of Tables	iv
List of Figures	v
<b>Chapter 1</b>	
<b>Introduction</b>	
1.1 What are chondrules?	3
1.2 Chondrule classification	5
1.3 Thermal histories of chondrules	9
1.4 Type-I and Type-II chondrules: genetically related?	11
1.5 Chemical and isotopic studies of chondrules	11
1.6 The setting for chondrule formation: Nebular or Planetary origin	15
1.7 Noble gases in chondrites	16
1.8 Noble gases in chondrules	16
1.9 In-situ produced noble gas components	17
1.10 Trapped noble gas components	18
1.11 Nitrogen in Meteorites	21
1.12 Objective of the present study	25
1.13 Earlier studies of noble gases and nitrogen related to present work	27
1.13.1 Noble gas studies on chondrules	27
1.13.2 Nitrogen studies on chondrules	29
<b>Chapter 2</b>	
<b>Experimental details</b>	
2.1 Introduction	31
2.2 Selection of chondrites	31
2.3 Separation of chondrules	32
2.4 The VG Micromass 1200	34
2.5 Gas extraction units	34
2.5.1 Laser microprobe (used for chondrule analyses)	35
2.5.2 The glass extraction system (used for bulk chondrite analysis)	41
2.6 Standard procedures	46
2.6.1 Gas extraction from chondrules	46
2.6.2 Gas extraction from bulk chondrite samples	47
2.6.3 Cleaning and separation (Laser microprobe)	48
2.6.4 Cleaning and separation (Glass extraction system)	49
2.6.5 Mass analysis	50
2.6.6 Data acquisition and reduction	50
2.6.7 Calibration of the mass spectrometer	53
2.7 Chemical characterization of chondrules	55
2.7.1 Method to determine the chemical composition of chondrule	55
2.7.2 Limitations of EPMA method	56
2.7.3 Petrographic and Mineralogical descriptions of chondrules	57

### **Chapter 3**

#### **Noble gases in chondrules -in situ produced components**

3.1	Introduction	72
3.2	Calculations of cosmogenic and radiogenic noble gases	73
3.3	Results	75
3.3.1	Cosmogenic noble gases ( $^3\text{He}$ , $^{21}\text{Ne}$ and $^{38}\text{Ar}$ )	75
3.3.2	Production rates ( $^3\text{He}$ , $^{21}\text{Ne}$ and $^{38}\text{Ar}$ ) and cosmic ray exposure age of chondrules	95
3.3.3	Radiogenic noble gases ( $^4\text{He}$ , $^{40}\text{Ar}$ and $^{129}\text{Xe}$ )	110
3.3.4	Gas retention ages ( $T_4$ , $T_{40}$ ) of chondrules	119
3.4	Discussion	121
3.4.1	Loss of cosmogenic and radiogenic noble gases from chondrules	121
3.4.2	Precompaction exposure of chondrules and duration of their formation	122
3.4.3	Precompaction irradiation and exposure to solar cosmic rays	125
3.5	Summary	127

### **Chapter 4**

#### **Noble gases in chondrules -trapped components**

4.1	Introduction	130
4.2	Calculations of trapped noble gases	131
4.3	Results	133
4.3.1	Trapped $^{20}\text{Ne}$	133
4.3.2	Trapped $^{36}\text{Ar}$	142
4.3.3	The elemental ratio $^{36}\text{Ar}/^{20}\text{Ne}$ in chondrules	142
4.4	Discussion	145
4.4.1	Presence of different noble gas components in chondrules	145
4.4.2	Solar type noble gases in chondrules	150
4.5	Summary	154

### **Chapter 5**

#### **Trapped nitrogen in chondrules**

5.1	Introduction	157
5.2	Corrections of the measured $\delta^{15}\text{N}$ for cosmogenic contribution	157
5.3	Results	159
5.4	Discussion	171
5.4.1	Did the chondrule-forming event affect the N-compositions?	173
5.4.2	Did chondrules act as open systems during their formation?	175
5.4.3	N-components in chondrules/ chondrule precursors	177
5.4.4	Nature of N-component required for chondrules of ordinary and carbonaceous chondrites in addition to HL and Q components	179
5.4.5	Heterogeneity in chondrule precursors and survival of various N-components	181
5.4.6	Uniform N-composition of EC chondrules	185
5.5	Summary	186

### **Chapter 6**

#### **Implications to the chondrule formation process and future directions**

6.1	Introduction	189
6.2	Cosmogenic noble gases and precompaction irradiation records in chondrules	189
6.3	Evidence of fractionation between metal and silicate phases during chondrule formation	189
6.4	Solar type noble gases in chondrules	191

6.5	Trapped components of nitrogen in chondrules: presence of Insoluble organic matter in chondrules	191
6.6	Possible scenario to account for trapped N and noble gas compositions	194
6.7	Uniform N-composition of EC chondrules: are chondrules formed in planetary environment?	195
6.8	Future Directions	197
	Appendix	198
	References	204

## Acknowledgements

Finally, a pleasant and equally difficult task (since this is surely the most or may be the only read page of this thesis!) is to thank all the people that have accompanied, encouraged and supported me during the very interesting time of my Ph.D. studies at PRL, Ahmedabad. The present thesis would not have been possible without the constant support and cooperation of a number of people. I would like to take this opportunity to thank all of them.

Prof. S V S Murty introduced me to the challenging world of noble gas and nitrogen cosmochemistry. I remember his words when I joined the lab 'Ph.D. is nothing but training, a beginning of the long journey ahead'. And during this training, there are numerous moments when I asked thoughtless questions and thousands of instances when I scribbled erroneous scientific ideas. His patience in response was beyond my imagination. His exceptional guidance and care always provided the perfect '*pressure*' and '*temperature*' required for my metamorphism. However, I have never expressed my thanks. Today, I thank him for his infinite supports and encouragements during this training.

Ramakant taught me the intricacies of the 'mass spectrometer' and the associated techniques. His enormous energy for work and organized way of maintaining lab has inspired me during all these years. It was nice to have Vinai and Sudeshna as my seniors (never like seniors!) when I joined the lab. Later entry of Shreyas made life more interesting and entertaining in lab especially during the toughest periods (e.g., degassing of mass spec). They contributed largely to the positive and intimate atmosphere in lab, allowing for a lot of fun and friendship, conversations, and also helpful and inspiring discussions.

I was lucky to have Prof. J. N. Goswami as my expert during synopsis. He has always shown great interest in my work and his questions (during reviews, area seminars, short visits to his lab and in lift!) always propelled me forward. I am grateful to Prof. Krishnaswami, Prof. Bhattacharya, Prof. Ramesh, Prof. Singhvi, Dr. P. N. Shukla and Prof. Sarin for their inputs during various area seminars. I cannot forget my first year courses taken by Prof. Goswami, Prof. Krishnaswami, Prof. Bhattacharya, Prof. Sarin, Prof. Ramesh and late Dr. Kulkarni. The training given by them has helped me at various stages of this work and will be helping throughout my scientific career. I wish to express my sincere appreciation to the members of academic committee at PRL for critically reviewing my work at various stages. The informal (and strictly regular) Friday talks (*TGIF*) were extremely beneficial for me where I learned how to present our own view and ideas.

I am always grateful to Dr. Maibam who taught me how to prepare sections for EPMA studies. Special thanks to Neerjari and Devmurariji for their total support during using facilities at Ion Probe Lab. I am thankful to Prof. Ulrich Ott, Max-Planck-Institut für Chemie, Mainz, Germany and Dr. EVSK Babu, NGRI, India for providing EPMA facility. Without their support this thesis work would have been incomplete.

I must mention the cooperation of Dr. M. Yadava and Mr. N.B. Vaghela in whose lab I weighed my samples before analyses. My sincere appreciation to Mr. M.P. Kurup and Mr. K.K. Sivasankaran (for glass blowing), Mr. M. L. Mathew and Mr. J.A. Patel (liquid nitrogen) and Mr. Ubale and his team for their excellent support and expertise. Without any one of them, it would be impossible to keep the instrument running in the lab. I am thankful to the library staff for their help. I would like to express special thanks to Mr. Pranav for excellent 'labview' software and maintaining the instrument in proper working conditions in the lab. I should appreciate his interest in learning new things other than electronics. I must thank Deepak, Neeraj and Shanmugam for their support during using PLANEX facilities at Thaltej.

I was lucky to have Jyoti, Sunil, Ravi, Dipuda, Anil-ds, Bhavsarbhai, Sudheer, and Deepak (pandaji) around me. I always wonder how these senior people became my friends in just a few interactions. I will always cherish the wide range (starting from rubbish to scientific) of discussions during afternoon tea with them.

I am thankful to seniors like Anirban, Kuljeet, Alam, Prasanta, Neeraj (Bhaisaab), Manish, Jayendra, Lokesh, Tarak, Santosh, Pathakji, Sanjeev, Manoj and many for cultivating unique culture of PRL in me and for their friendly attitude, interactions and supports. My batch mates: Morthekai, Dilip, Nagar, Bhavesh, Murari, Sanjoy, Murali, Pavan, Rakesh and Rajendra have always reminded me my college years. Young guns like Satya, Gowda, Amit, Subimal, Sanat (& Uma) Shasdhara, Naveen, Rohit, Salman, Nabi, Rajesh, Rehman, Anil, Ashwini, Gyan, Kirpa, Jitendra, Alok and Ritesh have always inspired me by their unlimited energy and joy. The tea time encounters with them were like energy boosters.

Papa, Mummy, Kaka, Munna and Montu have always shown faith and support in me. Didibhai and Burkhard always prompted me to do the best. I am at the lost of words how to acknowledge the efforts of Ma and Baba who have always tried to accelerate me at various stages of my work and finally during thesis. How can I thank little *Arne*, the first member of my family's next generation? He has always reminded me *the child* inside me.

And here comes the most difficult part..... thanking Archita who is not different than me. She is so close that I feel like thanking me for this thesis! I can only say: Dear, let's move ahead... I am enjoying the shower of your faith, care, love, friendship and support...which is as usual beyond my comprehension.

J P Das

Ahmedabad

## Abstract

Nitrogen (for the first time) and noble gases (mainly He, Ne and Ar), were analyzed in 76 individual chondrules from 6 ordinary (O), 2 enstatite (E) and 2 carbonaceous (C) chondrites by using laser microprobe technique. Isotopic signatures of trapped nitrogen and noble gases reveal about the precursors of chondrules and the environment(s) and process(es) of their formation whereas cosmogenic noble gases give precompaction irradiation records supporting their nebular origin.

This first systematic study of nitrogen in individual chondrules has provided the following important results: (1)  $\delta^{15}\text{N}$  of chondrules in OC and CC are different from their host chondrite, while for EC, they are similar. (2) There is a large spread in  $\delta^{15}\text{N}$  of chondrules even from a given OC and CC as well as splits from same chondrule show different  $\delta^{15}\text{N}$  values. These imply that (a) The precursors of OC and CC chondrules are different and preserve their original  $\delta^{15}\text{N}$  heterogeneity; (b) the precursors of EC chondrules are homogeneous and match those of E chondrites. (c) Three N components (HL, Q and IOM) are indicated for OC and CC chondrules (d) chondrules of OC and CC formed in a location different from those of EC chondrules, which are formed in the same location as their parent chondrite.

Some chondrules show higher concentration of cosmogenic noble gases compared to host chondrites, which cannot be explained by differences in target chemistry and show evidence of precompaction cosmic ray exposure. From these, couple of chondrules shows presence of solar cosmic ray component. The chondrules of the studied meteorite mostly contain low but measurable amounts of trapped neon ( $^{20}\text{Ne}$ ) and argon ( $^{36}\text{Ar}$ ). The trapped ( $^{36}\text{Ar}/^{20}\text{Ne}$ ) ratio of chondrules can be explained by presence of two noble gases components: HL and Q in different proportions indicating heterogeneity in chondrule precursors. Loss of trapped  $^{36}\text{Ar}$  is evident from chondrules compared to their host chondrites especially in OC and CC chondrules whereas EC chondrules show different trend. Loss of trapped noble gases (mainly Ar) seems a result of fractionation between metal and silicate phases during chondrule formation which is well supported by relation between trapped noble gases with FeO content of chondrules. Two chondrules from Dhajala reflect the presence of solar type noble gases based on their isotopic and elemental ratios as well as petrographic feature, supporting the precompaction radiation in chondrule precursors.

## List of Tables

1.1	Abundances of chondrite constituents and size of chondrules in different classes of chondrites	4
1.2	Formulae of common minerals in chondrules	4
1.3	Chondrule classification systems	5
1.4	Cosmogenic isotopic compositions and major target elements	17
1.5	Ne and Ar isotopic and elemental compositions of phase Q, presolar diamonds (HL), and other reservoirs	19
2.1	Chondrites analyzed from different groups of chondrites, number of chondrules analyzed and chemically characterized in this work	33
2.2	Typical amount of blanks observed in two-extraction system	51
2.3	Mass spectrometer calibration parameters	54
2.4	Details of EPMA analysis used for chemical characterization of chondrules	55
2.5	Details of the standards used during EPMA analysis for different elements	56
3.1	Maximum values of radiogenic $^4\text{He}$ and elemental ratio $^4\text{He}/^{40}\text{Ar}$ expected in different classes of chondrites	74
3.2	$^3\text{He}_c$ , $^{21}\text{Ne}_c$ , $^{38}\text{Ar}_c$ and $^4\text{He}_r$ , $^{40}\text{Ar}_r$ of chondrules from ordinary chondrites	78
3.3	$^3\text{He}_c$ , $^{21}\text{Ne}_c$ , $^{38}\text{Ar}_c$ and $^4\text{He}_r$ , $^{40}\text{Ar}_r$ of chondrules from enstatite chondrites	90
3.4	$^3\text{He}_c$ , $^{21}\text{Ne}_c$ , $^{38}\text{Ar}_c$ and $^4\text{He}_r$ , $^{40}\text{Ar}_r$ of chondrules from carbonaceous chondrites	93
3.5	Results of electron probe microanalysis (performed on chondrule splits)	98
3.6	$\text{Mg}/(\text{Al} + \text{Si})$ , $(^{22}\text{Ne}/^{21}\text{Ne})_c$ , Production rates and cosmic ray exposure ages of chondrules and respective chondrites	99
4.1	He, Ne and Ar isotopic and elemental compositions, $^{20}\text{Ne}_t$ , $^{36}\text{Ar}_t$ concentrations, and $(^{36}\text{Ar}/^{20}\text{Ne})_t$ ratios of chondrules from Dhajala, Chainpur, Bjurböle, Saratov, Tieschitz and Udaipur chondrites	134
4.2	He, Ne and Ar isotopic and elemental compositions, $^{20}\text{Ne}_t$ , $^{36}\text{Ar}_t$ concentrations, and $(^{36}\text{Ar}/^{20}\text{Ne})_t$ ratios of chondrules from Parsa and Qingzhen chondrites	138
4.3	He, Ne and Ar isotopic and elemental compositions, $^{20}\text{Ne}_t$ , $^{36}\text{Ar}_t$ concentrations, and $(^{36}\text{Ar}/^{20}\text{Ne})_t$ ratios of chondrules from Allende and Murray chondrites	139
5.1	Nitrogen results for the individual chondrules of ordinary chondrites	161
5.2	Nitrogen results for the individual chondrules of Parsa and Qingzhen chondrites	168
5.3	Nitrogen results for the individual chondrules of Allende and Murray chondrites	169
6.1	Important results of this thesis	192

## List of Figures

1.1	Different petrographic features of chondrules	7
1.2	Variation of chemical composition between Type-I and Type-II chondrules	12
1.3	The oxygen isotopic composition of chondrules from major chondrite groups.	14
1.4	Elemental abundances of major primordial noble gas components	20
1.5	N-compositions of major chondrites plotted against N-abundances.	22
1.6	Schematic to explain precompaction cosmic ray exposure of chondrules	26
2.1	Schematic for freeze-thaw method used for chondrule separation.	32
2.2	Schematic of the Laser Microprobe Setup	36
2.3	(a) Schematic of the sample chamber (b) photograph of sample chamber	38
2.4	Schematic diagram of the metal line	40
2.5	Schematic diagram of the extraction system	42
2.6	Schematic diagram of the extraction bottle	43
2.7	Flow diagram of standard experimental procedure	47
3.1	Elemental ratios ( ${}^3\text{He}/{}^{21}\text{Ne}$ ) <sub>c</sub> and ( ${}^{21}\text{Ne}/{}^{38}\text{Ar}$ ) <sub>c</sub> plotted against ${}^{21}\text{Ne}_c$ for chondrules from Dhajala chondrite	76
3.2	Elemental ratios ( ${}^3\text{He}/{}^{21}\text{Ne}$ ) <sub>c</sub> and ( ${}^{21}\text{Ne}/{}^{38}\text{Ar}$ ) <sub>c</sub> plotted with ${}^{21}\text{Ne}_c$ for chondrules from Bjurböle chondrite	83
3.3	Elemental ratios ( ${}^3\text{He}/{}^{21}\text{Ne}$ ) <sub>c</sub> and ( ${}^{21}\text{Ne}/{}^{38}\text{Ar}$ ) <sub>c</sub> plotted against ${}^{21}\text{Ne}_c$ for chondrules from four ordinary chondrites.	85
3.4	Elemental ratios ( ${}^3\text{He}/{}^{21}\text{Ne}$ ) <sub>c</sub> and ( ${}^{21}\text{Ne}/{}^{38}\text{Ar}$ ) <sub>c</sub> plotted ${}^{21}\text{Ne}_c$ for Parsa and Qingzhen chondrites	88
3.5	Elemental ratio ( ${}^3\text{He}/{}^{21}\text{Ne}$ ) <sub>c</sub> and ( ${}^{21}\text{Ne}/{}^{38}\text{Ar}$ ) <sub>c</sub> plotted ${}^{21}\text{Ne}_c$ for chondrules of Allende and Murray chondrites	91
3.6	Cosmogenic ${}^3\text{He}$ , ${}^{21}\text{Ne}$ , ${}^{38}\text{Ar}$ , the production rates of ${}^3\text{He}$ , ${}^{21}\text{Ne}$ , ${}^{38}\text{Ar}$ and the corresponding exposure ages respectively for Dhajala chondrules and bulk	101
3.7	Cosmogenic ${}^3\text{He}$ , ${}^{21}\text{Ne}$ , ${}^{38}\text{Ar}$ , the production rates of ${}^3\text{He}$ , ${}^{21}\text{Ne}$ , ${}^{38}\text{Ar}$ and the corresponding exposure ages respectively for Bjurböle chondrules	102
3.8	${}^3\text{He}_c$ , ${}^{21}\text{Ne}_c$ , ${}^{38}\text{Ar}_c$ , the production rates of ${}^3\text{He}$ , ${}^{21}\text{Ne}$ , ${}^{38}\text{Ar}$ and the corresponding exposure ages respectively for Tieschitz chondrule and bulk samples	104
3.9	Cosmogenic ${}^3\text{He}$ , ${}^{21}\text{Ne}$ , ${}^{38}\text{Ar}$ , the production rates of ${}^3\text{He}$ , ${}^{21}\text{Ne}$ , ${}^{38}\text{Ar}$ and the corresponding CRE ages respectively for Saratov chondrules and bulk samples	105
3.10	Cosmogenic ${}^3\text{He}$ , ${}^{21}\text{Ne}$ , ${}^{38}\text{Ar}$ , the production rates of ${}^3\text{He}$ , ${}^{21}\text{Ne}$ , ${}^{38}\text{Ar}$ and corresponding exposure ages for Chainpur chondrules and matrix samples	106
3.11	Cosmogenic ${}^3\text{He}$ , ${}^{21}\text{Ne}$ , ${}^{38}\text{Ar}$ , the production rates of ${}^3\text{He}$ , ${}^{21}\text{Ne}$ , ${}^{38}\text{Ar}$ and the corresponding exposure ages respectively for Parsa chondrule and bulk samples	107
3.12	Cosmogenic ${}^3\text{He}$ , ${}^{21}\text{Ne}$ , ${}^{38}\text{Ar}$ , the production rates of ${}^3\text{He}$ , ${}^{21}\text{Ne}$ , ${}^{38}\text{Ar}$ and the corresponding exposure ages respectively for Allende chondrules	108

3.13	Cosmogenic $^3\text{He}$ , $^{21}\text{Ne}$ , the production rates of $^3\text{He}$ , $^{21}\text{Ne}$ and the corresponding exposure ages respectively for Murray chondrule and bulk	110
3.14	Elemental ratio $^4\text{He}/^{40}\text{Ar}$ of chondrules from ordinary chondrites plotted with concentration of $^{40}\text{Ar}$ in chondrules	112
3.15	Elemental ratio $^4\text{He}/^{40}\text{Ar}$ of chondrules from enstatite chondrites plotted with concentration of $^{40}\text{Ar}$ in chondrules	116
3.16	Elemental ratio $^4\text{He}/^{40}\text{Ar}$ of chondrules from Allende and Murray chondrites plotted with concentration of $^{40}\text{Ar}$ in chondrules	118
3.17	$\text{K}-^{40}\text{Ar}$ and $\text{U}/\text{Th}-^4\text{He}$ gas retention ages of all chondrules and bulk	120
3.18	Plot of the $\text{Mg}/(\text{Al}+\text{Si})$ element concentration ratio against $(^{22}\text{Ne}/^{21}\text{Ne})_c$ for the chondrules with precompaction exposure history	126
4.1	Plot of measured $^{36}\text{Ar}/^{38}\text{Ar}$ values of all studied chondrules	132
4.2	Abundances of trapped $^{20}\text{Ne}$ and $^{36}\text{Ar}$ in chondrules and their bulk	141
4.3	$(^{36}\text{Ar}/^{20}\text{Ne})_t$ of all chondrules and chondrites is plotted against $^{36}\text{Ar}$	143
4.4	Elemental ratios $^{84}\text{Kr}/^{132}\text{Xe}$ and $^{36}\text{Ar}/^{132}\text{Xe}$ of chondrules	146
4.5	Concentrations of $^{36}\text{Ar}_t$ in studied chondrules versus $\text{FeO}$ of the chondrules	148
4.6	$^{20}\text{Ne}/^{22}\text{Ne}$ vs. $^{21}\text{Ne}/^{22}\text{Ne}$ of chondrules from Dhajala are plotted	151
4.7	$^4\text{He}$ in chondrules of Dhajala contributed by trapped and radiogenic components	153
5.1	Correction in nitrogen composition for cosmogenic contribution compared for (a) chondrites of different cosmic ray exposure ages (with similar N content) (b) from Dhajala with different N contents	158
5.2	Trapped N-composition ( $\delta^{15}\text{N}_t$ ) vs. nitrogen concentration is plotted for Dhajala chondrules and bulk	160
5.3	Trapped N-composition ( $\delta^{15}\text{N}_t$ ) vs. nitrogen content is plotted for chondrules and bulk sample of five ordinary chondrites	165
5.4	Trapped N-composition ( $\delta^{15}\text{N}_t$ ) vs. nitrogen content is plotted for chondrules and bulk sample of Parsa and Qingzhen chondrites	167
5.5	Trapped N-composition ( $\delta^{15}\text{N}_t$ ) vs. nitrogen content is plotted for chondrules and bulk sample of Allende and Murray chondrites	171
5.6	$\delta^{15}\text{N}$ vs. N content of splits analyzed from same chondrules	172
5.7	$\delta^{15}\text{N}$ vs. N content of Allende chondrules	174
5.8	Relation of size with $\delta^{15}\text{N}$ and N-content of chondrules from Dhajala, Bjurböle and Allende	176
5.9	Elemental ratio $^{36}\text{Ar}/^{14}\text{N}$ vs. $\delta^{15}\text{N}$ of individual chondrules and their bulk	178
5.10	Elemental ratio $^{36}\text{Ar}/^{14}\text{N}$ vs. $\delta^{15}\text{N}$ of individual chondrules and their (with IOM)	180
5.11	Concentrations of N in chondrules and their respective bulk	182
5.12	N-composition of Type-I and II chondrules vs. content of $\text{FeO}$ in chondrules	184
6.1	N-compositions of for chondrules from OC, EC and CC vs. the content of N	193

# Chapter 1

## Introduction

## ***Preamble***

Spherical objects of about ~1mm size called chondrules are major constituent of most chondrites. Chondrules are one of first solids to form in the solar system. Large abundance of chondrules suggests that their formation was an efficient and common process during the early stages of our solar system. Understanding of chondrule formation therefore has a potential astrophysical significance. However, after decades of research, little is known about the chondrule formation mechanism and the environment during chondrule formation. Several recent reviews on chondrules discuss their physicochemical properties and formation models (Grossmann et al., 1988, Hewins 1997, Brearley and Jones, 1998, Rubin 2000, Connolly and Desch, 2004, Jones et al., 2005, Lauretta et al., 2006). During Masursky Lecture at the 2000 Lunar and Planetary Science Conference, John Wood has summarized the present state of knowledge on meteorites and chondrule formation, as “*We still don’t understand what the meteorites are trying to tell us*” and “*I personally wonder whether we ever will. There’s just no convergence*” (Kerr, 2001). This describes the challenges involved in understanding chondrules and their origin. There have been three international conferences on chondrules (1982, 1995 and 2004) where the contemporary state of knowledge and the enigmatic aspects that need to be addressed have been discussed.

Isotopic signatures of trapped nitrogen and noble gases provide information about the precursors of chondrules, the environment(s) and process(es) of chondrule formation. This work is aimed at the study nitrogen and noble gases in individual chondrules from major classes of chondrites. Study of nitrogen is virtually an unexplored quarter in chondrule research and only a few studies have been done for noble gases in chondrules so far. This work is the first systematic approach for the simultaneous nitrogen and noble gas studies in chondrules.

Details of chondrule occurrences, their various properties and possible formation mechanisms are given in the first part of this chapter. Next, various nitrogen and noble gas components related to this study are explained. This is followed by a section, which summaries the results and implications of earlier studies (related to this work) on chondrules. The summary is mainly related to noble gas studies, as nitrogen studies are very rare. After that, the objectives of this work are described. Outline of this thesis is given in the last section.

## ***Chondrites***

Meteorites are fragments of asteroids-the leftover material in the formation of large solar system objects. Material from asteroids is pristine as it represents the most primitive solid matter of the solar system. Meteorites can be generally classified into two broad categories: Undifferentiated and Differentiated. Undifferentiated meteorites are also called chondrites, meteorites containing chondrules. Most of the meteorites that fall on the earth are chondrites. Chondrites are those solid objects, which have been subjected to minimum secondary processing (e.g. aqueous alteration and thermal metamorphism) since their formation and preserve primitive signatures in the form of elemental and isotopic compositions. Thus, chondrites and their components are the logical places to search for survived signatures of early stages of nebular history and solar system.

Based on small differences in their composition, chondrites are classified between the three major chondrite groups (ordinary (H, L, LL), enstatite (EH and EL) and carbonaceous (CI, CM, CO, CV)). Differences in their composition apparently were caused by the fractionation of various solid components and gas that existed in the nebula prior to the final accretion of the parent bodies. Their compositions suggest different environment of formation for example, ordinary chondrites formed under normal conditions and carbonaceous and enstatite chondrites formed under oxidizing and reducing conditions respectively.

Chondrites in general comprise of chondrules, fine matrix materials, aggregates of metal and troilite minerals (abundant in ordinary and enstatite chondrites, rare in carbonaceous chondrites) and non-igneous-textured Calcium Aluminum rich Inclusions (CAIs) (most abundant in CM, CO and CV chondrites). Chondrules are the major component in H, L, LL, EH, CM, CO and CV groups and are absent from the CI group.

### ***1.1 What are chondrules?***

Chondrules are the most significant components of chondrites, comprising up to ~80 vol%. Chondrules are small ( $\leq 1\text{mm}$ ), mainly ferromagnesian silicate spheres with igneous textures result of high temperature melting. Table 1.1 gives the sizes and abundances of chondrules in various chondrites, while Table 1.2 gives the major minerals found in chondrules. Their shape, textures and mineralogy suggest their formation by flash heating of freely floating precursor grains in presence of nebular gas and rapid crystallization of a molten droplet. Based on these properties and

**Table 1.1** Abundances of chondrite constituents and size of chondrules in different classes of chondrites

Chondrite class	Chondrule abundance <sup>1</sup> (vol%)	Matrix abundance (vol%)	Refractory Inclusion Abundance <sup>2</sup> (vol%)	Metal Abundance <sup>3</sup> (vol%)	Chondrule mean diameter (mm)
CI	<<1	>99	<<1	0	-
CM	20	70	5	0.1	0.3
CR	50-60	30-50	0.5	5-8	0.7
CO	48	34	13	1-5	0.15
CV	45	40	10	0-5	1.0
CK	15	75	4	<0.01	0.7
CH	~70	5	0.1	20	0.02
H	60-80	10-15	0.1-1?	10	0.3
L	60-80	10-15	0.1-1?	5	0.7
LL	60-80	10-15	0.1-1?	2	0.9
EH	60-80	<2-15?	0.1-1?	8	0.2
EL	60-80	<2-15?	0.1-1?	15	0.6
R	>40	36	0	0.1	0.4
K	27	73 <sup>4</sup>	<0.1	0 <sup>4</sup>	0.6

<sup>1</sup>Chondrule abundance includes mineral fragments <sup>2</sup>Refractory inclusion abundance includes CAI (Calcium Aluminum rich Inclusion) +AOI (Amoeboid Olivine Inclusion) <sup>3</sup>Metal abundance includes metal <sup>4</sup>Matrix abundance includes metal (Data source: Brearley & Jones, 1998).

**Table 1.2** Formulae of common minerals in chondrules

Mineral	Formula
Olivine	(Fe, Mg) <sub>2</sub> SiO <sub>4</sub>
Pyroxene	(Fe, Mg, Ca) <sub>2</sub> Si <sub>2</sub> O <sub>6</sub>
Plagioclase (feldspar)	CaAl <sub>2</sub> Si <sub>2</sub> O <sub>8</sub> – NaAlSi <sub>3</sub> O <sub>8</sub>
Spinel	MgAl <sub>2</sub> O <sub>4</sub>
Chromite	FeCr <sub>2</sub> O <sub>4</sub>
Troilite	FeS
Kamacite	Fe-Ni

subsequent arguments, formation of chondrules by flash heating and rapid cooling is one of the major constraint for the models explaining chondrule formation mechanism.

Chondrules show large variation in textures, mineral abundances; chemical properties (e.g. bulk and isotopic compositions) and physical properties (e.g. size sorting according to chondrite classes). Each major chondrite group (ordinary, carbonaceous, and enstatite) contains chondrules with a wide range of all these properties, generally reflecting variations among precursors and the formation regions of the chondrite groups. On one hand, this wide range of properties provides vital information about chondrule formation process(es) while on the other, it complicates our understanding about chondrules (Lauretta et al., 2006, Jones et al., 2005; Connolly and Desch, 2004; Rubin 2000; Hewins 1997).

### ***1.2 Chondrule classification***

An essential part of interpreting observations on chondrules, involves the relationship between chondrules (or groups of chondrules) and their properties. For simplicity in comparison between observations and chondrule properties, classification schemes for chondrules are employed. Classification schemes of chondrules are mainly based on

**Table 1.3** Chondrule classification systems (Table 3, Lauretta et al., 2006)

Textural Classification			
Abbreviation	Abundance in OCs (%)		Texture
POP	47–52		Porphyritic, both olivine and pyroxene
PO	15–27		Porphyritic, dominated by olivine (>10/1 by volume)
PP	9–11		Porphyritic, abundant pyroxene (>10/1 by volume)
RP	7–9		Radial pyroxene
BO	3–4		Barred olivine
CC	3–5		Cryptocrystalline
GOP	2–5		Granular olivine-pyroxene
M	<1		Metallic
Compositional Classification			
Type	Silicate Composition	Subtype	Silicate Abundances
I	FeO-poor (Fo, En > 90)	A	Abundant olivine (>80 vol%)
		AB	Intermediate abundances of olivine and pyroxene
II	FeO-rich (Fo, En < 90)	B	Abundant pyroxene (>80 vol%)

textural, chemical and cathodoluminescence properties of chondrules. Schemes based on textural and chemical properties of chondrules are widely accepted.

The classification scheme proposed by Gooding and Keil (1981) was based on textural properties of chondrules. They defined two broad categories of chondrules: porphyritic and nonporphyritic. Porphyritic chondrules contain abundant, relatively large (as large as the radius of the chondrule) phenocrysts of olivine and/or low-Ca pyroxene surrounded by glassy or microcrystalline mesostasis. Porphyritic chondrules that are dominated by olivine (>10/1 volume ratio) are referred to as porphyritic olivine (PO) chondrules, while those that contain abundant pyroxene (>10/1 volume ratio) are porphyritic pyroxene (PP) chondrules (as listed in Table 1.3). As for example, chondrule BB-29 and DH-11 from this study show PO and PP textures respectively as seen in Fig. 1.1.

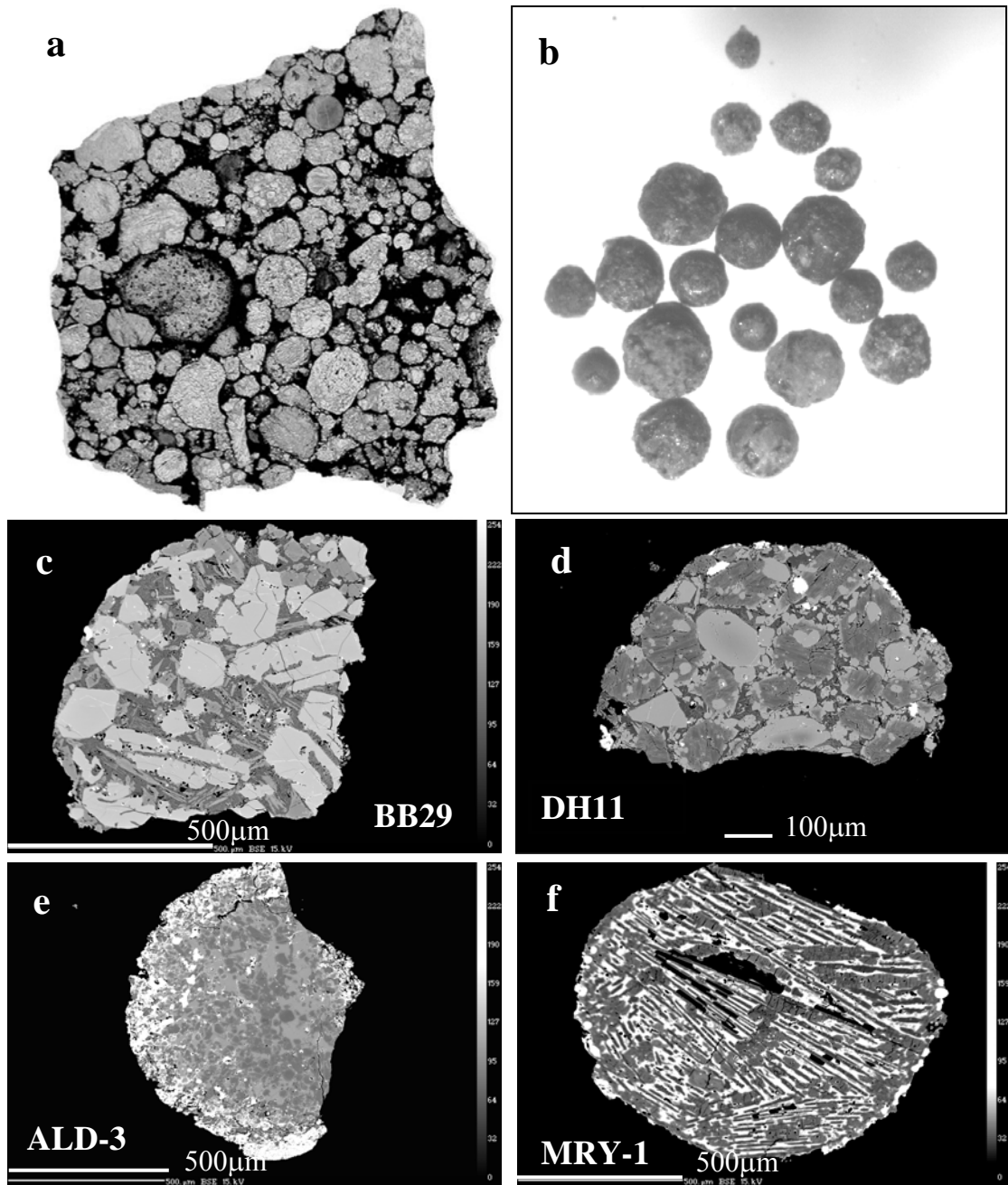


**Fig. 1.1** (a) Plane-polarized transmitted light image of the Semarkona (LL3.0) primitive chondrite (Fig. 1, Lauretta et al., 2006). ~70 vol% is made up of chondrules. Black interchondrule material is fine-grained matrix (b) separated chondrules of Allende chondrite, as seen in stereomicroscope. Back scattered electron (BSE) images of chondrules representing various textural properties observed in chondrules. (c) Porphyritic olivine (PO): large phenocrysts of olivine with few pyroxene minerals with interstitial mesostasis (d) Porphyritic pyroxene (PP): dark mineral are low-Ca pyroxenes and lighter grains are olivine minerals (e) Granular chondrule (G) with olivine minerals ( $< 10 \mu\text{m}$ ) with anorthitic mesostasis. Rim of metal sulfide is also visible. (f) Barred Olivine (BO): Bars of olivine minerals, with several sets of orientations, are visible with small dots of metal/metal sulfides at the rim.

Chondrules with silicate mineral abundances between these two extremes are called porphyritic olivine-pyroxene (POP) chondrules. Chondrules with many small grains of uniform size ( $<10\ \mu\text{m}$ ) with poorly defined crystal outlines are classified as Granular (G) (chondrule ALD-3, Fig. 1.1.). Granular chondrules are further subdivided into GO, GOP, and GP groups according to abundance of olivine and pyroxene minerals. Barred-olivine chondrules (BO) contain olivine crystals that have one dimension that is markedly longer than the other two when viewed in thin section. All olivine grains in barred chondrules either have the same crystallographic orientation or contain several sets of such oriented grains. Chondrule MRY-1 of this study shows BO texture with sets of olivine bars with different orientations. Radial-pyroxene chondrules (RP) consist of fan-like arrays of low-Ca pyroxene, which radiate from one or more points near their surface. Cryptocrystalline chondrules are objects that do not exhibit any recognizable crystal structure under an optical microscope. They have a high abundance of glassy material. Neither chondrule size nor shape is strongly correlated with textural type.

Another chondrule classification scheme has been developed based on bulk FeO contents (compositional classification) of chondrules (listed in Table 1.3). This scheme divides chondrules into two broad categories: Type-I and Type-II (McSween, 1977; Scott and Taylor, 1983). Type-I chondrules are characterized by the presence of FeO-poor olivine and pyroxene (**F**orsterite ( $\text{Mg}_2\text{SiO}_4$ ) and **E**nstatite ( $\text{Mg}_2\text{SiO}_3$ )  $> 90$ ). Type-II chondrules contain FeO-rich olivine and pyroxene (Fo and En  $< 90$ ). These two main categories are further subdivided into subtypes A and B based on their abundances of olivine and pyroxene. Type-IA and IIA chondrules contain abundant olivine ( $>80\ \text{vol}\ \%$ ), Type-IB and IIB chondrules contain abundant pyroxene ( $>80\ \text{vol}\ \%$ ), and chondrules with intermediate abundances of olivine and pyroxene are classified as Type-IAB or IIAB.

A simplified chemical classification scheme, derived from the above mentioned scheme is also used by some workers. As in one scheme, Type-I refers to chondrules that have low Fe/ (Fe + Mg) atomic ratios ( $<10\%$ ) in their olivine and low-Ca pyroxene; type-II refers to chondrules that have higher Fe/ (Fe + Mg) atomic ratios ( $>10\%$ ) in their silicate minerals (Jones et al., 2005). While in the scheme adopted by Hanon et al. (1998), for Type-II chondrules, higher than 12 wt% content of FeO in olivine and low-Ca pyroxene is taken as the criterion and chondrules with less than this amount of FeO is considered as Type-I. It is observed that by using these different

schemes, no significant changes occurred to classification of chondrules in a given suit. More important is the content of FeO in a given chondrule which has significance related to chondrule precursors and environment during chondrule formation.

These above mentioned schemes (based on FeO content of chondrules) along with the Gooding and Keil (1981) classification scheme (based on textural properties) are often used in conjunction with one another and widely accepted in chondrule research fraternity.

In addition to these schemes, independent chondrule classification scheme has been proposed by Sears et al. (1992) and DeHart et al. (1992). This scheme does not rely on textural properties or modal mineralogy of chondrules. Instead, chondrules are classified based on their cathodoluminescence properties and mineral compositions. Cathodoluminescence refers to the emission of visible light from a solid that is excited by interaction with an electron beam. Cathodoluminescence is highly dependent on trace-element abundances and crystal lattice defects. Chondrules that luminesce brightly are classified as group-A chondrules, while those that show little or no luminescence are group-B chondrules. These two groups are further subdivided based on the mean FeO and CaO concentration in olivine and the composition of the chondrule mesostasis. Sears et al. (1992) identified four groups of chondrules as primitive and suggested that the other groups represent alteration of primitive chondrules on meteorite parent asteroids. Cathodoluminescence is a less widely available technique, and as a result the Sears et al. classification is not commonly used (Lauretta et al., 2006). In the present study, we used the scheme based on compositional classification (McSween, 1977; Scott and Taylor, 1983). Type-I chondrules are defined as FeO < 7.8 wt% and Type-II chondrules are defined as FeO content higher than 7.8%.

### ***1.3 Thermal histories of chondrules***

Besides its use for chondrule classification, texture of chondrules can also be used to constrain the thermal histories of chondrules. Textures (as discussed above in classification schemes) of chondrules carry information related to peak temperature and heating duration experienced by individual chondrules. With the help of chondrule observations as well as experimental simulations, several constraints on

thermal histories of chondrules are made. Recently Lauretta et al. (2006) has discussed this approach in detail.

For the crystallization of a melt, the presence of crystal nuclei is prerequisite. The abundance of crystal nuclei is a major factor in determining chondrule textures (Lofgren, 1996). Spontaneous formation of nuclei in the chondrule melt is relatively slow process compared to the timescales of chondrule formation. Hence, peak temperature experienced by chondrules controls the abundance of nuclei in chondrules available during cooling and crystallization. Porphyritic and granular textures form when abundant nuclei are present during cooling of chondrules. This suggests that for the formation of porphyritic and granular chondrules, the peak temperatures were slightly below the liquidus temperature of chondrules (Lofgren and Russell, 1986). As observed in experimental simulations, unmelted relicts provided abundant nucleation sites that generated the characteristic porphyritic textures on cooling (Lofgren, 1989; Hewins and Radomsky, 1990). The unmelted relicts of precursors in case of porphyritic chondrules suggest incomplete removal of trapped gases from these precursors. Okazaki et al. (2001a) has reported higher concentrations of trapped  $^{36}\text{Ar}$  in porphyritic chondrules from the enstatite chondrite Yamato (Y)-791790. They argue that this high concentration is due to the presence of irradiated solar wind noble gases received from young sun during chondrule formation (as suggested by X-wind model) and survived in these porphyritic chondrules.

Barred olivine (BO) and radial pyroxene (RP) are the other major textures observed in chondrules. Nuclei free chondrule melts can cool well below liquidus temperature of chondrule. In such case, when a nucleus forms, there is a burst of rapid crystal growth, producing textures similar to barred-olivine and radial-pyroxene chondrules (Lofgren and Lanier 1990; Radomsky and Hewins 1990). Barred olivine (BO) texture is the result of crystallization of nuclei-free melt droplets and significant amount of undercooling may have occurred in these melt droplets. Comparison of the olivine morphology in barred chondrules with analog textures produced in experiments indicates that these chondrules cooled at rates of  $500^0$ -  $2300^0\text{C/h}$  (Lofgren and Lanier, 1990; Tsuchiyama et al., 2004).

#### ***1.4 Type-I and Type-II chondrules: genetically related?***

The definition of Type-I and Type-II chondrules are given in section 1.2. There are few typical properties of these two types of chondrules. For example, Type-I chondrules show variable amount of metallic phases and with olivine having high Mg/Fe ratios and Type-II chondrules are almost free of metallic phases and with olivine having low Mg/Fe ratio (Hanon et al., 1998). As shown in Fig. 1.2 and recently reviewed by Jones et al. 2005, Lauretta et al. 2006, the trend suggests that relative to CI-abundances, Type-II chondrules are generally more volatile rich and refractory poor than Type-I chondrules. Sears et al. (1996) proposed that initially chondrule precursors were FeO-rich, similar to Type-II chondrules. Subsequent heating in oxygen rich environment formed Type-II chondrules; whereas heating in low oxygen fugacity caused reduction of the precursors forming Type-I chondrules. Recent evaporation experiments show that Type-IIAB (FeO rich, olivine and pyroxene) starting material, when heated for 5-15 min above liquidus temperature gradually becomes Type-IB (FeO-poor, pyroxene) in composition and due to reduction and evaporation the Na loss is nearly 100% (Hewins et al., 1996). Though the Fe-loss trend of the experiments is indicating formation of Type-I chondrules from Type-II chondrules, for natural chondrules it cannot be applied directly as natural Type-I chondrules have higher Na. However, this suggestion is still valid, if Na and elements that are more volatile are reintroduced in, chondrules after their formation (as for example re-condensation of fine grained objects derived from dust plus volatiles). To summarize, it is clear that Type-I chondrules are more reduced compared to Type-II chondrules and possibly derived from precursors similar to Type-II chondrules.

#### ***1.5 Chemical and isotopic studies of chondrules***

Based on chemical compositions of chondrules, issues related to their formation and thermal histories can be constrained. As reviewed by Grossman and Wasson (1983), Jones et al. (2005) and Lauretta et al. (2006), chondrules show large diversity in chemical composition compared to bulk chondrites. Generally it is observed that chondrules are depleted in FeO compared to bulk chondrite (except EH chondrites which have very little FeO). In ordinary and enstatite chondrites, chondrules are generally depleted in metal and sulfide compared to whole rock and depletion in Fe is greater than that of FeO. Minor and trace elements also show wide range in

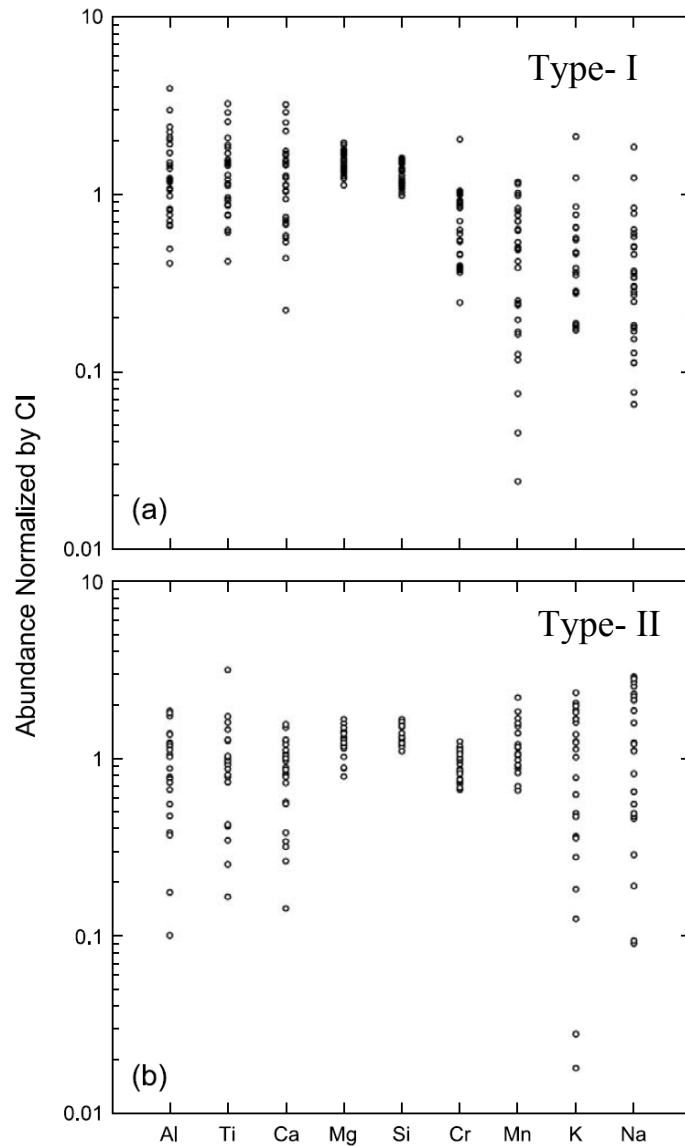


**Fig. 1.2** Variation of chemical composition between Type-I and Type-II chondrules from Semarkona (LL3.0) and Renazzo chondrite. Elemental abundances are plotted relative to silicon and to CI chondrite abundances. Elements on the ordinate are arranged in order of increasing volatility. (a), (b) Data for Semarkona (Jones & Scott 1989; Jones 1990, 1994, 1996) and Renazzo (Kong and Palme, 1999). Fig. 3, Lauretta et al., (2006)

chondrules. The most obvious difference in chondrules and host chondrite group is depletion in siderophile and chalcophile elements and depletion is different in different chondrite groups. Grossman and Wasson (1983) suggested that the large variations in the compositions of chondrules are highly systematic. They showed that elements of similar volatility and mineral affinity vary together. To sum up, it is established that chondrules show very different composition compared to host chondrites.

### **1.5.1 Complementarity between chondrules and matrix**

Anders (1964) proposed two-component model to explain the varying volatile contents in chondritic meteorites. This two-component model is related to chondrule formation where a volatile rich component (matrix, of CI composition) accreted with volatile depleted chondrules (because of evaporative loss of volatiles during chondrule formation). Recently Bland et al. (2005) also found that matrix of carbonaceous chondrites are rich in volatiles compared to bulk chondrites. Authors suggested that this complementarity is due to thermal processing during chondrule formation and exchange of volatiles between chondrules and matrix. Their result favors the nebular origin of chondrules and suggests shorter duration for the accretion of chondrules and adjacent matrix material.

### **1.5.2 Oxygen isotopic composition of chondrules**

Study of isotopic composition in individual chondrules is another important tool to investigate chondrule origins and effect of surrounding environment on chondrules. Like bulk chemical compositional data, oxygen isotopic compositions of chondrules show large diversity both among and within the various chondrite groups (Clayton et al., 1984; Clayton et al., 1991; Clayton 1993; Rubin et al., 1990; Clayton and Mayeda 1999). In a three-isotopic diagram ( $\delta^{18}\text{O}$  vs.  $\delta^{17}\text{O}$ ), bulk O-isotopic compositions of most chondrules in ordinary, enstatite and carbonaceous chondrites plot above, along and below terrestrial fractionation line (with slope 0.5 and result of mass dependent fraction between oxygen isotopes) respectively (as shown in Fig. 1.3). These observations are commonly interpreted as presence of isotopically heterogeneous precursor materials in chondrules and O-isotopic exchange between  $^{16}\text{O}$ -rich and  $^{16}\text{O}$ -poor reservoirs during chondrule formation event (Clayton 1993). These results can also be explained by mass-independent fractionation processes (Thiemens 1996) and by various self-shielding models (as summarized by Kuramoto and Yurimoto 2005). In addition, bulk O-isotopic compositions of chondrules were probably modified to various degrees during post crystallization alteration, most likely in an asteroidal setting (e.g. Young et al., 2002).

In a nutshell, the current interpretation of oxygen isotope data for chondrules suggests: 1) that there were isotopic differences among chondrule precursors in different chondrite groups as well as among chondrules, and 2) that chondrules preserve evidence for isotopic interaction with the ambient gas while they were

molten. The ambient gas may have been common to all chondrite groups (Jones et al., 2005).

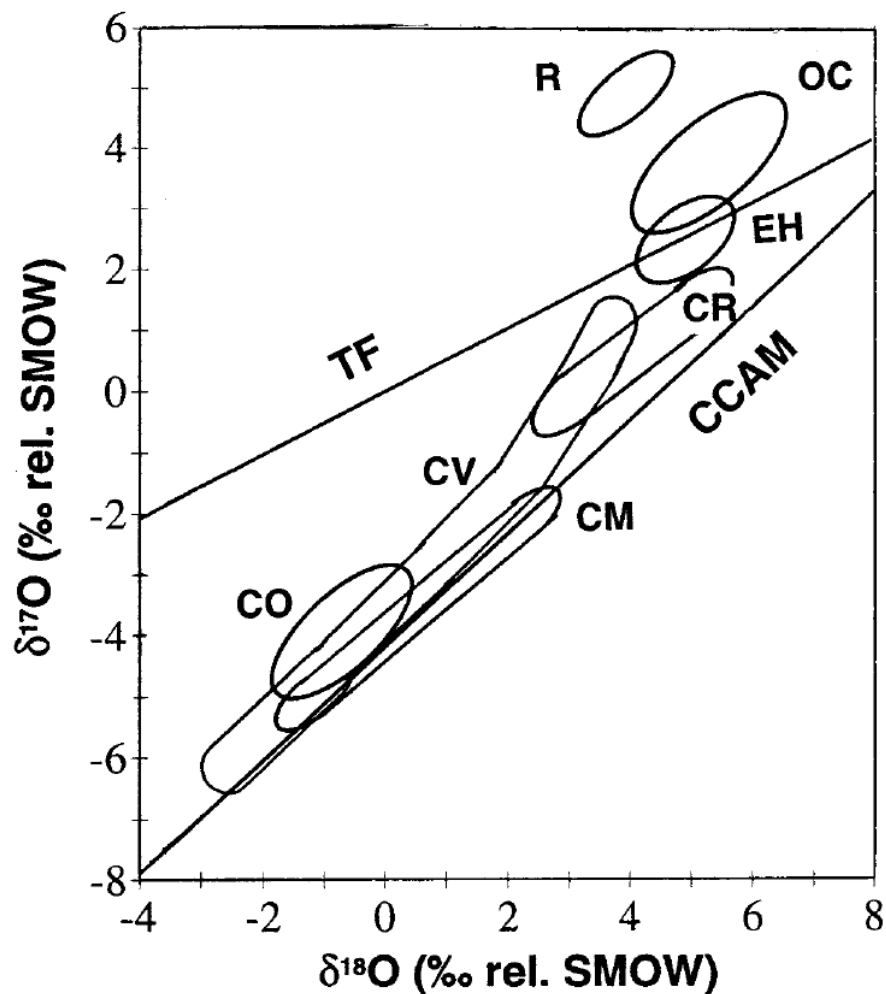


**Fig. 1.3** The oxygen isotopic composition of chondrules from major chondrite groups. Oxygen-bearing terrestrial materials lie on a mass-fractionation line of slope 0.52 called the terrestrial fractionation (TF) line. The CCAM (carbonaceous chondrite anhydrous mineral) line has a slope of 0.94 and is defined by the composition of refractory inclusions in CV chondrites. Data for represented groups include R chondrites (Weisberg et al., 1991), ordinary chondrites (Clayton et al., 1991), EH enstatite chondrites (Clayton and Mayeda, 1985), and CO (Rubin et al., 1990), CV (Clayton et al., 1983; Rubin et al., 1990), CM (Rowe et al., 1994) and CR (Weisberg et al., 1993) carbonaceous chondrites. Fig. 1, Rubin (2000)

### 1.5.3 Lack of isotopic fractionation in chondrules

Chondrules show fundamental discrepancy between chemical and isotopic fractionations. It is generally observed that chondrules are depleted in volatile elements like S, K, Na, Fe, Mg etc., and suggesting chemical fractionation compared to refractory elements like Al. However, chondrules are not found isotopically fractionated for these elements. Both evaporation and condensation generally

accompanied by mass dependent fractionation. As for example, evaporation can result in enrichment of heavy isotopes in the residue. The largest isotopic fractionation occurs during Rayleigh fractionation and the isotopic fractionations correlate with the extent of volatile loss or gain. However, lack of isotopic fractionations is observed in chondrules. It was first reported by Humayun and Clayton (1995) who measured K-isotopic composition in a single Allende chondrule and found no isotopic fractionation. Later several other workers also found similar observations (see review by Lauretta et al., 2006). Lauretta et al. (2006) summarize the present status as follows: (1) moderately volatile components from chondrule precursors were lost during heating due to evaporation. The degree of evaporative loss depended on melt composition, evaporative loss, rate of heating, total heating time and the physical conditions such as pressure and temperature (2) Evaporated gas was not lost from the system and significant amount of it condensed back during cooling (crystallization of chondrules) (3) During early stage of evaporation, isotopic fractionation should have been significant. However, isotopic re-equilibration occurred later during cooling, which resulted in little isotopic fractionation preserved in chondrules.

### ***1.6 The setting for chondrule formation: Nebular or Planetary origin***

There is no clear consensus for the environment in which chondrule formed (Nebular or planetary) like the uncertainties in chondrule formation mechanism. Some mechanisms like lightning (Whipple, 1966, Horányi et al., 1995), X-winds (Shu et al., 1996), shock waves (Wood, 1984; Ruzmaikina and Ip, 1996; Connolly and Love, 1998) and collisions between smaller objects (Kieffer, 1975) requires nebular setting for chondrule formation. On the other hand, mechanisms like impacts on parent bodies (Urey, 1967; Zook, 1980; Symes, 1997; Sanders, 1996; Hutchison et al., 2005), magmatic processes on planetary bodies (e.g. Chen et al., 1998; Lugmair and Shukolyukov, 2001) and ejection from planetary bodies by volcanoes (Merrill, 1920) favor chondrule formation in planetary environment. Based on various properties of chondrules, there are attempts to prove or disprove various models. Another stream of thinking is that either both kinds of mechanisms were involved in chondrule formation or similar to chondrites, chondrules might have formed in different locations in solar system.

### ***1.7 Noble gases in chondrites***

The noble gases extracted from a bulk primitive meteorite mainly represent mixtures of at least two or more noble gas components. For example, there exists noble gas components that were produced *in-situ* in the meteorite, in particular noble gases produced due to cosmic ray exposure (cosmogenic) and by decay of radioactive parents (radiogenic). All other noble gas components are called “trapped” components. These trapped noble gas components can be further subdivided into primordial and non-primordial components. Primordial components are the noble gas components directly inherited from the solar nebula, carried by certain phases. Noble gases were trapped in these carrier phases very early in the history of the solar system or even in the parent molecular cloud. Among these components, the two most prominent ones are the so-called **phase Q** and **HL (Presolar diamonds)**. Whereas non-primordial trapped component comprise noble gases implanted into the minerals. This implantation on minerals is possible mainly in two ways. For example, during the early stages of solar system evolution, **solar wind** from active sun can be implanted on grains freely floating into interplanetary space and/or much later on regolith of a parent body.

### ***1.8 Noble gases in chondrules***

In the context of chondrules, all these above-mentioned components of noble gases are expected. However, there is difference in abundances of trapped noble gases in chondrules compared to chondrites. Previous noble gas studies on chondrules suggested low to zero noble gas concentrations apart from cosmogenic gases (Smith et al., 1977, Swindle et al., 1991a, b; Miura and Nagao 1996, Nakamura et al., 1999, Okazaki et al., 2001b, Vogel et al., 2004) and radiogenic gases. The lower abundance of trapped noble gases in chondrules is generally attributed to extensive gas loss during melting of a more gas-rich precursor (Alexander 1989, Connolly et al., 2001, Kong and Ebihara 1997, Kong and Palme 1999, Scott and Taylor 1983).

The following sections contain a description of the most common noble gas components that might be present in unequilibrated chondrites and chondrules. In addition, possible sources of the noble gas components and/or their carrier phases are described.

**Table 1.4** Cosmogenic isotopic compositions and major target elements required for production of cosmogenic He, Ne and Ar.

Isotope	Cosmogenic isotopic composition	Major Targets
${}^3\text{He}_c$	$({}^4\text{He}/{}^3\text{He}) = 5.2 \pm 0.3$ <sup>1</sup>	O, Mg, Al, Si, Fe
${}^{21}\text{Ne}_c$	${}^{22}\text{Ne}/{}^{21}\text{Ne} = 1.05 - 1.25$ <sup>2</sup>	Mg, Al, Si, Ca, Fe
	${}^{20}\text{Ne}/{}^{21}\text{Ne} = 0.88 - 0.98$	
${}^{38}\text{Ar}_c$	${}^{36}\text{Ar}/{}^{38}\text{Ar} \sim 0.65$ <sup>2</sup>	Ca, Ti, Fe, Ni

1: Heymann (1967) 2: Wieler (2002)

## 1.9 In-situ produced noble gas components

### 1.9.1 Cosmogenic noble gases

Cosmogenic noble gases are produced by nuclear reactions by energetic particles from the galactic cosmic radiation (GCR) with meteoritic material. The mean attenuation length of GCR in solid material is  $\sim 150 \text{ g/cm}^2$ . This is in the “preatmospheric” size range of many meteorites, which means the size of an object, before it loses a large part of its mass due to the passage through the Earth’s atmosphere. Although many nuclides are formed by these reactions, effects are detectable only for those, whose original abundance in the target material is extremely low. For example, in many meteorites  ${}^3\text{He}$ ,  ${}^{21}\text{Ne}$ , and  ${}^{38}\text{Ar}$  are predominantly of cosmogenic origin. Some important cosmogenic ratios and their principal target elements are given in Table 1.4.

The production rate of a certain cosmogenic nuclide strongly depends on the chemistry of the target material. Ne is mainly produced from Mg, Al, and Si, whereas the main Ar-producing targets are Ca, Ti, Fe, and Ni (Leya et al., 2000). Helium is an exception, being produced in similar amounts from essentially all elements. Furthermore, the production rate depends on the shielding depth of a sample, which means the depth of a meteorite sample within the respective meteoroid. The unknown shielding depth can be estimated via the cosmogenic  ${}^{22}\text{Ne}/{}^{21}\text{Ne}$  or the  ${}^3\text{He}/{}^{21}\text{Ne}$  ratios (Wieler, 2002). With the help of the production rate and the absolute amount of cosmogenic nuclides in a meteorite sample, it is possible to estimate meteorite’s exposure age- the time span between the separation of a meteoroid from a parent body, where it was shielded from the GCR, and its arrival on Earth. Results of cosmogenic component of noble gases from this work are discussed in Chapter 3.

### **1.9.2 Importance of sample chemistry for chondrules**

The variation of abundances and ratios of cosmogenic noble gases in chondrules and chondrites depends on cosmic ray fluence (time x flux), composition of target chemistry and shielding depth. As far as shielding depth of chondrules is concerned, a uniform value can be taken as the suit of chondrules from each chondrite studied is separated from small bulk chondrite fragment of few grams. To identify the correct reason for the observed variation in a given cosmogenic noble gas abundance, hence knowledge of sample chemistry is important at least in case of individual chondrules.

### **1.9.3 Radiogenic and fissiogenic noble gases**

Radiogenic and fissiogenic noble gases are produced by the decay and fission of radionuclides, respectively. For example,  $^{235}\text{U}$ ,  $^{238}\text{U}$ , and  $^{232}\text{Th}$  are the main parent nuclides for radiogenic  $^4\text{He}$ , and  $^{40}\text{K}$  decays into  $^{40}\text{Ar}$ . The relatively short-lived, now extinct,  $^{129}\text{I}$  was an important source for  $^{129}\text{Xe}$  in meteorites. The heavy isotopes of Kr and Xe are produced by neutron-induced fission of  $^{235}\text{U}$  and by spontaneous fission of  $^{238}\text{U}$  and the extinct  $^{244}\text{Pu}$  (e.g., Swindle, 2002).

With the help of radiogenic nuclides the absolute gas-retention age or, in the case of the relatively short-lived nuclides, a relative chronology can be established. However, for this purpose, information about concentrations of the parent nuclides is essential. Results of  $^4\text{He}$ ,  $^{40}\text{Ar}$  and  $^{129}\text{Xe}$  from this work are discussed in Chapter 3.

## ***1.10 Trapped noble gas components***

### **1.10.1 Noble gases carried by phase Q**

Some typical isotopic and elemental ratios of trapped noble gas components are given in Table 1.5. Most of the heavy trapped noble gases (Ar, Kr, Xe) in unequilibrated chondrites, (in absence of solar implanted gases), reside in the carrier phase Q. The definition of phase Q is operational: It survives the treatment of a meteorite with hydrofluoric (HF) and hydrochloric acid (HCl) (only ~1% of a bulk chondrite survives this treatment) together with the bulk of noble gases. However, all noble gases carried by phase-Q are released essentially during subsequent oxidation with  $\text{HNO}_3$  (Lewis et al., 1975). The decrease in mass during the oxidation of the HF/HCl-residue with  $\text{HNO}_3$ , is however very small and variable (Busemann, 1998).

Although the carrier phase Q seems to have a minor mass only, the noble gas concentrations of phase Q are high (on the order of  $10^{-5} \text{ cm}^3\text{STP/g } ^{36}\text{Ar}$ ; see, e.g., Busemann et al., 2000). However, it has not been possible to define precisely the

nature of the carrier phase Q so far, though it seems established that Q is a carbonaceous phase (e.g., Ott et al., 1981). Based on carbonaceous nature of Q, Vogel et al. (2004) have suggested that phase Q got associated with metal phase during the chondrule formation event.

**Table 1.5** Ne and Ar isotopic and elemental compositions of phase Q, presolar diamonds (HL), and other reservoirs relevant in this thesis during discussion.

	$^{20}\text{Ne}/^{22}\text{Ne}$	$^{21}\text{Ne}/^{22}\text{Ne}$	$^{36}\text{Ar}/^{38}\text{Ar}$	$^{36}\text{Ar}/^{20}\text{Ne}$	References
Q	10.05(5)- 10.7(2)	0.0291(16)- 0.0294(10)	5.34(2)	14-84	Busemann et al., 2000
HL	8.50(6)	0.036(1)	4.41(6)	0.103(42)	Huss and Lewis, 1994
SW	13.8(1)	0.0328(5)	5.58(3)	~0.04	Benkert et al., 1993
Air	9.80(8) a)	0.0290(3) a)	5.32(1) b)	1.9 c)	a) Eberhardt et al., 1965, b) Nier 1950, c) Ozima and Podosek, 2002
GCR	0.70-0.93	0.80-0.95	0.65(3)		Wieler, 2002

It is further unclear whether the Q gases are of solar system origin (local) or presolar origin. Due to “normal” isotopic composition (could have been derived by mass fractionation of noble gases having a solar origin) Q-gases generally assumed are of local origin (Ott, 2002). The elemental composition of noble gases from phase Q shows a strong depletion of the light noble gases relative to the heavier ones as well as when compared to solar composition (Fig. 1.4). However, it is also possible that the carrier of phase Q obtained its noble gas inventory already in the parent molecular cloud or even earlier in the interstellar space (Huss and Alexander, 1987; Ott, 2002) and was injected into the solar system similar to the presolar diamonds (discussed next).

### 1.10.2 Noble gases in presolar diamonds

Diamond was the first presolar mineral identified in meteorites (Lewis et al., 1987). The light noble gas inventory of unequilibrated chondrites (free of SW-gases) is dominated by He and Ne from presolar diamonds. These have sizes of up to a few nanometers. On the basis of different average release temperatures during pyrolysis, three different sub-components within the diamonds (P3, HL, and P6) are identified. Huss and Lewis (1994) discussed these components in detail. According to these authors, the major component is the so-called HL-component with a wide range of release temperatures between 1100 and 1600 °C. He and Ne in this component are

correlated with smaller amounts of the heavier noble gases, of which Xe is the most important one. This Xe (known as Xe-HL) displays an exotic isotopic composition, which is characterized by the enrichment of the heavy ( $^{134,136}\text{Xe}$ ) and the light ( $^{124,126}\text{Xe}$ ) isotopes compared to the intermediate masses and the solar Xe isotopic composition. In contrast to a “normal”, solar-like isotopic composition, stellar nucleosynthesis processes are required to explain this exotic noble gas composition.

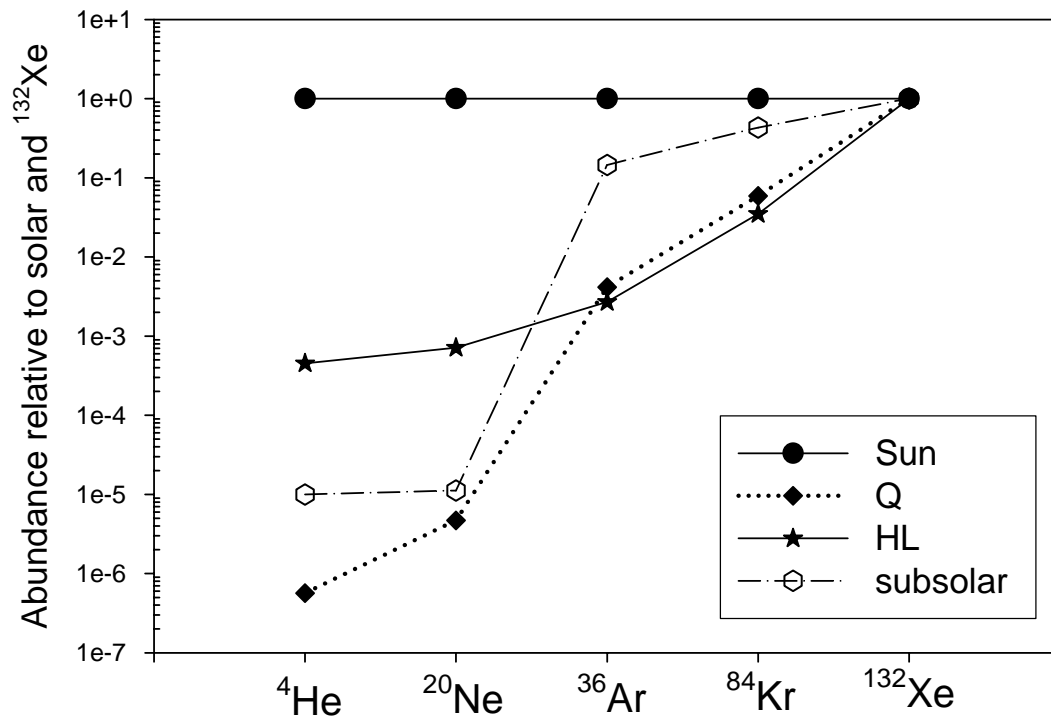


**Fig. 1.4** Elemental abundances of major primordial noble gas components relevant to this study in meteorites (Ott, 2002), normalized to abundances estimated for the Sun (Wieler, 2002). As clearly seen Q is the heavy noble gas (Ar, Kr, and Xe) carrier whereas HL is light noble gas (He, Ne) carrier.

In the case of Xe-HL, the light Xe isotopes are produced in p-, the heavy ones in r-process, whereas the intermediate masses show contributions from the s-process (see Ott (2002) for a comprehensive review). This possibly indicates a supernova origin of the HL component and thus a presolar origin of its carrier phase. Therefore, also the associated He and Ne isotopes (He-HL, Ne-HL) are suggested to be of presolar origin despite their rather normal isotopic compositions.

Furthermore, there exists the normal so-called P3 component, which releases its noble gases at lower temperatures (200-900 °C) than the HL-gases during pyrolysis. Therefore, P3 gases are already lost in chondrites, which had suffered mild thermal metamorphism. The so-called P6 noble gases, cannot be fully separated from the bulk

of HL gases during pyrolysis, therefore, also the P6 composition is somewhat uncertain. Huss and Lewis (1994) propose a roughly normal isotopic composition of the P6 noble gases. However, despite the (probably) normal noble gas isotopic composition of the P3 and P6 carrying diamonds, the authors suggest a presolar origin for both components. The large range of noble gas release temperatures of the different sub-groups of presolar diamonds points to the presence of different populations of diamonds probably with different physical properties (e.g., Ott, 2002).

### **1.10.3 Solar wind noble gases**

Solar wind (SW) noble gases are emitted from the chromosphere of the Sun. The particles have velocities between 300 - 800 km/s and are implanted into the outermost grain layers (several 10 nm (Mewaldt et al., 2001)) of material exposed to SW radiation, e.g. the fine-grained regolith surfaces of meteorite parent bodies or the moon.

SW noble gas implantation might also have been active in the very early history of the solar system, when infalling dust was directly exposed to SW radiation at the innermost part of the accretion disk (Okazaki et al., 2001a). Subsequent processing of this irradiated dust by heating or melting may have even produced specific meteorite noble gas components by mass fractionation of the SW noble gases, as, e.g., the subsolar noble gas component (as seen in Fig. 1.4, not discussed here).

## ***1.11 Nitrogen in Meteorites***

Although nitrogen is the sixth most abundant element in solar system and a key element in the terrestrial atmosphere and biosphere, we know surprisingly little about its cosmochemical behavior during the formation of solar system. Nitrogen isotope systematic for the early solar system is complex. The origin of the large range of nitrogen isotopic compositions in extraterrestrial samples is not well understood. Stony meteorites exhibit a range of bulk  $\delta^{15}\text{N}$  from  $-45$  to  $+860\%$  (Kung and Clayton, 1978; Grady and Pillinger, 1990), and Bencubbin, an unusual stony breccia, has a bulk  $\delta^{15}\text{N}$  of about  $1000\%$  (Prombo and Clayton, 1985; Franchi et al., 1986). Nitrogen measurements from iron meteorite range from  $-96$  to  $+156\%$ , with most of them having values more negative than  $-50\%$  (Prombo and Clayton, 1993; Franchi et al., 1993; Murty and Marti 1994; Mathew et al., 2000). The nitrogen isotopic composition of solar wind as measured in lunar soil samples appears to have undergone a secular change from  $-278\%$  (Carr et al., 1985) to  $150\%$  (Clayton and

Thiemens, 1980; Norris et al., 1983). The large heterogeneity in N-composition is not well understood. It is not established that whether there was once uniform primordial N-composition, which was later modified by chemical, physical, and nuclear processes or primordial inhomogeneities were dominant in determining the nitrogen isotopic compositions of solar system objects. The existing database for nitrogen isotopic measurements of chondrites, achondrites, iron meteorites and solar wind does not suggest a uniform ‘planetary’ nitrogen component analogous to the ‘planetary’ noble gases. In Fig. 1.5, range of N-composition observed in major chondrites is plotted against range of N abundances. The heterogeneity of nitrogen within chondrites is evident in this figure.

The most probable form of nitrogen in chondrites (and chondrules) is molecular

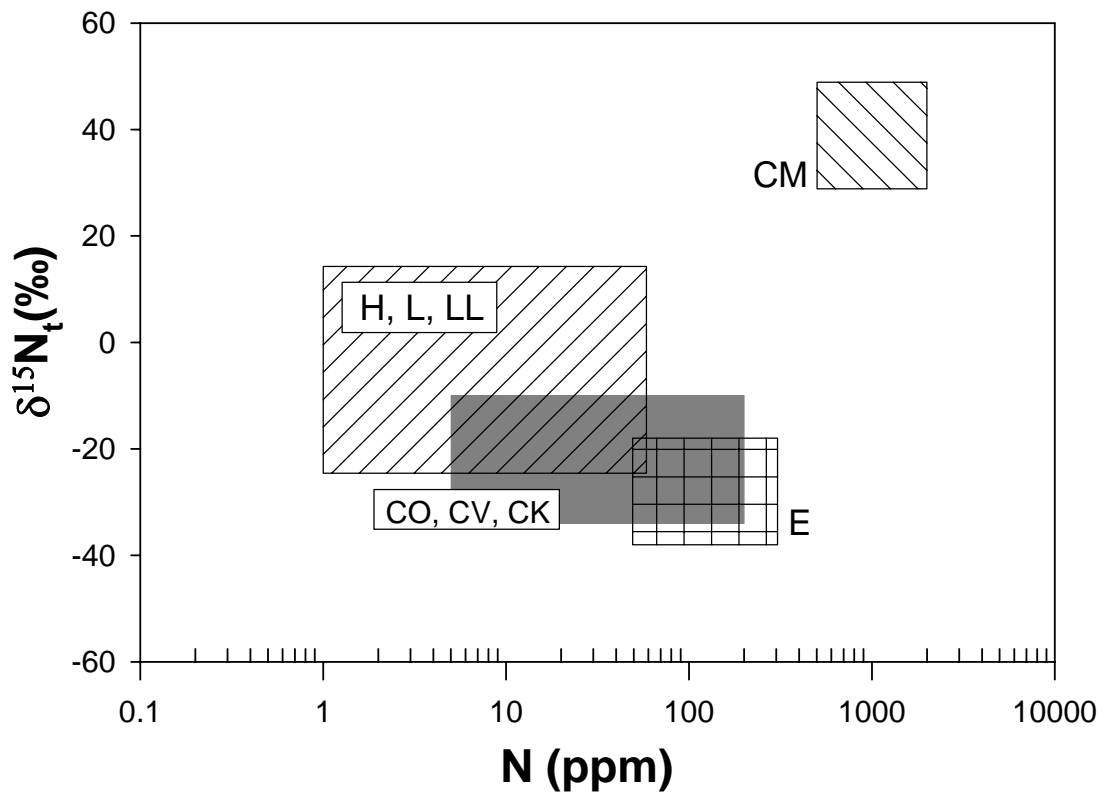


**Fig. 1.5** N-compositions of major chondrites plotted against N-abundances. Data are taken from Grady and Wright (2003). The ranges occupied by chondrites are different and show wide range of  $\delta^{15}\text{N}$ , suggesting heterogeneous N-compositions in a given chondrite class.

nitrogen. In this form, nitrogen behaves similar to noble gases. Often N has also been trapped by similar processes as noble gases. Due to similarity of nitrogen and noble gases on these aspects, it is logical to have accompanying nitrogen components with defined noble gas components. Here such components are discussed.

### 1.11.1 Nitrogen in Phase-Q

As discussed above in noble gases carried by phase-Q, Q gases are uniform in almost all the chondrites. It is logical to look for the nitrogen (and its composition), accompanying/carried by the Q component together with noble gases. Several attempts have been made to identify and characterize the nitrogen associated with phase Q. In case of Dhajala chondrite, the composition of nitrogen associated with Q noble gases is -15‰ (Murty, 1996). N-composition observed in phase Q is -50‰ in CO3 meteorites by Hashizume and Nakaoka (1998). Independent to this, a component in ureilites most similar to Q has a  $\delta^{15}\text{N}$  value of -21‰ (Rai et al., 2003). Based on these observations it is clear that N-composition of phase Q is not well constrained or it is possible that N-composition of phase Q may not be uniform. In this work,  $\delta^{15}\text{N} = -15‰$  is assumed however, considering the whole range of observed N-composition for phase Q is not affecting the final conclusions severely.

### 1.11.2 Nitrogen in presolar diamonds

Nitrogen is abundant in the presolar diamonds, with concentrations of up to 1.3 wt% (Russell et al., 1991). There is no evidence for any significant variation in the N-composition of the diamonds and  $\delta^{15}\text{N}$  in diamonds ranges from -330‰ to -350‰ (Lewis et al., 1987, Russell et al., 1996). This range is below the values observed in various types of meteorites (~ -100‰ to +200‰) but is close to the upper limit of < -240‰ for solar wind implanted into the lunar regolith, and to the N-composition of Jupiter ( $\delta^{15}\text{N} = -374‰$ , Owen et al., 2001), which is probably more representative for the solar system. The  $^{12}\text{C}/^{13}\text{C}$  ratio of 92-93 of bulk diamond in primitive meteorites (Lewis et al., 1987, 1989; Russell et al., 1991, 1996) is close to solar ratio of 89. The similarity of C- and N-isotopic signatures with solar compositions indicates that not all presolar diamonds originate from supernovae unlike noble gas indicators (especially Xe-HL). However, the observed large range in  $\delta^{15}\text{N}$  values for different materials generally accepted to form in solar nebula (meteorites, Jupiter, the Sun) makes it difficult to argue for solar origin of diamonds based on N-composition. On the other hand, recently Russell et al. (1996) inferred the  $^{12}\text{C}/^{13}\text{C}$  ratio possibly as high as 120 in the N-rich nanodiamond fraction does offer some support to the argument for a presolar origin for the N-rich nanodiamonds. In this work, -350‰ value is taken as the N-composition for the presolar diamond phase.

### 1.11.3 Nitrogen in Organic Material

Most of the Carbon in meteorites exists as organic material and probably contains no distinct noble gas components (Wieler et al., 2006). However, organic matter is most abundant nitrogen-bearing component in carbonaceous chondrites, which can account for up to 5 wt% of the meteorite. In carbonaceous chondrites, N-composition of organic matter ranges from +25‰ to +150‰ (Table 1, Sephton et al., 2003). According to Sephton et al. (2003), the organic material in carbonaceous chondrites can be divided into three components: (1) free organic matter (FOM), which is easily extractable from whole-rock meteorites and is enriched in  $^{13}\text{C}$  and  $^{15}\text{N}$ ; (2) labile organic matter (LOM), which has a macromolecular structure but is liberated by hydrous pyrolysis; LOM is the parent structure for some FOM and is also enriched in  $^{13}\text{C}$  and  $^{15}\text{N}$ ; and (3) refractory organic matter (ROM), which is also macromolecular but is virtually unaffected by hydrous pyrolysis and is relatively depleted in  $^{13}\text{C}$  and  $^{15}\text{N}$ .

There is a hypothesis that carbonaceous and enstatite chondrites inherited a common organic progenitor (Alexander et al., 1998). However as suggested by Sephton et al. (2003), reductive thermal metamorphism (resulted into graphitization of organic matter) incorporates and partially preserves free and labile organic matter with  $^{13}\text{C}$  enrichments and the associated  $^{15}\text{N}$  enrichments are lost at high levels of metamorphism. The composition of nitrogen in separated organic material from enstatite chondrites is found in range of bulk N-composition (-30‰ to -10‰, Grady and Wright (2003)) of enstatite chondrites by Sephton et al. (2003).

In case of unequilibrated ordinary chondrites inorganic species are present, equivalent to 700-4000 ppm carbon and 5-50 ppm nitrogen with ( $^{13}\text{C}$  of -20‰ to -10‰ and ( $^{15}\text{N}$  of -10‰ to +200‰. The most primitive of the UOCs have the heaviest compositions, and might have the highest complement of organic matter (Alexander et al., 1998).

On the origin of organic material in chondrites, there are mixed views. Traditionally organic matter considered as low temperature later condensate of the solar nebula (e.g. Hayatsu and Anders, 1981) while isotopic compositions (e.g. D/H ratio) contradict the solar origin theory for organic matter (Grady and Wright, 2003)

In case of chondrules, it is very unlikely to have physical presence of organic matter, as chondrules are the high temperature products. However, the presence of organic matter in chondrule precursors cannot be ignored. As suggested by Kong and Palme (1999) and references therein, during chondrule melting, organic matter was possibly

decomposed, dissolved into the metal and later released to form thin layers around the metal grains. In this scenario, as far as N is concerned, the loss of nitrogen during melting of organic matter is most probable; however, the N-composition should reflect presence of dissolved organic matter in metal. C content of this organic matter released on decomposition is expected to play a role of reducing agent during chondrule formation. The results of Connolly et al. (1994) and Hannon et al. (1998) demand for higher C/O ratio in the chondrule forming region to yield type-I chondrules by reduction process. It is possible that the decomposition of organic matter from the precursors of chondrules provided high C/O ratio locally.

### ***1.12 Objective of the present study***

By using isotopic composition of nitrogen and noble gases as a tool, the information about the precursors of chondrules, the environment(s) and process(es) of chondrule formation can be extracted which can further provide important clues in understanding chondrules. The major objective behind this study is discussed in this section in detail.

***Precursors of chondrules:*** To understand the effect of chondrule formation process(es), it is necessary to know about the precursors of the chondrules. Isotopic compositions of both oxygen ( $\Delta^{17}\text{O}$ ) and nitrogen ( $\delta^{15}\text{N}$ ) show distinct values for each class of chondrites (Clayton 1993; Grady et al., 2002) and have been attributed to differences in their formation location. As discussed earlier in this chapter, oxygen isotopic composition of chondrules has provided important clues to chondrule precursors. In this study of N-compositions ( $\delta^{15}\text{N}$ ) in chondrules from three major groups, the objectives are (1) a comparison between chondrules and their host chondrites as well as among the chondrules from different chondrite classes (2) trend according to chondrite group (3) identification of various phases in chondrules (or in chondrule precursors).

***Environment of chondrule formation:*** Various trapped noble gas elemental and isotopic ratios are the best indicator of different environments and phases, which were present in chondrule precursors. This work is aimed to look for evidences related to chondrule forming environment (e.g. whether chondrules formed near to young sun) and presence of various phases in chondrule precursors (e.g. presolar diamonds and phase Q). Additionally, as molecular N behaves similar to Ar in adsorption, solubility, diffusion etc, analyses of nitrogen and noble gases together in chondrules, therefore

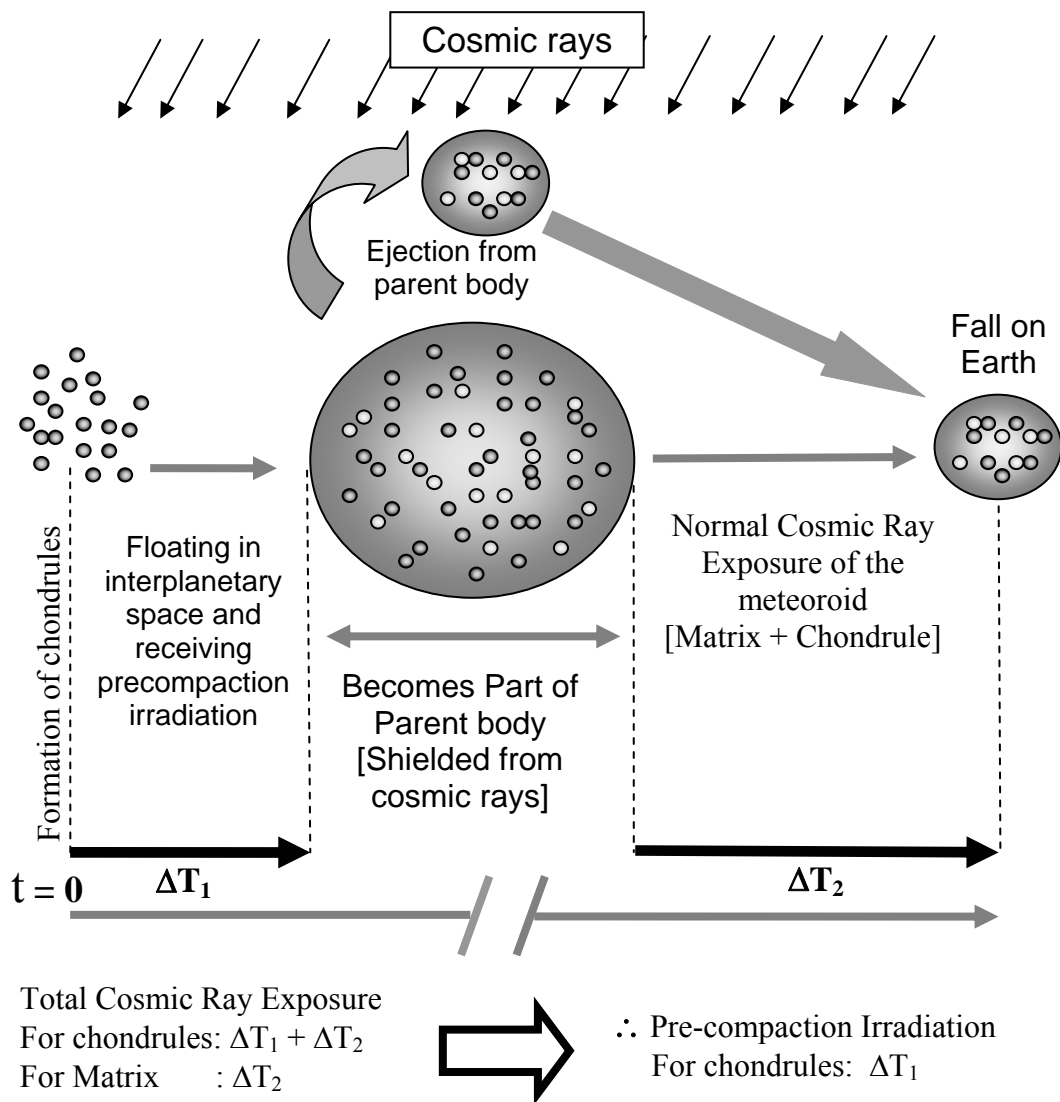


**Fig. 1.6** Schematic to explain precompaction cosmic ray exposure of chondrules

provides a better approach to look for specific chemical processes (like metal silicate fractionation) and components (like trapping of solar gases during chondrule formation) in chondrules.

***Pre-compaction irradiation of chondrules:*** It is expected that chondrules preserve pre-compaction irradiation records (for example, excess of cosmogenic noble gases compared to parent chondrite), which can be visualized, in favorable cases (chondrites with exposure ages  $< 2$  Ma). In this work, we have looked for such excess in chondrules compared to their host chondrites. Fig. 1.6 depicts the schematic to explain the possibility of precompaction exposure in chondrules. Based on short-lived radionuclides the chondrule formation duration is constrained up to 2 Ma. If chondrules are nebular products, it is expected that some chondrules were freely

floating in the space before accreting with fine-grained material to form chondritic parent bodies.

As shown in Fig. 1.6, if chondrule formation time is taken as initial time then maximum up to  $\Delta T_1$  time chondrules were freely floating. During this time, their exposure to cosmic rays (both solar as well as galactic cosmic rays) is expected. Once chondrule became part of larger bodies, they get shielded from cosmic rays. Later an impact event on this parent body ejects the small fragment to interplanetary space. This fragment of parent body receives second stage of cosmic ray exposure (for time  $\Delta T_2$ ) until it reaches earth as meteorite. Hence, the exposure age of bulk meteorite is  $\Delta T_2$  whereas as chondrules should show exposure age  $\Delta T_1 + \Delta T_2$  compared to bulk. The time  $\Delta T_1$  can be defined as precompaction exposure duration of chondrules. As mentioned, earlier this time can be maximum up to  $\sim 2$  Ma based on constraint provided by short-lived nuclides. To detect this low duration, chondrites with lower cosmic ray exposure ages (low  $\Delta T_2$ ) are the suitable samples. In present study, chondrites like Dhajala, Bjurböle and Allende have exposure ages less than  $\sim 8$  Ma.

***Effect of chondrule formation process on noble gas and nitrogen composition:***

Noble gases and nitrogen are highly volatile elements. The volatiles in chondrules play an important role to understand the effect of chondrule formation process(es) and further useful to constrain the formation process itself. They have major implications related with Type-I and Type-II chondrules. The evolution of  $\delta^{15}\text{N}$  and various noble gas compositions in chondrules with respect to the chondrule forming process (effect registered independently in FeO content of chondrules) is one of the objectives.

***1.13 Earlier studies of noble gases and nitrogen related to present work***

**1.13.1 Noble gas studies on chondrules**

There are several studies on noble gases in chondrules (Fredriksson et al., 1985; Kim and Marti 1994; Miura and Nagao 1996; Nakamura et al., 1999; Okazaki et al. 2001a; Smith et al., 1977, Swindle et al., 1991a,b; Polnau et al., 1999, 2001; Whitby et al., 2002 etc). These works are mainly comparisons of trapped, cosmogenic and radiogenic noble gases in chondrules with respective bulk chondrites and/or other components of chondrites like matrix material. Most of these studies are done on an ensemble of chondrules or on individual chondrules for dating.

### ***Studies of trapped noble gases in chondrules:***

Previous study on trapped noble gases in chondrules has revealed low to zero noble gas concentrations compared to matrix and bulk chondrites (Smith et al. 1977; Swindle et al. 1991 a, b; Kim and Marti 1994; Miura and Nagao 1996; Nakamura et al. 1999; Okazaki et al. 2001b; Vogel et al., 2004 etc) generally attributed to extensive loss during chondrule formation event. However, recently Okazaki et al. (2001b) reported high noble gas concentrations (e.g. up to  $7 \times 10^{-6} \text{ cm}^3\text{STP/g } ^{36}\text{Ar}$ ) in chondrules of the enstatite chondrite Yamato (Y)-791790. Matrix surrounding these chondrules is found with lower gas concentrations. These authors explain this higher concentration observed mainly in porphyritic chondrules based on irradiation of solar wind (SW) noble gases from the young sun on chondrule precursors as predicted by X-wind model, whereas another recent work of Vogel et al. (2004) found absence of any solar type noble gases and observed very small amount of trapped  $^{36}\text{Ar}$ . Compared to chondrules they found higher concentration of trapped  $^{36}\text{Ar}$  in metal/metal sulfide coating of chondrules. They proposed that during metal-silicate fractionation in the course of chondrule formation, the Ar-carrying phase Q became enriched in the metal-sulfide-rich chondrule coatings and in the silicate rich chondrule interior, only the most stable Ne-carrying presolar diamonds survived the melting event. Based on earlier studies it is clear that trapped noble gases are present in chondrules and these gases are contributed by various noble gas components like Q, presolar diamond (HL) and solar wind.

### ***Cosmogenic noble gas studies on chondrules:***

A Few studies have been done related to precompaction irradiation of individual chondrules, based on cosmogenic noble gases and nuclear track study (Allen et al., 1980; Pellas et al., 1969; Polnau et al., 1999, 2001). Polnau et al. (1999) found excess cosmogenic noble gases ( $^3\text{He}$ ,  $^{21}\text{Ne}$  and  $^{38}\text{Ar}$ ) in a chondrule from the H6 chondrite ALH76008. This excess translates into a precompaction exposure time of 0.90 Ma. More recently, work on chondrule and matrix samples of eight ordinary chondrites shows larger concentrations of cosmogenic noble gases compared to matrix (Polnau et al., 2001). They concluded that differences in exposure ages are due to different precompaction exposures of chondrules, or components thereof, before final assembly of the meteorite. These evidences of precompaction exposure supported the formation of chondrules in solar nebula as well as suggest that precursors of chondrules were exposed to either galactic or solar cosmic rays.

### ***Radiogenic noble gas studies in chondrules:***

Few radiogenic noble gas studies have been attempted on chondrules, which are mainly for I-Xe ages for chondrules from carbonaceous, low-petrologic type ordinary chondrites and enstatite chondrites (Nichols et al., 1990; Swindle et al., 1991a, b; Whitby et al., 2002). The study on enstatite chondrites by Whitby et al., (2002) (their study on chondrules and interchondrule matrix from Qingzhen (EH3) and Kota Kota (EH3)) suggests that the timing of chondrule-forming episode brackets the I-Xe closure age of planetesimal bodies such as the Shallowater aubrite parent body. This evidence related to existence of planetesimals at the time of chondrule formation provides important constraints to chondrule formation models especially for the case of chondrules from enstatite chondrites.

#### **1.13.2 Nitrogen studies on chondrules**

Studies of nitrogen on chondrules are very scarce and this thesis is the first major attempt to look into details of the N-composition of individual chondrules from major chondrite groups. The first nitrogen study was on bunch of five chondrules of Soko Banja (LL4) by Kung and Clayton (1978). The N composition (uncorrected for cosmogenic contribution) for these chondrules was 11‰ compared to 7‰ observed for bulk chondrite. Other previous nitrogen studies on individual chondrules of Bjurböle (L4) and Dhajala (H3.8) suggested that chondrules are depleted in heavier isotope of nitrogen compared to their bulk chondrites (Fredriksson et al., 1985). Authors explained this on the basis of mixing between silicate phases (carriers of light nitrogen whose isotope signature may overlap with values of enstatite chondrites) and some sulfide-rich phases (enriched in heavy nitrogen whose isotope signature may be similar to the respective chondrite matrix) in chondrules. This study suggests that various phases in chondrules (with distinct N-composition) can affect the nitrogen compositions of bulk chondrules. In addition to this, the heterogeneity in N-composition is evident in this limited study. Recent study of Mahajan and Murty (2003) on chondrules of Dhajala chondrite suggests that chondrules are different compared to bulk chondrite. Based on these limited number of studies related to nitrogen in chondrules it can be inferred that the study can be used to understand the various phases involved in chondrule (as well as chondrule precursors) and effect of chondrule forming event on them.

## Chapter 2

# Experimental details

## ***2.1 Introduction***

In this chapter, the sample selection criteria, separation and characterization of individual chondrules are first discussed. Then detailed procedures and the laser probe set up for the nitrogen and noble gas measurements are described. The chapter can be divided into three sections as follows.

- ✓ Selection of chondrites
- ✓ Separation of chondrules from chondrites
- ✓ Procedure for Nitrogen and noble gases analyses of chondrules & chondrites
- ✓ Chemical characterization of chondrules

## ***2.2 Selection of chondrites***

Prime objective of this work is to understand the processes related to chondrule formation by the help of trapped nitrogen and noble gas compositions in chondrules and their host chondrites. Chondrites have experienced secondary processes such as thermal, shock metamorphism, and aqueous activity mainly on parent bodies. These secondary processes are expected to reset composition of chondrites eventually erasing (or altering) signatures of primary events experienced by them. Few chondrites groups contain members that have escaped thermal metamorphism. These are the petrographic type 3 H, L, LL, EH, CO and CV chondrites, the CM chondrites (type 2) and the CI chondrites (type 1). In turn, these groups contain members that are not heavily altered by shock. Aqueous activity has extensively affected all the CI and CM chondrites and may have affected (to a much smaller degree) some type-3 ordinary, CV and EH chondrites. Therefore, chondrites that have not undergone extensive changes by these processes are ideal samples for studies related to early stages of nebular history. For this work, we have selected mainly type 3 and 4 chondrites which are less affected by secondary processes.

Low cosmic ray exposure age was another criterion for the selection of chondrites. Maximum pre-compaction irradiation time for chondrules can be of the order of 1Ma. Based on short-lived radionuclides, 1 to 2 Ma time is suggested for chondrule formation duration (Mostefaoui et al., 2002). The excess of cosmogenic noble gases in chondrules, compared to host chondrites, is very low for this duration. To detect pre-compaction duration of this order, chondrules from low cosmic ray exposure age chondrites will be most suitable. The other criterion was the ease of chondrule separation. Also, chondrule > 1 mg size are preferred as a spilt from chondrule can be

used for chemical characterization while the other split is used for nitrogen and noble gas studies. Hence, chondrites of type 3/4, hosting larger chondrules which could be isolated with relative ease (like Dhajala, Bjurbole, Chainpur, Saratov, Parsa and Allende) were preferred for this study.

Based on these criteria six ordinary chondrites, two enstatite chondrites and two carbonaceous chondrites were selected for this work. All the samples were available from PRL meteorite collection. Details of these samples are given in Table 2.1.

### 2.3 Separation of chondrules

Chondrules are cemented into the matrix material of chondrites. Sometimes, separation of chondrules is easy when matrix material is not so hard like in case of Dhajala, Bjurbole, Allende and Parsa chondrites. For these meteorites by gently crushing in an agate mortar, chondrules can be dislodged from matrix. However, in case of nearly unbreakable matrix, easy disaggregation of material is difficult. Breaking of these tough chondrites also reduces chance to get complete chondrules. In such cases, the technique of freeze-thaw is used for better chondrule separation process. A small system, for performing freeze-thaw on chondrites with hard matrix is fabricated (schematic is given in Fig. 2.1).

A small system is made for the freeze-thaw cycling of the sample in double distilled water. To ensure that the oxygen from dissolved air does not react with sample water, the water has been degassed

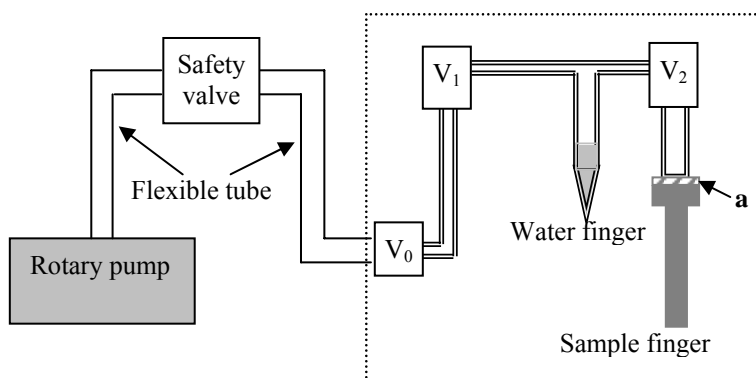


**Fig. 2.1** Schematic for freeze-thaw method used for chondrule separation. Double-lined volume is made up of glass.  $V_0$ ,  $V_1$  and  $V_2$  are valves. Water can be introduced from point 'a' connecting sample finger with glass system through Teflon gasket.

thoroughly by cycling through freezing – pumping - thawing – freezing – pumping , several times. This is followed by loading sample (by attaching sample finger at point 'a', Fig. 2.1). After evacuating sample finger, the degassed water then introduced onto the sample under vacuum and taken through several cycles of freeze – thaw and ultrasonication cycles. After about 200 cycles the sample disintegrated. Chondrules

are then picked from the disintegrated sample, decanting the water and washing with alcohol.

This process is performed under vacuum as it reduces the possible alteration of samples in presence of air by water as well as enhances entry of water inside the micro-cracks of the sample. Once water gets inside micro cracks the process of freezing (by using liquid nitrogen) and thawing (boiling water) from outside of the sample finger can be repeated alternatively. The repeated freezing and thawing expands the cracks, which can finally lead to complete disintegration of sample. Depending on the hardness of samples, 100 to 200 steps of freeze-thaw are adequate for the complete breakup of the sample. Chondrules then are separated from disintegrated chondrites under the microscope. Generally, few minutes of ultrasonication is sufficient for the removal of any adherent matrix material on individual chondrule. In extreme cases, this material is removed by either scratching or by using dentist's tools. After careful inspection and documentations with the help of microscope, chondrules have been selected for the analysis.

**Table 2.1** Chondrites analyzed from different groups of chondrites, number of chondrules analyzed and chemically characterized in this work.

Samples	Chondrules Analysed	Chemically characterized
<b>Ordinary chondrite</b>		
Dhajala (H3.8)	21	5
Udaipur (H3)	3	-
Tieschitz (H3.6)	5	1
Saratov (L4)	5	2
Chainpur (LL3.4)	4	3
Bjurböle (L/LL4)	9	5
<b>Enstatite chondrite</b>		
Qingzhen (EH3)	5	1
Parsa (EH3)	4	3
<b>Carbonaceous chondrite</b>		
Allende (CV3.2)	16	7
Murray (CM2)	4	1
<b>Total</b>	<b>76</b>	<b>28</b>

**Documentation of chondrules:** Documentation of chondrules is the important task before finalizing chondrules for the analyses. Digital camera attached with microscope, is used for the photographic documentation of chondrules. Weights of individual chondrules are measured by using Sartorius microbalance (model no: MC-5; Germany). For chondrules > 1 mg, splits were taken for the chemical, mineralogical and petrologic characterizations. Electron Probe Micro Analysis (EPMA) method is used for the chemical characterization of these chondrule splits. Details of chemical characterization as well as description of each chondrule are given in section 2.7. With a hand magnet, each chondrule has been checked to determine, whether it is magnetic or otherwise.

#### **2.4 The VG Micromass 1200**

VG Micromass 1200 is a noble gas mass spectrometer from the Vacuum Generators Ltd. U.K. Sensitivity of this mass spectrometer allows measurement of small amount of noble gases. The operating resolution is 170. Like all mass spectrometers, the operation involves ionization of gases, then acceleration of ions and finally analyses of the ions according to their mass to charge ratio. Nier type ion source with a source magnet is used to increase the ionization efficiency. Usually, a trap current of 100 $\mu$ A is employed to control electron beam for ionization. The ionized species are accelerated by electrostatic potential of 4 KV. The VG Micromass 1200 is a magnetic deflection mass spectrometer with 60<sup>0</sup> electromagnetic sector that acts as a mass analyzer. By varying the magnetic field, different mass to charge signals are measured. The mass spectrometer is having Faraday cup and electron multiplier for the detection of wide range of signals varying more than six orders of magnitude. Ultra High Vacuum (UHV)  $\sim 10^{-9}$  torr is maintained inside the mass spectrometer by the help of ion pump connected by UHV valves. The mass spectrometer is also equipped with SAES<sup>TM</sup> getter useful to keep hydrogen background at low. This getter also helps in maintaining low background of hydrocarbons. During the analysis of nitrogen, this getter has to be isolated from mass spectrometer as this getter also acts as a chemical getter for nitrogen. For the degassing (after exposure to air), the entire mass spectrometer is covered by an oven, which can reach up to 300<sup>0</sup>C.

#### **2.5 Gas extraction units**

This work is dealing with two types of samples like chondrules whose masses are small (0.5 - 3 mg) and their respective bulk chondrite, which are relatively large ( $\geq$

50 mg). Hence, for bulk chondrite samples, traditional glass system with RF heater (for gas extraction) is used for analyses. In case of chondrule samples, as the expected amount of gas release is very small, a specially designed metal system with Laser (for gas extraction from microscopic samples) collectively called *Laser microprobe* is used. Except two different extraction systems, all other procedures for the analyses of nitrogen and noble gases are same for chondrules and bulk chondrites. The following sections describe (a) Laser microprobe (b) The glass extraction system

### **2.5.1 Laser microprobe (used for chondrule analyses)**

Laser microprobe is the assigned name to a system, which is specially designed at Physical Research Laboratory (PRL) for the simultaneous analysis of nitrogen and noble gases especially in submicroscopic samples on VG-1200 mass spectrometer (above discussed). The schematic of this set up is given in Fig. 2.2. Nd-YAG Laser is used for the melting of tiny samples. During the measurement of small amount of gases, keeping low background of gases is mandatory. The cleanup and separation system is made of stainless steel to achieve very low background. In this section, this specially designed laser microprobe system is discussed.

#### **2.5.1.1 Nd-YAG Laser:**

The laser used in this study is an Nd: YAG (Neodymium: Yttrium Aluminium Garnet) laser (Model SL900GT, Spectron Laser Systems, U. K.). This laser can be operated in continuous wave (CW) as well as pulse (Q-switched) mode. In CW mode fundamental wavelength is 1064 nm. The maximum output at this wavelength is 16W and the divergence of the output beam is 1.8 milliradian. In the pulsed mode, the average output power is 8W. The laser can also be operated at second harmonic, and has an average output power of 3W at 532 nm, operated at the pulsed mode. The pulse width of the Q-switched laser output is 120 ns. The operation of laser in the CW mode is of use for uniform heating of a grain while in the pulsed mode operation laser can be used for selective melting of any part of the sample by dumping energy in short pulses. For individual chondrule analyses, the laser is used in CW mode.

A He-Ne laser is also given with the main laser assembly. The output of the He-Ne laser is directed through two mirrors in such a way that it will travel the same path as followed by both the fundamental and second harmonic outputs of the main laser. The output of the main laser (~ 16W in CW mode) is high, forbidding the use of main laser for adjusting the sample under the focusing spot, as this process can preheat the sample and can result in partial gas loss from the sample. In contrast, the output

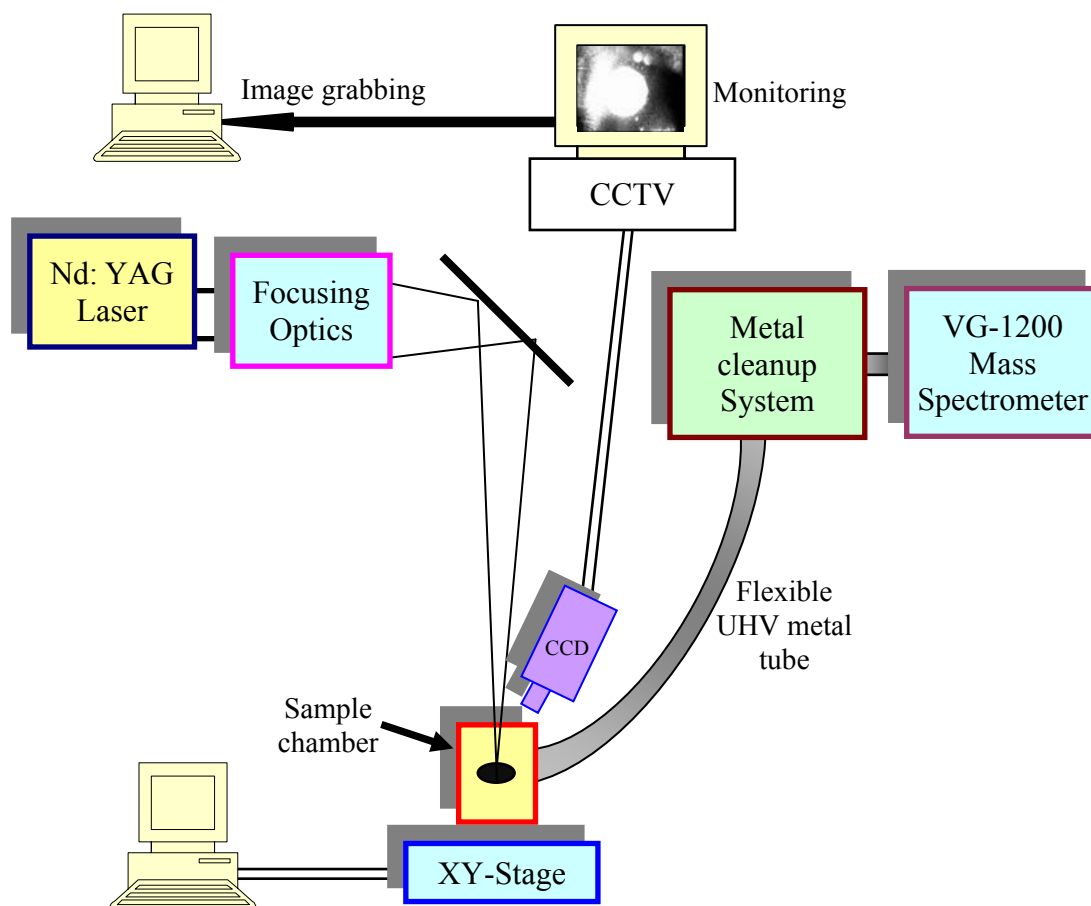


**Fig. 2.2** Schematic of the Laser Microprobe Setup

power of the He-Ne laser is only 2 mW and its wavelength [632.8 nm] is in the visible (red) region, making it a good tool for focusing the laser beam on to the sample. Furthermore, He-Ne laser can be used for optical alignment of the different components of the laser system, some of which have to be changed for switching the laser output from fundamental to second harmonic. Collimation is one of the important operations, essential for getting parallel size of output laser beam. A telescope is used for collimating the laser beam. The collimated laser beam is focused to a small spot by the help of convex lens. Characterization of the laser output power as a function of the input current has been done periodically with the help of power meter. Moreover, measurement of laser power was mandatory before flashing the laser to samples. Normally it was observed that for continuous wave [CW] mode at 1064 nm, at a lamp current of 16.5 A, the laser output power is 15 W. The lamp current can be varied from 11 A to 18 A, so a desired power output can be set for a particular irradiation step. For the individual chondrule, mostly three steps of laser irradiations were performed (details of the extraction steps are given in section 2.6.1).

### **2.5.1.2 XY stage:**

The sample chamber is mounted on XY stage. The movement of XY stage can be programmed and precisely controlled by computer. This mechanism is useful to set the individual samples mounted on Cu-plate in sample chamber under the laser beam. For this the laser beam, kept on at fixed position and by controlled movement of XY stage, the desired sample is set under the beam. Additionally this XY stage is fixed on a platform that allows fine vertical movement. This vertical movement can be used for the focusing/defocusing of laser beam. For this work, defocused beam is used to cover the total sample size by the laser beam.

### **2.5.1.3 Sample chamber:**

The sample chamber consists of three different parts made from stainless steel (SS-316) (Fig. 2.3a and 2.3b). The top flange is specially made with optical quartz window. A laser beam can be focused on the samples through this window. This top flange is fixed on the double-sided flange (middle flange). The other side of the double-sided flange is fixed with the bottom flange, which can be fixed on X-Y stage. The double-sided flange has an arrangement to connect with flexible UHV stainless steel tube leading to cleanup and separation system. Sample holder made of copper with thickness of 3 mm is fixed on bottom flange. As copper is good conductor of heat, it conducts away heat faster than spot heating and hence releases very low gases during the sample irradiation, which helps in achieving low blank. Blind pinholes of required size (1 to 3 mm) and depth (1 to 2 mm) are drilled on this sample holder to keep the individual chondrule samples. During laser irradiation, the sample gets vaporized. To avoid this vapour deposition on quartz optical window (which affects the transmission characteristics of laser radiation through it) an arrangement of quartz cover glass has been made over the samples in the chamber. Quartz cover slip is fixed in such a way that it can be maneuvered with an external magnet and positioned above the particular sample to be heated.

### **2.5.1.4 CCD camera**

Monochrome Charged-Coupled Device (CCD) is used for the online monitoring of the sample for recording the processes before, during and after the laser irradiation on the chondrule samples. CCD camera is also coupled to a zoom lens (Leica monozoom 7) to get magnified image on the tiny samples. A CCTV (monochromatic display unit) and a computer are used for online monitoring as well as image grabbing as part of the documentation.

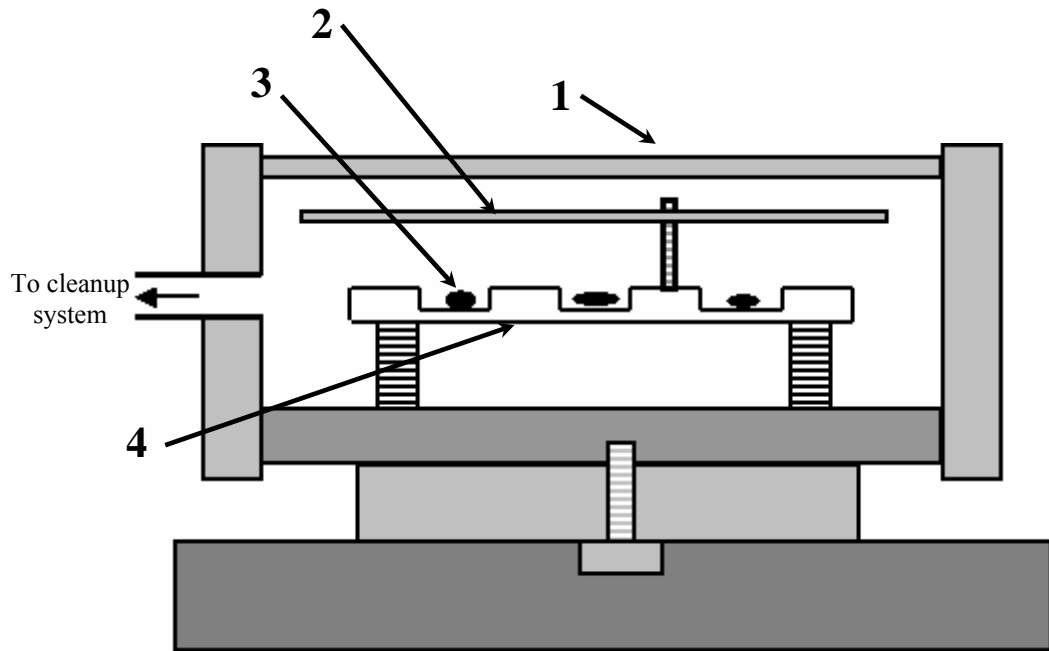


**Fig. 2.3a** Schematic of the sample chamber. (1) Optical window (2) Cover slip (3) Sample (4) Sample holder (made of Cu)

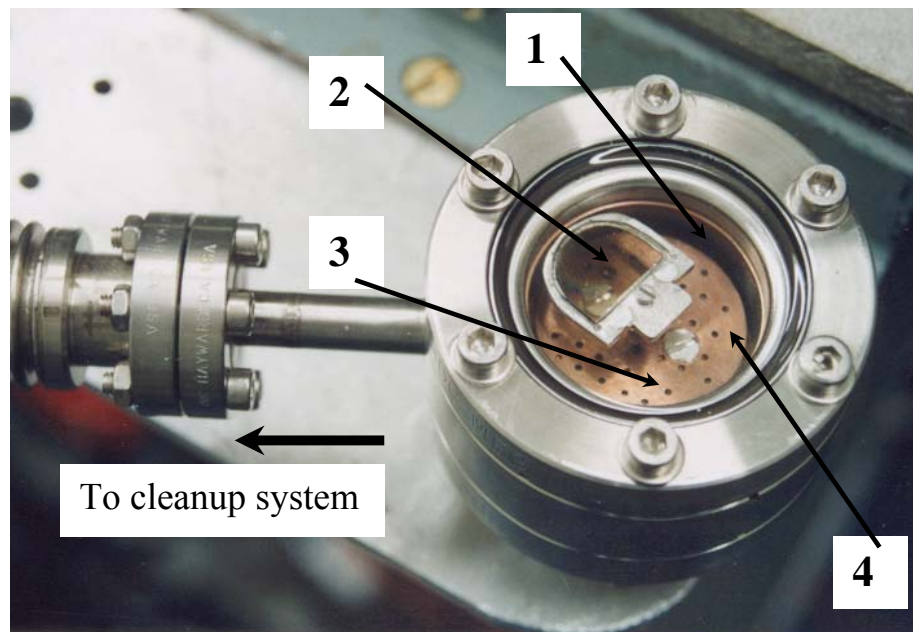


**Fig. 2.3b** Actual photograph of the sample chamber connected to cleanup system through flexible UHV metal tubes. Numbers are carrying same name as mentioned above.

### 2.5.1.5 Metal cleanup and separation system

Very low background is essential for the analysis of small amount of sample gases. A specially designed all metal UHV system has been used for the cleaning and separation of extracted gases from chondrules. The schematic of the metal cleanup system is shown in Fig 2.4. Special care was taken to keep the total volume of this system small to achieve the lowest possible blanks. The salient features of the

extraction system are the following: All metal configurations are used to obtain very low blanks especially for He and Ne. During the initial phases of assessing the performance of the extraction, system (made by all metal) it was realized that the system does not give low and reproducible blanks for nitrogen, although no such problem existed for noble gases. This could be due to some metal surfaces in the UHV system serving as active sites for N<sub>2</sub> to be chemisorbed. To avoid prolonged exposure of N<sub>2</sub> released from the sample to metal surfaces of the extraction system, a separate branch line made of pyrex<sup>TM</sup> glass is introduced for nitrogen processing. The glass line has been integrated in the metal cleanup system in such a way that, after irradiation of sample by the laser, a fraction of the total extracted gas is isolated into the glass line within a minute for the nitrogen analysis, while the rest of the gas is processed for noble gases in the metal system. The whole system can be covered and baked to 300°C to achieve UHV and very low blanks. We employ a turbo molecular pump backed by diaphragm pump to obtain hydrocarbon free UHV of 10<sup>-9</sup> torr and an ion pump to maintain the UHV conditions during sample analysis. Stainless steel mesh (SSM) is used for adsorption of noble gases and nitrogen. SSM can be degassed up to 700°C thereby obtaining ultra clean conditions, without affecting its adsorption/desorption characteristics.

The different components of the cleanup system are two SSM fingers, two charcoal fingers, two CuO fingers, two cold fingers, one Ti-sponge getter finger, and one Ti-Zr getter finger.

The SSM is used for collecting noble gases [Ar, Kr, and Xe] and Nitrogen by cooling it to liquid nitrogen temperature (LNT). The adsorbed gases on SSM can be desorbed, by heating the finger up to 150°C. The second SSM finger (near the Mass Spectrometer) is used to collect the sample gas; these gases can further be introduced into the mass spectrometer. The cold finger is used to trap the unwanted and condensable gases (H<sub>2</sub>O, CO<sub>2</sub> etc.) at LNT. The charcoal is used for collecting the noble gases as well as for their separation [into Ar, Kr, and Xe]. Usually the noble gas amounts (specially Xe & Kr) remain very small in chondrules so separation of noble gases is not performed. A Ti-Zr getter is used to remove all the chemically reactive gases. CuO- finger is used to generate oxygen in the cleanup system at desired pressure. Oxygen is needed to oxidize the hydrocarbons etc. into condensable gases, which can then be removed from the gas (nitrogen fraction) by using the cold trap. The condensable gases can further be removed using either Ti-Zr or Ti-sponge getter.

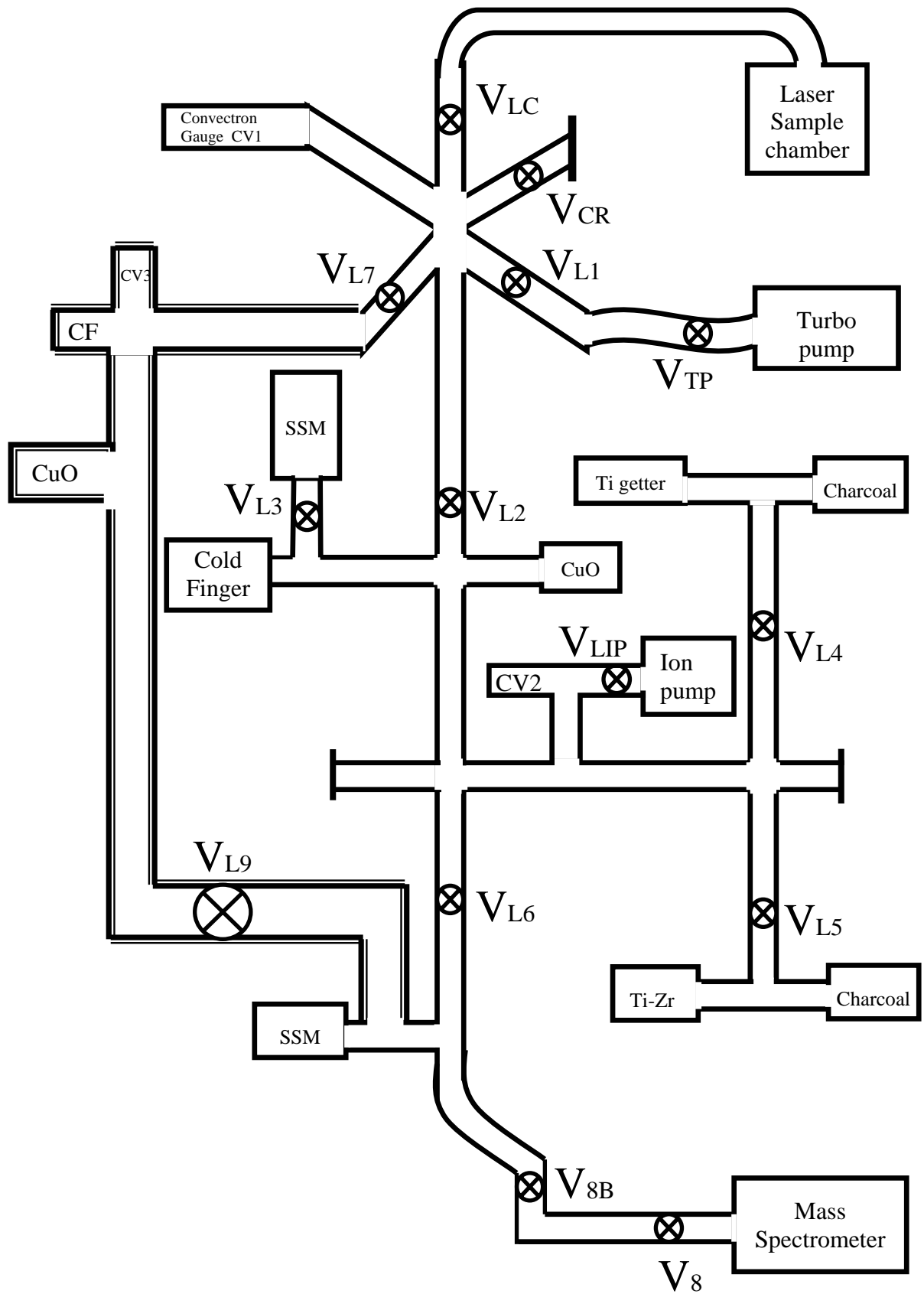


**Fig. 2.4** Schematic diagram of the metal line

The CuO setup in separate glass-line (for Nitrogen fraction) is used for cleaning of nitrogen. This cleaning was mandatory for every step of chondrule analysis. Three pressure gauges (convectron by GP<sup>TM</sup>) are connected to the cleanup system to monitor the vacuum level, as well as to measure the pressure generated by the extracted gases from the sample and the pressure of oxygen generated from the CuO. The protocol to use this metal separation and cleanup system for released gases from chondrules are discussed in section 2.6.3.

### **2.5.2 The glass extraction system (used for bulk chondrite analysis) for large samples**

The mass spectrometer is attached to a gas extraction system through a UHV valve. This system, suitable for separation and cleaning of nitrogen and noble gases extracted from samples for the mass spectrometry, has been fabricated at PRL using commercially available UHV components. Though nitrogen (N<sub>2</sub>) behaves like the noble gases under normal conditions of temperature and pressure, in ultra high vacuum, the clean surfaces of certain metals are active to getter nitrogen (Fast, 1965). Stainless steel, aluminum, copper oxide (CuO), molybdenum (Mo), tungsten (W), nickel (Ni) at room temperature are inert to nitrogen, while titanium (Ti), titanium zirconium (Ti-Zr) alloy, titanium-palladium (Ti-Pd) alloy, SAES getter, some forms of charcoal and hot Ni are some of the materials which scavenge nitrogen very fast. These aspects have been well considered while fabricating the extraction system. Proper isolation valves have been incorporated in the line by which the materials that act as a getter for nitrogen can be isolated from the extraction system while nitrogen is being processed. Fig.2.5 is a schematic diagram of the extraction system. It essentially consists of three parts (excluding the pumps and pressure measuring devices).

1. Gas extraction unit.
2. A standard gas reservoir (Air standard reservoir) that provides standard sample for calibration. This is a reservoir containing standard air, which is connected to the main line through a pipette valve (V11 and V12, *see* Fig. 2.5). Known volumes of the air - standard are pipetted for calibration purposes.
3. The main line used for purification and separation of the gases.

Following is a brief description of these sub units.

#### **2.5.2.1 The gas extraction unit**

It consists of a combustion finger and an extraction bottle for the extraction of gases from solid samples. The extraction unit is connected to an online sample tree where the



samples are kept prior to their gas extraction. For gas extraction the samples are manoeuvred from the sample -tree into the combustion finger and/or the extraction bottle by an external hand magnet and nickel pieces (which are loaded into the sample tree along with the samples).

### 2.5.2.2 Combustion Finger

The extraction system is attached to a double-walled (vacuum jacketed) quartz finger that can be heated up to 1075 °C (the safe limit without collapsing the quartz) by means of an external resistance heater. The outer vacuum line of this finger is connected to the diffusion pump. Sample is introduced into this finger by a quartz boat that can be manoeuvred with an external hand magnet. For combustion purposes, samples are heated within this finger in an environment of oxygen generated from an inline Cu/CuO getter.

### 2.5.2.3 Extraction bottle

In stepwise pyrolysis, the sample gases were extracted in specially designed glass bottle by the help of Radio frequency heater (explained in section 2.6.2.3). This bottle

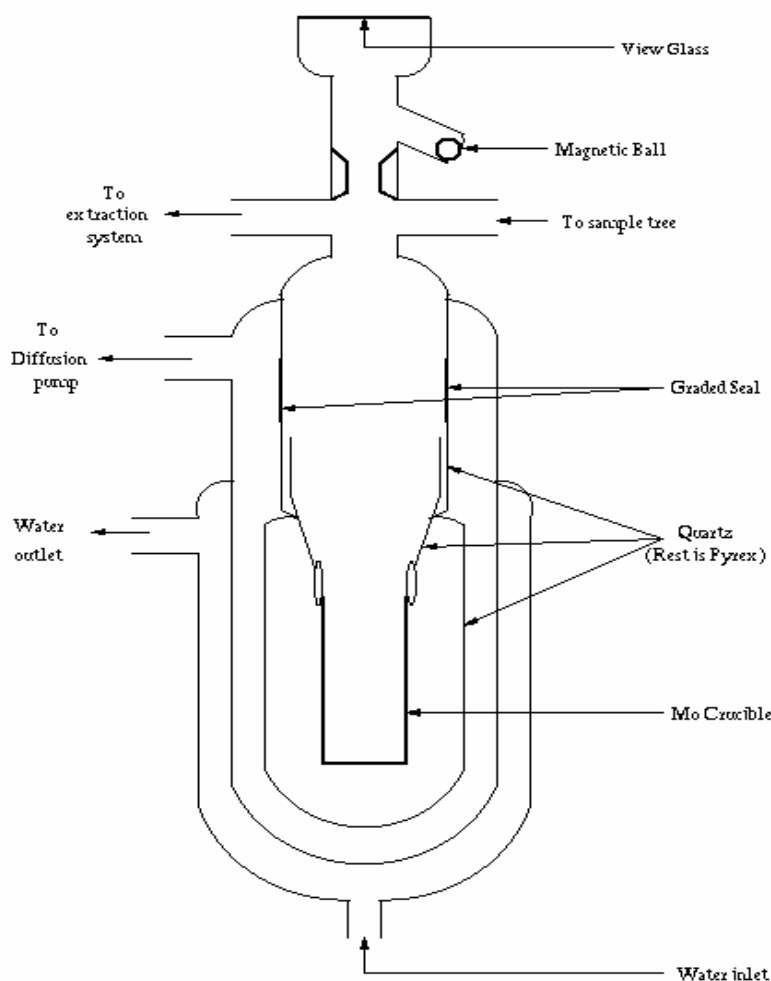


**Fig.2.6** Schematic diagram of the extraction bottle, made up of Pyrex, with quartz at places.

is a double-vacuum bottle that can be cooled externally by a water jacket (Fig. 2.6). It is partially made of quartz and partially by Pyrex™ (See Fig 2.6). Quartz is used in regions that are subjected to higher temperatures (innermost wall of bottle) and rest of the bottle is made of Pyrex. The extraction bottle contains a Molybdenum (Mo) crucible (melting point >2500 °C) that is suspended through a funnel shaped quartz tube and is heated inductively by Radio frequency (RF) power. Sample has to be dropped in this Mo crucible for extraction of gases. One has to do this work with utmost care. An outer chilled water jacket provides cooling to the Pyrex layer that is subjected to high temperatures due to the radiation heating from the crucible. The intermediate vacuum layer between the water jacket and the quartz wall is intended to serve two purposes:

- (1) After the degassing of quartz volume, both sides of quartz wall remains in vacuum, which eliminates the possibility of constant loading of gases into quartz volume.
- (2) This vacuum also minimizes the diffusion of Helium (He) into quartz volume. These two advantages lead to low blank levels hence enable analysis of small samples.

The optically flat view glass, at the top of the bottle allows viewing of the crucible bottom required for temperature calibration (using an optical pyrometer) and visual inspection of sample during melting. A magnetic ball and the seating can be used to block the route, when not required to prevent the vapor deposits on the view glass.

#### **2.5.2.4 The main line**

Subsequent to its extraction, the sample gas passes through a series of cleaning and separation processes in the main line. It consists of a series of fingers (for the adsorption or condensation of gases) and getters (for removing the unwanted gases) many of which can be isolated from the main line by UHV valves. The essential features of this unit are described below.

#### **The line fingers**

The gas-separations, in the inert gas mass spectrometry, are based on the differential adsorption and desorption properties of the gases He, Ne, Ar, Kr, Xe and N<sub>2</sub>. The main line has two stainless steel meshes (SSM-2 and SSM-4) that contain inside them meshes made up of stainless steel powder of 2 μm size (sintered into crucible shapes). The adsorption/desorption properties of these meshes are similar to those of the activated charcoal or zeolite, with an added advantage that they can be baked up to

800 °C thus enabling thorough degassing and UHV conditions. The conventional activated charcoal and zeolite, if baked beyond 400°C, undergo structural damages, which affect their adsorption/desorption properties. Additionally in the case of charcoal, there may be a possibility of carbon monoxide (CO) contamination to nitrogen. Thus for processing of nitrogen, only the SSM fingers are used. The main line has also two Pyrex fingers (CH-3 and CH-6) containing activated charcoal inside them for processing the noble gases. The charcoal and SSM fingers have been connected to the main line by UHV valves. Besides these fingers, which can be isolated from the main line when required, the main line contains a Pyrex cold-finger that is used for separating the unwanted condensable species (like H<sub>2</sub>O and CO<sub>2</sub>) from the rest of the gases.

Gases extracted from the samples contain many other unwanted species in addition to the noble gases and nitrogen. These species are troublesome, as their signals often interfere with those of interest and therefore desirable to get rid of these interfering species, prior to the analysis of the sample gas, by adopting suitable cleaning procedures. The extraction line is provided with a Cu/CuO finger and two getters (Ti-Zr and SAES) that are used for cleaning the sample gas.

#### **Cu/CuO finger**

It is often convenient to clean the sample gas by oxidizing the interfering species (like CO, H<sub>2</sub> and the hydrocarbons etc), followed by a cryogenic separation of the condensable oxides that form (CO<sub>2</sub>, H<sub>2</sub>O etc.). For this purpose, the main line is equipped with an online Cu/CuO getter. Essentially, it is a double-walled quartz finger that contains wires (~0.65 × 6 mm) of copper oxide (MERCK™) wrapped in Pt-foil. Pt-foil serves two purposes: (1) work as catalyst during generation of O<sub>2</sub> (2) prevent direct contact between CuO and quartz finger. Ultra-pure O<sub>2</sub> can be generated in the main line by heating the quartz finger with an external heater (usually) at 700 °C. This oxygen is used for both the combustion of the samples as well as for cleaning of the sample gas (*as mentioned earlier*). By cooling the Cu/CuO finger to 400C, the O<sub>2</sub>, which has not taken part in reaction, can be taken back.

#### **The Ti-Zr and SAES getters**

These materials chemically react with the reactive species such as N<sub>2</sub>, carbon dioxide (CO<sub>2</sub>), O<sub>2</sub>, hydrogen (H<sub>2</sub>) and the hydrocarbons to form refractory compounds. Noble gases can be effectively cleaned of these species by exposing them to these getters.

The main line has been provided with two getters for this purpose. The Ti-Zr getter is a double-walled quartz tube containing sponges of an alloy of Ti and Zr, which is heated by an external heater. The Ti-Zr getter works in the following way. At temperatures  $>700\text{ }^{\circ}\text{C}$ , Ti continuously reacts with  $\text{N}_2$ ,  $\text{O}_2$ ,  $\text{CO}_2$ , CO and decomposes the hydrocarbons by taking up C from them, and leaving behind the  $\text{H}_2$  gas that is adsorbed at temperatures below  $400\text{ }^{\circ}\text{C}$ . Zirconium (Zr) decomposes  $\text{H}_2\text{O}$  vapor, reacts with  $\text{O}_2$  to form refractory oxide and sorbs  $\text{H}_2$  at temperatures  $\sim 300\text{ }^{\circ}\text{C}$ .

The SAES (AP-10GJ) getter that contains a non-evaporating getter material (ST 101 Zr-Al alloy) has an action similar to that of the Ti-Zr getter. It is used for further finer cleaning of the noble gases that have already been cleaned by the Ti-Zr getter, to remove the further traces of the interfering species. For cleaning, the SAES getter is usually heated to  $750\text{ }^{\circ}\text{C}$  and then is cooled to  $300\text{ }^{\circ}\text{C}$  in slow steps.

The Ti-Zr and SAES getters that are very useful for the noble gases are detrimental for nitrogen, as they can scavenge nitrogen. Therefore, during the processing of the nitrogen fraction, these getters are isolated from the main line by UHV valves (V3, and V6, *see* Fig. 2.5). After each experiment, the Ti-Zr and SAES getters are degassed at  $800\text{ }^{\circ}\text{C}$  before further use.

## ***2.6 Standard procedures***

Fig. 2.7 is a flow diagram illustrating the standard procedures adopted for the experiment. The experiment involves the extraction and cleaning of the sample gas, followed by the separation into individual gas fractions and their subsequent analysis in the mass spectrometer and the data acquisition.

### **2.6.1 Gas extraction from chondrules**

As mentioned earlier, to extract gases from the chondrule samples, Nd:YAG laser is used. Chondrules are roughly a milligram samples, which constrains the number of gas extraction steps. Generally, the gas extraction from chondrules is carried out in three steps. For the first step, which is mainly meant for removal of surficial contaminants, the output power of laser kept less than  $0.3\text{W}$ . The second step is the main step for the gas release and complete melting of the chondrule in most of the cases. Laser power used in this step is around  $12\text{W}$ , which is sufficient to melt chondrules. In most cases,  $> 90\%$  of gas is released from chondrule during this step. The third step is a repetition of second step with same/ slightly higher laser power, to

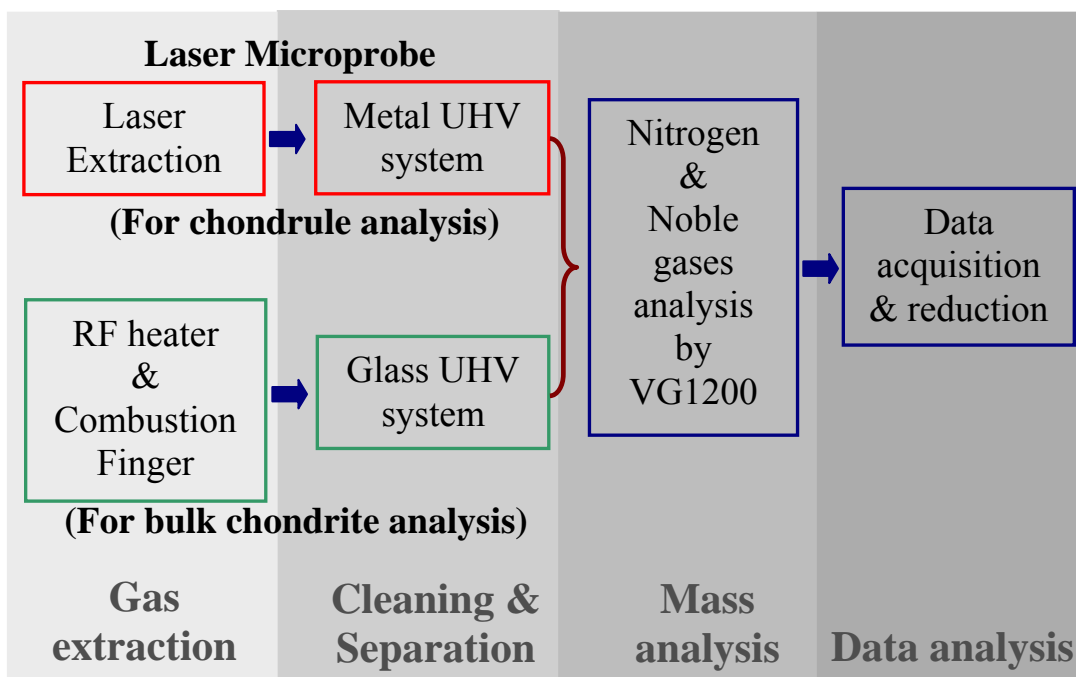


**Fig. 2.7** Flow diagram of standard experimental procedure

ensure complete release of gas from the chondrule. For larger chondrules (> 4 mg e.g. ALD-1 and 2 from Allende chondrite) one intermediate (with moderate laser power ~6W) step is introduced before the main extraction step.

## 2.6.2 Gas extraction from bulk chondrite samples

For the nitrogen and noble gas, analysis of bulk chondrites mainly gas extracted in three temperature steps. In first step, combustion (discussed next) of the sample was done at ~400°C to remove surficial contaminants. After this, two steps (1000°C and 1600°C-melting step) of stepwise pyrolysis (discussed next) were performed.

### 2.6.2.1 Combustion

In this method, the sample is heated inside the combustion finger in an environment of oxygen. The oxygen for combustion is obtained from the on-line Cu/CuO by heating it to ~850 °C. For most of the bulk samples, an initial combustion at 400 °C in 2 torr of oxygen is carried out to remove the surficial contaminants. Heating is usually done for 45 minutes during which the combustion finger is isolated from the main line by an UHV valve. After the heating is over the gas is expanded to the glass UHV system (discussed later) and processed for analysis. The combustion finger is a double-walled (vacuum jacketed) quartz finger that can be heated up to 1050°C (the safe limit without collapsing the quartz) by means of an external resistance heater. The outer vacuum line of this finger is connected to the diffusion pump. Sample is

introduced into this finger by a quartz boat that can be maneuvered with an external hand magnet.

### **2.6.2.2 Stepped Pyrolysis**

The process of stepped pyrolysis involves heating the samples in a pre-degassed Mo crucible (as discussed in section 2.5.2.3) in temperature steps up to 1850 °C, using RF power heater (discussed next). The sample is heated at each step for 45 minutes (30 minutes at the -melting step); the gases released being simultaneously adsorbed on a stainless steel mesh (SSM), maintained at liquid nitrogen temperature. Subsequent to heating, the main line is isolated from the extraction bottle and the gases from the stainless steel mesh are desorbed for further processing.

### **2.6.2.3 Radio frequency (RF) power heater**

RF power heater used for stepped pyrolysis is the industrial triode converter type induction-heating unit, which converts power line energy to high frequency electrical energy suitable for induction heating applications. When inductively coupled through a suitable work coil, this high frequency energy can be used to heat a metal crucible (with high melting point, like Mo) to temperatures of up to >1800 °C. This metal crucible in turn, passively heats the silicate materials dropped into it, causing them to melt and degass.

### **2.6.3 Cleaning and separation (Laser microprobe)**

The extracted gas contains many species other than noble gases and nitrogen that contaminate the mass spectrometer and create interference during mass analysis. Hence, cleaning and separation of noble gases and nitrogen from this released gas is an important and mandatory part of analysis. Following the gas extraction by laser, the released gases are expanded by opening valves  $V_{LC}$  and  $V_{L2}$  for one minute (See Fig. 2.2). After this expansion, valve  $V_{L2}$  is closed. The gas fraction between valves  $V_{L2}$  and  $V_{L6}$  is used for noble gas analyses (NG fraction). On the other hand, valve  $V_{L7}$  is opened to expand the remaining fraction of gas to the Pyrex-line branch volume. The gas between valves  $V_{L7}$  and  $V_{L9}$  is used for nitrogen analysis ( $N_2$  fraction). This step of taking separate fraction of nitrogen in Pyrex-line, takes about two minutes, which minimizes the exposure of nitrogen to metal.

From the NG-fraction, the helium and neon gases are then cleaned by exposing it to the heated Ti-sponge getter, while the Ar/Kr/Xe from this fraction, is trapped by cooling the charcoal finger (and by opening  $V_{L4}$ ) to liquid Nitrogen trap (LNT).

Ti-sponge getter removes all chemically active gases including hydrocarbons. After this cleaning, the helium and neon fraction is introduced to the mass spectrometer by opening valve  $V_{8B}$ . During the He, Ne analysis with  $V_{8B}$  open, the LNT kept under SSM finger to minimize the amounts of  $^{40}\text{Ar}$ ,  $\text{CO}_2$  and water in mass spectrometer. This reduces the interferences of  $^{40}\text{Ar}^{++}$ ,  $\text{H}_2^{18}\text{O}^+$  (in  $^{20}\text{Ne}$  signals) and  $\text{CO}_2^{++}$  (in  $^{22}\text{Ne}$  signals). Nitrogen gas fraction is cleaned by exposing it to CuO (wrapped in Pt foil) at  $750^\circ\text{C}$  for 20 minutes to oxidize CO and hydrocarbons to  $\text{CO}_2$  and  $\text{H}_2\text{O}$  and subsequently to CuO at  $400^\circ\text{C}$  to remove excess  $\text{O}_2$ .  $\text{CO}_2$  and  $\text{H}_2\text{O}$  are condensed on cold finger and cleaned  $\text{N}_2$  fraction is introduced to mass spectrometer for measurements. The remaining Ar/Kr/Xe amount in the volume between the valve  $V_{L2}$  and the sample chamber is collected on the same charcoal finger ( $V_{L4}$ ) by the help of LNT. The total fraction of gas is cleaned once again by Ti-sponge getter and then introduced to the mass spectrometer for analysis.

#### **2.6.4 Cleaning and separation (Glass extraction system)**

As noted earlier, the extracted gas contains many unwanted species that contaminate the mass spectrometer and could cause mass interference. These are removed from or minimized in the sample gas at various stages of cleaning. Initially, the gases are cleaned by exposing them to the Cu/CuO that is heated to  $700^\circ\text{C}$  for 20 minutes followed by cooling to  $400^\circ\text{C}$  in steps. During heating the non-condensable species like C, CO,  $\text{H}_2$  are oxidized to condensable species  $\text{CO}_2$  and  $\text{H}_2\text{O}$ , which are isolated from sample gas by using liquid nitrogen trap. A portion of this clean sample gas (typically 10 %), free from the interfering species, is isolated for the analysis of nitrogen before collecting the rest of the fraction on charcoal finger for exposure to getters for the noble gases study. Cleaning by the Cu/CuO is an essential procedure for processing nitrogen. As this is the only way of cleaning for the nitrogen fraction. Sometimes the sample gas is cleaned by the Cu/CuO more than one time. Usually, if the amounts of condensable gases generated are large a second Cu/CuO clean up is done. The noble gas fraction is then cleaned by exposing it to the Ti-Zr getter, after which the heavy noble gases (xenon, krypton and argon) are adsorbed on a charcoal finger (Ch-6) at liquid nitrogen temperature. The helium-neon fraction that remains in the gas phase is further exposed to the SAES getter, and then introduced into the mass spectrometer via a let-in valve. However, during the analysis of the helium-neon fraction, a liquid nitrogen trap is constantly maintained on the SSM in the let-in

volume. This serves two purposes: a) it adsorbs any water, CO<sub>2</sub> or argon that might have escaped from the cleaning stage; b) it also adsorbs the background species built up in the mass spectrometer during the analysis. Both these reduce the interfering background species for neon. The split of noble gas fraction trapped in the charcoal finger is now a mixture of xenon, krypton and argon. These are separated in two steps, by allowing selective adsorption of the species on a charcoal finger at suitable temperature (−108 °C for Xe and −154 °C for Kr) using a variable temperature probe. Each of these is transferred to the let-in volume before introducing them into the mass spectrometer.

*After the cleaning and separation of gases, the procedure followed for mass spectrometric analysis is same, irrespective of gas extraction or use of glass / metal cleanup system, and is detailed below.*

### **2.6.5 Mass analysis**

Each of the separated fractions from the extraction line is introduced into the mass spectrometer through an UHV valve, and analyzed for the masses by scanning the peaks manually in a number of cycles. In addition to the masses of interest, peak signals at masses 2 (H<sub>2</sub><sup>+</sup>), 18 (H<sub>2</sub>O<sup>+</sup>), 40 (<sup>40</sup>Ar<sup>+</sup>) and 44 (CO<sub>2</sub><sup>+</sup>) in the He–Ne fraction, and 40 (<sup>40</sup>Ar<sup>+</sup>) in the Kr–fraction are monitored to assess the background contributions (*discussed later*). The noble gases are measured usually on the electron multiplier except for mass 4 and 40 in some samples that are measured on the Faraday cup. Nitrogen is measured in the molecular form on the Faraday cup for mass 28, 29 and 30. For smaller nitrogen samples, the peaks 29 and 30 were run on the multiplier, after scanning on Faraday for mass peaks 28 and 29. Measuring mass 30 in the nitrogen fraction allows a precise estimation and correction for the interference from CO (*discussed later*).

### **2.6.6 Data acquisition and reduction**

The signals from the mass spectrometer are acquired and recorded on an on-line computer by using suitable interface and programs. A parallel XY recorder gives a graphic view of the scan and helps in the identification of the peaks. The digitized ‘time vs. signal’ data is processed for the time and peak-heights. The time zero (T<sub>0</sub>) values for the peak heights and the ratios are found out from this data by offline data reduction. The data thus acquired is corrected for the blank, interferences and the instrumental mass discrimination.

## Blanks

The blank of complete system is most important part of the analysis. It is mandatory to establish a low blank (< 5-10 % of the expected sample gases) before starting any sample analysis. Additionally it is also necessary that analysis of blank must be performed in identical fashion to the sample steps, both before and after the sample analysis.

In case of chondrules, laser irradiation (at power equals to maximum power step taken for chondrule analysis) was done on an empty spot of the Cu-plate of the sample chamber. The analysis of released gases was then carried out in an identical fashion as for sample gases. Very small level of blank gases is found by this way. In case of bulk chondrite, analysis blanks have been analysed for 400<sup>0</sup>C combustion step and for 1000<sup>0</sup>C and 1600<sup>0</sup>C steps of pyrolysis. The procedures followed are similar to the sample gas analysis. The blank contributions of nitrogen in most of the chondrule remain less than 10-20% and rarely reached 50% of the sample signals. Blank contribution for the noble gases usually remained 10% to 30% and seldom exceeds 50%. Analyses are discarded when blank contribution is found more than 50%.

**Table 2.2** Typical amount of blanks observed in two-extraction system

UHV Extraction system	<sup>4</sup> He	<sup>22</sup> Ne	<sup>36</sup> Ar	<sup>84</sup> Kr	<sup>132</sup> Xe	N
	10 <sup>-12</sup> cm <sup>3</sup> STP					pg
Metal system (Max. Laser Power)	50	4	2	0.06	0.06	87
Glass system (1600 <sup>0</sup> C)	150000	100	75	0.08	0.07	300

## Interference corrections

The measured signals often have a contribution from the interfering species. With the usual resolving powers of the mass spectrometer, it is not always possible to resolve these contributions from the measured signals. It is however possible to identify the interfering species and correct for their contributions, which are outlined below.

### *a. Interference at mass 3*

The molecular ions of hydrogen (H<sub>3</sub><sup>+</sup> + HD<sup>+</sup>) interfere with the <sup>3</sup>He mass. These peaks cannot be resolved with the resolution of 170 of the mass spectrometer as the resolution > 600 is needed to resolve <sup>3</sup>He<sup>+</sup> from H<sub>3</sub><sup>+</sup> and HD<sup>+</sup>. The contribution of (H<sub>3</sub><sup>+</sup> + HD<sup>+</sup>) at mass 3, however, can be assessed and corrected for, by measuring the

peak at mass 2 ( $\text{H}_2^+$ ) and estimating the corresponding ( $\text{H}_3^+ + \text{HD}^+$ ) contribution using a predetermined ( $\text{H}_3^+ + \text{HD}^+$ )/ $\text{H}_2^+$  ratio (using pure  $\text{H}_2$ ) which is typically  $\sim 4.62 \times 10^{-4}$  ( $\pm 10\%$ ). As the SAES getter in the mass spectrometer keeps the  $\text{H}_2$  background very low, the contribution due to ( $\text{H}_3^+ + \text{HD}^+$ ) is in general very low ( $< 1\%$ ).

*b. Interference at masses 20 and 22*

Contributions from  $\text{H}_2^{18}\text{O}^+$  and  $^{40}\text{Ar}^{++}$  at mass 20 and  $^{44}\text{CO}_2^{++}$  at mass 22 cannot be resolved from the neon peak signals by the mass spectrometer. The neon data is, therefore, corrected for these background contributions from the measured peak signals of the masses 18, 40 and 44 and using the  $^{18}\text{O}/^{16}\text{O}$ ,  $40^{++}/40^+$ , and  $44^{++}/44^+$  abundance ratios, respectively. The abundance ratios  $40^{++}/40^+$ , and  $44^{++}/44^+$ , in the above correction, are periodically determined for the operating conditions of the mass spectrometer from the air standard. The typical values of  $40^{++}/40^+$ , and  $44^{++}/44^+$  are 0.036 ( $\pm 10\%$ ) and 0.007 ( $\pm 10\%$ ) respectively.

*c. CO correction*

Peak height at mass 30 can have contributions from  $^{15}\text{N}^{15}\text{N}$ ,  $^{12}\text{C}^{18}\text{O}$  and possibly from the hydrocarbons. Assuming that all the hydrocarbon contribution at masses 30 and 31 would be comparable, and considering the near absence of any 31 peak in the signal, it is considered that the hydrocarbon peak at mass 30 is negligible. Therefore, the excess over  $^{15}\text{N}^{15}\text{N}$  at mass 30 is assigned wholly to CO contribution. The effect of CO contribution, which shifts the  $\delta^{15}\text{N}$  to more positive value, is corrected for by routinely measuring mass 30 along with the masses 28 and 29 in the nitrogen-fraction. The correction procedure is as follows.

1. First, the excess of at mass 30 estimated based on measured and expected ratio of 30/29 as follows.

$$30_{\text{excess}} = [(30/29)_{\text{meas.}} - (30/29)_{\text{expect.}}] \times 29_{\text{meas.}}$$

Where,  $(30/29)_{\text{expect.}} = 1/4 \times (29/28)_{\text{meas.}}$  (from the abundance of  $^{15}\text{N}$  and  $^{14}\text{N}$ )

This (30 excess) is assigned, wholly, as the contribution of 30 from CO.

2. Contribution at mass 29 from CO ( $^{29}\text{CO}$ ) is now estimated from the amount of  $^{30}\text{CO}$  derived in the previous step, using the  $^{29}\text{CO}/^{30}\text{CO}$  ratio of 5.711 for normal C, O isotopic compositions. The  $^{29}\text{CO}$ , which has a  $^{28}\text{CO}/^{29}\text{CO}$  ratio of 85.939, is subtracted from the measured nitrogen ( $29_{\text{meas.}}$ ) to obtain the CO-corrected 28/29. Using this corrected 28/29 value steps 1 and 2 are repeated.

After less than five iterations, the 28/29 values converge, and this value is used as the CO-corrected 28/29. The  $^{29}\text{CO}$  obtained in the last iteration is subtracted from the measured 29 to obtain the CO-corrected nitrogen amount. For deriving the  $^{28}\text{CO}/^{29}\text{CO}$  and  $^{30}\text{CO}/^{29}\text{CO}$  ratios, the terrestrial C, O isotopic compositions are assumed. The CO correction on  $\delta^{15}\text{N}$  is usually less than 1‰.

#### *B4. Correction for the contribution of $^{40}\text{Ar}_2^+$ at mass 80*

$^{40}\text{Ar}_2^+$  has an irresolvable contribution at mass 80. This is assessed from the  $^{40}\text{Ar}^+$  measured in the krypton fraction, and using a ratio of  $^{40}\text{Ar}_2^+ / ^{40}\text{Ar}^+$  measured in the krypton fraction of an air standard. The Kr fraction of an air standard always has some  $^{40}\text{Ar}$ , because of incomplete separation of Ar and Kr. Therefore, the  $^{40}\text{Ar}$  in the Kr fraction of an air standard is always monitored, and used in estimating the  $^{40}\text{Ar}_2^+ / ^{40}\text{Ar}^+$  ratio the following way.

i. Estimating the [80/84] ratio corrected for mass discrimination

$$[80/84]_{\text{corr.}} = [80/84]_{\text{meas.}} - (4 \times \text{mass discrimination} \times [80/84]_{\text{meas.}})$$

ii. Estimating the excess at 80:

$$80_{\text{excess}} = ([80/84]_{\text{corr.}} - [80/84]_{\text{Air}}) \times 84_{\text{meas.}}$$

iii.  $^{40}\text{Ar}_2^+ / ^{40}\text{Ar}^+ = 80_{\text{excess}} / 40_{\text{meas.}}$  in Kr fraction.

A typical value of this ratio is  $4 \times 10^{-7} (\pm 10\%)$ .

### **2.6.7 Calibration of the mass spectrometer**

Known amount air standards, processed in a fashion similar to the samples, are run periodically to calibrate the mass spectrometer, for its sensitivity and mass discrimination. An Air standard is also used to find out the separation efficiency of Ar, Kr and Xe in a mixture of these gases. Typical values of the air standard parameters that are used in calibration are given in Table 2.3. The sensitivities lie within 10 % between standards, analyzed over several months. For a particular experiment, the most closely spaced (in time) air standard parameters are used. The mass discrimination is more reproducible for long periods of time. For most of the analysis, the separation yields of Ar, Kr and Xe have been calculated for individual measurements to get precise elemental abundance values.

**Table 2.3** Mass spectrometer calibration parameters

Species	Detectors and Resistance (ohms) used	Sensitivity cm <sup>3</sup> STP/counts	Yield (%)	M.D.* % / amu
<sup>4</sup> He	M, 10 <sup>8</sup>	2.11 x 10 <sup>-13</sup>		12(3)
<sup>22</sup> Ne	M, 10 <sup>8</sup>	1.18 x 10 <sup>-13</sup>		1.77 (.56)
<sup>28</sup> N <sub>2</sub>	F, 10 <sup>10</sup>	6.06 x 10 <sup>-8</sup> #		1.95(.07)
<sup>36</sup> Ar	M, 10 <sup>8</sup>	1.83 x 10 <sup>-14</sup>	94	0.99(.08), F 1.01(.05), M
<sup>40</sup> Ar	F, 10 <sup>10</sup>	4.42 x 10 <sup>-11</sup>		
<sup>132</sup> Xe	M, 10 <sup>9</sup>	1.14 x 10 <sup>-15</sup>	80	0.44(.05)
<sup>84</sup> Kr	M, 10 <sup>9</sup>	1.49 x 10 <sup>-15</sup>	68	0.82(.05)

100 counts/sec = 1 mV; M.D.\* = mass discrimination, # Sensitivity of N<sub>2</sub> is in micrograms/count, M = Electron multiplier, F = Faraday cup, number in brackets with MD values are the error in last significant digit

### Mass Discrimination

The sensitivity of the mass spectrometer for different isotopes of an element is different. This causes a systematic difference in measured isotopic ratios compared to actual isotopic ratios. The correction factor for mass discrimination can be calculated using reference gas (air) with known isotopic composition using the following equation:

$$\text{m.d.} = \left[ \frac{R_{\text{meas.}}}{R_{\text{true.}}} - 1 \right] \times \frac{100}{m_j - m_i} \quad (\% / \text{amu})$$

$$R_{\text{true.}} = \left[ \frac{\text{m.d.}}{100} (m_j - m_i) + 1 \right]^{-1} R_{\text{meas.}}$$

$$\text{Where, } R = \frac{(m_i)}{(m_j)}, \quad \text{and if } \left[ \frac{\text{m.d.}}{100} \times (m_j - m_i) \right] \ll 1 \quad \text{then}$$

$$R_{\text{true}} = R_{\text{meas.}} \left[ 1 - \frac{\text{m.d.}}{100} (m_j - m_i) \right] = R_{\text{meas.}} \times \text{mdf}$$

$$\text{Where, } \text{mdf} = \left[ 1 - \frac{\text{m.d.}}{100} (m_j - m_i) \right]$$

So to get the  $R_{\text{true}}$  (true/actual isotopic ratio), the  $R_{\text{meas}}$  (measured isotopic ratio) is multiplied with the factor  $\text{mdf}$ .

For He, the sensitivity and the mass discrimination are determined by an artificial mixture of He, which is cross-calibrated using Bruderheim meteorite standard.

## 2.7 Chemical characterization of chondrules

Chemical characterization of chondrules has been done by Electron Probe Micro Analysis (EPMA) method. By this non-destructive method, chemical composition of important elements in the form of their oxides can be analysed. 27 chondrules have been characterized in two phases of EPMA (details are given in Table 2. 4).

First phase of characterization has been done at the EPMA facility at Max-Planck-Institut für Chemie, Mainz, Germany. Second phase of EPMA has been carried out at National Geophysical Research Institute (NGRI), Hyderabad, India.

**Table 2.4** Details of EPMA analysis used for chemical characterization of chondrules. Numbers in brackets are showing number of chondrules analysed from each chondrites

Facility	Model	Accelerating voltage, Gun current	Samples (chondrules)
Mainz, Germany	Jeol (Superprobe) JXA-8900 RL	15 kV, 40 nA	Dhajala (5), Chainpur (3) Parsa (3)
NGRI, India	Cameca (SX100)	15 kV, 40 nA	Allende (7), Bjurbole (5) Saratov (2), Tieschitz (1) Murray (1), Qingzhen (1)

EPMA performed on the splits kept for 28 chondrules (as mentioned in section 2.1). Epoxy mounts (circular buttons of ~ 3mm thickness) are made keeping these splits on one surface. To remove the surface roughness, fine polishing of these buttons have been done in steps (coarser to finer). The final polishing is done with the help of Alumina powder with grain size ~0.3 $\mu$ m. Before EPMA, sections were coated with carbon to avoid the charging of surface during the electron probe analysis. Various details of EPMA and the standards used for each element are given in Table 2.4 and 2.5.

### 2.7.1 Method to determine the chemical composition of chondrule

Major element compositional data are determined for 28 chondrules using electron microprobe facilities listed in Table 2.4. Using back scattered electron (BSE) image the different topography present on chondrule sections are first determined. Using a focused (~1  $\mu$ m diameter) beam in point mode, 15kV accelerating voltage, and 40nA gun current, spot analysis performed for each topography. This helped in (1) deciding the mineral (2) composition of mineral. Usually 3-4 spots were taken per topography in a given chondrule. Data from these spot analyses averaged to calculate the mineral

composition. By using ENVI (environment for visualizing images) software, the modal distribution percentage of identified minerals in given chondrule section has been calculated. To calculate composition of a chondrule, composition of each mineral (weighted by mineral's modal percentage in a chondrule) is added. Percentages of minerals in each chondrule are given in chondrule description (section 2.7.2). Major element composition of all chondrules is given in Table 3.5, Chapter 3.

### 2.7.2 Limitations of EPMA method:

There are limitations with EPMA method during estimating chemical composition of chondrules. EPMA is a surface analysis method hence the estimated chemical composition represents the surface whereas by volume the sample may have different composition. In addition to this as mentioned by Jones et al., (2005) chemical composition estimated by EPMA is based on spot analyses (1 to 10  $\mu\text{m}$ ) which may not be a true representative of the mineral/grain composition. But for chondrule splits, EPMA offers the best way for composition determination and has been adopted by other workers (Polnau et al., 1999, 2001).

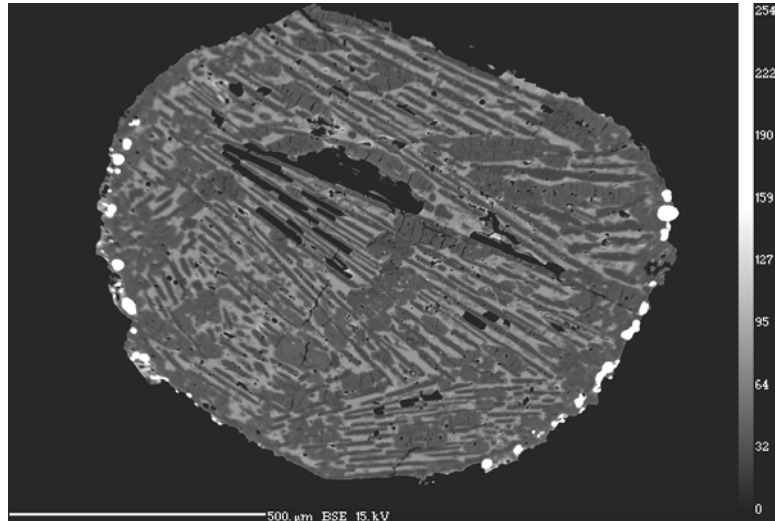
**Table 2.5** Details of the standards used during EPMA analysis for different elements

NGRI, India		
Signal	Standard	Type
Na Ka	Albite	Natural
Mg Ka	Periclase	Natural
Al Ka	Corundum	Natural
Si Ka	Wollastonite	Natural
S Ka	Pyrite	Natural
K Ka	Orthoclase	Natural
Ca Ka	Wollastonite	Natural
Ti Ka	Ti	Element
Cr Ka	Cr	Element
Mn Ka	Mn	Element
Fe Ka	Andradite	Natural

### 2.7.3 Petrographic and Mineralogical descriptions of chondrules

**Murray-1:** BO, Type-I (FeO 0.3 %) (Ol 68, Feldspathic material 25) An unusually large chondrule (~1100 $\mu$ m) compared to average size of chondrules (~300  $\mu$ m) in CM chondrites. Chondrule has barred olivine texture with interstitial feldspathic mesostasis. At few places, bars are cross-cutting. The olivine is fosteritic (Fo 99)

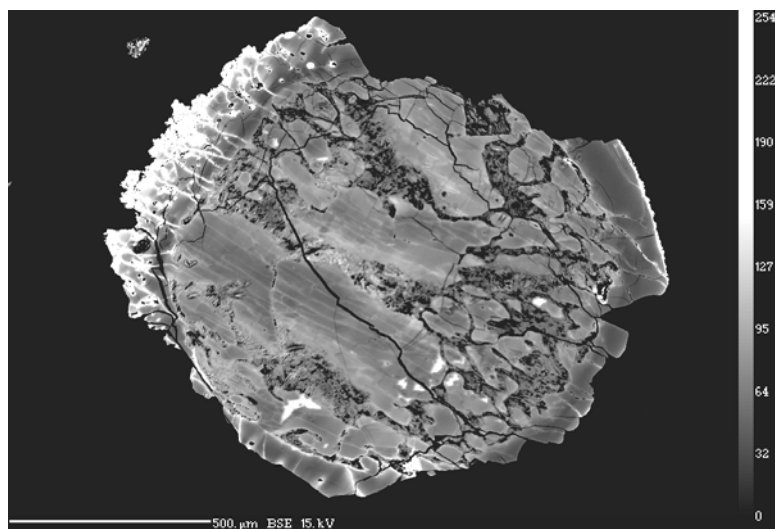
whereas interstitial material is calcic feldspar (An 96, Ab 4). Chondrule has very different rim made from the small spherules of metal/metal sulfide. Rim is not related with inside minerals suggesting rim



formation as a separate event for this chondrule.

**Allende-1:** PO, Type I (FeO 4.6%), (Ol 58, Px 24). Large crystals of olivine with faint bar texture in half of the chondrule are the special features observed in this chondrule. The other half comprises fragmented olivine and pyroxene crystals. The other curious feature is the rim of this chondrule. The chondrule is having thick (~140 $\mu$ m) olivine rim with veins of iron sulfide at one edge. The olivine present in rim is found to be Fe

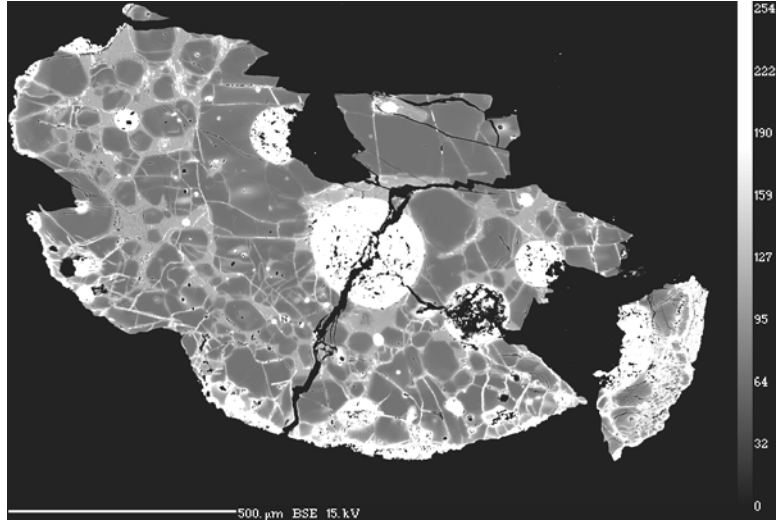
rich compare to olivine present in inner chondrule. The iron sulfide veins in olivine rim are connected with inner fragmented pyroxene crystals. These pyroxene crystals are interstitially present



with large size (~700 $\mu$ m) olivine crystals. At the other edge of chondrule, clear olivine rim without iron sulfide is present. At this edge, small olivine crystals with

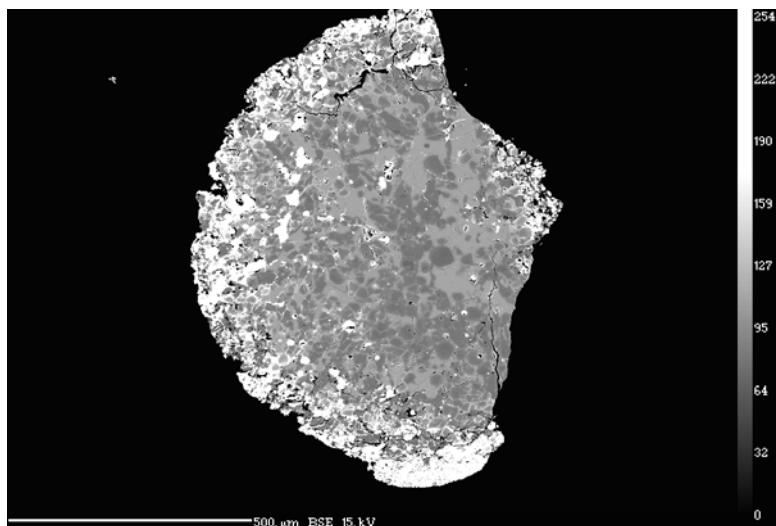
interstitial pyroxene fragments are present. On average olivine in this chondrule is found to Mg-rich (Fo 97, Fa 3) similar to pyroxene (En 91, Fs 8).

**Allende-2:** PO, Type I (FeO 2%) (Ol 53, feldspathic material 30, metal 15) This is unique chondrule with pure Fe-Ni metal-spherules (15%). Olivine is Mg-rich (Fo 98, Fa 2) and having interstitial spectacular network of feldspathic glass rich in Calcium (An: 91, Ab: 9). The network of feldspathic material is also includes



Fe-Ni metal-spherules. Some independent metal spherules are also observed. At some places, effect of rapid cooling can be seen with barred texture in feldspar. A big Fe-Ni blob with ~260 μm size is also curious feature of this chondrule. The feldspathic glass network is only observed at the edges of the chondrule and in this region, sizes of olivine crystals (50-20μm) are smaller compared to olivine crystals (100-200μm) present in core.

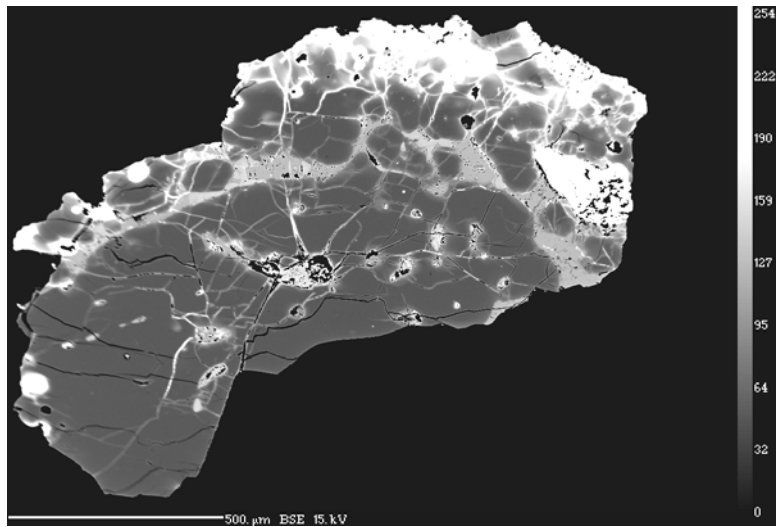
**Allende-3:** MPO, Al-rich, Type I (FeO 1.4%) (Ol 53, feldspathic material 34, metal sulfide 13) Texture of the chondrule is micro-porphyritic with rim of metal sulfide (FeS). Micro-porphyritic euhedral crystals of



olivine (maximum size ~40 μm) are present with interstitial feldspathic glass. Olivine is almost fosteritic (Fo: 97, Fa: 3) whereas interstitial material is calcic feldspar with some Na and Al amount (An: 88%, Ab: 12%). Due to higher amount of feldspar

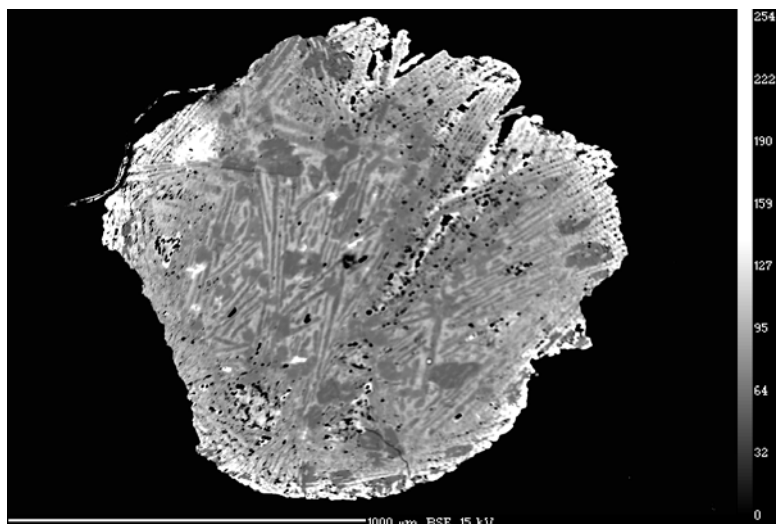
(54%) in this chondrule compared to other Allende chondrules, this chondrule is showing highest concentration of Al (~5 %). Chondrule has ~150 $\mu$ m size rim mainly troilite grains connected with fine veins of troilite coming from inner olivine and feldspathic glass crystals. The size of olivine crystals is decreasing from core to rim. This chondrule is showing maximum depletion in  $^{15}\text{N}$  isotope in all chondrules of Allende.

**Allende-13:** PO, Type-I (FeO 0.4%) (Ol 61, feldspathic material 17, metal sulfide 10, pyroxene 8) Chondrule is having porphyritic olivine texture where olivine is almost fosteritic. The curious feature is the presence



of thick feldspathic glass vein between olivine structure and rim. In this calcic feldspathic material (An: 89, Ab: 8), which is poor in Na and Al, Al-rich pyroxene grains (~10 $\mu$ m) are present at several places. This feldspathic glass further observed to feed the iron sulfide coating of the chondrule.

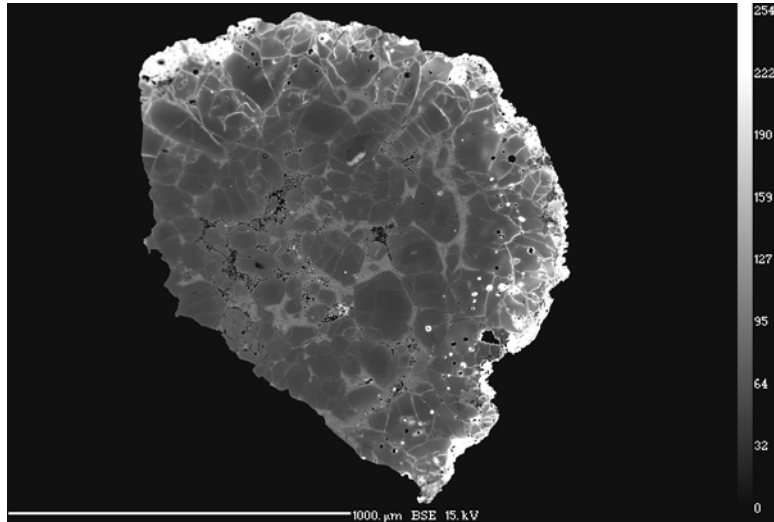
**Allende-14:** BO/BP, Type-I (FeO 2.4%), (Ol 47, Px 46). This is a lone chondrule from Allende suite, which is showing barred texture. It comprises almost equal amount of olivine and pyroxene. Olivine is found to be Mg-rich (Fo



97, Fa 3) similar to pyroxene (En 96, Fs 2.5). The barred structure in this chondrule is multiple and cross-cutting at several places. Edges are probably metal rich suggesting

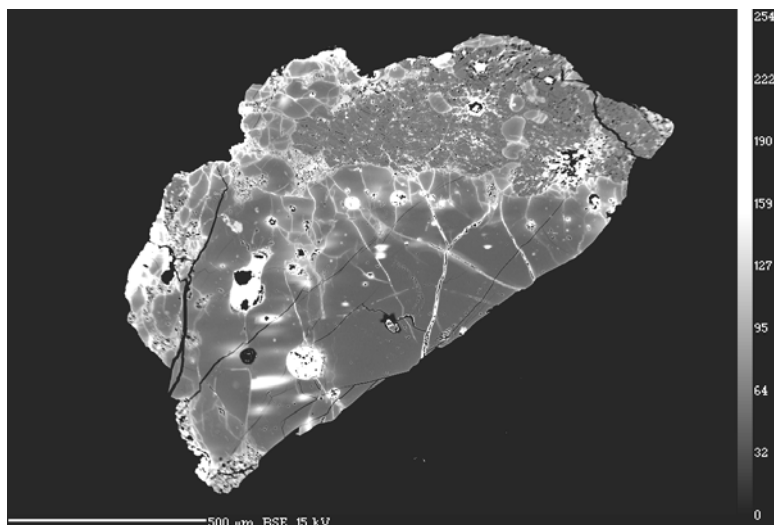
zoning of Fe from the core to the edge. The possible rim structure is not different from the inner barred structure as bars are present even up to the edges of chondrule.

**Allende-15:** PO, Type-I (FeO 4.5%) (Ol 62, feldspathic material 27, metal sulfide 9) Presence of euhedral crystals ( $250 \times 200 \mu\text{m}^2$ ) with interstitial feldspathic mesostasis is observed. Feldspathic material is mainly calcic (An 92, Ab 7). Olivine is found to be Mg-rich (Fo 94, Fa 6). Olivine crystals near the rim of chondrule are found to be Mg-poor and Fe-rich compared to olivine crystals at the core suggesting Fe is increasing from core to rim. A network of troilite veins is present



near the rim. These veins are connected to the metal sulfide rim indicating the exclusion of metal sulfide from core to rim possibly due to metal silicate fractionation during chondrule formation. The above mentioned zoning of Fe in this chondrule is also the metal silicate fractionation. Similar kind of zoning is not observed for sulfur which is only present in the rim area. Small drops of iron sulfide independent to vein network are also present. This may be due to re-condensation of metal when chondrule was still in molten stage.

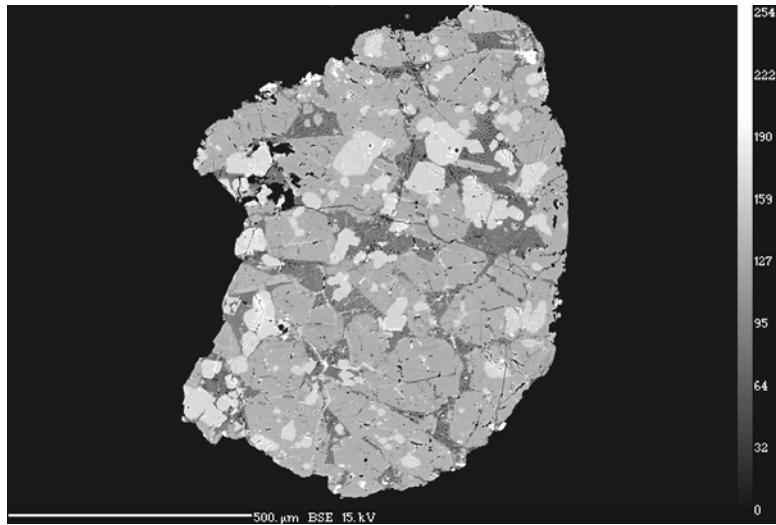
**Allende-16:** PO, Type-I (FeO 1.4%) (Ol 60, feldspathic material 20) More than half of the chondrule is showing porphyritic olivine texture however; at one end, presence of feldspathic mesostasis is observed. Few crystals



of olivine ( $\sim 50\mu\text{m}$ ) are observed in this mesostasis, which are found to be Fe-rich

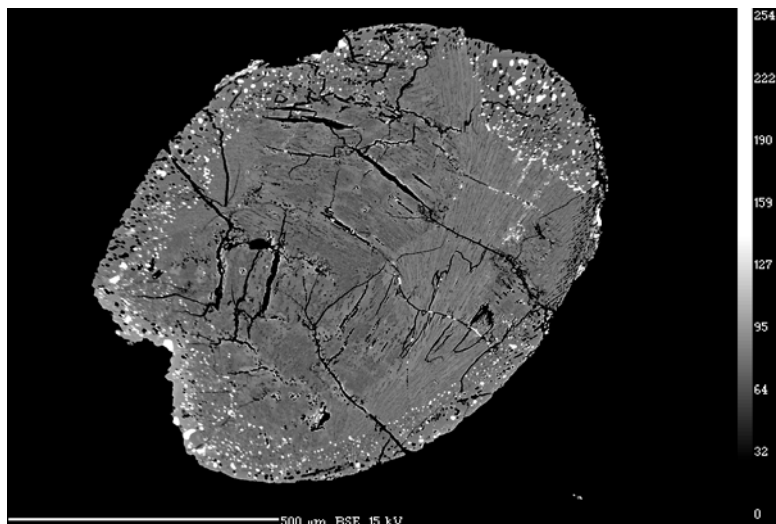
compared to porphyritic crystals of olivine present at the other end. At some places, presence of metal (Fe, Ni) blobs can be seen. Metal veins are also visible in large olivine crystals.

**Bjurbole-15:** PP, Type-II (FeO 13.3%) ( Px 57, Ol 21, Feldspathic material 19) Pyroxene crystals (400 x 300  $\mu\text{m}$ ) are major minerals in this chondrule. Small olivine crystals (<100 $\mu\text{m}$ ) which are mainly euhedral are also



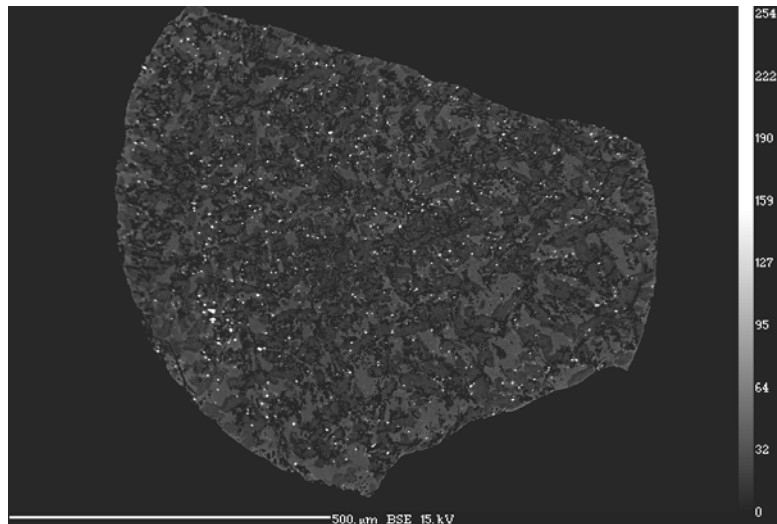
present. Some olivine crystals within pyroxene crystals are observed. Feldspathic glass mainly Albite (Ab 78, An 20), is found to be interstitially present with crystals of pyroxene and olivine. Very small laths of pyroxene are observed in feldspathic material.

**Bjurbole-18:** Pyroxene, Type-II (FeO 13%) This is a lone elliptical chondrule without any defined crystals almost a pyroxene sphere. This pyroxene (En 74, Fs 21) is mainly enstatite. Rim is clearly visible made by tiny dots of iron



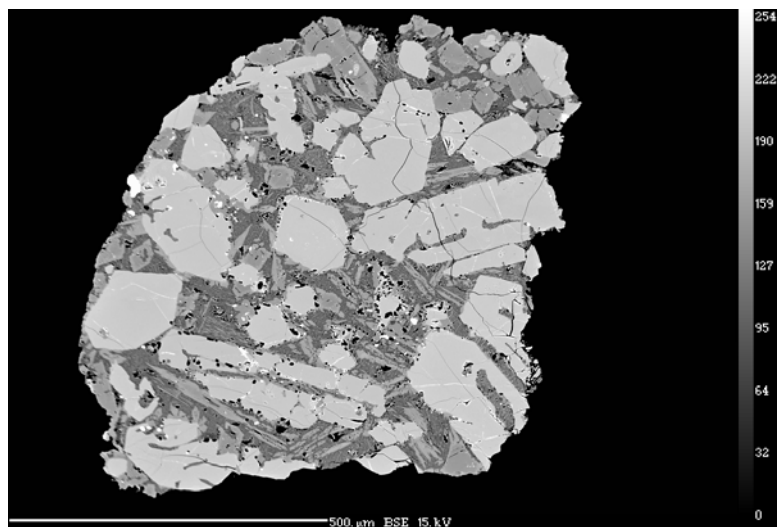
sulfide. Fine laths of pyroxene rich in Al, is visible in this chondrule at the outer region. At the interaction of inner region with these laths, higher concentration of Ca is observed. Elliptical shape of chondrule may have a relation with velocity of chondrule as well as rotation of chondrule. Very fine cracks are present in chondrules at several places. Cracks are most likely due to secondary processes.

**Bjurbole-25:** MP, Type-II (FeO 15%), (Ol 32, Px 60, feldspathic material 19) This chondrule is a lone chondrule from Bjurbole with micro-porphyritic texture made by both pyroxene and olivine. Very small



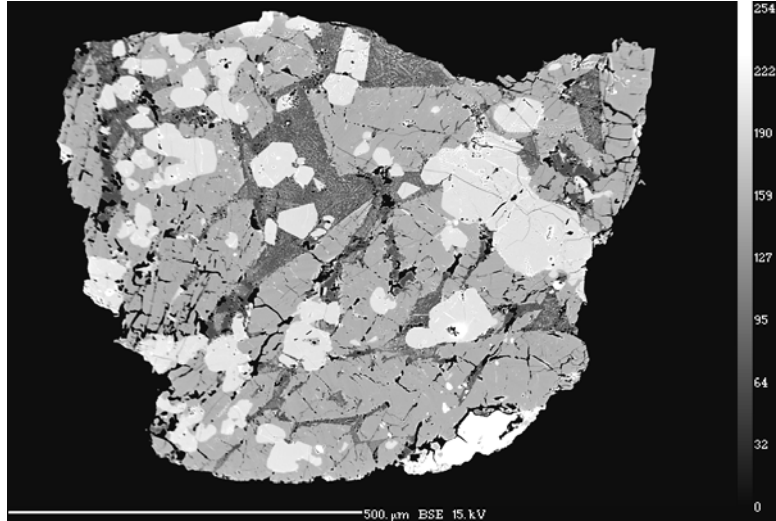
dots of metal/metal sulfides are visible at some places. The pyroxene is the major constituent and found to be Mg-rich however, it has significant amount of Fe (En 70, Fs 20) similar to olivine which also Mg-rich with some amount of Fe (Fo 76, Fa 24).

**Bjurbole-26:** PP, Type-II (FeO 14%) (Px 53, Ol 24, feldspathic material 15, metal/metal sulfide 3) Euhedral crystals (500 x 200 μm) of pyroxene (En 77, Fs 21) are the major minerals. No evidence of any elemental zoning is observed. Euhedral olivine crystals of varying sizes are also present. In some cases, olivine crystals are within the pyroxene crystals and feldspathic material. These olivine crystals do not have sharp boundaries. Olivine (Fo 74, Fa 25)

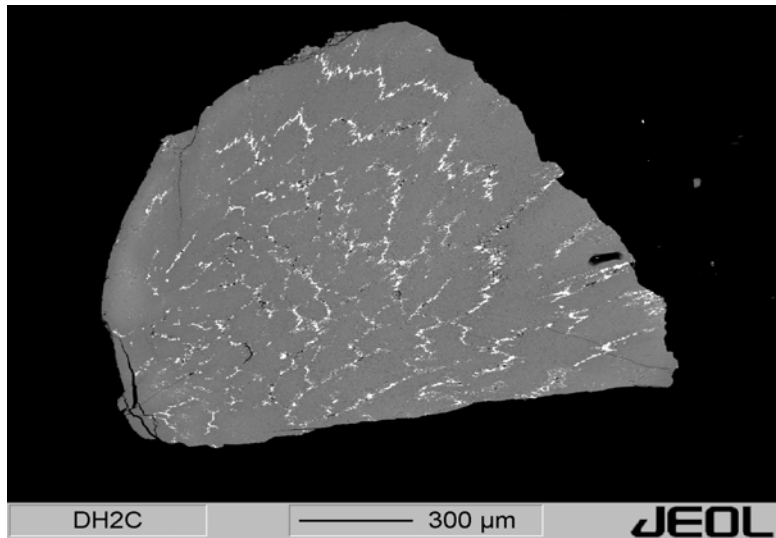


found to be mainly Mg-rich. Feldspathic material is interstitially present with pyroxene and olivine crystals. Feldspathic glass is mainly Albite (Ab 65, An 33). A ~200μm size metal blob is found to present in this chondrule. Tiny laths of pyroxene are seen this feldspathic glass. Porphyritic pyroxene rich, less amount of olivine crystals, embedded in anorthitic mesostasis.

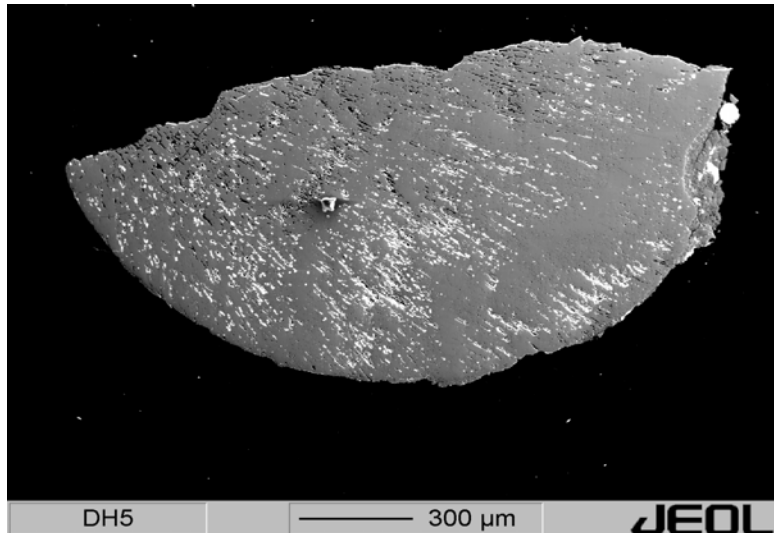
**Bjurbole-29:** PO, Type-I (FeO 15%) (Ol 47, Px 23 Feldspathic mesostasis 24, metal/metal sulfide 2%) Euhedral crystals (300 x 100  $\mu\text{m}$ ) of olivine (Fo 74, Fa 25) are the major constituents. Two kinds of pyroxene crystals are present together with olivine crystals. Few pyroxene crystals are euhedral in shape and small (100 x 50  $\mu\text{m}$ ), whereas other pyroxenes crystals are longer (~350 x 20  $\mu\text{m}$ ). These long pyroxene crystals show core and rim structure with elemental zoning. In details, Core is Mg-rich (En 74, Fs 21) whereas rim is found to be Mg-poor, Ca, Al rich (Wo 25, En 59, Fs 14) in these crystals. All together, the crystals of olivine and pyroxenes are having interstitial feldspathic glass (An 53, Ab 41). A small amount of metal/metal sulfide (~2%) is also found as fine dots.



**Dhajala-2:** Pyroxene, type-II (FeO 14 %) The is having mostly pyroxene (En 71, Fs 22) mainly enstatite with some amount of FeO. Pyroxene does not have any crystal structure. The curious feature is that the highly reflecting white lines like wave into the chondrule possibly metal sulfide as lines are found to be Fe, S and Ca rich. For the splits of this chondrule, different N-composition is observed.

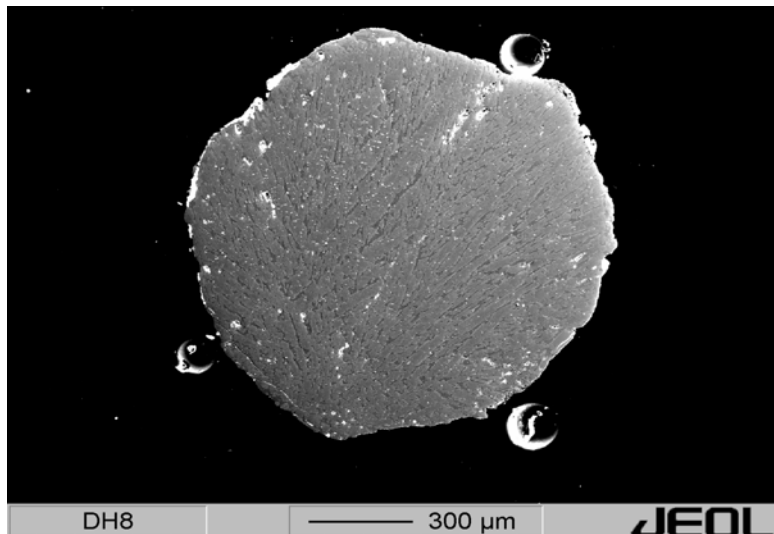


**Dhajala-5:** RP, Type-II (FeO 20%) (Px 95, Iron sulfide 3, metal 2) Very fine laths of pyroxene are radiating from single point to the edge of chondrule. Pyroxene is mainly enstatite with some amount of FeO (En 73, Fs 24). There is



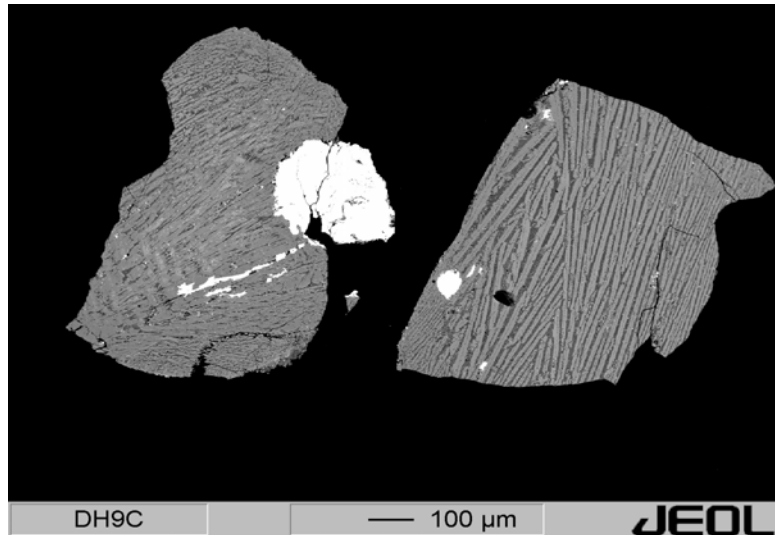
a possibility of Fe and/or S interstitially present in radial lines as reflecting radiating lines clearly visible in BSE image. At the edge a Fe-Ni blob and a troilite grain is also visible.

**Dhajala-8:** BP Type-II (FeO 8.5%) (Px 97, metal/metal sulfide 3) Bars of pyroxene laths are showing radial texture typically <math>50\mu\text{m}</math> wide. The bars are with branches and cross-cutting at several places. Pyroxene is the major



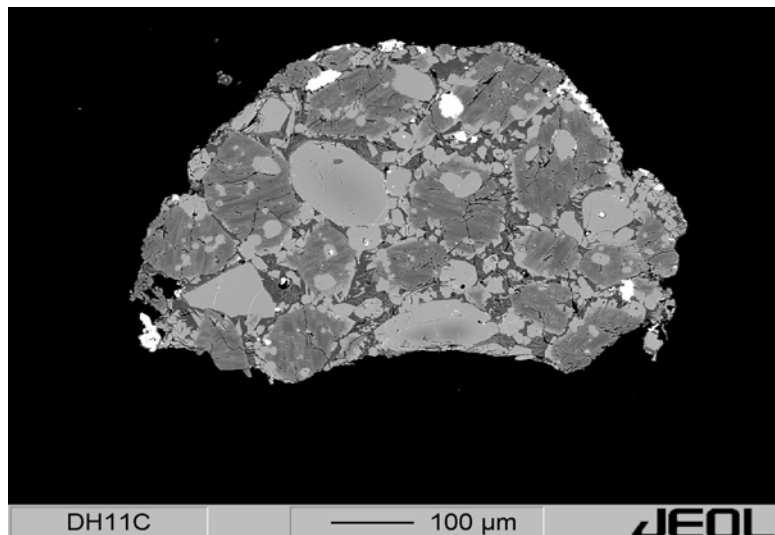
mineral with enstatite as a major end member (En 76, Fs 11). At the edges very small amount (3%) of metal inclusions are visible. Between the pyroxene, laths there is a presence of interstitial material may be feldspathic in nature.

**Dhajala-9:** BP, type-II (FeO 19%) (Px 92, metal 8) Laths of pyroxene typically ~20µm wide are making perfect barred texture for this chondrule. This Pyroxene is found to be metal rich however significant amount of Fe



is also present (En 71, Fs 20) A big metal sulfide inclusion is present between the barred structures. The Size of this metal sulfide inclusion: is ~280µm. A small drop of pure Fe-Ni blob is also present in this chondrule.

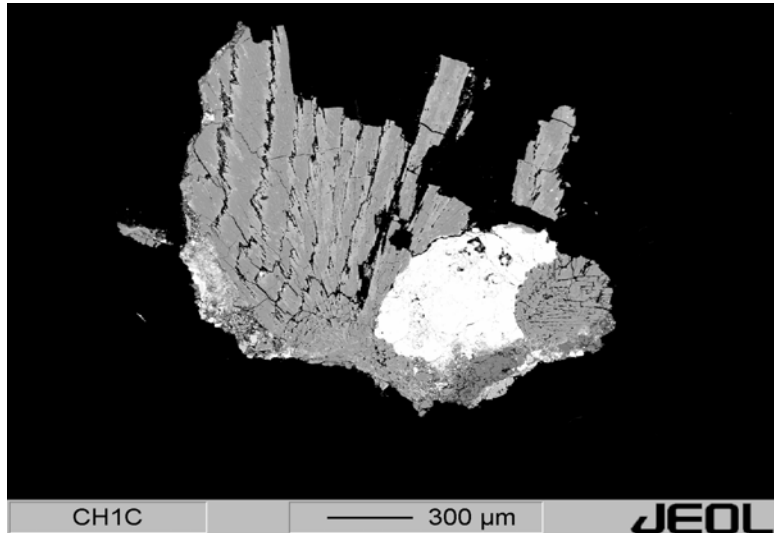
**Dhajala-11:** PO Type-II (FeO 12.6%), (ol 47, Px 32, feldspathic material 15, metal sulfide 3) Euhedral phenocrysts of olivine and pyroxene are the major constituents of this chondrule. Crystals of pyroxene (160 x 100 µm<sup>2</sup>) are generally



bigger compared to olivine crystals (140 x 80 µm<sup>2</sup>). The important feature is that in almost all pyroxene crystals presence of small olivine grains (30 x 20 µm<sup>2</sup>) mainly at the boundaries of mineral are observed. In addition, pyroxene minerals are showing barred texture. Interstitially, feldspathic glass is present with olivine and pyroxene phenocrysts. In fact, small olivine grains (10- 20 µm) are also present in this feldspathic material. Very thin laths (most probably pyroxene) are also observed in this interstitial material. Olivine are Mg-rich however some amount of Fe is also present (Fo 81, Fa 18) similar to pyroxene (En 87, Fs 12). Interstitial feldspar is found

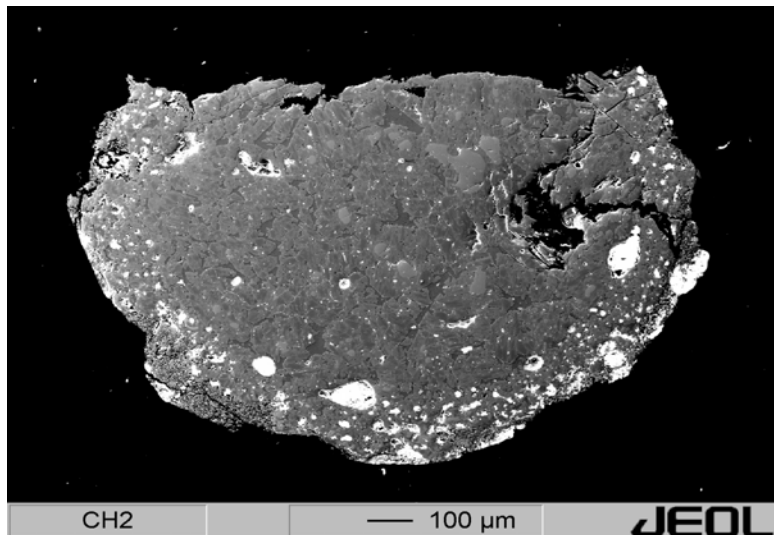
to be Ca and Na rich (An 47, Ab 53). At few places, presence of iron sulfide is seen in this chondrule.

**Chainpur-1:** BP, Type-II (FeO 13%), (Px 78, metal sulfide 17) This chondrule is having big (~ 700 $\mu$ m) size metal blob with a smaller spherical object (probably a small chondrule) of ~370  $\mu$ m size. This small object is showing barred texture. The other part of the chondrule is also showing barred



structure. Bars are typically ~50 $\mu$ m wide. Different gray scales between the bars are suggesting a possibility of some elemental zoning at the edges of the bars. The major mineral constituent is pyroxene, which is found to be Mg-rich (En 78, Fs 13, Ac 7)

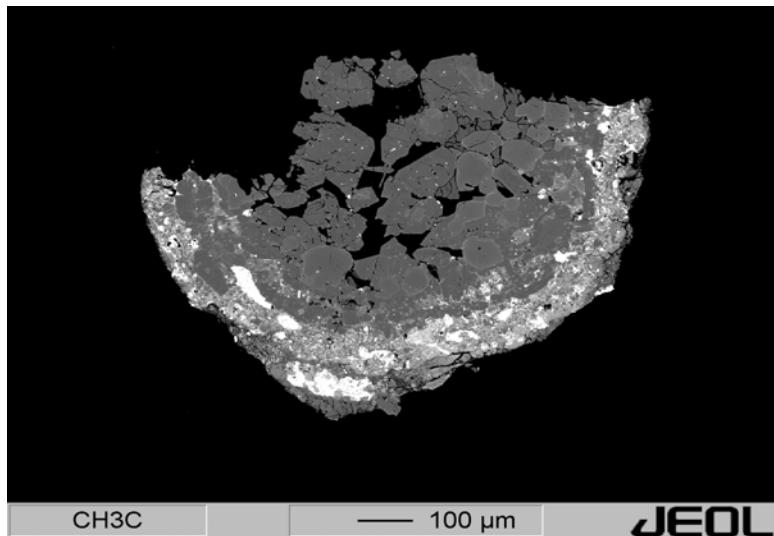
**Chainpur-2:** MP, Type-II (FeO 8.7%) presence of micro-porphyritic crystals with interstitial feldspathic glass is observed. Small grains of olivine are also present. Rim is made by metal blobs of varying size. Rim with such texture can be due to re-condensation of metal spherules probably expelled during chondrule



forming event. Although rim is formed mainly by small metal blobs, at least four bigger metal spherules with 100 to 50  $\mu$ m diameter are also present. At rim, compared to inner part of the chondrule, smaller sized minerals are observed probably due to interaction with dust during molten stage. Like other Chainpur chondrule (ch-3), rim

is found to be thick (Rim width: 150  $\mu\text{m}$ ). Pyroxene in this chondrule is found to be Mg-rich with some amount of Fe content (En 79, Fs 20).

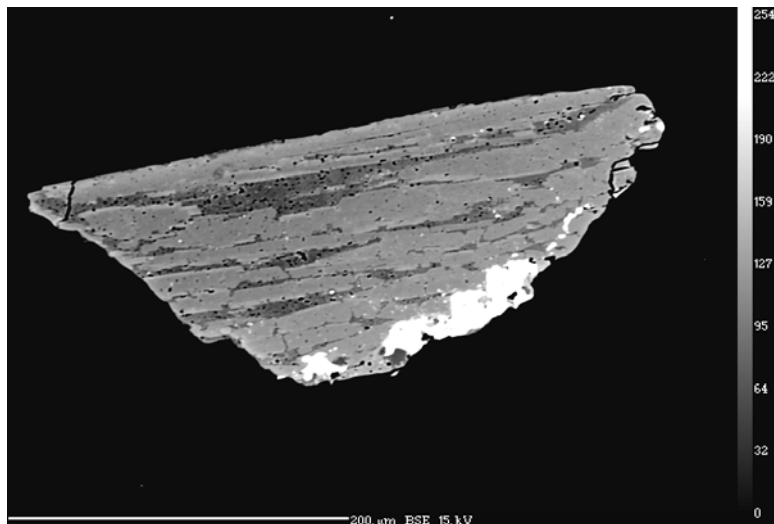
**Chainpur-3:** PP, type-I (FeO 6.4%) (Ol 36%, Px 53%, metal sulfide 7%) Euhedral pyroxene crystals with sharp boundaries are the major mineral constituents. Rim is mainly metal and feldspathic glass. This



chondrule is having a thick rim ( $\sim 140 \mu\text{m}$ ) and the outer rim is found to be Fe-rich suggesting Fe zoning in the rim. Few crystals of olivine with sharp boundaries are present between the pyroxene crystals. In addition, it is observed that smaller olivine grains are within the porphyritic pyroxene grains.

**Saratov-2:** BP, Type-II (FeO 8.5%) (Px 80, feldspathic material 12, metal sulfide 6)

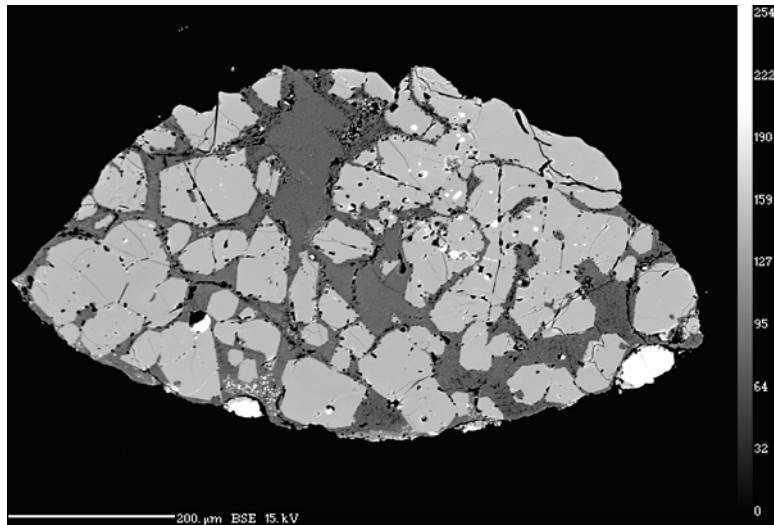
Pyroxene bars typically 15-25  $\mu\text{m}$  wide are observed in this chondrule. Pyroxene is Mg-rich (En 83, Fs 14). Sodium and Aluminium rich feldspathic glass is present interstitially between bars of pyroxene. Small amount



of metal sulfide is present at the edge of the chondrule.

**Saratov-3:** PO, Type-II (FeO 14%) (Ol 61, Feldspathic material 32, and metal sulfide

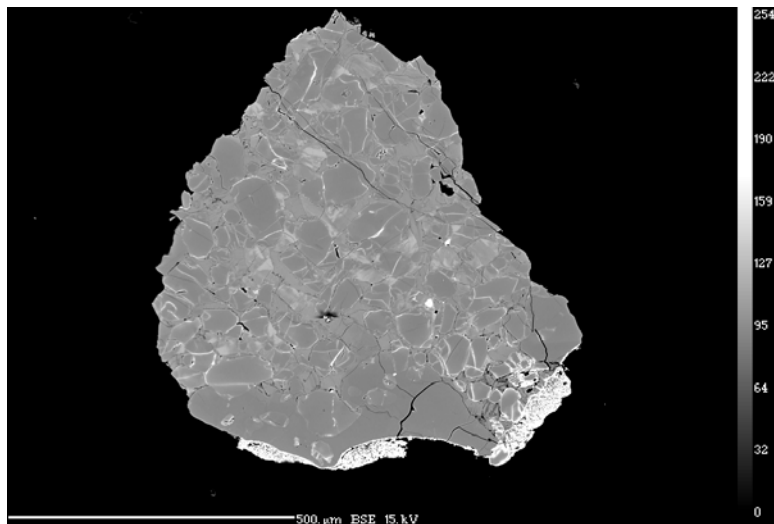
2) Olivine crystals with varying size are the major mineral constituents of this chondrule. Olivine is found to be Mg-rich (Fo 77, Fa 22). Olivine crystals (200 to 20  $\mu\text{m}$ ) with interstitial feldspathic material are



showing different shapes but mainly euhedral. Feldspathic mesostasis is Sodium and Aluminium rich (Ab 89, An 8). On the chondrule edge, two troilite blobs are found. A curious observation is that the feldspathic material is becoming Si-rich and Fe-poor from core to the edge of the chondrule. On the edges of most of the olivine crystals, black dots are found suggesting empty space. This indicates interaction between olivine and interstitial feldspathic material.

**Tieschitz-2:** PO, Type-I (FeO 4%) (Ol 44, feldspathic material + Px 50) Porphyritic

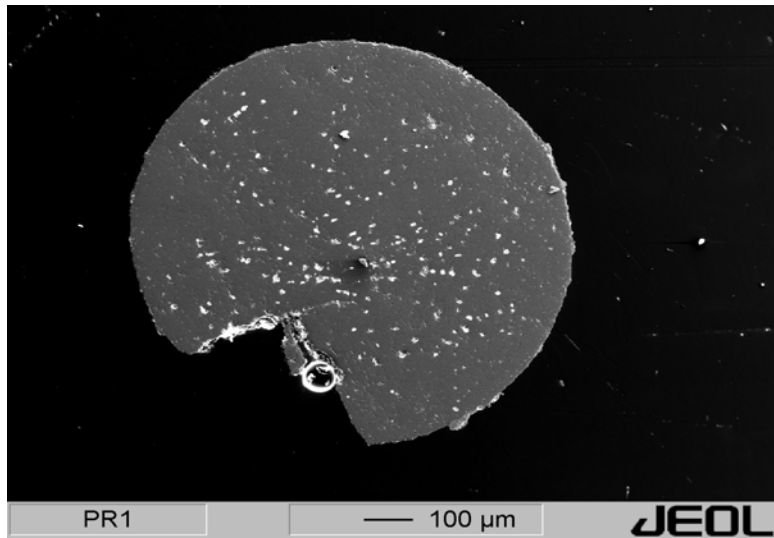
olivine crystals are present with interstitial feldspathic material. In most of the cases, boundaries of these crystals are not sharp whereas in few cases, boundaries are having white lines most likely to be metal like



material. At few places in feldspathic material presence of pyroxene is observed. The important feature observed in this chondrule is that blurred edges of the olivine crystals suggesting equilibration with interstitial feldspathic material. For this chondrule, the difference observed in gray scale of olivine and feldspar in BSE image is very less.

**Parsa-1:** Pyroxene, Type-I (FeO 1.4%) The complete chondrule is pyroxene sphere with very tiny crystals.

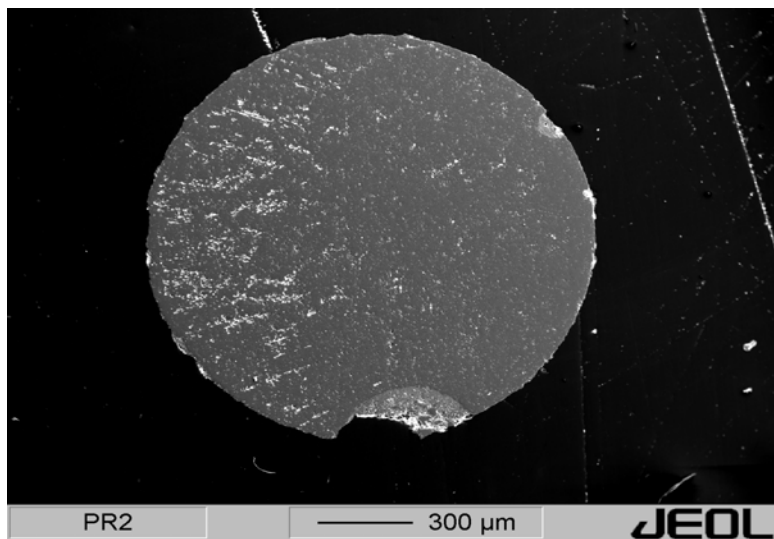
Very small ( $< 10\mu\text{m}$ ) size of crystals with compact arrangement does not allow to characterize the ground mass. Individual spot analyses support pyroxene as the only mineral present in this



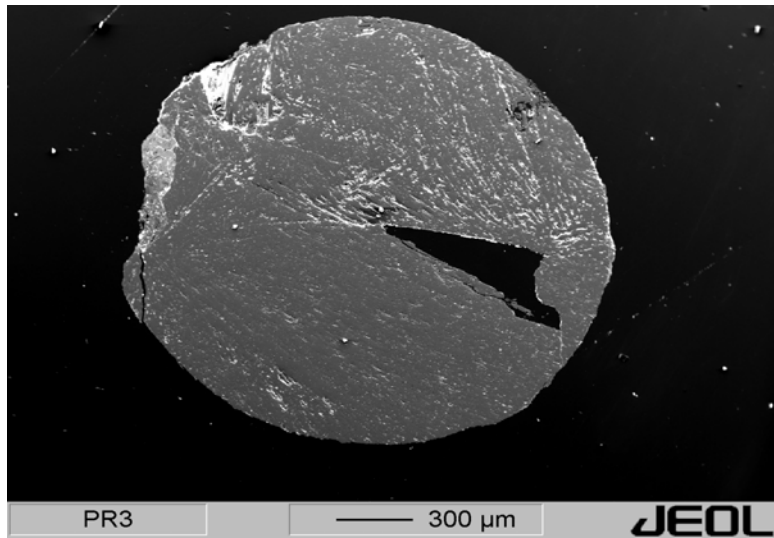
chondrule. Fine highly reflecting dots can be seen mainly in the core of the chondrule separated by 20-50  $\mu\text{m}$  distance. These fine circles may be representing metal/metal sulfide. Chondrule is perfect sphere. The pyroxene is mainly Mg-rich (En 88, Ac 5) with presence of  $\text{Na}_2\text{O}$  around 1.4%.

**Parsa-2:** Pyroxene, Type-I (FeO 1%). This chondrule is a pyroxene sphere with very small crystals.

Pyroxene is Mg-rich (En 93). One side of the chondrule is showing presence of some highly reflecting material most probably metal/metal sulfide. This material seems to be radial from core to edge. Chondrule is perfect sphere.



**Parsa-3:** pyroxene Type-I (FeO 1%). Chondrule is only pyroxene, which is mainly enstatite (95%). Laths radiate from a single point at the edge to core of the chondrule, are present in half of the chondrule. These laths are  $<10\mu\text{m}$  wide and difficult to resolve from the ground mass. The other half of the chondrule seems to have different texture with presence of metal/metal sulfide radiating to the edge of the chondrule. The laths from two halves of the chondrule are cross-cutting roughly at half-line of the chondrule.



## Chapter 3

# Noble gases in chondrules *-in situ* produced components

### **3.1 Introduction**

The measured noble gases in meteorites and their constituents are mainly a mixture of *in situ* and trapped components. The *in situ* label designates a nuclear component like cosmogenic and radiogenic, ideally that is still in the same location in which it was generated. This chapter concentrates on the cosmogenic and radiogenic noble gas nuclides in chondrules and their host chondrites. In next chapter (chapter 4), results of trapped noble gases are discussed.

Although chondrules are the major constituent of chondrites they are very different compared to bulk chondrite (e.g., their chemical and isotopic compositions for some elements are different compared to host chondrite). In case of chondrule formation in nebular environment, it is expected that chondrules were formed first and later they became part of the chondritic parent body. Based on short-lived radionuclides the chondrule formation duration is constrained to be ~1 Ma (Mostefaoui et al., 2002). Hence, it is expected that the first formed chondrules, before becoming a part of larger parent body, receive some cosmic ray exposure for a duration of up to 1 Ma and preserve this pre-compaction irradiation records (for example, excess cosmogenic noble gases in chondrules compared to parent chondrite) which can be visualized in favourable cases (chondrites with small exposure ages < 1-3 Ma). In this work, we have looked for such evidences in chondrules from the major classes of chondrites.

Study of radiogenic noble gases ( $^4\text{He}$ ,  $^{40}\text{Ar}$  and  $^{129}\text{Xe}$ ) gives the clue about the ages of chondrules. The variation in concentrations of these radiogenic gases can be related to different gas retention ages of chondrules and/or different amount of parent nuclides in chondrules (as K content variation can yield differences in  $^{40}\text{Ar}$  amount).

The comparison between radiogenic concentration and cosmogenic concentration in a given sample provides the information to identify and characterize loss of gases from a sample. Usually the loss of radiogenic noble gases is expected to be more compared to cosmogenic noble gases. As for example, if the radiogenic  $^{40}\text{Ar}$  in sample is not affected by any loss, then it can be inferred that there should not be any loss of  $^{38}\text{Ar}$  from this sample. This work mainly deals with cosmogenic  $^3\text{He}$ ,  $^{21}\text{Ne}$  and  $^{38}\text{Ar}$  and radiogenic  $^4\text{He}$ ,  $^{40}\text{Ar}$  and  $^{129}\text{Xe}$  in individual chondrules and their comparison with host chondrites. The production reactions of these isotopes are given in details in *Appendix*.

The measured noble gases in chondritic samples are generally mixture of various components. By using standard established methods, these components can be separated into cosmogenic, radiogenic and trapped components.

We first discuss details of methods used for separating various components.

In this chapter, various subscripts are used with concentrations and ratios to identify different components. Subscripts **m**, **c**, **t**, **r** and **rt** are used to represent measured, cosmogenic, trapped, radiogenic and radiogenic + trapped components respectively.

### ***3.2 Calculations of cosmogenic and radiogenic noble gases***

To decouple mixture of cosmogenic, radiogenic and trapped components a few assumptions are required. Following is the details of the assumptions. Methods of calculation for various noble gas components based on these assumptions are given in *Appendix*.

#### **Helium (<sup>3</sup>He<sub>c</sub>, <sup>4</sup>He<sub>r</sub>)**

Helium has two isotopes: <sup>3</sup>He and <sup>4</sup>He. In chondrites, Helium is mainly dominated by <sup>4</sup>He, which is mostly radiogenic where as <sup>3</sup>He is cosmogenic and is lower in amount.

To decouple these two components following assumptions are made.

- 1  ${}^3\text{He}_t = 0$ , hence  ${}^3\text{He}_m = {}^3\text{He}_c$
- 1  $({}^4\text{He}/{}^3\text{He})_c = 5.2$
- 2  ${}^4\text{He}_{rt} = {}^4\text{He}_m - (5.2 \times {}^3\text{He}_c)$
- 3 If  ${}^4\text{He}_{rt} < \text{maximum } {}^4\text{He}_r$ , then  ${}^4\text{He}_t = 0$  and  ${}^4\text{He}_{rt} = {}^4\text{He}_r$
- 4 In case of  ${}^4\text{He}_{rt} > \text{maximum } {}^4\text{He}_r$ , then  ${}^4\text{He}_t = {}^4\text{He}_{rt} - \text{maximum } {}^4\text{He}_r$
- 5 This leads to  ${}^3\text{He}_t = {}^4\text{He}_t \times ({}^3\text{He}/{}^4\text{He})_t$ 
  - $({}^3\text{He}/{}^4\text{He})_t$  decided based on trapped end member assumed for Ne (for most chondrules: Q composition and for few chondrules solar composition).
- 6 Then measured <sup>3</sup>He is corrected for trapped <sup>3</sup>He contribution if necessary, to obtain cosmogenic <sup>3</sup>He amount.

*Maximum <sup>4</sup>He<sub>r</sub>*: Maximum amount of radiogenic <sup>4</sup>He expected during the age of the chondrule (4.56 Ga), for the chondritic abundances of U, Th and complete retention of the radiogenic component. In Table 3.1, the maximum <sup>4</sup>He<sub>r</sub> expected in different classes of chondrites are listed.

### Neon ( $^{21}\text{Ne}_c$ , $^{20}\text{Ne}_t$ )

Ne has three isotopes, which makes the partition of cosmogenic, and trapped components of neon relatively more accurate compared to He and Ar. Following assumptions are made for calculation of  $^{21}\text{Ne}_c$  and  $^{20}\text{Ne}_t$  (results of  $^{20}\text{Ne}_t$  are discussed in chapter 4).  $(^{20}\text{Ne}/^{22}\text{Ne})_t$  and  $(^{21}\text{Ne}/^{22}\text{Ne})_t$ : the trapped end members of Ne are decided based on criteria as suggested by Eugster (1988).

- $(^{20}\text{Ne}/^{22}\text{Ne})_c = 0.80 \pm 0.03$  (Begemann et al., 1976)

If,

- $(^{20}\text{Ne}/^{36}\text{Ar})_t < 1$  :  $(^{20}\text{Ne}/^{22}\text{Ne})_t = 8.4$ ,  $(^{21}\text{Ne}/^{22}\text{Ne})_t = 0.035$  (Tang and Anders, 1988)
- $(^{20}\text{Ne}/^{36}\text{Ar})_t \sim 1$  :  $(^{20}\text{Ne}/^{22}\text{Ne})_t = 11.0$ ,  $(^{21}\text{Ne}/^{22}\text{Ne})_t = 0.034$
- $(^{20}\text{Ne}/^{36}\text{Ar})_t > 1$  :  $(^{20}\text{Ne}/^{22}\text{Ne})_t = 13.7$ ,  $(^{21}\text{Ne}/^{22}\text{Ne})_t = 0.033$  (Geiss, 1973)

It is observed that assumption of trapped Ne end member is not critical in deciding  $^{21}\text{Ne}_c$  and  $^{20}\text{Ne}_t$ .

- In most of the cases,  $(^{21}\text{Ne}/^{22}\text{Ne})_c$  remains 0.8 to 0.95 as observed in chondrites (Wieler 2004). For very few cases when  $(^{21}\text{Ne}/^{22}\text{Ne})_c$  was not within 0.8 to 0.95, it is taken as 0.9 as considered for the case of average shielding depth in chondrites.

(Details of the calculations are given in *Appendix*)

**Table 3.1** Maximum values of radiogenic  $^4\text{He}$  and elemental ratio  $^4\text{He}/^{40}\text{Ar}$  expected in different classes of chondrites based on concentrations of U, Th and K.

Chondrites	U (ppb)	Th (ppb)	K (ppm)	$^4\text{He}_r$	$^4\text{He}/^{40}\text{Ar}$
H <sup>a</sup>	12	42	780	2047	1.83
L/LL <sup>a</sup>	13	43	825 (L), 790(LL)	2181	1.83
EH <sup>b</sup>	10	34	800	1691	1.37
CV <sup>a</sup>	17	60	310	2907	6.70
CM <sup>a</sup>	11	40	400	1898	3.36

Concentrations of U, Th and K are from; <sup>a</sup>: Wasson and Kallemeyn (1988)

<sup>b</sup>: Mason, (1979)

### Argon ( $^{36}\text{Ar}_t$ , $^{38}\text{Ar}_c$ , $^{40}\text{Ar}_r$ )

In case of Ar, three isotopes represent different noble gas components. To decouple between these three components following assumptions are made.

- $^{40}\text{Ar}_m = ^{40}\text{Ar}_r$
- $(^{36}\text{Ar}/^{38}\text{Ar})_c = 0.65 \pm 0.02$

- $(^{36}\text{Ar}/^{38}\text{Ar})_t = 5.34 \pm 0.02$  (Q composition, Busemann et al., 2000), as phase Q is the major Ar-carrier phase in unequilibrated chondrites
- In meteorites with large pre-atmospheric size, a possible contribution to  $^{36}\text{Ar}$  from  $^{35}\text{Cl}$  ( $n,\gamma$ )  $^{36}\text{Cl}$  ( $\beta^-$ )  $^{36}\text{Ar}_{\text{Cl}}$  can result in an underestimate of cosmogenic  $^{38}\text{Ar}_c$ . Such cases have been discussed where relevant during the discussion.

### **Xenon ( $^{129}\text{Xe}_r$ )**

$^{129}\text{Xe}$  is the major radiogenic Xenon isotope (produced due to decay of  $^{129}\text{I}$ ) and in a few chondrules, it could be detected. For calculations of  $^{129}\text{Xe}_r$  we assumed Q as trapped end member with  $(^{129}\text{Xe}/^{132}\text{Xe})_t = 1.042 \pm 0.002$  (Busemann et al., 2000)

Results of cosmogenic  $^3\text{He}$ ,  $^{21}\text{Ne}$  and  $^{38}\text{Ar}$  calculated based on these assumptions are discussed in section 3.3.1

Results of radiogenic  $^4\text{He}$ ,  $^{40}\text{Ar}$  and  $^{129}\text{Xe}$  obtained based on these calculations are given in section 3.3.2

## **3.3 Results**

### **3.3.1 Cosmogenic noble gases ( $^3\text{He}$ , $^{21}\text{Ne}$ and $^{38}\text{Ar}$ )**

The results of cosmogenic  $^3\text{He}$ ,  $^{21}\text{Ne}$  and  $^{38}\text{Ar}$ , calculated for each chondrule from ordinary, enstatite and carbonaceous chondrites are given in Tables 3.2, 3.3 and 3.4 respectively. For all chondrules and their respective chondrites elemental ratios  $(^3\text{He}/^{21}\text{Ne})_c$  and  $(^{21}\text{Ne}/^{38}\text{Ar})_c$  are plotted against concentrations of  $^{21}\text{Ne}_c$  in Figs. 3.1, 3.2, 3.3, 3.4 and 3.5 for Dhajala, Bjurböle, rest of the ordinary chondrites (Tieschitz, Udaipur, Saratov, Chainpur), enstatite chondrites (Parsa, Qingzhen) and carbonaceous chondrites (Allende, Murray) respectively, to visualize differential loss and/or large chemical composition differences.

#### **3.3.1.1 Chondrules from ordinary chondrites**

Of the 47 chondrules analysed from OC, 22 are from Dhajala and 9 are from Bjurböle. Due to the large number of individual chondrule analysis from Dhajala and Bjurböle, it would be easy to see, if there are any significant differences among the chondrules from a given meteorite. For this reason, the chondrules of Dhajala and Bjurböle will be discussed separately while the chondrules from the other four ordinary chondrites (16) will be discussed together.

**Dhajala (H3.8):** Chondrules of Dhajala show a range from 0.2 to  $6 \times 10^{-8}$   $\text{cm}^3\text{STP/g}$  of  $^3\text{He}_c$  concentrations whereas the bulk sample of Dhajala shows  $6.0 \times 10^{-8}$   $\text{cm}^3\text{STP/g}$  concentration (Table 3.2). Most chondrules except DH-S8 show lower  $^3\text{He}$

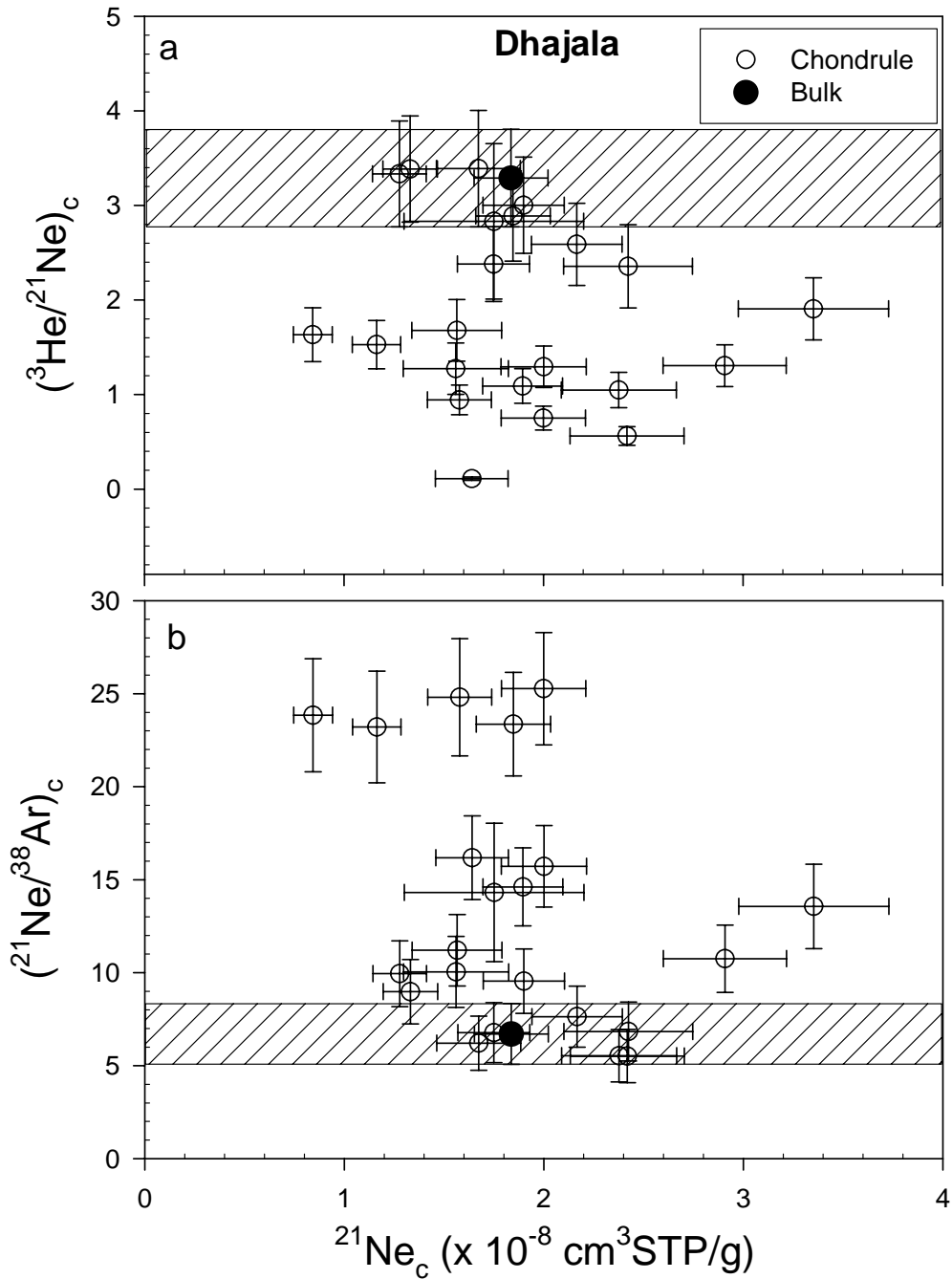


**Fig. 3.1** Elemental ratios  $(^3\text{He}/^{21}\text{Ne})_c$  and  $(^{21}\text{Ne}/^{38}\text{Ar})_c$  plotted against concentrations of  $^{21}\text{Ne}_c$  for chondrules from Dhajala chondrite, hatched areas show the range observed for bulk Dhajala **(a)** Loss of  $^3\text{He}_c$  in chondrule is evident compared to bulk. **(b)** Similar loss is not reflected in case of  $^{21}\text{Ne}_c$  compared to bulk.

concentrations compared to bulk Dhajala sample. In chondrules DH-11 and DH-8, the abundance of cosmogenic corrected  $^4\text{He}$  is higher compared to *maximum*  $^4\text{He}_r$  (Table 3.2). As mentioned in section 3.2,  $^3\text{He}_c$  is calculated after correcting for trapped  $^3\text{He}$  in these chondrules. For chondrules DH-S18 and DH-S19, the amount of  $^4\text{He}$  observed is slightly higher compared to *maximum*  $^4\text{He}_r$  (as listed in Table 3.1). Correction for trapped  $^3\text{He}$ , has not significantly affected the concentration of  $^3\text{He}_c$ . Other chondrules

show lower concentrations of  $^3\text{He}_c$ . Chondrule DH-V38 shows lowest concentration of  $^3\text{He}$  among all chondrules.

On the other hand,  $^{21}\text{Ne}_c$  ranges from 1 to  $3 \times 10^{-8} \text{ cm}^3\text{STP/g}$ , a narrow range compared to  $^3\text{He}_c$ . Most chondrule values are around  $1.5 \times 10^{-8} \text{ cm}^3\text{STP/g}$  and similar within 10%.  $^{21}\text{Ne}_c$  concentration is  $1.84 \times 10^{-8} \text{ cm}^3\text{STP/g}$  in bulk Dhajala. A Few chondrules show higher concentration of  $^{21}\text{Ne}_c$  compared to bulk.

The range of  $^{38}\text{Ar}_c$  in Dhajala chondrules is from 0.04 to  $0.82 \times 10^{-8} \text{ cm}^3\text{STP/g}$  encompassing  $0.27 \times 10^{-8} \text{ cm}^3\text{STP/g}$  of  $^{38}\text{Ar}_c$  in bulk Dhajala. Three chondrules (DH-5, DH-S18 and S19) show higher value compared to bulk Dhajala. Chondrule DH-5 shows highest value of  $^{38}\text{Ar}$  ( $0.42 \times 10^{-8} \text{ cm}^3\text{STP/g}$ ) which is four times compared to value observed for bulk Dhajala.

In Fig. 3.1, elemental ratios  $(^3\text{He}/^{21}\text{Ne})_c$  and  $(^{21}\text{Ne}/^{38}\text{Ar})_c$  are plotted against  $^{21}\text{Ne}_c$  concentrations of chondrules and bulk from Dhajala. As evident in Fig. 3.1a, most chondrules show lower values of  $(^3\text{He}/^{21}\text{Ne})_c$  compared to bulk. The hatched region shown in figure represents the expected range in H chondrites. This range is calculated from the production rates (for average chemical composition) of  $^3\text{He}$  and  $^{21}\text{Ne}$  suggested by Eugster (1988) for average chemical composition as well as shielding depth. As production of  $^3\text{He}_c$  is less sensitive to chemical variation, the observed depletion in  $(^3\text{He}/^{21}\text{Ne})_c$  values can be either due to loss of  $^3\text{He}_c$  or higher concentration of  $^{21}\text{Ne}_c$ . However as evident in figure, except a few, most chondrules have similar or lower  $^{21}\text{Ne}_c$  and still their  $(^3\text{He}/^{21}\text{Ne})_c$  is lower compared to bulk and expected H-chondrite range. This clearly indicates loss of  $^3\text{He}_c$  from these chondrules compared to bulk. Loss of  $^{21}\text{Ne}_c$  from chondrules is not significant as  $^{21}\text{Ne}/^{38}\text{Ar}$  ratio of chondrules is higher compared to bulk (Fig. 3.1b). In case of diffusive loss,  $^{21}\text{Ne}_c$  is expected to be lost more easily than  $^{38}\text{Ar}_c$ . Hence, higher than bulk values of  $(^{21}\text{Ne}/^{38}\text{Ar})_c$  are clearly due to differences in chemical composition. Either high Mg and low Ca or a combination of both can explain higher values of  $(^{21}\text{Ne}/^{38}\text{Ar})_c$ . Above all, the variation observed in abundances of  $^{21}\text{Ne}_c$  and  $^{38}\text{Ar}_c$  seems to relate with different chemical composition of chondrules whereas  $^3\text{He}_c$  is clearly affected by loss most probably due to diffusion.

**Table 3.2**  $^3\text{He}_c$ ,  $^{21}\text{Ne}_c$ ,  $^{38}\text{Ar}_c$  and radiogenic  $^4\text{He}_r$ ,  $^{40}\text{Ar}_r$  of chondrules from ordinary chondrites. Elemental ratios ( $^3\text{He}/^{21}\text{Ne}$ )<sub>c</sub>, ( $^{21}\text{Ne}/^{38}\text{Ar}$ )<sub>c</sub>, ( $^4\text{He}/^{40}\text{Ar}$ )<sub>r</sub> as well as gas retention ages ( $T_4$  and  $T_{40}$ ) based on  $^4\text{He}$  and  $^{40}\text{Ar}$  are also given. Concentrations are given in units of  $10^{-8} \text{ cm}^3\text{STP/g}$ .

Sample	$^3\text{He}_c$	$^{21}\text{Ne}_c$	$^{38}\text{Ar}_c$	( $^3\text{He}/^{21}\text{Ne}$ ) <sub>c</sub>	( $^{21}\text{Ne}/^{38}\text{Ar}$ ) <sub>c</sub>	$^4\text{He}_r$	$^{40}\text{Ar}_r$	( $^4\text{He}/^{40}\text{Ar}$ ) <sub>r</sub>	$T_4$	$T_{40}$
<b>Dhajala (H3.8)</b>										
<b>DH-8</b>	4.96 ±0.67	1.75 ±0.45	0.12 ±0.02	2.83 ±0.82	14.3 ±3.7	64391	13153	4.90	-	-
<b>DH-2</b>	4.92 .64	1.59 .16	0.11 .02	3.14 .52	16.2 2.3	1408	1310	1.32	3.14	4.02
<b>DH-9</b>	5.71 .75	1.90 .20	0.20 .03	3.00 .51	9.54 1.73	1067	1754	0.61	2.38	2.46
<b>DH-5</b>	2.49 .33	2.38 .29	0.43 .06	1.05 .19	5.53 1.41	987	6174	0.16	2.20	3.96
<b>DH-11</b>	1.99 .24	1.57 .26	0.16 .02	1.26 .26	10.1 1.9	13990	6129	2.28	-	-
<b>DH-V35</b>	1.38 .18	0.84 .10	0.04 .01	1.63 .29	23.8 3.0	401	920	0.44	0.89	1.42
<b>DH-V30</b>	2.07 .27	1.90 .20	0.13 .02	1.09 .18	14.6 2.1	784	1906	0.41	1.75	2.24
<b>DH-V7</b>	2.59 .34	2.00 .21	0.13 .02	1.29 .22	15.7 2.2	1449	438	3.30	3.23	0.81
<b>DH-NO25</b>	1.49 .20	1.58 .16	0.06 .01	0.94 .16	24.8 3.2	478	531	0.90	1.06	0.95
<b>DH-V18</b>	1.78 .23	1.16 .12	0.05 .01	1.53 .26	23.2 3.0	594	3297	0.18	1.32	3.00
<b>DH-V38</b>	0.18 .02	1.64 .18	0.10 .02	0.11 .02	16.2 2.2	86	161	0.53	0.19	0.34
<b>DH-V11</b>	1.50 .20	2.00 .21	0.08 .01	0.75 .13	25.3 3.0	391	3930	0.10	0.87	3.26
<b>DH-S8</b>	6.39 .84	3.35 .38	0.25 .05	1.91 .33	13.6 2.8	1728	12900	0.13	3.85	-

Sample	$^3\text{He}_c$	$^{21}\text{Ne}_c$	$^{38}\text{Ar}_c$	$(^3\text{He}/^{21}\text{Ne})_c$	$(^{21}\text{Ne}/^{38}\text{Ar})_c$	$^4\text{He}_r$	$^{40}\text{Ar}_r$	$(^4\text{He}/^{40}\text{Ar})_r$	$T_4$	$T_{40}$
<b>DH-S11</b>	5.67	1.67	0.27	3.39	6.21	1580	2291	0.69	3.52	2.49
	.74	.21	.04	.62	1.46					
<b>DH-S18</b>	5.71	2.42	0.35	2.36	6.84	2060	19104	0.11	-	-
	.75	.32	.06	.44	1.59					
<b>DH-S19</b>	1.36	2.42	0.44	0.56	5.52	2523	13828	0.18	-	-
	.18	.29	.07	.10	1.43					
<b>DH-S24</b>	2.63	1.57	0.14	1.68	11.2	696	2006	0.35	1.55	2.31
	.34	.23	.02	.33	1.92					
<b>DH-S1</b>	4.26	1.28	0.13	3.33	9.94	854	1278	0.67	1.90	1.76
	.56	.13	.02	.56	1.77					
<b>DH-S23</b>	4.16	1.75	0.26	2.38	6.77	807	9367	0.09	1.80	4.65
	.55	.18	.04	.40	1.61					
<b>DH-S27</b>	3.80	2.91	0.27	1.31	10.8	875	935	0.94	1.95	1.43
	.50	.31	.04	.22	1.8					
<b>DH-S28</b>	5.61	2.17	0.28	2.59	7.64	1681	2010	0.84	3.74	2.31
	.74	.23	.04	.43	1.64					
<b>DH</b>	6.04	1.84	0.27	3.29	6.70	1309	7032	0.19	2.92	4.58
<b>(bulk)</b>	.73	.19	.04	.52	1.63					
<b>Bjurböle (L/LL4)</b>										
<b>BB-26</b>	10.4	2.81	0.31	3.71	8.95	1378	4328	0.32	2.88	3.85
	1.4	.28	.04	.61	1.47					
<b>BB-25</b>	7.14	2.67	0.62	2.67	4.31	1879	7242	0.26	3.93	4.69
	.93	.29	.09	.45	.79					
<b>BB-18</b>	7.75	3.32	0.50	2.34	6.67	4850	2321	2.09	-	2.90
	1.16	.37	.06	.44	1.06					
<b>BB-28</b>	9.32	2.35	0.34	3.96	7.00	1026	2376	0.43	3.42	2.93
	1.20	.25	.06	.66	1.54					
<b>BB-15</b>	10.7	2.98	0.33	3.59	8.98	944	3384	0.28	1.97	3.46
	1.4	.30	.04	.59	1.47					
<b>BB<sup>#</sup></b>	15.2	4.62	0.41	3.29	11.2	1912	7207	0.27	-	4.63
<b>(chonds.)</b>	.5	.14	.05	.14	1.4					
<b>BB<sup>#</sup></b>	13.8	4.01	0.34	3.44	11.9	1523	7794	0.20	-	4.76
<b>(matrix)</b>	.4	.13	.05	.16	1.9					

Sample	$^3\text{He}_c$	$^{21}\text{Ne}_c$	$^{38}\text{Ar}_c$	$(^3\text{He}/^{21}\text{Ne})_c$	$(^{21}\text{Ne}/^{38}\text{Ar})_c$	$^4\text{He}_r$	$^{40}\text{Ar}_r$	$(^4\text{He}/^{40}\text{Ar})_r$	$T_4$	$T_{40}$
<b>BB*</b>	-	3.76	0.49	-	7.67	-	5430	-	-	4.21
(matrix)										
<b>Tieschitz (H3.6)</b>										
<b>TCZ-8</b>	18.0	4.38	0.58	4.12	7.61	745	973	0.77	1.66	1.84
	2.7	.47	.09	.70	1.40					
<b>TCZ-9</b>	14.8	2.23	0.90	6.62	2.48	204	3761	0.05	0.45	3.72
	1.9	.25	.13	1.15	.47					
<b>TCZ-5</b>	18.5	3.67	0.64	5.04	5.70	632	1324	0.48	2.22	1.41
	2.4	.37	.12	.83	1.22					
<b>TCZ-2</b>	23.0	5.31	0.85	4.31	6.28	1382	1082	1.28	3.08	1.55
	3.0	.55	.17	.72	1.40					
<b>TCZ-1</b>	13.2	2.77	0.98	4.78	2.81	562	1935	0.29	1.25	2.73
	1.7	.45	.15	1.00	.62					
<b>TCZ (bulk)</b>	41.6	7.04	1.20	5.90	5.84	2269	2249	1.01	-	3.94
	5.4	.71	.18	.98	1.06					
<b>Udaipur (H3)</b>										
<b>UD-1</b>	19.0	3.45	0.78	5.51	4.43	654	3673	0.18	1.46	3.69
	2.5	.35	.12	.91	.80					
<b>UD-2</b>	18.1	3.96	1.04	4.58	3.81	862	43177	0.02	1.92	-
	2.4	.43	.16	.78	.70					
<b>UD-3</b>	7.25	4.09	0.93	1.77	4.41	266	8139	0.03	0.59	-
	.95	.46	.14	.31	.82					
<b>UDP (bulk)</b>	43.0	6.87	0.55	6.27	12.4	1474	3179	0.46	3.28	3.46
	5.2	.69	.08	.98	2.2					
<b>Saratov (L4)</b>										
<b>STV-2</b>	12.6	3.18	0.60	4.16	5.45	1004	9018	0.11	2.10	4.57
	1.7	.33	.10	.70	1.08					
<b>STV-6</b>	14.2	4.53	0.46	3.14	9.88	836	4735	0.18	1.75	3.55
	1.9	.46	.06	.52	1.69					

Sample	$^3\text{He}_c$	$^{21}\text{Ne}_c$	$^{38}\text{Ar}_c$	$(^3\text{He}/^{21}\text{Ne})_c$	$(^{21}\text{Ne}/^{38}\text{Ar})_c$	$^4\text{He}_r$	$^{40}\text{Ar}_r$	$(^4\text{He}/^{40}\text{Ar})_r$	$T_4$	$T_{40}$
<b>STV-3</b>	11.3	4.69	0.42	2.42	11.2	778	8753	0.09	2.59	4.53
	1.5	.47	.08	.40	2.4					
<b>STV-7</b>	6.88	2.90	0.48	2.38	6.04	380	2739	0.14	0.79	2.73
	.90	.34	.07	.42	1.15					
<b>STV (bulk)</b>	27.8	7.79	0.88	3.56	8.89	1736	6821	0.25	3.63	4.55
	3.6	.78	.13	.59	1.61					
<b>Chainpur (LL3.4)</b>										
<b>CH-1</b>	33.5	7.04	1.73	4.77	4.52	1408	1854	0.89	2.94	1.58
	4.4	.71	.28	.79	.90					
<b>CH-2</b>	30.4	8.41	1.57	3.62	5.36	1853	1708	1.08	3.88	1.54
	4.0	.84	.24	.60	.97					
<b>CH-3</b>	45.0	12.0	2.14	3.76	5.60	1992	3512	0.57	4.17	2.40
	5.9	1.2	.32	.62	1.01					
<b>Matrix (fine)</b>	21.0	8.16	0.75	2.57	10.9	2483	2472	1.00	-	2.94
	2.3	.85	.11	.39	2.0					
<b>Matrix (Coarse)</b>	17.5	8.40	1.09	2.09	7.72	2943	3009	0.98	-	3.23
	2.7	.82	.16	.39	1.38					

Errors in concentrations of  $^4\text{He}_r$  and  $^{40}\text{Ar}_r$  are  $\pm 10\%$ . Errors in gas retention ages are  $\pm 20\%$   
<sup>#</sup> Polnau et al., (2001), <sup>\*</sup> Fredriksson et al., (1985).

**Bjurböle (L/LL4):**  $^3\text{He}_c$  concentrations are from 7 to  $10 \times 10^{-8} \text{ cm}^3\text{STP/g}$  in nine chondrules analyzed from Bjurböle chondrite, which is a narrow range compared to other chondrules. As reported by Polnau et al (2001), Bjurböle chondrules show  $^3\text{He}_c$  concentration  $\sim 15.2 \times 10^{-8} \text{ cm}^3\text{STP/g}$  (value from bunch of chondrules analyzed together) whereas matrix material shows concentrations  $\sim 14 \times 10^{-8} \text{ cm}^3\text{STP/g}$  (also listed in Table 3.2). The concentrations observed in nine chondrules in this study are lower compared to the reported values (Polnau et al., 2001). The average of  $^3\text{He}_c$  of these nine chondrules is  $8.9 \times 10^{-8} \text{ cm}^3\text{STP/g}$ .

$^{21}\text{Ne}_c$  in these chondrules is from 2 to  $4 \times 10^{-8} \text{ cm}^3\text{STP/g}$  with average  $^{21}\text{Ne}_c$  around  $2.7 \times 10^{-8} \text{ cm}^3\text{STP/g}$ . This average value is lower by factor of 2 compared to concentrations of Bjurböle chondrules ( $4.6 \times 10^{-8} \text{ cm}^3\text{STP/g}$ , value from bunch of chondrules analyzed together) and Bjurböle matrix ( $4.0 \times 10^{-8} \text{ cm}^3\text{STP/g}$ ) as reported by Polnau et al. (2001). The range observed for  $^{21}\text{Ne}_c$  includes the earlier value of  $^{21}\text{Ne}_c$  reported for Bjurböle matrix by Fredriksson et al. (1985).

$^{38}\text{Ar}_c$  in Bjurböle chondrules ranges from 0.3 to  $0.8 \times 10^{-8} \text{ cm}^3\text{STP/g}$ . Chondrule BB-29 shows highest concentration of  $^{38}\text{Ar}$  compared to all other chondrules. Average concentration of  $^{38}\text{Ar}_c$  in chondrules is  $0.46 \times 10^{-8} \text{ cm}^3\text{STP/g}$ . Unlike concentrations of  $^3\text{He}_c$  and  $^{21}\text{Ne}_c$ , average concentration of  $^{38}\text{Ar}_c$  is similar to values ( $0.4 \times 10^{-8} \text{ cm}^3\text{STP/g}$ ) reported by Polnau et al. (2001) as well as ( $0.4 \times 10^{-8} \text{ cm}^3\text{STP/g}$ ) reported by Fredriksson et al. (1985).

In Fig. 3.2,  $(^3\text{He}/^{21}\text{Ne})_c$  and  $(^{21}\text{Ne}/^{38}\text{Ar})_c$  of chondrules are plotted with abundances of  $^{21}\text{Ne}_c$ . In Fig. 3.2a, it is clearly seen that a few chondrules have higher values of  $(^3\text{He}/^{21}\text{Ne})_c$  compared to range observed in matrix by Polnau et al. (2001). As mentioned above  $^{21}\text{Ne}_c$  of chondrules are lower compared to matrix. The specific chemistry of these chondrules may be reason for lower  $^{21}\text{Ne}_c$ . Four chondrules show lower  $(^3\text{He}/^{21}\text{Ne})_c$  values. As the abundances of  $^{21}\text{Ne}_c$  in these chondrules are similar to other chondrules, it can be argued that lower value of  $(^3\text{He}/^{21}\text{Ne})_c$  is an evidence of higher loss of  $^3\text{He}_c$  (Fig. 3.2a) from these chondrules compared to other chondrules.  $(^3\text{He}/^{21}\text{Ne})_c$  observed in bunch of chondrules by Polnau et al. (2001) is slightly lower compared to range observed in matrix. Chondrules from this work show lower or higher values compared to value observed in bunch of chondrules. Average value of  $(^3\text{He}/^{21}\text{Ne})_c$  from our chondrules also falls in hatched region (Fig. 3.2). It is possible that individual chondrule has different  $(^3\text{He}/^{21}\text{Ne})_c$  depending on variation in their chemical composition and/or differential loss of  $^3\text{He}_c$  from these chondrules.

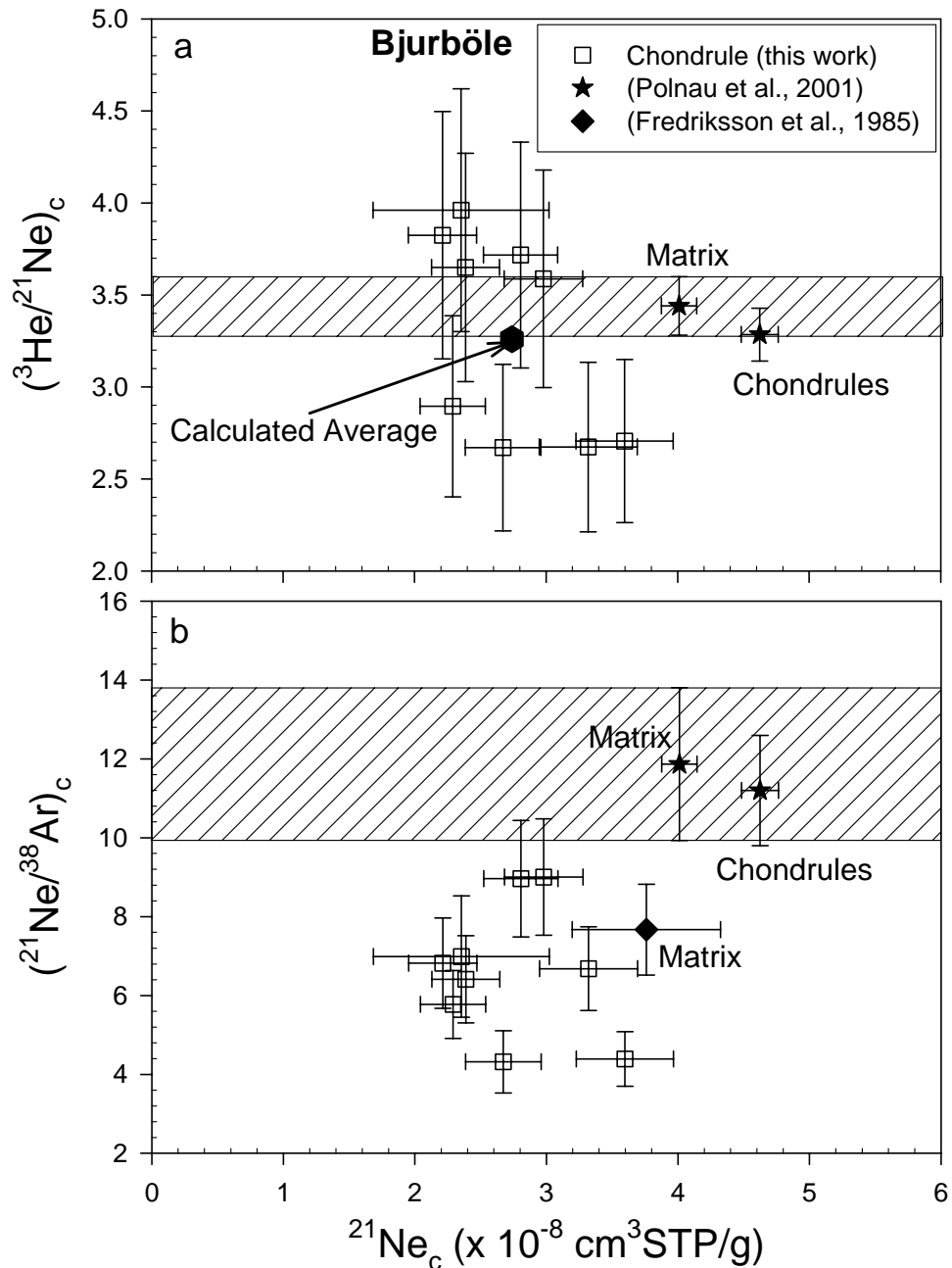


**Fig. 3.2** Elemental ratios  $(^3\text{He}/^{21}\text{Ne})_c$  and  $(^{21}\text{Ne}/^{38}\text{Ar})_c$  plotted with concentrations of  $^{21}\text{Ne}_c$  for chondrules from Bjurböle chondrite (a) Chondrules show higher values of  $(^3\text{He}/^{21}\text{Ne})_c$  compared to reported range in Bjurböle matrix (b) lower values of  $(^{21}\text{Ne}/^{38}\text{Ar})_c$  observed in chondrules. For comparison, values of chondrules and matrix are also plotted from Polnau et al., (2001). Value reported for matrix by Fredriksson et al., (1985) is also given in (b). Average calculated based on data from this work show value of  $(^3\text{He}/^{21}\text{Ne})_c$  similar to value reported for bunch of chondrules.

However, when  $(^3\text{He}/^{21}\text{Ne})_c$  seen in bunch of chondrules (or average of individual chondrules) it falls within the expected range.

All the chondrules show lower value of  $(^{21}\text{Ne}/^{38}\text{Ar})_c$  compared to matrix and average chondrule range which is mainly due to lower concentration of  $^{21}\text{Ne}_c$  in these

chondrules as mentioned above, the abundance of  $^{38}\text{Ar}_c$  in chondrules are similar to values reported by Polnau et al. (2001). Values reported by Fredriksson et al. (1985) fall within the range observed for chondrules.

#### **Chondrules from Tieschitz, Udaipur, Saratov and Chainpur chondrites:**

16 chondrules are analyzed from four different ordinary chondrites. In case of Tieschitz chondrite, five chondrules are analyzed. As listed in Table 3.2, all chondrules show lower  $^3\text{He}_c$  ( $13$  to  $23 \times 10^{-8} \text{ cm}^3\text{STP/g}$ ) compared to that of Tieschitz bulk ( $42 \times 10^{-8} \text{ cm}^3\text{STP/g}$ ).  $^{21}\text{Ne}_c$  in chondrules is also less than Tieschitz bulk and ranging from  $2$  to  $5 \times 10^{-8} \text{ cm}^3\text{STP/g}$ ; compared to  $7 \times 10^{-8} \text{ cm}^3\text{STP/g}$  of  $^{21}\text{Ne}_c$  in bulk.  $^{38}\text{Ar}_c$  in Tieschitz bulk is  $1.2 \times 10^{-8} \text{ cm}^3\text{STP/g}$ . Similar to  $^3\text{He}_c$  and  $^{21}\text{Ne}_c$ , abundances of  $^{38}\text{Ar}_c$  in chondrules is lower compared to bulk chondrite ranging from  $0.14$  to  $1 \times 10^{-8} \text{ cm}^3\text{STP/g}$  (Table 3.2).

$^3\text{He}_c$  in Udaipur chondrite is  $43 \times 10^{-8} \text{ cm}^3\text{STP/g}$ .  $^3\text{He}_c$  in chondrules is depleted.  $^3\text{He}_c$  in chondrule UD-3 ( $\sim 7 \times 10^{-8} \text{ cm}^3\text{STP/g}$ ) is lower by factor of 6 compared to bulk. This chondrule is smallest ( $0.25 \text{ mg}$ ) compared to other two chondrules (UD-1 =  $1.42 \text{ mg}$  and UD-2 =  $0.8 \text{ mg}$ ). Three chondrules show  $^{21}\text{Ne}_c$  ( $\sim 3.5$  to  $4 \times 10^{-8} \text{ cm}^3\text{STP/g}$ ) compared to  $7 \times 10^{-8} \text{ cm}^3\text{STP/g}$  of  $^{21}\text{Ne}_c$  in bulk Udaipur whereas unlike the cases of  $^3\text{He}_c$  and  $^{21}\text{Ne}_c$ , bulk sample shows lower  $^{38}\text{Ar}_c$  ( $0.55 \times 10^{-8} \text{ cm}^3\text{STP/g}$ ) compared to three chondrules in which  $^{38}\text{Ar}_c$  ranges from  $0.8$  to  $1 \times 10^{-8} \text{ cm}^3\text{STP/g}$ .

$^3\text{He}_c$  in four chondrules from Saratov chondrite ranges from  $7$  to  $14 \times 10^{-8} \text{ cm}^3\text{STP/g}$  and falling short of concentration ( $\sim 28 \times 10^{-8} \text{ cm}^3\text{STP/g}$ ) observed in Saratov bulk (Table 3.2). It is observed that  $^{21}\text{Ne}_c$  in bulk Saratov is  $\sim 8 \times 10^{-8} \text{ cm}^3\text{STP/g}$ . On the other hand, chondrules show  $^{21}\text{Ne}_c$  from  $2.4$  to  $4.7 \times 10^{-8} \text{ cm}^3\text{STP/g}$ . All chondrules show lower  $^{38}\text{Ar}_c$  compared to Saratov bulk and values range from  $0.4$  to  $0.8 \times 10^{-8} \text{ cm}^3\text{STP/g}$  compared to  $0.9 \times 10^{-8} \text{ cm}^3\text{STP/g}$  of  $^{38}\text{Ar}_c$  in Saratov bulk (Table 3.2). Together with fine ( $< 100\mu\text{m}$ ) and coarse-grained ( $100\text{-}200\mu\text{m}$ ) matrix samples, three individual chondrules have been analyzed from Chainpur chondrite. In chondrules,  $^3\text{He}_c$  ranges from  $30$  to  $45 \times 10^{-8} \text{ cm}^3\text{STP/g}$ , whereas both fine and coarse matrix of show lower  $^3\text{He}_c$ ,  $21 \times 10^{-8} \text{ cm}^3\text{STP/g}$  and  $17 \times 10^{-8} \text{ cm}^3\text{STP/g}$  respectively (Table 3.2). The chondrule CH-3 shows highest  $^3\text{He}_c$  ( $45 \times 10^{-8} \text{ cm}^3\text{STP/g}$ ) compared to other two chondrules. All chondrules show higher  $^3\text{He}_c$  compared to matrix.  $^{21}\text{Ne}_c$  in matrix samples (fine and coarse-grained) is  $\sim 8 \times 10^{-8} \text{ cm}^3\text{STP/g}$ . The three chondrules except CH-3 show similar  $^{21}\text{Ne}_c$ . Chondrule CH-3 shows  $12 \times 10^{-8} \text{ cm}^3\text{STP/g}$ , which is  $\sim 50\%$

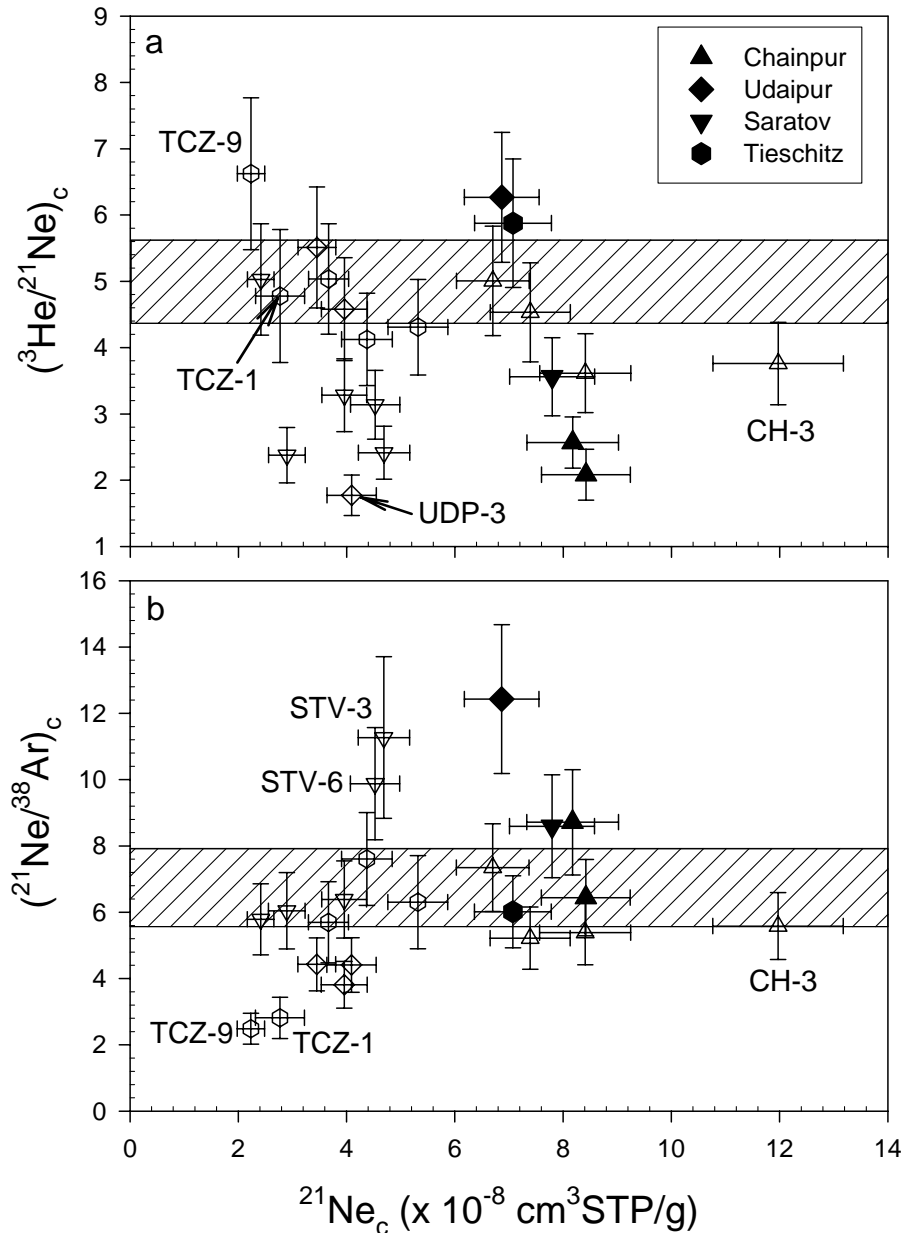


**Fig. 3.3** Elemental ratios  $(^3\text{He}/^{21}\text{Ne})_c$  and  $(^{21}\text{Ne}/^{38}\text{Ar})_c$  plotted against concentrations of  $^{21}\text{Ne}_c$  for chondrules from four ordinary chondrites. The hatched bars show the range of these elemental ratios calculated based on production rates given by Eugster (1988). (a) most chondrules show similar or lower  $(^3\text{He}/^{21}\text{Ne})_c$  values compared to expected range (b) Two chondrules from Saratov show higher values of  $(^{21}\text{Ne}/^{38}\text{Ar})_c$  suggesting different chemical composition of these chondrules. Symbol: open – for chondrules, filled – for bulk chondrites

higher compared to other two chondrules and matrix samples (Fig 3.3a). Chondrule CH-3 shows  $2.15 \times 10^{-8} \text{ cm}^3 \text{STP/g } ^{38}\text{Ar}_c$  highest among all three chondrules whereas matrix materials (fine and coarse-grained) show  $^{38}\text{Ar}_c$  ( $0.7 \times 10^{-8} \text{ cm}^3 \text{STP/g}$  and  $1 \times 10^{-8} \text{ cm}^3 \text{STP/g}$  respectively).  $^{38}\text{Ar}_c$  in chondrules CH-1, CH-2 is comparable to matrix materials.

In Fig. 3.3, elemental ratios  $(^3\text{He}/^{21}\text{Ne})_c$  and  $(^{21}\text{Ne}/^{38}\text{Ar})_c$  of chondrules and bulk are plotted with concentrations of  $^{21}\text{Ne}_c$  for Tieschitz, Udaipur, Saratov and Chainpur chondrites. The hatched areas in this plot represents range of  $(^3\text{He}/^{21}\text{Ne})_c$  and  $(^{21}\text{Ne}/^{38}\text{Ar})_c$  in ordinary chondrites calculated based on production rates (suggested for average chemical composition) of  $^3\text{He}$ ,  $^{21}\text{Ne}$  and  $^{38}\text{Ar}$  (Eugster, 1988) for ordinary chondrites.

In case of Tieschitz, except chondrule TCZ-9, all chondrules show lower values of  $(^3\text{He}/^{21}\text{Ne})_c$  compared to bulk suggesting loss of  $^3\text{He}_c$ . As seen in Fig. 3.2b, most chondrules except TCZ-1 and TCZ-9 show values of  $(^{21}\text{Ne}/^{38}\text{Ar})_c$  similar to Tieschitz bulk and ordinary chondrites. Higher value of  $(^3\text{He}/^{21}\text{Ne})_c$  in TCZ-9 chondrule is due to lower abundance of  $^{21}\text{Ne}$  in this chondrule. This is also reflected in lowest value of  $(^{21}\text{Ne}/^{38}\text{Ar})_c$  in this chondrule. In case of loss by diffusion, loss of  $^3\text{He}_c$  can be easier than  $^{21}\text{Ne}_c$ . However, for TCZ-9 chondrule, the observation is opposite. This suggests different chemical composition (Mg- poor) of this chondrule compared to other chondrules.

In case of Udaipur,  $(^3\text{He}/^{21}\text{Ne})_c$  of chondrule UD-3 is lowest because of lower  $^3\text{He}_c$ . Values of  $(^3\text{He}/^{21}\text{Ne})_c$  is varying according to sizes of the chondrules (Table 3.2) and indicate that loss of  $^3\text{He}_c$  from these chondrules is related to size ( $\sim$ mass) as expected in case of loss by diffusion.  $(^{21}\text{Ne}/^{38}\text{Ar})_c$  of chondrules shows fewer differences however, the values are lower compared to bulk and expected range of ordinary chondrite. High value of (highest among all the chondrites in plot)  $(^{21}\text{Ne}/^{38}\text{Ar})_c$  for Udaipur bulk is related with lower abundance of  $^{38}\text{Ar}$  in this chondrite probably due to Ca-poor composition.

Chondrules and bulk from Saratov show lower  $(^3\text{He}/^{21}\text{Ne})_c$  compared to expected range of ordinary chondrites. Chondrules are mostly depleted compared to bulk in  $(^3\text{He}/^{21}\text{Ne})_c$  suggesting loss of  $^3\text{He}$  from these chondrules.  $(^{21}\text{Ne}/^{38}\text{Ar})_c$  values of two chondrules (STV-3 and STV-6) are higher than bulk as well as expected range of ordinary chondrites which can be only explained by different chemical composition of these chondrules. Other three chondrules show lower values compared to bulk.

In case of Chainpur,  $(^3\text{He}/^{21}\text{Ne})_c$  of chondrules and matrix materials are lower compared to expected range of ordinary chondrites. Matrix of Chainpur is more depleted in these values compared to chondrules, suggesting higher loss of  $^3\text{He}$  from matrix.  $(^{21}\text{Ne}/^{38}\text{Ar})_c$  values of chondrules and matrix are similar to expected range of ordinary chondrites. Chondrule CH-3 shows  $(^3\text{He}/^{21}\text{Ne})_c$  and  $(^{21}\text{Ne}/^{38}\text{Ar})_c$  within the

range expected for ordinary chondrites. Most probably, in the case of Chainpur, where the chondrule sizes are large (0.8 to 1.6 mm in diameter), the loss of cosmogenic gases is more prominent in the matrix (fine grained <100 $\mu$ m, coarse grained (100-200 $\mu$ m) samples.

### 3.3.1.2 Chondrules from enstatite chondrites

**Parsa (EH3):** Three chondrules analyzed from Parsa chondrite show slightly higher concentrations of  $^3\text{He}_c$  (29 to 40  $\times 10^{-8}$  cm<sup>3</sup>STP/g) compared to bulk Parsa ( $\sim 29 \times 10^{-8}$  cm<sup>3</sup>STP/g). Except Parsa-1 chondrule, all chondrules show  $^{21}\text{Ne}_c$  similar to Parsa bulk ( $\sim 6 \times 10^{-8}$  cm<sup>3</sup>STP/g). The splits analyzed for Parsa-3 chondrules show similar  $^{21}\text{Ne}_c$  that is slightly lower compared to bulk chondrite (as can be seen in Table 3.3). Chondrules show  $^{38}\text{Ar}_c$  within 0.19 to 0.36  $\times 10^{-8}$  cm<sup>3</sup>STP/g, which is less compared to bulk Parsa (0.56  $\times 10^{-8}$  cm<sup>3</sup>STP/g) as can be seen in Table 3.3. Among all four samples, Parsa-1 chondrule shows slightly higher  $^{38}\text{Ar}_c$  compared to other chondrules. In Fig. 3.4,  $(^3\text{He}/^{21}\text{Ne})_c$  and  $(^{21}\text{Ne}/^{38}\text{Ar})_c$  values of Parsa and Qingzhen chondrules and bulk are plotted with  $^{21}\text{Ne}_c$ . Parsa chondrules and bulk show values of  $(^3\text{He}/^{21}\text{Ne})_c$  that fall in the range observed for bulk (Fig 3.4a).  $(^{21}\text{Ne}/^{38}\text{Ar})_c$  of chondrules are higher by factor of two compared to Parsa bulk (Fig. 3.4b). This can be explained by different chemical composition (resulting in less production of  $^{38}\text{Ar}_c$  in chondrules compared to bulk) of chondrules, or preferential loss of  $^{38}\text{Ar}_c$  compared to  $^{21}\text{Ne}_c$ . Patzer et al. (2001) have demonstrated the vulnerability of Ca rich phases (e.g. oldhamite-CaS) to water. Weathering of these phases results in preferential loss of  $^{38}\text{Ar}_c$  over  $^{21}\text{Ne}_c$  as Ne is mainly produced from Mg, which is generally found in minerals resistant to water leaching.

**Qingzhen (EH3):** Four chondrules are analyzed from Qingzhen chondrite, two of which QZN-3 and QZN-5 are small and we could not measure Helium in these samples. The other two chondrules show  $^3\text{He}_c$  of 0.25 and 0.82  $\times 10^{-8}$  cm<sup>3</sup>STP/g, lower compared to  $^3\text{He}_c$  (2  $\times 10^{-8}$  cm<sup>3</sup>STP/g), in bulk Qingzhen chondrite. These values observed in chondrules and bulk Qingzhen chondrite, are in agreement with earlier reported values by Crabb and Anders (1982).

Chondrules show  $^{21}\text{Ne}_c$  concentration either lower or similar to bulk. For chondrule, Qzn-5 lowest  $^{21}\text{Ne}_c$  (1  $\times 10^{-8}$  cm<sup>3</sup>STP/g) is observed. In Fig. 3.4a, it is clearly seen that value of  $(^3\text{He}/^{21}\text{Ne})_c$  in chondrules is lower compared to bulk.  $(^3\text{He}/^{21}\text{Ne})_c$  observed in Qingzhen bulk is also lower compared to the range expected based on

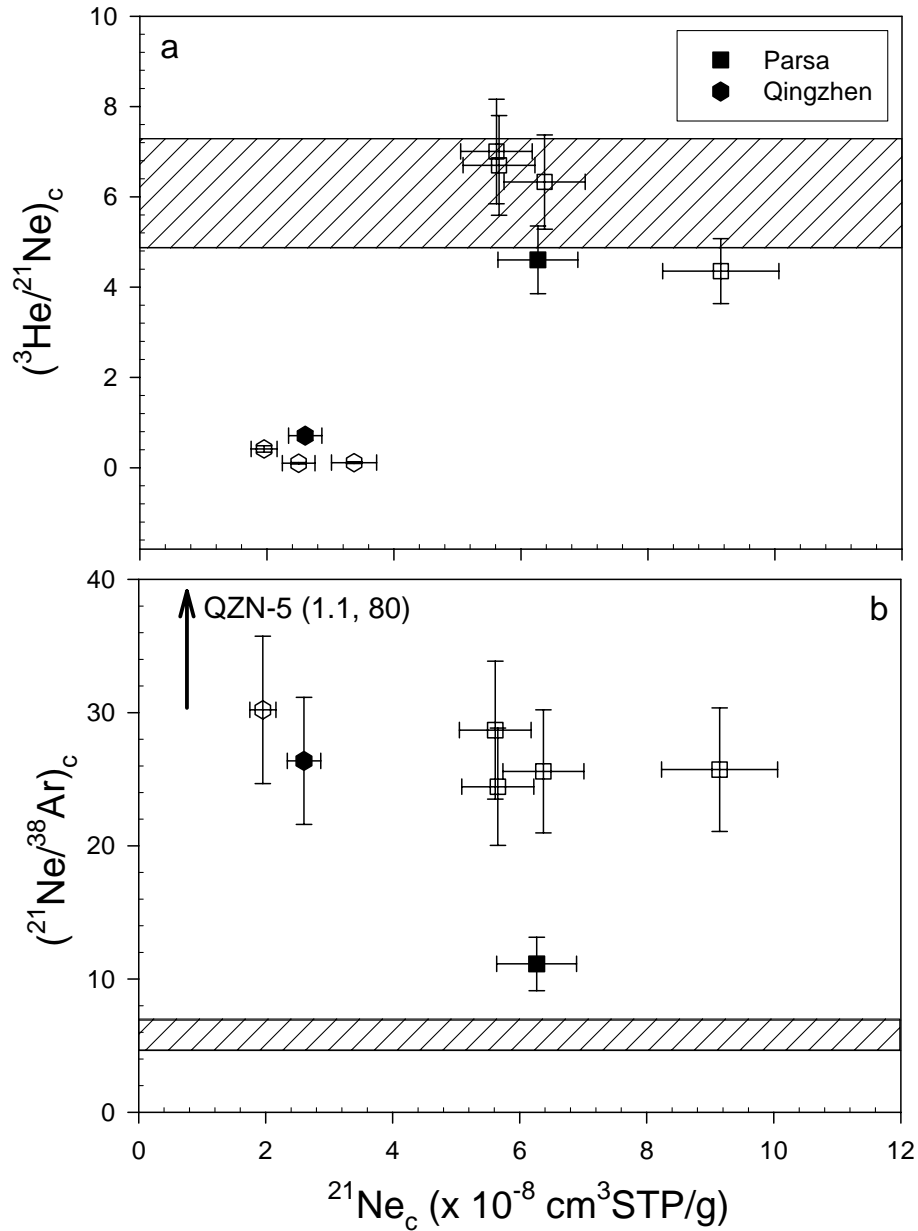


**Fig. 3.4** Elemental ratios  $(^3\text{He}/^{21}\text{Ne})_c$  and  $(^{21}\text{Ne}/^{38}\text{Ar})_c$  plotted with concentrations of  $^{21}\text{Ne}_c$  for Parsa and Qingzhen chondrites. Hatched regions in plot represent the expected ranges for  $(^3\text{He}/^{21}\text{Ne})_c$  and  $(^{21}\text{Ne}/^{38}\text{Ar})_c$  based on production rates suggested by Eugster (1988). **(a)** Parsa chondrites are similar to expected range, chondrules and bulk of Qingzhen show loss of  $^3\text{He}_c$ . **(b)** Values of  $(^{21}\text{Ne}/^{38}\text{Ar})_c$  are higher in both chondrites and their chondrules compared to expected range. Symbol: open – chondrules, filled – chondrites

production rates of  $^3\text{He}_c$  and  $^{21}\text{Ne}_c$  as suggested by Eugster (1988).  $(^3\text{He}/^{21}\text{Ne})_c$  value of Qingzhen bulk is similar to value reported by Patzer and Schultz (2001). In this case, loss of  $^3\text{He}_c$  is evident in bulk (more in chondrules).

**Neutron produced  $^{36}\text{Ar}$  in Qingzhen:**

In chondrules of Qingzhen, it is observed that measured  $(^{38}\text{Ar}/^{36}\text{Ar})$  is less than 0.188 usually taken as ratio of  $^{38}\text{Ar}/^{36}\text{Ar}$  for trapped Ar component. The lower value of

$^{38}\text{Ar}/^{36}\text{Ar}$  in chondrules suggests the presence of a pure  $^{36}\text{Ar}$  component in these chondrules. It is possible to have cosmogenic  $^{36}\text{Ar}$  contribution, which can be produced by neutron-capture on  $^{35}\text{Cl}$  and subsequent  $\beta^-$  - decay ( $^{36}\text{Ar}_{\text{cl}}$ ). This contribution strongly depends on the preatmospheric size of the meteoroid and the shielding depth of the sample and generally negligible compared to  $^{36}\text{Ar}_{\text{t}}$  concentrations. However, it can severely affect the concentrations of  $^{38}\text{Ar}_{\text{c}}$  as calculation of  $^{38}\text{Ar}_{\text{c}}$  is based on assumptions that  $^{36}\text{Ar}$  has only two components: trapped Ar ( $^{38}\text{Ar}/^{36}\text{Ar} \sim 0.188$ ) and spallogenic Ar ( $^{38}\text{Ar}/^{36}\text{Ar} \sim 1.5$ ). Similar kind of  $^{38}\text{Ar}/^{36}\text{Ar}$  values are also reported by Crabb and Anders (1982) for their analyses of an ensemble of chondrules from Qingzhen chondrite. They also found higher concentrations of  $^{129}\text{Xe}_{\text{r}}$  in chondrules compared to bulk. Independently Grossmann et al. (1985) reported higher content of Cl in chondrules of Qingzhen compared to bulk. As discussed later in this chapter calculated  $^{129}\text{Xe}_{\text{r}}$  in these chondrules are higher than Qingzhen bulk. Based on these evidences, we suggest that chondrules from Qingzhen have higher content of halogens compared to bulk chondrite. Due to higher concentrations of Cl,  $^{36}\text{Ar}$  produced by neutron-capture is more, which is responsible for lowering the measured  $^{38}\text{Ar}/^{36}\text{Ar}$  of chondrules. Although the recovered mass of Qingzhen is a single piece (2.6Kg, Eugster et al., 1992), the presence of  $^{36}\text{Ar}_{\text{cl}}$  suggests a preatmospheric size of radius  $>22\text{cm}$  (Eugster et al., 2002, Murty et al., 2004).

Although, we could calculate  $^{38}\text{Ar}_{\text{c}}$  in chondrules QZN-1 and QZN-5, the values are very low ( $\sim 0.01 \times 10^{-8} \text{ cm}^3\text{STP/g}$ ), compared to  $0.1 \times 10^{-8} \text{ cm}^3\text{STP/g}$  of  $^{38}\text{Ar}_{\text{c}}$  in Qingzhen bulk indicating effect of neutron-capture produced  $^{36}\text{Ar}$  in these chondrules, as well as partly due to loss of  $^{38}\text{Ar}_{\text{c}}$  from humidity prone CaS phase.  $(^{21}\text{Ne}/^{38}\text{Ar})_{\text{c}}$  value of QZN-5 is higher compared to bulk (not shown in Fig. 3.4b) which is due to low abundance of  $^{38}\text{Ar}_{\text{c}}$ . This cannot be attributed to different chemistry of this chondrule as the calculated  $^{38}\text{Ar}_{\text{c}}$  in this chondrule is seem to be affected by the presence of neutron capture produced  $^{36}\text{Ar}$ . QZN-1 chondrule however show similar value of  $(^{21}\text{Ne}/^{38}\text{Ar})_{\text{c}}$  when compared to bulk.

**Table 3.3**  $^3\text{He}_c$ ,  $^{21}\text{Ne}_c$ ,  $^{38}\text{Ar}_c$  and radiogenic  $^4\text{He}_r$ ,  $^{40}\text{Ar}_r$  of chondrules from enstatite chondrites. Elemental ratios ( $^3\text{He}/^{21}\text{Ne}$ )<sub>c</sub>, ( $^{21}\text{Ne}/^{38}\text{Ar}$ )<sub>c</sub>, ( $^4\text{He}/^{40}\text{Ar}$ )<sub>r</sub> as well as gas retention ages ( $T_4$  and  $T_{40}$ ) based on  $^4\text{He}$  and  $^{40}\text{Ar}$  are also given. Concentrations are given in units of  $10^{-8} \text{ cm}^3\text{STP/g}$ .

Sample	$^3\text{He}_c$	$^{21}\text{Ne}_c$	$^{38}\text{Ar}_c$	( $^3\text{He}/^{21}\text{Ne}$ ) <sub>c</sub>	( $^{21}\text{Ne}/^{38}\text{Ar}$ ) <sub>c</sub>	$^4\text{He}_r$	$^{40}\text{Ar}_r$	( $^4\text{He}/^{40}\text{Ar}$ ) <sub>r</sub>	$T_4$	$T_{40}$
<b>Parsa-1</b>	39.8	9.15	0.36	4.35	25.7	1141	2537	0.45	3.08	3.08
	5.2	.92	.05	0.72	4.6					
<b>Parsa-2</b>	40.3	6.37	0.25	6.33	25.6	1306	2503	0.52	3.52	3.06
	5.3	.64	.04	1.04	4.6					
<b>Parsa-3</b>	38.6	5.63	0.21	6.85	26.6	1356	2634	0.57	3.62	2.58
	5.1	.56	.03	1.13	4.8					
<b>Parsa (bulk)</b>	28.9	6.27	0.56	4.61	11.1	2298	1885	1.22	4.56	2.66
	3.7	.63	.08	0.75	2.0					
<b>QZN-1</b>	0.60	2.66	0.02	0.27	-	49	609	0.09	0.13	1.3
	.08	.28		.04						
<b>QZN-2</b>	0.25	2.50		0.10	-	0.43	1371	0.0003	0.001	2.23
	.03	.26		.02						
<b>QZN-3</b>	-	2.34		-	-	-	2821	-	-	3.24
		.27								
<b>QZN-5</b>	-	1.09	0.01	-	80.0	-	2402	-	-	3.00
		.14	.002		15.6					
<b>QZN (Bulk)</b>	1.99	2.60	0.10	0.76	24.9	5405	1298	4.16	4.56	3.32
	.26	.26	.02	.13	4.5					

Errors in concentrations of  $^4\text{He}_r$  and  $^{40}\text{Ar}_r$  are  $\pm 10\%$ . Errors in gas retention ages are  $\pm 20\%$

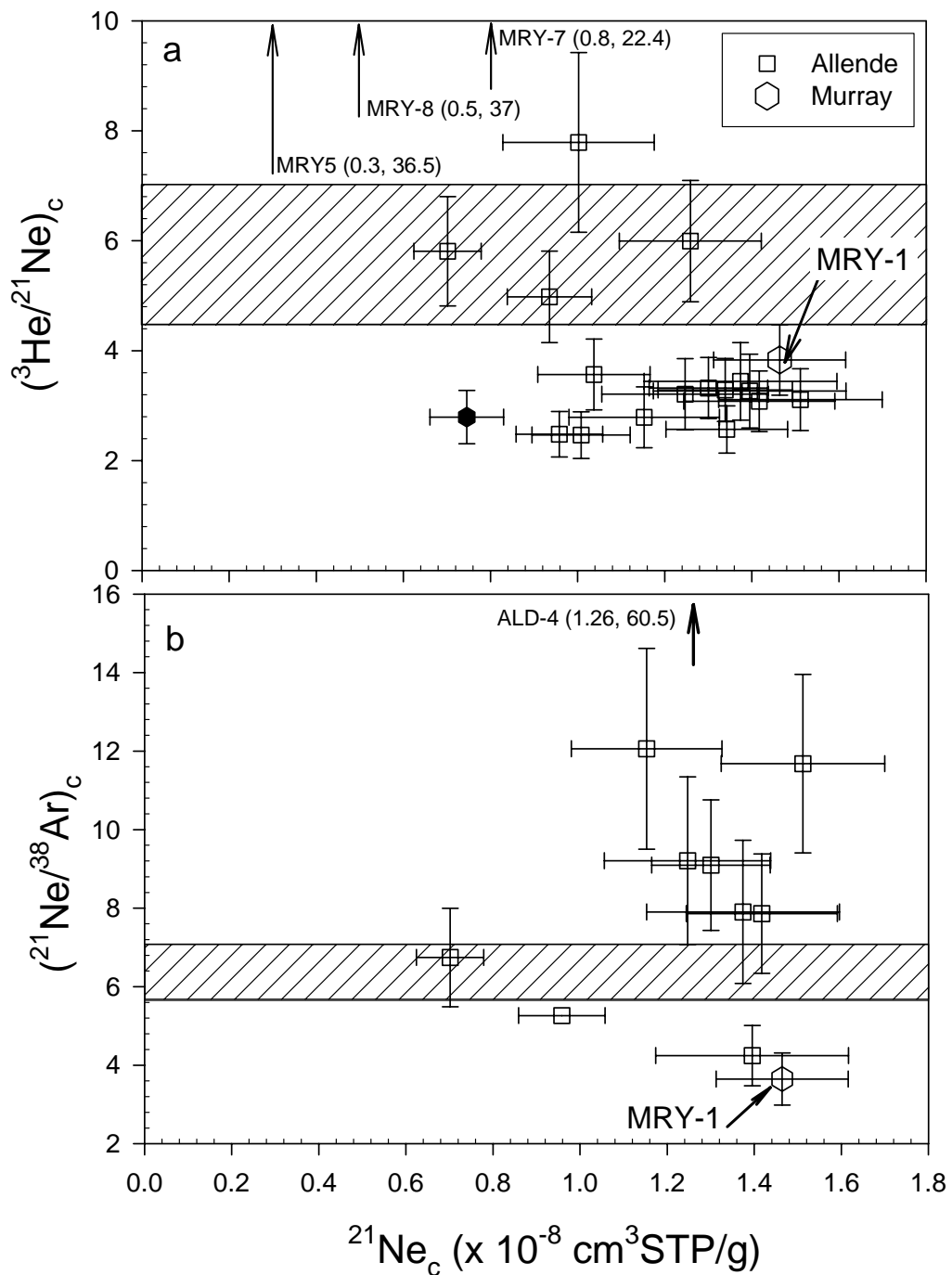


**Fig. 3.5** Elemental ratio  $(^3\text{He}/^{21}\text{Ne})_c$  and  $(^{21}\text{Ne}/^{38}\text{Ar})_c$  plotted with concentrations of  $^{21}\text{Ne}_c$  for chondrules of Allende and Murray chondrites (a) Most chondrules show loss of He compared to Ne. Chondrule MYR-1 shows higher concentration of  $^{21}\text{Ne}_c$  compared to bulk. (b) Most chondrules show higher value of  $(^{21}\text{Ne}/^{38}\text{Ar})_c$  which can be explained by different chemical composition of these chondrules. Symbol: open – for chondrules, filled – for bulk chondrites

### 3.3.1.3 Chondrules from carbonaceous chondrites

**Allende (CV3.2):**  $^3\text{He}_c$  in sixteen chondrules from Allende show a range from 1 to 7  $\times 10^{-8} \text{ cm}^3 \text{STP/g}$  with average concentration  $4 \times 10^{-8} \text{ cm}^3 \text{STP/g}$ .  $^{21}\text{Ne}_c$  in chondrules

from Allende chondrite ranges from  $0.7$  to  $1.5 \times 10^{-8}$   $\text{cm}^3\text{STP/g}$ . Chondrule ALD-11 shows lowest  $^{21}\text{Ne}_c$  compared to all chondrules in Allende (Table 3.4).

During the analysis of a set of six Allende chondrules, we had some technical problem, which resulted in imprecise Ar-data. For these chondrules, we could not get good  $^{38}\text{Ar}/^{36}\text{Ar}$  ratios and hence their cosmogenic  $^{38}\text{Ar}$  will not be discussed. For another ten samples, we observed that  $^{38}\text{Ar}_c$  varies from  $0.02$  to  $0.33 \times 10^{-8}$   $\text{cm}^3\text{STP/g}$ . However, most of the samples show a value around  $0.15 \times 10^{-8}$   $\text{cm}^3\text{STP/g}$  (Table 3.4). In Fig. 3.5,  $(^3\text{He}/^{21}\text{Ne})_c$  and  $(^{21}\text{Ne}/^{38}\text{Ar})_c$  values of Allende and Murray chondrules are plotted with  $^{21}\text{Ne}_c$ .  $(^3\text{He}/^{21}\text{Ne})_c$  values of Allende chondrules are lower compared to range expected for CV chondrites (shown by hatched region in plot) mainly due to loss of  $^3\text{He}_c$ .  $(^{21}\text{Ne}/^{38}\text{Ar})_c$  values for these chondrules mostly higher compared to expected range depending on chemical compositions in chondrules. The lowest concentration of  $^{38}\text{Ar}_c$  in chondrule ALD-4 is also reflected in highest value of  $(^{21}\text{Ne}/^{38}\text{Ar})_c$  (not shown in Fig. 3.5b).

**Murray (CM2):** Four chondrules analyzed from Murray chondrite show  $^3\text{He}_c$  higher by factor of 7 compared to bulk Murray. The  $^3\text{He}_c$  ranges from  $6$  to  $17 \times 10^{-8}$   $\text{cm}^3\text{STP/g}$  compared to  $2 \times 10^{-8}$   $\text{cm}^3\text{STP/g}$   $^3\text{He}_c$  in bulk chondrite (as can be seen in Table 3.4). The chondrule MRY-1, biggest among four chondrules, shows lowest  $^3\text{He}_c$ .

In contrast to this except MRY-1 chondrule, all the three chondrules show low  $^{21}\text{Ne}_c$  compared to Murray bulk. MRY-1 shows  $^{21}\text{Ne}_c$  twice compared to bulk (Table 3.4). We could not detect Ar in three smaller ( $60$  to  $80 \mu\text{g}$ ) samples except MRY-1. During analysis of Murray bulk we had some technical problem, which resulted in imprecise Ar-data hence, no Ar data can be discussed for Murray bulk.

$(^3\text{He}/^{21}\text{Ne})_c$  values of three chondrules (with higher  $^3\text{He}_c$ ) are higher by factor of 12 (not shown in plot). The other chondrule MRY-1 is similar or slightly higher compared to bulk may be due to different chemical composition.

**Table 3.4**  $^3\text{He}_c$ ,  $^{21}\text{Ne}_c$ ,  $^{38}\text{Ar}_c$  and radiogenic  $^4\text{He}_r$ ,  $^{40}\text{Ar}_r$  of chondrules from carbonaceous chondrites. Elemental ratios ( $^3\text{He}/^{21}\text{Ne}$ )<sub>c</sub>, ( $^{21}\text{Ne}/^{38}\text{Ar}$ )<sub>c</sub>, ( $^4\text{He}/^{40}\text{Ar}$ )<sub>r</sub> as well as gas retention ages ( $T_4$  and  $T_{40}$ ) based on  $^4\text{He}$  and  $^{40}\text{Ar}$  are also given. Concentrations are given in units of  $10^{-8} \text{ cm}^3\text{STP/g}$ .

Sample	$^3\text{He}_c$	$^{21}\text{Ne}_c$	$^{38}\text{Ar}_c$	( $^3\text{He}/^{21}\text{Ne}$ ) <sub>c</sub>	( $^{21}\text{Ne}/^{38}\text{Ar}$ ) <sub>c</sub>	$^4\text{He}_r$	$^{40}\text{Ar}_r$	( $^4\text{He}/^{40}\text{Ar}$ ) <sub>r</sub>	$T_4$	$T_{40}$
<b>Allende (CV3.2)</b>										
<b>ALD-1</b>	3.45	1.34	-	2.56	-	1630	-	2.56	-	-
	$\pm 0.45$	$\pm 0.14$		$\pm 0.43$				-		
<b>ALD-2</b>	4.66	0.94	-	4.97	-	1828	-	-	2.87	-
	.61	.10		.83						
<b>ALD-3</b>	2.48	1.01	-	2.46	-	2285	-	-	3.58	-
	.33	.11		.42						
<b>ALD-4</b>	7.55	1.26	0.02	5.99	60.5	1395	663	2.10	2.19	2.21
	.99	.16	.003	1.10	12.0					
<b>ALD-5</b>	2.38	0.96	0.18	2.48	5.26	1154	-	-	1.85	-
	.31	.10		.41						
<b>ALD-6</b>	4.40	1.34	0.04	3.28	36.4	1080	3306	0.33	1.69	4.62
	.58	.15	.01	.57	6.89					
<b>ALD-8</b>	3.70	1.04	-	3.56	-	701	-	-	1.10	-
	.48	.13		.64						
<b>ALD-9</b>	7.81	1.01	-	7.75	-	1277	-	-	2.00	-
	.93	.17		1.62						
<b>ALD-11</b>	4.08	0.70	0.10	5.81	6.74	974	2868	0.34	1.53	4.39
	.53	.08	.02	.99	1.25					
<b>ALD-12</b>	4.32	1.30	0.14	3.32	9.09	1538	4576	0.34	2.41	-
	.57	.14	.02	.56	1.66					
<b>ALD-13</b>	4.36	1.31	0.16	3.32	8.52	1234	642	1.92	1.94	2.17
	.56	.21	.03	.68	2.00					
<b>ALD-14</b>	4.55	1.37	0.33	3.33	4.16	2748	1050	2.62	4.31	2.83
	.60	.22	.03	.69	0.76					
<b>ALD-15</b>	4.53	1.47	0.16	3.09	9.67	1437	3628	0.40	2.10	4.77
	.59	.18	.02	.56	1.88					
<b>ALD-16</b>	3.21	1.15	0.10	2.78	12.0	649	2074	0.31	1.22	3.86
	.42	.17	.01	.55	2.5					

Sample	$^3\text{He}_c$	$^{21}\text{Ne}_c$	$^{38}\text{Ar}_c$	$(^3\text{He}/^{21}\text{Ne})_c$	$(^{21}\text{Ne}/^{38}\text{Ar})_c$	$^4\text{He}_r$	$^{40}\text{Ar}_r$	$(^4\text{He}/^{40}\text{Ar})_r$	$T_4$	$T_{40}$
<b>Murray (CM2)</b>										
<b>MRY-1B</b>	5.61	1.45	0.42	3.87	3.42	1554	157	9.89	3.98	0.67
	.73	.15	.06	.65	0.63					
<b>MRY-5</b>	11.8	0.32	-	36.5	-	329	-	-		
	1.5	.07		9.1						
<b>MRY-7</b>	17.2	0.77	-	22.4	-	1403	-	-		
	2.2	.12		4.6						
<b>MRY-8</b>	17.2	0.47	-	37.0	-	549	-	-		
	2.2	.07		7.4						
<b>Murray</b>	2.08	0.70	-	3.0	-	9321	-			
<b>(bulk)</b>	0.27	.08		.5						

Errors in concentrations of  $^4\text{He}_r$  and  $^{40}\text{Ar}_r$  are  $\pm 10\%$ . Errors in gas retention ages are  $\pm 20\%$

### ***3.3.2 Production rates ( $^3\text{He}$ , $^{21}\text{Ne}$ and $^{38}\text{Ar}$ ) and cosmic ray exposure age of chondrules:***

As discussed above, analyses of several chondrules from ordinary, enstatite and carbonaceous chondrites yielded variable amounts of cosmogenic noble gases compared to their respective bulk chondrite as well as among chondrules. For some cases, we found that chondrules are depleted in cosmogenic gases while for a few cases cosmogenic gases in chondrules are higher compared to bulk.

The higher or lower concentrations of cosmogenic gases in chondrules compared to their bulk chondrite can be due to one or a combination of the three reasons: **(a)** Loss of cosmogenic gases from the chondrules as well as bulk chondrites. **(b)** Higher cosmic ray fluence (time  $\times$  flux of cosmic rays) experienced by samples (especially when chondrules show higher concentration of cosmogenic gases) **(c)** Different production rates of these cosmogenic isotopes in chondrules and bulk chondrites. Production rates in turn depend on composition of target chemistry and shielding depth of the chondrules within the meteoroid.

#### ***(a) Loss of cosmogenic gases from the chondrules as well as bulk chondrites***

In a gas loss event (solar heating or collisional heating) during recent cosmic ray exposure, all the components (radiogenic, trapped and cosmogenic) can be lost to varying degrees. However, in a gas loss event on the parent body or during ejection of meteoroid, only radiogenic and trapped components will be lost (cosmogenic component is yet to be produced). Hence, if a sample shows expected cosmogenic component, but loss of trapped/radiogenic components, the gas loss must have occurred prior to the recent cosmic ray exposure and on parent body. In general, the retentivities of the various noble gas components are as follows: cosmogenic  $>$  trapped  $>$  radiogenic and lighter gas (e.g. He) is less retentive than heavier gas (Ar). In any event leading to gas loss, the most labile species will hence be radiogenic and lighter gas (as for example, loss of  $^4\text{He}$  is easy and more likely compared to  $^{40}\text{Ar}$ ).

#### ***(b) Different production rate of these cosmogenic isotopes in chondrules and bulk chondrites***

In general, the production rates of sub-samples (chondrules and bulk) coming from a single meteorite fragment of  $\sim 1$  gm and having same shielding depth, are independent of shielding depth. In such case, production rates of cosmogenic gases only depend on chemical composition of targets. As for example,  $^{21}\text{Ne}_c$  and  $^{38}\text{Ar}_c$  in individual

chondrules show strong dependence of principal target element abundances Mg ( and Al, Si) and Ca (and Ti, Fe) respectively, whereas  ${}^3\text{He}_c$  will be relatively independent of chemical composition differences (target elements for these three cosmogenic noble gas isotopes are listed in Table 1.4, Chapter 1). Hence, any differences in  ${}^3\text{He}_c$  contents among chondrules from a small ( $\sim 1$  gm) piece are more likely due to diffusive loss of  ${}^3\text{He}$ ; whereas such difference in  ${}^{21}\text{Ne}_c$  and  ${}^{38}\text{Ar}_c$  are either due to compositional differences or in certain cases due to differences in exposure duration. Knowledge of target chemical composition is hence important to calculate the production rates of cosmogenic noble gases, which normalize the abundances of these gases according to chemical composition of chondrules. Henceforth, only the cases of chemically characterized chondrules are discussed.

**(c) Higher cosmic ray fluence**

As mentioned earlier, the difference in cosmic ray fluence for the samples can result in difference in their cosmic ray exposure ages. This can be either due to difference in duration of exposure at the same CR flux or exposure (for short duration) to cosmic rays with higher flux. As discussed in introduction of this chapter, such a case of different cosmic ray fluence is expected in case of chondrules together with differences in chemical compositions.

As shown in Figs. 3.1a, 3.2a, 3.3a, 3.4a and 3.5a, for most chondrules, loss of  ${}^3\text{He}_c$  is evident compared to more retentive  ${}^{21}\text{Ne}_c$  as well as their respective chondrites. Except three chondrules from Parsa chondrite (Fig. 3.4a) and chondrules from Chainpur (compared to matrix), all other chondrules show lower or similar value of  $({}^3\text{He}/{}^{21}\text{Ne})_c$  when compared to bulk chondrites. The higher concentration of  ${}^3\text{He}$  in chondrules from Chainpur and Parsa chondrite can be due to either target chemistry or higher duration of cosmic ray exposure.

It is found that the difference of  ${}^{21}\text{Ne}_c$  in chondrules with respect to more retentive  ${}^{38}\text{Ar}$  is less when compared to loss of  ${}^3\text{He}$  with respect to  ${}^{21}\text{Ne}_c$ . In a few chondrules, higher value of  $({}^{21}\text{Ne}/{}^{38}\text{Ar})_c$  is observed compared to bulk chondrite indicating higher concentration of  ${}^{21}\text{Ne}$ . As mentioned above, this can be due to target chemistry or higher cosmic ray exposure of chondrules.

To take care of chemical composition differences, it is appropriate to compare the normalized abundances of cosmogenic isotope abundances. Calculation of production rates serves this purpose. Usually production systematics of cosmogenic nuclides are studied by two different approaches mainly: (a) by survey of many meteorites of a

specific class (e.g., work by Eugster, 1988) (b) physical models - based on nuclide production models (based on meteorite data), thin target cross section analyses, or simulation experiments of cosmic radiation by bombarding thick target with energetic protons (e.g., Leya et al., 2000). However, the method suggested by Eugster (1988) is widely accepted and as mentioned in recent review by Wieler (2002), the production rates according to Eugster (1988) are usually matches within some  $\pm 15\%$  for average shielding ( $^{22}\text{Ne}/^{21}\text{Ne} = 1.08-1.13$ ) with physical models.

In this work, hence the production rates of  $^3\text{He}$ ,  $^{21}\text{Ne}$  and  $^{38}\text{Ar}$  are calculated for chemically characterized chondrules using the method suggested by Eugster (1988). As mentioned earlier production rates depends on shielding depth and target chemistry of the sample. As used in method suggested by Eugster (1988),  $(^{22}\text{Ne}/^{21}\text{Ne})_c$  is used as shielding parameter for each chondrule (listed in Table 3.6). Another parameter required in this method is chemical correction factors  $F$ . This chemical correction factor is defined as:  $F = P_i/P_L$ , where  $P$  is the production rate of a given cosmogenic noble gas calculated based on chemical composition of sample. 'i' indicates the sample and 'L' indicates the L-chondrite. Production rate of  $^3\text{He}_c$  for the samples calculated as suggested by Eugster and Michel (1995) where as production rates of  $^{21}\text{Ne}_c$  calculated based on formula given by Schultz and Freundel (1985). Production rate of  $^{38}\text{Ar}_c$  is calculated as suggested by Marti and Graf (1992). The value of  $P_L$  (production rate based on chemical composition of L-chondrite and average shielding depth corresponding to  $(^{22}\text{Ne}/^{21}\text{Ne})_c = 1.11$ ) is fixed for all chondrules. ' $P_L$ ' is 1.61, 0.332 and 0.0462 (in units of  $10^{-8} \text{ cm}^3\text{STP/g/Ma}$ ) for  $^3\text{He}$ ,  $^{21}\text{Ne}$  and  $^{38}\text{Ar}$  respectively. Value of  $P_i$  changes for each chondrules based on the chemical composition of that chondrule. Chemical compositions of chondrules are listed in Table 3.5, used for calculation of production rates. The production rates and cosmic ray exposure ages of bulk chondrites are calculated by using method suggested by Eugster (1988) by taking appropriated chemical correction factor ( $F$ ) according to class of chondrite. Details of production rate calculations are given in *Appendix*.  $(^{22}\text{Ne}/^{21}\text{Ne})_c$ , production rates of  $^3\text{He}_c$ ,  $^{21}\text{Ne}_c$  and  $^{38}\text{Ar}_c$  for each of the chemically characterized chondrules are given in Table 3.6. Cosmic ray exposure ages based on these production rates are also given.

**Table 3.5** Results of electron probe microanalysis (performed on chondrule splits) used for the calculation of the production rates.

<b>Samples</b>	<b>Mg</b>	<b>Al</b>	<b>Ca</b>	<b>Fe</b>	<b>Si</b>
<b>weight %</b>					
<b>Dhajala</b>					
<b>DH-2</b>	16.0	0.5	1.1	11.0	26.0
<b>DH-5</b>	16.4	0.5	1.1	15.3	23.0
<b>DH-8</b>	15.2	1.1	1.8	6.6	26.7
<b>DH-9</b>	15.1	0.6	1.5	14.4	23.3
<b>DH-11</b>	23.1	0.2	0.5	9.8	22.6
<b>Bjurböle</b>					
<b>BB-15</b>	15.6	1.1	0.6	10.3	23.8
<b>BB-18</b>	16.0	0.2	1.3	10.1	25.1
<b>BB-25</b>	17.3	0.2	4.3	11.8	21.7
<b>BB-26</b>	16.4	0.7	1.0	11.1	23.7
<b>BB-29</b>	16.6	0.6	2.9	11.8	21.5
<b>Chainpur (CH), Saratov (STV), Tieschitz (TCZ)</b>					
<b>CH-1</b>	18.4	0.1	1.6	10.1	26.1
<b>CH-2</b>	17.4	1.1	1.6	6.8	26.0
<b>CH-3</b>	24.8	0.3	1.6	5.0	23.6
<b>STV-2</b>	17.4	0.4	0.9	6.6	26.0
<b>STV-3</b>	15.7	2.0	0.5	11.0	21.3
<b>TCZ-2</b>	16.7	2.6	5.0	3.3	22.5
<b>Parsa</b>					
<b>PR-1</b>	17.8	0.7	0.8	1.1	30.3
<b>PR-2</b>	19.2	0.8	0.9	1.0	29.6
<b>PR-3</b>	22.7	0.3	0.2	0.7	27.7
<b>Allende (ALD) and Murray (MRY)</b>					
<b>ALD-1</b>	32.2	< 0.1	0.2	3.6	19.2
<b>ALD-2</b>	23.1	2.3	4.7	1.5	20.2
<b>ALD-3</b>	12.4	5.4	8.0	1.1	20.3
<b>ALD-13</b>	25.1	1.9	4.0	0.3	20.0
<b>ALD-14</b>	28.1	0.4	0.5	1.9	22.2
<b>ALD-15</b>	24.0	1.8	3.1	3.5	20.0
<b>ALD-16</b>	25.5	0.6	0.7	1.1	24.0
<b>MRY-1</b>	18.3	2.5	4.1	0.2	24.7

Additional concentrations of Na, K, Cr, Mn and Ti were adopted from Rubin (1986) for ordinary and CM chondrules. For Allende and EH3 chondrules, these values are adopted from Rubin and Wasson (1977) and Grossman et al., (1985).

**Table 3.6** Mg/(Al+ Si), (<sup>22</sup>Ne/<sup>21</sup>Ne)<sub>c</sub>, Production rates and cosmic ray exposure ages of chondrules and respective chondrites.

Sample	Mg/(Al+Si)	<sup>22</sup> Ne/ <sup>21</sup> Ne <sub>c</sub>	P <sub>3</sub>	P <sub>21</sub>	P <sub>38</sub>	T <sub>3</sub>	T <sub>21</sub>	T <sub>38</sub>	T <sup>^</sup> <sub>CREA</sub>
			(10 <sup>-8</sup> cm <sup>3</sup> STP/g/Ma)			Ma			
<b>Dhajala</b>									
DH-2	0.6	(1.02)	1.673	0.350	0.030	2.94 ±0.29	4.54 ±0.82	3.82 ±0.69	4.18 ±0.75
DH5	0.7	1.12	1.642	0.332	0.042	1.52 .15	7.15 1.29	10.3 1.8	8.72 1.55
DH8	0.5	-	1.699	0.344	0.044	2.92 .29	5.10 .92	2.78 .50	5.10 .92
DH9	0.6	-	1.652	0.333	0.044	3.45 .35	5.70 1.03	4.51 .81	5.10 .91
DH11	1.0	(1.31)	1.686	0.478	0.029	1.18 .12	3.29 .59	5.40 .97	5.40 .97
DH (Bulk)	0.8	1.10	1.584	0.322	0.046	3.82 .38	5.71 1.03	5.91 1.06	5.81 1.04
<b>Bjurböle</b>									
BB-15	0.6	(1.00)	1.678	0.340	0.028	6.37 .64	8.76 1.58	11.9 2.1	10.3 1.79
BB-18	0.6	(1.02)	1.679	0.349	0.037	4.62 .46	9.50 1.71	13.5 2.4	11.5 2.0
BB-25	0.8	1.06	1.668	0.357	0.082	4.28 .43	7.49 1.35	7.53 1.35	7.51 1.35
BB-26	0.7	1.11	1.672	0.351	0.034	6.24 .62	8.00 1.44	9.18 1.65	8.59 1.54
BB-29	0.7	(1.15)	1.670	0.350	0.059	5.83 .58	10.30 1.85	14.0 2.5	12.2 2.2
BB* (mat)	0.8	1.11	-	0.501	0.043	-	7.50 1.35	11.5 2.1	9.5 1.7
BB <sup>#</sup> (chonds.)	0.7	1.11	1.670	0.398	0.050	9.12 1.64	11.61 2.09	8.29 1.49	9.67 1.74
BB <sup>#</sup> (mat)	0.9	1.11	1.650	0.501	0.043	8.37 1.51	8.01 1.44	7.92 1.42	8.1 1.5
<b>Tieschitz</b>									
TCZ-2	0.7	1.11	1.719	0.363	0.088	13.3 1.3	14.6 2.6	9.60 1.73	14.6 2.6
TCZ (Bulk)	0.8	(1.26)	1.580	0.308	0.046	26.3 2.6	23.4 4.2	26.4 4.7	25.4 3.8
<b>Saratov</b>									
STV-2	0.7	1.12	1.61	0.394	0.032	7.37 .74	8.21 1.48	18.6 3.3	18.6 3.3
STV-3	0.7	1.10	1.616	0.39	0.029	6.75 .68	13.3 2.4	14.2 2.6	13.7 2.5
STV (Bulk)	0.8	1.10	1.615	0.341	0.046	17.2 1.7	22.9 4.1	19.0 3.4	22.9 4.1
<b>Chainpur</b>									
CH-1	0.7	1.10	1.67	0.39	0.053	20.0 2.0	18.0 3.2	32.1 5.8	18.0 3.2
CH-2	0.6	(1.13)	1.691	0.347	0.048	18.0 1.8	24.2 4.4	32.7 5.9	24.2 4.4
CH-3	1.0	(1.09)	1.721	0.546	0.050	26.2 2.6	21.9 3.9	42.9 7.7	21.9 3.9

Sample	Mg/(Al+Si)	$(^{22}\text{Ne}/^{21}\text{Ne})_c$	$P_3$	$P_{21}$	$P_{38}$	$T_3$	$T_{21}$	$T_{38}$	$T_{\text{CREA}}^{\wedge}$
			$(10^{-8} \text{ cm}^3 \text{ STP/g/Ma})$			Ma			
Matrix(fine)	0.8	1.14	1.611	0.325	0.044	13.0	25.1	17.2	25.1
(< 100 $\mu\text{m}$ )						1.3	4.5	3.1	4.5
Matrix(coa.)	0.8	1.09	1.611	0.325	0.047	10.9	25.9	23.1	24.5
(100-200 $\mu\text{m}$ )						1.1	4.6	4.1	4.3
<b>Parsa</b>									
Parsa-1	0.6	(1.13)	1.725	0.36	0.022	23.1	25.4	16.3	25.4
						2.3	4.6	2.9	4.6
Parsa-2	0.6	(1.11)	1.737	0.421	0.024	23.2	15.1	10.4	15.1
						2.3	2.7	1.9	2.7
Parsa-3	0.8	1.11	1.740	0.470	0.014	22.2	11.9	15.0	11.9
						2.2	2.1	2.7	2.1
Parsa (Bulk)	0.8	(1.19)	1.564	0.259	0.046	18.4	24.2	12.3	24.2
						1.8	4.35	2.2	4.3
<b>Allende</b>									
ALD-1	1.7	(0.91)	1.720	0.590	0.011	2.00	2.28	-	2.28
						.20	0.41		0.41
ALD-2	1.0	-	1.731	0.457	0.023	2.69	2.05	-	2.05
						.27	0.37		0.37
ALD-3	0.5	-	1.735	0.316	0.121	1.43	3.19	-	3.19
						.14	.58		.58
ALD-13	1.1	(1.03)	1.75	0.493	0.062	2.49	2.66	2.50	2.55
						.25	.48	.45	.39
ALD-14	1.2	(1.18)	1.732	0.493	0.035	2.63	2.55	9.32	9.32
						.26	.46	1.68	1.68
ALD-15	1.1	1.13	1.710	0.49	0.054	2.65	3.32	2.91	2.95
						.26	.60	.52	.46
ALD-16	1.0	(1.23)	1.745	0.537	0.013	1.84	2.32	7.49	7.49
						.18	.42	1.35	1.35
<b>Murray</b>									
MRY-1	0.7	(1.29)	1.740	0.396	0.066	3.22	3.66	6.39	3.66
						.32	.66	1.15	.66
Murray (Bulk)	0.8	1.11	1.612	0.261	0.041	1.29	2.68	-	2.68
						.13	.48		.48

Abbreviations:  $P_3$ ,  $P_{21}$ ,  $P_{38}$  = production rates of  $^3\text{He}_c$ ,  $^{21}\text{Ne}_c$ ,  $^{38}\text{Ar}_c$ .  $T_3$ ,  $T_{21}$ ,  $T_{38}$  = cosmic ray exposure ages calculated with  $^3\text{He}_c$ ,  $^{21}\text{Ne}_c$ ,  $^{38}\text{Ar}_c$ . \* Data taken from Fredriksson et al., (1985), #Data are taken from Polnau et al., (2001) (also shown in italics).  $(^{22}\text{Ne}/^{21}\text{Ne})_c$  values given in bracket are not used for the calculations of production rates for chondrules, instead  $(^{22}\text{Ne}/^{21}\text{Ne})_c$  value of bulk or value for average shielding depth (e.g. for Parsa) is considered.  $T_{\text{CREA}}^{\wedge} = T_{21}$  (if  $T_3$ ,  $T_{21}$  and  $T_{38}$  are different) or  $(T_{21}+T_{38})/2$ .  $T_{\text{CREA}} = (T_3+T_{21}+T_{38})/3$  for very similar values of  $T_3$ ,  $T_{21}$  and  $T_{38}$ .

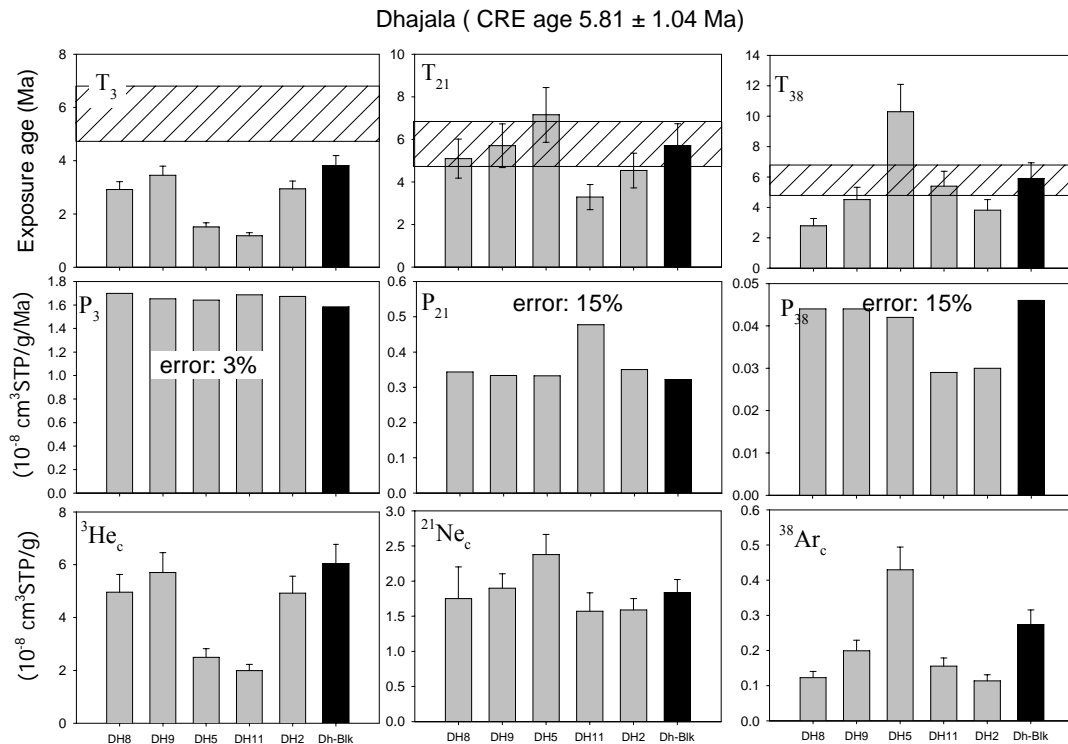


**Fig. 3.6** Three panels show cosmogenic  $^3\text{He}$ ,  $^{21}\text{Ne}$ ,  $^{38}\text{Ar}$ , the production rates of  $^3\text{He}$ ,  $^{21}\text{Ne}$ ,  $^{38}\text{Ar}$  and the corresponding exposure ages respectively for Dhajala chondrules and bulk samples. Chondrule DH-5 shows higher exposure age compared to bulk. Other chondrules show lower exposure ages. Hatched area represents the average cosmic ray exposure age ( $5.81 \pm 1.04$ ) of Dhajala chondrite.

### Dhajala (H3.8)

The calculated production rates and exposure durations  $T_3$ ,  $T_{21}$  and  $T_{38}$  are listed in Table 3.6. Fig. 3.6 presents the production rates as well as exposure durations  $T_3$ ,  $T_{21}$  and  $T_{38}$  for five chondrules and bulk sample of Dhajala. As production of  $^3\text{He}_c$  is relatively independent of chemical differences, production rate of  $^3\text{He}_c$  ( $P_3$ ) of chondrules and bulk are similar whereas production rates of  $^{21}\text{Ne}_c$  ( $P_{21}$ ) and  $^{38}\text{Ar}_c$  ( $P_{38}$ ) are different for chondrules and bulk. Cosmic Ray Exposure (CRE) age based on  $^3\text{He}_c$  ( $T_3$ ) for most chondrules is lower compared to bulk. Lower CRE age ( $T_3$ ) of bulk compared to  $T_{21}$  and  $T_{38}$  ages indicates loss of  $^3\text{He}_c$  from bulk. To calculate the  $T_{\text{CREA}}$  (average cosmic ray exposure age) for bulk hence, value of  $T_3$  is not included (Table 3.6) Chondrules that show lower  $T_3$  compared to bulk suggest even higher loss of  $^3\text{He}_c$  compared to bulk. As evident in Fig.3.6, maximum loss is evident in chondrules DH-5 and DH-11 (which is also evident in their  $(^3\text{He}/^{21}\text{Ne})_c$  values). The production rates  $P_{21}$  for chondrules and bulk is similar except that of DH-11, which is showing highest production rate (Fig. 3.6). The content of Mg in this chondrule is 23 wt. %

compared to ~16 wt.% of Mg in other chondrules (Table 3.5) explaining higher production rate of  $^{21}\text{Ne}_c$ . Neon exposure ages  $T_{21}$  of chondrule DH-5 and bulk are  $7.15 \pm 1.29$  Ma and  $5.71 \pm 1.03$  Ma respectively. The neon exposure age of chondrule exceeds that of bulk by 25%. Except DH-11, all other chondrules show similar exposure duration compared to bulk. DH-5 chondrule also shows higher cosmic ray exposure age ( $10.3 \pm 1.8$  Ma) based on  $^{38}\text{Ar}_c$  compared to bulk Dhajala ( $5.91 \pm 1.06$ ) which is higher by 74%. Similar kind of higher exposure ages are not observed in any other chondrule from Dhajala. Variable loss of cosmogenic noble gases is observed in chondrules. As for example, for chondrules DH-5 and DH-11, the exposure ages show trend:  $T_{38} > T_{21} > T_3$ , where as for chondrule DH-8, DH-2, and DH-9, the trend is:  $T_{21} > T_3, T_{38}$ . Based on these observation, for all chondrules neon exposure age ( $T_{21}$ ) seems to be least affected by secondary loss.

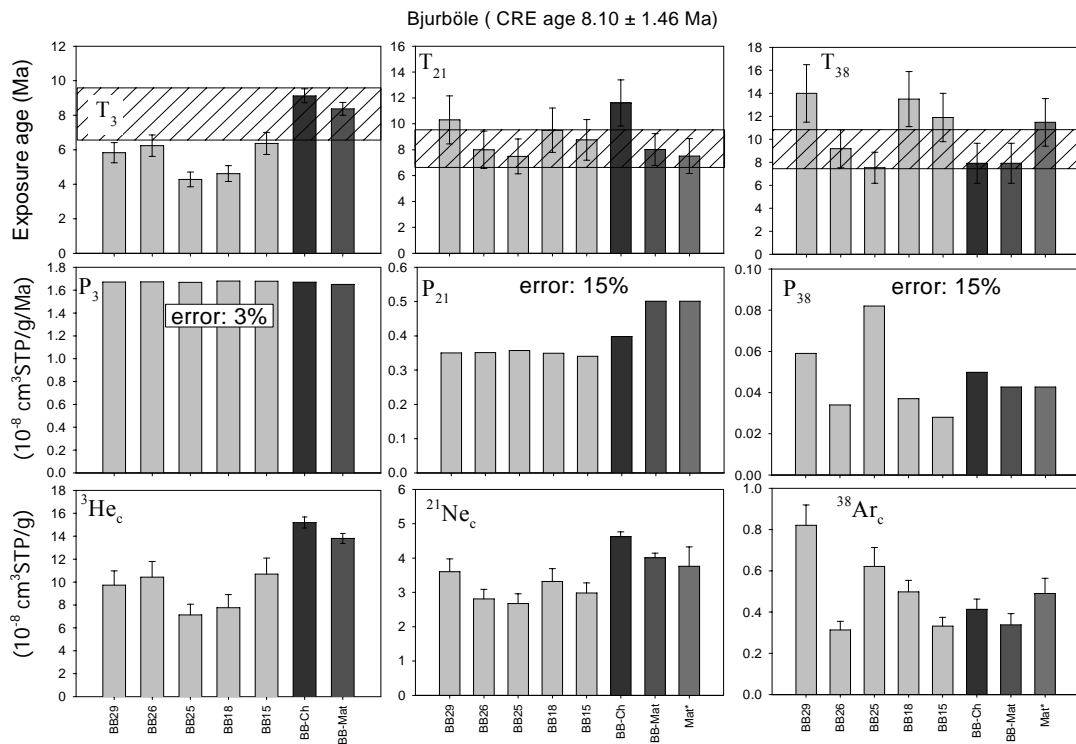


**Fig. 3.7** Three panels show cosmogenic  $^3\text{He}$ ,  $^{21}\text{Ne}$ ,  $^{38}\text{Ar}$ , the production rates of  $^3\text{He}$ ,  $^{21}\text{Ne}$ ,  $^{38}\text{Ar}$  and the corresponding exposure ages respectively for Bjurböle chondrules. Data of from Fredriksson et al., (1985) (last bar, for Ne and Ar) and Polnau et al., (2001) also plotted for comparison with this work. Few chondrules show higher CRE ages ( $T_{21}$ ) compared to reported data. Hatched area represents the average cosmic ray exposure age ( $8.01 \pm 1.46$ ) of Bjurböle chondrite.

### Bjurböle (L/LL4)

Five chondrules from Bjurböle chondrite were chemically characterized. In Table 3.6, the details of the production rates and cosmic ray exposure ages are given with earlier literature data taken from Fredriksson et al. (1985) and Polnau et al. (2001). In Fig.

3.7 concentrations, production rates and exposure ages of cosmogenic noble gases for chondrules are compared with those of matrix (Fredriksson et al., 1985) values.  $^3\text{He}_c$  in chondrules show variation whereas production rates of  $^3\text{He}_c$  are similar for all chondrules. The CRE ages based on  $^3\text{He}_c$  are lower for chondrules varying between 4-6 Ma indicating variable losses of  $^3\text{He}_c$  from chondrules.

Unlike the case of  $^3\text{He}_c$ , CRE ages of most chondrules based on  $^{21}\text{Ne}_c$  are similar to values suggested by Fredriksson et al. (1985) (also plotted in Fig. 3.7) and Polnau et al. (2001) for matrix except for BB-29 and BB-18 (Table 3.6). The CRE age ( $T_{21}$ ) of BB-29 ( $10.30 \pm 1.85$  Ma) is higher compared to matrix ( $7.50 \pm 1.35$  Ma) (Fig. 3.7) by 37%. Chondrule BB-18 shows neon exposure age higher by 27% compared to bulk. The other chondrule BB-15 also shows slightly higher neon exposure but similar to that of bulk within error.  $T_{21}$  age of BB-29 chondrule is similar to reported values for bunch of chondrules (Polnau et al., 2001, Table 3.6).  $^{38}\text{Ar}_c$  in these chondrules also varies largely compared to  $^3\text{He}_c$  and  $^{21}\text{Ne}_c$ . Similar variations are also observed in production rates of  $^{38}\text{Ar}_c$  for these chondrules suggesting mainly variation of Ca in these chondrules (e.g., ~ 4 % of Ca in chondrule BB-25, Table 3.5). CRE age ( $T_{38}$ ) of BB-29 is also found higher compared to matrix (Table 3.6, Fig. 3.7).

Polnau et al. (2001) analyzed powder of chondrules (representing an average of many chondrules) and matrix for Bjurböle chondrite. In this work, five individual chondrules are analyzed which show either higher or similar CRE age when compared to matrix.  $T_{21}$  ages of BB-29 and BB-18 chondrule suggests excess duration of cosmic ray exposure of 2-3 Ma compared to matrix. Based on  $^{129}\text{I}$ - $^{129}\text{Xe}$  dating method, Caffee et al. (1982) suggested that Bjurböle chondrules were formed 1.5 Ma earlier to 0.5 Ma later than Bjurböle whole rock. This suggests that chondrules or precursors of chondrules might have experienced cosmic ray exposure for longer duration indicating formation of chondrules over an extended period.

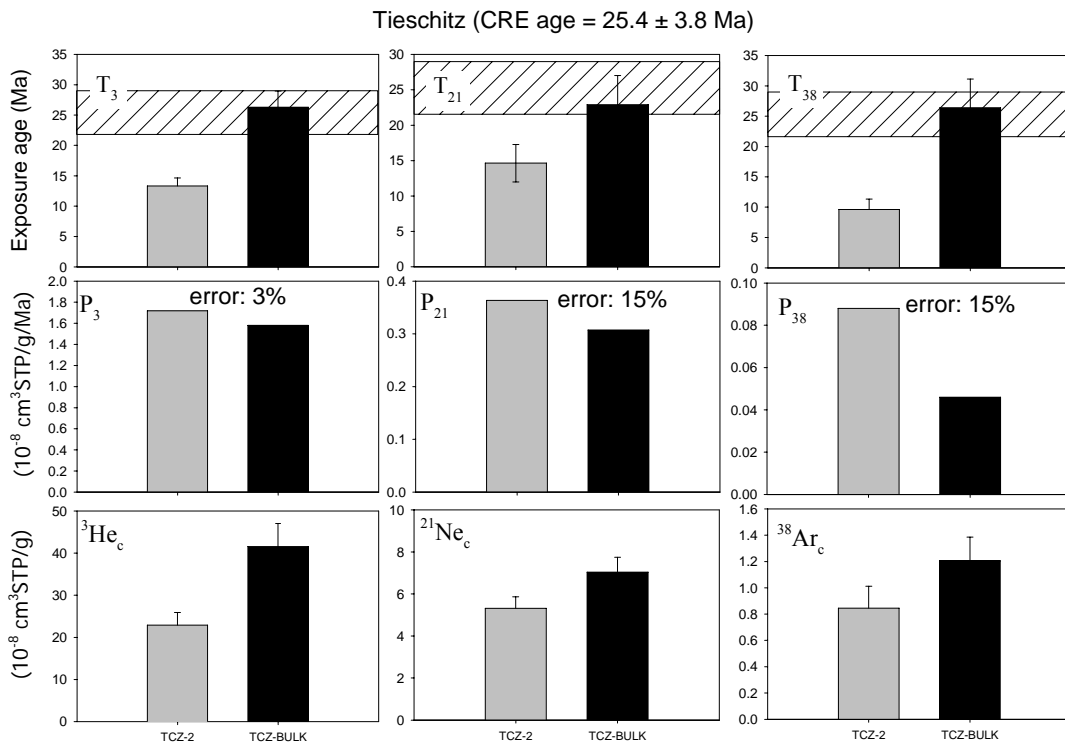


**Fig. 3.8** Three panels show  $^3\text{He}_c$ ,  $^{21}\text{Ne}_c$ ,  $^{38}\text{Ar}_c$ , the production rates of  $^3\text{He}$ ,  $^{21}\text{Ne}$ ,  $^{38}\text{Ar}$  and the corresponding exposure ages respectively for Tieschitz chondrule and bulk samples. Chondrule TCZ-2 shows lower exposure ages compared to bulk. Hatched area represents the average cosmic ray exposure age ( $25.4 \pm 3.8$ ) of Tieschitz chondrite.

### Tieschitz (H3.6)

TCZ-2 chondrule is chemically characterized and as can be seen in Fig. 3.8,  $^3\text{He}_c$  in this chondrule is lower by factor of 2 compared to bulk whereas production rates ( $P_3$ ) are similar. Similarly lower concentrations of  $^{21}\text{Ne}_c$  and  $^{38}\text{Ar}_c$  are observed in chondrule compared to bulk (Table 3.6, Fig. 3.8). The exposure age ( $T_{\text{CREA}}$ ) of bulk is  $\sim 23$  Ma consistent with earlier reported age by Nichols et al. (1991). The exposure ages ( $T_3$ ,  $T_{21}$ ,  $T_{38}$ ) of chondrule are around 10-15 Ma which almost half compared to bulk suggesting loss of all cosmogenic noble gases from this chondrule.

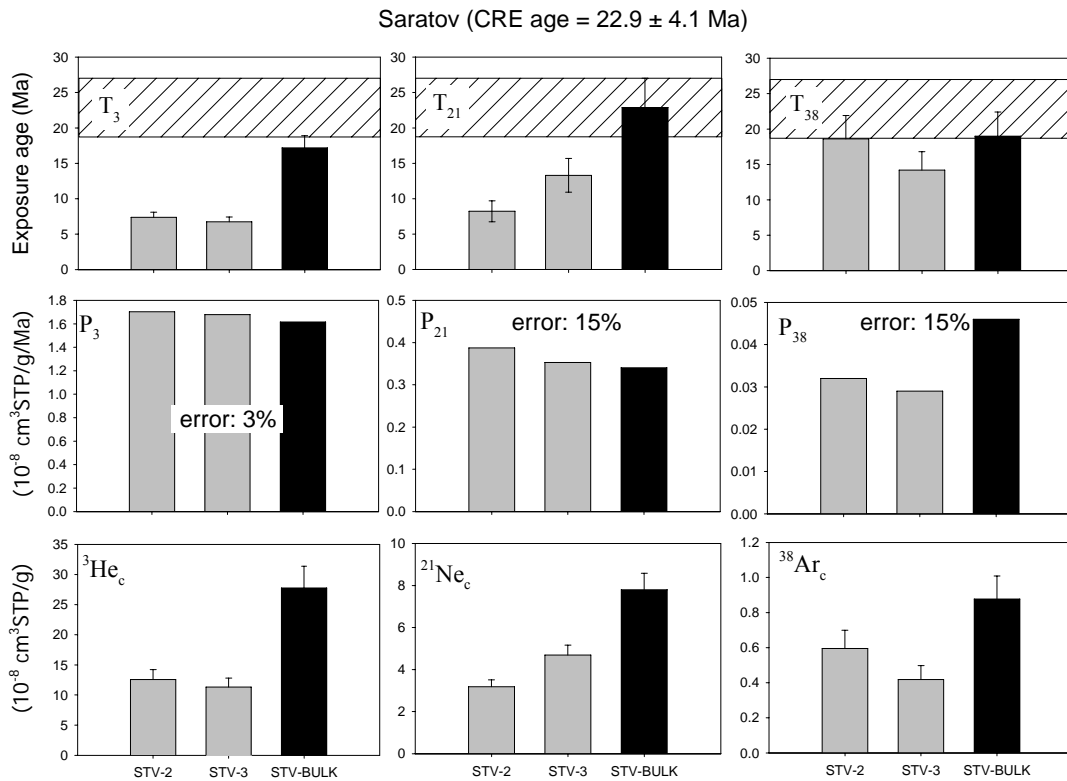


**Fig. 3.9** Three panels show cosmogenic  $^3\text{He}$ ,  $^{21}\text{Ne}$ ,  $^{38}\text{Ar}$ , the production rates of  $^3\text{He}$ ,  $^{21}\text{Ne}$ ,  $^{38}\text{Ar}$  and the corresponding CRE ages respectively for Saratov chondrules and bulk samples. Loss of cosmogenic gases is evident from chondrules compared to bulk. Hatched area represents average CRE age ( $22.9 \pm 4.1$ ) Ma of Saratov chondrite.

### Saratov (L4)

Two chondrules from Saratov have been chemically characterized. These chondrules STV-2 (average of two splits) and STV-3 show lower  $^3\text{He}_c$  compared to bulk where as CRE ages ( $T_3$ ) based on  $^3\text{He}_c$  production rates are lower by factor of 3 (Fig. 3.9, Table 3.6). The  $T_3$  age of Saratov bulk is also low compared to  $T_{21}$  and  $T_{38}$ , which can be most probably due to loss of  $^3\text{He}_c$ . Chondrules are also found depleted in abundances of  $^{21}\text{Ne}_c$  and  $^{38}\text{Ar}_c$  compared to bulk, which is translated into their lower  $T_{21}$  and  $T_{38}$  ages, as production rates ( $P_{21}$  and  $P_{38}$ ) are similar for chondrules and bulk. Similar to the case of chondrule from Tieschitz, loss of cosmogenic noble gases from these chondrules is also evident when compared with bulk.

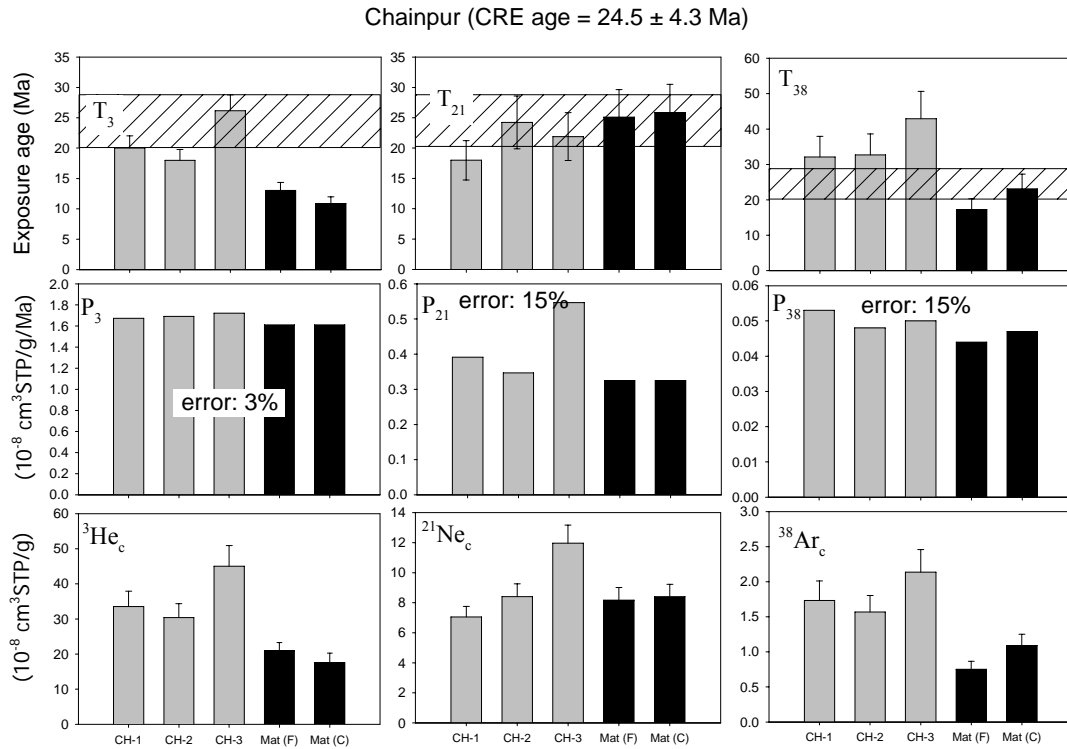


**Fig. 3.10** Three panels show cosmogenic  $^3\text{He}$ ,  $^{21}\text{Ne}$ ,  $^{38}\text{Ar}$ , the production rates of  $^3\text{He}$ ,  $^{21}\text{Ne}$ ,  $^{38}\text{Ar}$  and the corresponding exposure ages for Chainpur chondrules and matrix samples (*mat(f)* = Fine-grained matrix, *mat(c)* = Coarse grained matrix). Chondrules show similar or lower exposure ages compared to bulk. CRE ages ( $T_{38}$ ) are higher compared to matrix.

### Chainpur (LL3.4)

As mentioned in the results section of  $^3\text{He}_c$ , chondrules from Chainpur show higher  $^3\text{He}_c$  compared to matrix material (fine as well as coarse grained). As evident in Fig 3.10, the production rates of  $^3\text{He}_c$  for all chondrules are similar to matrix. Helium exposure ages ( $T_3$ ) of chondrules are higher compared to matrix.  $T_3$  age of chondrule CH-3 is almost higher by factor of 2 compared to matrix. The reported exposure age of Chainpur is  $\sim 25$  Ma (Eugster, 1988). The lower  $T_3$  ages of Chainpur matrix clearly indicate loss of  $^3\text{He}_c$ . The relative higher  $T_3$  ages observed for chondrules compared to matrix are hence due to higher loss of  $^3\text{He}_c$  from the matrix samples. As discussed earlier,  $^3\text{He}/^{21}\text{Ne}$  ratios of matrix materials are also lower compared to chondrule samples (Fig. 3.3). As listed in Table 3.6,  $T_{21}$  and  $T_{38}$  of matrix material is  $\sim 25$  Ma consistent with reported exposure age. Among four chondrules, chondrule CH-3 shows higher concentration of  $^{21}\text{Ne}_c$ . Production rate of  $^{21}\text{Ne}_c$  is also higher compared to other chondrules and matrix. Variation of production rates are also observed in these chondrules however within 15% estimated error these rates are similar. Neon exposure ages of chondrules are either similar or lower compared to matrix. The

exposure ages of chondrules based on  $^{21}\text{Ne}$  is higher compared to that of based on  $^3\text{He}$ . Such is also the case with matrix suggesting loss of He from chondrules as well as matrix material. CRE ages based on cosmogenic  $^{38}\text{Ar}$  suggest different trend (Fig. 3.10). Production rates of  $^{38}\text{Ar}_c$  for chondrules are similar compared to matrix materials within error. CRE age ( $T_{38}$ ) of chondrule CH-3 is higher compared to matrix by 72% where as chondrules CH-1 and CH-2 are higher by 28%. This translates in to 8 to 18 Ma difference between chondrule and matrix. High concentration of  $^{38}\text{Ar}_c$  especially in chondrule CH-3 as well as partial loss of Ar from matrix seems responsible for such large difference in exposure age. As mentioned by Patzer and Schultz (2001), argon exposure ages ( $T_{38}$ ) can have higher uncertainty for samples with higher amounts of trapped Ar due to possible discrepancy between the assumed  $^{36}\text{Ar}/^{38}\text{Ar}$  ratio of 5.32 and the real (but unknown) value.

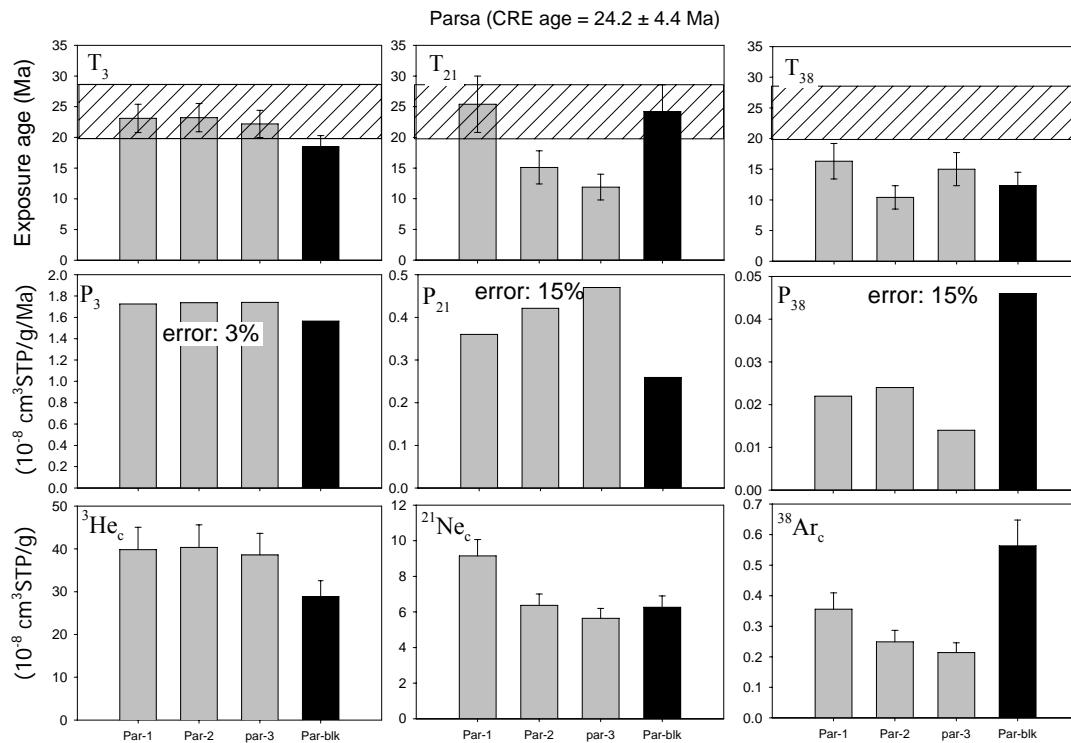


**Fig. 3.11** Three panels show cosmogenic  $^3\text{He}$ ,  $^{21}\text{Ne}$ ,  $^{38}\text{Ar}$ , the production rates of  $^3\text{He}$ ,  $^{21}\text{Ne}$ ,  $^{38}\text{Ar}$  and the corresponding exposure ages respectively for Parsa chondrule and bulk samples. Chondrules show similar or lower exposure ages compared to bulk. Exposure ages based on  $^{21}\text{Ne}$  are lower compared to bulk.

### Parsa (EH3)

As clearly seen in Fig.3.11 and Table 3.6, all the Parsa chondrules show higher  $^3\text{He}_c$  compared to bulk. The production rates of  $^3\text{He}_c$  for chondrules are similar to bulk as observed in chondrules from other chondrites. Subsequent calculation of CRE ages

suggests slightly higher exposure duration for chondrules compared to bulk. However, within estimated errors of exposure ages, the difference is not significant. Chondrule Parsa-1 shows highest  $^{21}\text{Ne}_c$ , however lower production rate of  $^{21}\text{Ne}_c$  for this chondrules finally result into cosmic ray exposure duration similar to bulk. Other chondrules show  $^{21}\text{Ne}_c$  similar to bulk however, their higher production rates yield  $T_{21}$  ages lower compared to bulk. Argon exposure ages ( $T_{38}$ ) for chondrules are similar to bulk within error, except the case of Parsa-2 chondrule, which shows lower  $T_{38}$  age compared to bulk. The cosmic ray exposure ages of Parsa, bulk shows a trend:  $T_{21} > T_3 > T_{38}$ . This can be explained by partial loss of  $^{38}\text{Ar}_c$  from oldhamite (CaS) which is possible in enstatite chondrite as discussed earlier.

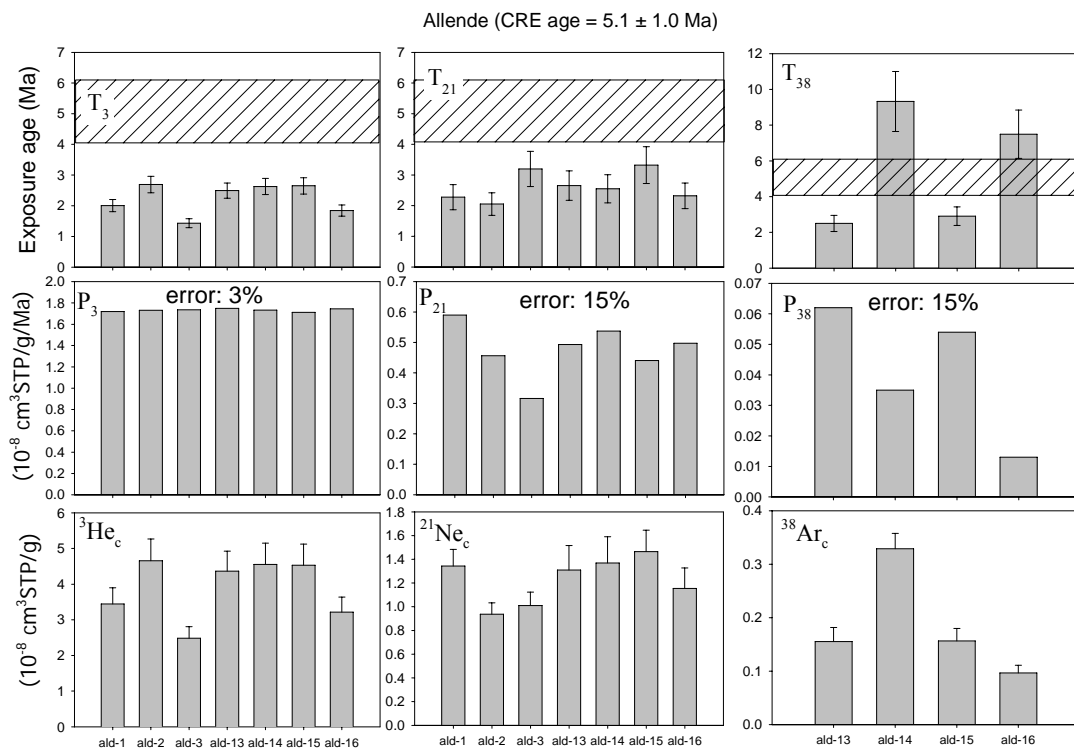


**Fig. 3.12** Three panels show cosmogenic  $^3\text{He}$ ,  $^{21}\text{Ne}$ ,  $^{38}\text{Ar}$ , the production rates of  $^3\text{He}$ ,  $^{21}\text{Ne}$ ,  $^{38}\text{Ar}$  and the corresponding exposure ages respectively for Allende chondrules. The hatched area gives the range of CRE age calculated for Allende bulk based on literature data (see text for details). Chondrules ALD-14 and ALD-16 show  $T_{38}$  age higher compared to reported value for bulk. Other chondrules show lower exposure ages.

### Allende (CV3.2)

The production rates of  $^3\text{He}_c$  observed for Allende chondrules are similar. However due to variation in  $^3\text{He}_c$  the CRE ages ( $T_3$ ) of chondrules vary from 1.5 to 2.5 Ma. Chondrules show CRE ages lower by almost factor of 2 or higher compared to  $\sim 5 \pm 1$  Ma CRE age of bulk Allende chondrite (Fig. 3.12). This CRE age of Allende bulk is

estimated via bulk  $^{21}\text{Ne}_c$  concentrations from Schultz and Franck (2000), and average shielding ( $^{22}\text{Ne}/^{21}\text{Ne}$ )<sub>c</sub> of 1.11 (Wieler 2002) and production rates calculated according to Eugster (1988).

Due to variation in target chemistry, differences in concentrations and production rates of  $^{21}\text{Ne}_c$  are observed for Allende chondrules. The CRE ages ( $T_{21}$ ) of chondrules mostly less than 4 Ma. This range of CRE ages is lower than the cosmic ray exposure age of bulk (Table 3.6 and Fig. 3.12).

Argon exposure ages ( $T_{38}$ ) of chondrules are also lower except ALD-14 and ALD-16, which show exposure duration ( $9.32 \pm 1.68$ ) Ma and ( $7.49 \pm 1.35$ ) Ma respectively, which is almost 3.4 Ma more, compared to bulk Allende exposure age ( $5.1 \pm 1.02$ ). Chondrules like ALD-13 and ALD-15 show exposure ages  $\sim 2$  Ma similar to cosmic ray exposure ages based on  $^3\text{He}$  of these chondrules. The production rates of  $^{38}\text{Ar}$  in these chondrules are similar. If the assumed K content (Table 3.1) is valid, gas retention age ( $T_{40}$ ) of chondrule ALD-13 (2.2 Ga) suggests loss of Ar where as for chondrule ALD-15, loss of Ar cannot be argued as the  $T_{40}$  age is  $\sim 4.8$  Ga. At the same time, it is possible that the low value of  $T_{38}$  is an artifact due to the presence of neutron-produced  $^{36}\text{Ar}_n$  from the  $(n,\gamma)$  reaction on  $^{35}\text{Cl}$ . However, in the absence of much radiogenic  $^{129}\text{Xe}$  abundances from these chondrules not much can be argued similar to the case of chondrules from Qingzhen chondrite.

### **Murray (CM2)**

For chondrule MRY-1, we could determine the chemical composition as it was large chondrule. As discussed earlier, higher concentrations of  $^3\text{He}_c$  and  $^{21}\text{Ne}_c$  are observed in this chondrule compared to bulk.

As shown in Fig. 3.13, chondrule MRY-1 shows  $^3\text{He}_c$  higher by factor of 3 compared to bulk. Helium exposure age ( $T_3$ ) of chondrule is  $3.22 \pm 0.32$  Ma almost twice compared to bulk ( $1.29 \pm 0.13$  Ma). CRE age ( $T_3$ ) of Murray chondrite is less compared to neon exposure age ( $T_{21}$ ) (Fig. 3.12) and earlier result (2 to 6 Ma, Herzog et al., 1990). Based on lower CRE age of bulk, the loss of  $^3\text{He}$  is evident. The difference of exposure duration between chondrules and Murray bulk may be a result of differential loss of  $^3\text{He}_c$  from chondrule and bulk.

$^{21}\text{Ne}_c$  in this chondrule as mentioned earlier is higher by factor of 2 compared to bulk. When normalized with production rate of  $^{21}\text{Ne}$ , based on the target composition of chondrule, the calculated CRE age of chondrule ( $T_{21} = 3.66 \pm 0.66$  Ma) is higher

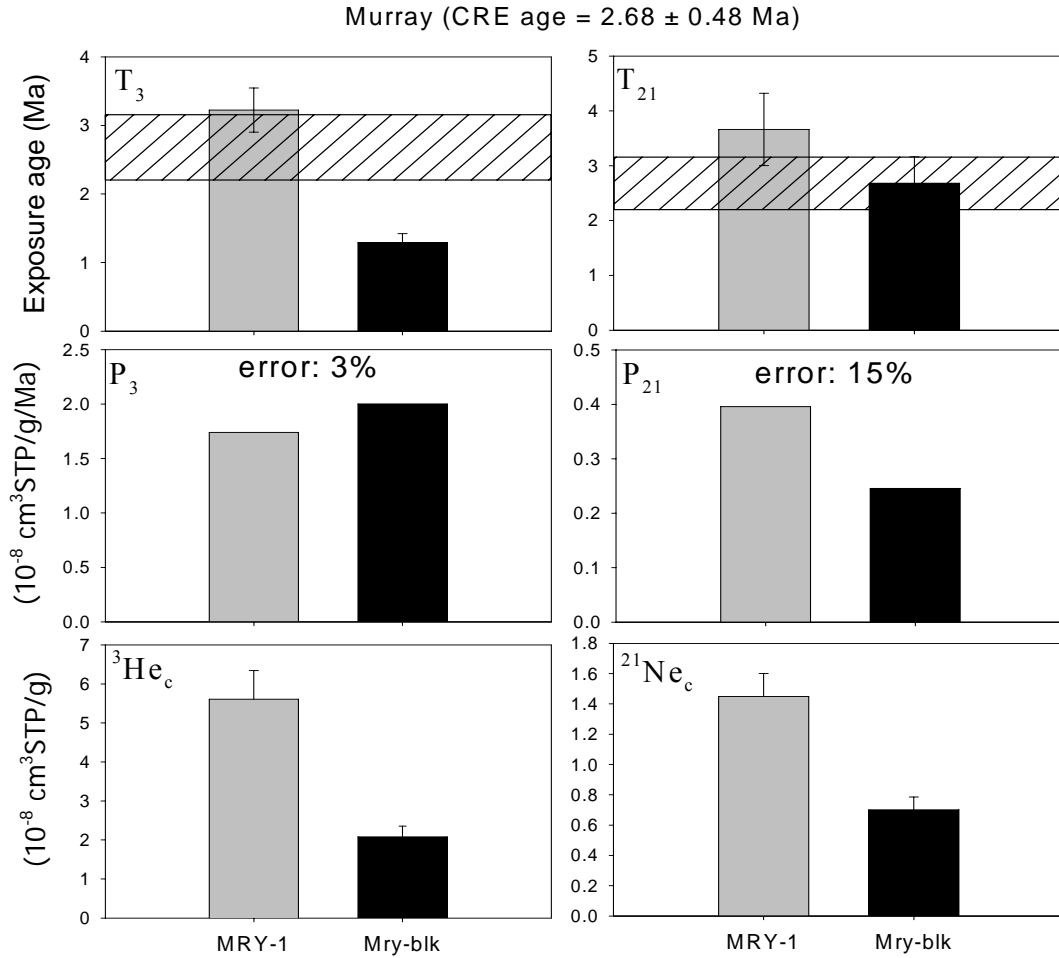


**Fig. 3.13** Three panels show cosmogenic  $^3\text{He}$ ,  $^{21}\text{Ne}$ , the production rates of  $^3\text{He}$ ,  $^{21}\text{Ne}$  and the corresponding exposure ages respectively for Murray chondrule and bulk. Chondrule (MRY-1) shows ~ 2 Ma higher exposure age compared to bulk. Hatched area represents the cosmic ray exposure age ( $2.68 \pm 0.48$  Ma) of Murray bulk.

compared to bulk ( $T_{21} = 2.68 \pm 0.48$  Ma) by 37%. Values are listed in Table 3.6 as well as presented in Fig. 3.12. Argon exposure age for chondrule MRY-1 is  $6.39 \pm 1.15$  Ma. Unfortunately, this cannot be compared with argon exposure age of bulk, as Ar measurement could not be performed for Murray bulk due to some technical problem.

### 3.3.3 Radiogenic noble gases ( $^4\text{He}$ , $^{40}\text{Ar}$ and $^{129}\text{Xe}$ )

Results of  $^4\text{He}$ ,  $^{40}\text{Ar}$  and  $^{129}\text{Xe}$  in chondrules from all chondrites are listed in Tables 3.2, 3.3 and 3.4. In Figs. 3.14, 3.15 and 3.16 elemental ratio  $^4\text{He}/^{40}\text{Ar}$  is plotted against  $^{40}\text{Ar}_r$  in chondrules and their chondrites for ordinary, enstatite and carbonaceous chondrites respectively. ‘Cosmogenic corrected  $^4\text{He}$ ’ term is used to indicate that calculated  $^4\text{He}$  is mixture of trapped and radiogenic contributions. In absence of trapped  $^4\text{He}$ , cosmogenic corrected  $^4\text{He}$  refers to radiogenic  $^4\text{He}$ . Amount

of  $^4\text{He}$  and  $^{40}\text{Ar}$  in chondrules and chondrites are governed by amount of U, Th and K respectively. However, the preferential loss expected for radiogenic  $^4\text{He}$  can affect the elemental ratio significantly. Simultaneously, presence of non-radiogenic  $^4\text{He}$  (trapped) or  $^{40}\text{Ar}$  (air contamination, though less probable) can influence  $^4\text{He}/^{40}\text{Ar}$  ratios in chondrules as well as chondrites. Although, presence of such trapped component is rare, such cases are discussed in Chapter 4.

### 3.3.3.1 Chondrules from ordinary chondrites

#### Dhajala (H3.8):

The cosmogenic corrected  $^4\text{He}$  in the Dhajala bulk is  $(1309 \pm 131) \times 10^{-8} \text{ cm}^3\text{STP/g}$  and lower when compared to the maximum  $^4\text{He}_r$  ( $2050 \times 10^{-8} \text{ cm}^3\text{STP/g}$  as listed in Table 3.1). Most of the chondrules show lower  $^4\text{He}_r$  compared to the bulk Dhajala sample (Table 3.2). It is found that chondrules DH-8 and DH-11 are enriched in  $^4\text{He}$  by a factor of 50 and 11 respectively when compared to Dhajala bulk (Fig. 4.7, chapter 4).

$^3\text{He}_c$  in DH-8 and DH-11 are hence corrected for the presence of trapped He component (as discussed in section 3.2). Chondrules DH-S8, DH-S18 and DH-S19 also show marginally higher  $^4\text{He}$  compared to Dhajala bulk as listed in Table 3.2. In contrast to these results, a few chondrules show very low  $^4\text{He}_r$  compared to Dhajala bulk. Chondrule DH-5 shows  $^4\text{He}$  lower by 25% compared to bulk whereas  $^{40}\text{Ar}_r$  ( $\sim 6174 \times 10^{-8} \text{ cm}^3\text{STP/g}$ ) similar to bulk within error (Table 3.2). This indicates higher loss of He compared to Ar. Chondrule DH2 shows similar  $^4\text{He}$  whereas amount of  $^{40}\text{Ar}$  is found less compared to bulk. In case of DH-9 chondrule, amount of  $^4\text{He}$  and  $^{40}\text{Ar}$  are similar to bulk. This is consistent with the observation of cosmogenic noble gases in this chondrule where exposure ages are found similar to bulk. Although chondrule DH-8 shows presence of excess  $^4\text{He}$ , lower amount of  $^{40}\text{Ar}$  is observed in this chondrule indicating the effect of secondary events on this chondrule. Lowest  $^{40}\text{Ar}_r$  is observed for chondrule DH-V38 as observed similarly for  $^4\text{He}_r$  and cosmogenic gases of this chondrule. It seems that the loss of noble gases from this chondrule is very severe.

In Fig. 3.14, the elemental ratio  $^4\text{He}/^{40}\text{Ar}$  and  $^{40}\text{Ar}_r$  is plotted for Dhajala chondrules with other chondrules from ordinary chondrites. Most chondrules show depleted value of  $^4\text{He}/^{40}\text{Ar}$  compared to maximum expected value (shown as hatched band) in ordinary chondrites. The overall trend suggests the loss of  $^4\text{He}$  from chondrules compared to  $^{40}\text{Ar}$  as similarly observed for  $^3\text{He}_c$ . As mentioned above, chondrules

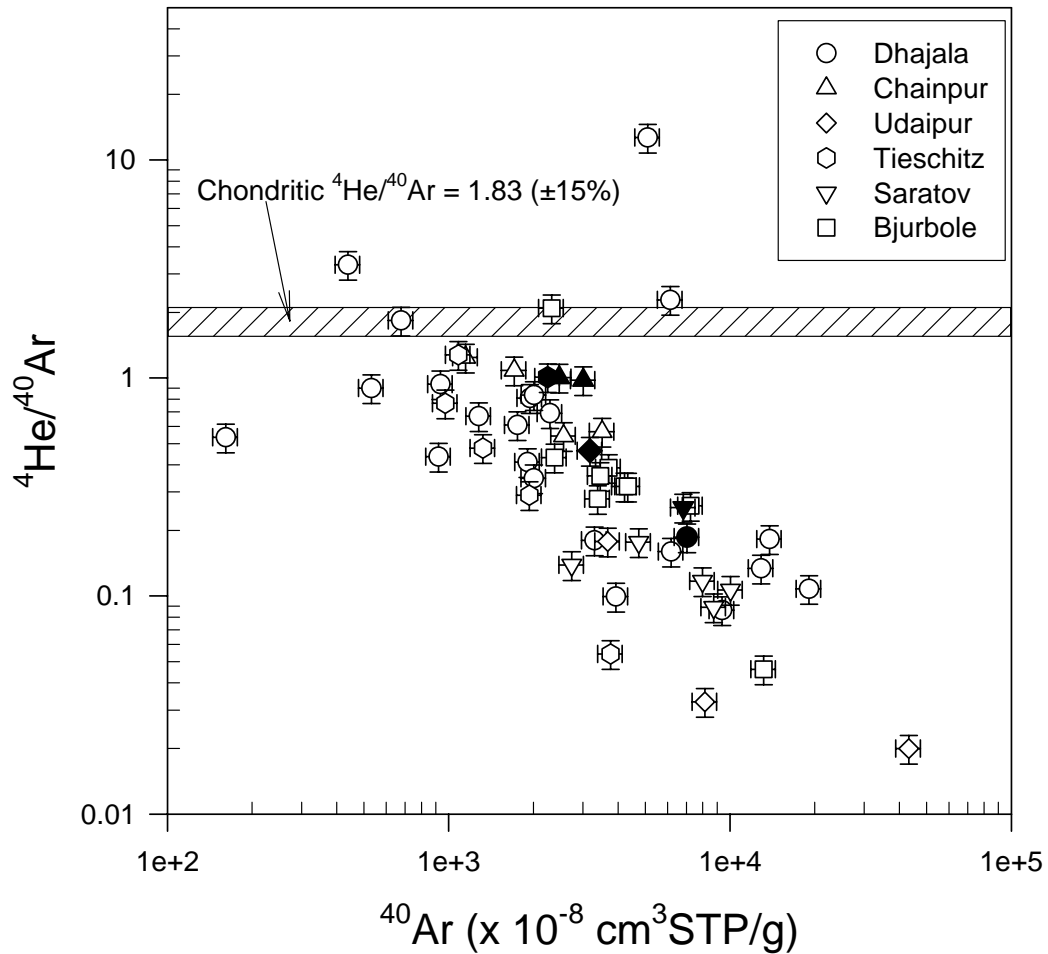


**Fig. 3.14** Elemental ratio  ${}^4\text{He}/{}^{40}\text{Ar}$  of chondrules from ordinary chondrites plotted with concentration of  ${}^{40}\text{Ar}$  in chondrules. The band (with hatched lines) gives the expected value of  ${}^4\text{He}/{}^{40}\text{Ar}$  for the ordinary chondrites (see Table 3.1, for details). In most chondrules (and chondrites), value of  ${}^4\text{He}/{}^{40}\text{Ar}$  is lower compared to expected chondritic value most possibly due to loss of radiogenic  ${}^4\text{He}$ .

DH-8 and DH-11 have presence of higher  ${}^4\text{He}$ , which is also reflected in their  ${}^4\text{He}/{}^{40}\text{Ar}$  values. The value for bulk Dhajala is also lowest among all ordinary chondrites investigated suggesting loss of He.

In nine chondrules, we could measure the Xe contents.  ${}^{129}\text{Xe}_r$  in bulk Dhajala is  $869 \times 10^{-12} \text{ cm}^3\text{STP/g}$ , which is an order of magnitude higher compared to chondrules. Only DH-S28 has concentration around  $543 \times 10^{-12} \text{ cm}^3\text{STP/g}$  whereas all other chondrules show a range between 18 to  $235 \times 10^{-12} \text{ cm}^3\text{STP/g}$ . The range observed in amount of  ${}^{129}\text{Xe}_r$  in chondrules (from other chondrites also) suggest initial heterogeneous distribution of parent elements indicating existence of heterogeneous precursors for chondrules.

**Bjurböle (L/LL4):**

Cosmogenic corrected  $^4\text{He}$  in nine chondrules from Bjurböle chondrite varies from 607 to  $4850 \times 10^{-8} \text{ cm}^3\text{STP/g}$ . Chondrule BB-18 shows higher value of  $^4\text{He}$  compared to maximum  $^4\text{He}_r$  ( $2181 \times 10^{-8} \text{ cm}^3\text{STP/g}$ , Table 3.1) whereas other chondrules have lower  $^4\text{He}$ . Polnau et al. (2001) reported  $1912 \pm 60 \times 10^{-8} \text{ cm}^3\text{STP/g}$  of  $^4\text{He}_r$  for chondrules and  $1523 \times 10^{-8} \text{ cm}^3\text{STP/g}$  for matrix material. Results of nine chondrules suggest that  $^{40}\text{Ar}_r$  does not vary much except for chondrules BB-29 and BB-25. For BB-29 and BB-25 chondrules,  $13160 \times 10^{-8} \text{ cm}^3\text{STP/g}$  and  $7242 \times 10^{-8} \text{ cm}^3\text{STP/g}$  of  $^{40}\text{Ar}_r$  is observed respectively. Other chondrules show  $^{40}\text{Ar}_r$  from 2321 to  $4328 \times 10^{-8} \text{ cm}^3\text{STP/g}$  as seen in Fig 3.14. Polnau et al. (2001) have reported  $7200 \times 10^{-8} \text{ cm}^3\text{STP/g}$  and  $7800 \times 10^{-8} \text{ cm}^3\text{STP/g}$  of  $^{40}\text{Ar}$  in Bjurböle chondrules and matrix respectively. We could not detect Xe in Bjurböle chondrules. Fredriksson et al. (1985) reported  $5430 \times 10^{-8} \text{ cm}^3\text{STP/g}$  of  $^{40}\text{Ar}$  for matrix whereas as high as  $19800 \times 10^{-8} \text{ cm}^3\text{STP/g}$  of  $^{40}\text{Ar}$  for chondrule. The large range of values observed in chondrules and matrix probably suggests large difference in K-content of these samples as well as differential effects of secondary processes.

**Tieschitz (H3.6):**

It is observed that cosmogenic corrected  $^4\text{He}$  in Tieschitz bulk is similar within errors compared to expected maximum  $^4\text{He}_r$  in Tieschitz chondrite. Cosmogenic corrected  $^4\text{He}$  in chondrules is ranging from 204 to  $1382 \times 10^{-8} \text{ cm}^3\text{STP/g}$  as listed in Table 3.2. Among chondrules, TCZ-2 shows  $^4\text{He}$  abundance almost half compared to bulk, similar to  $^3\text{He}_c$  in this chondrule. The amount of cosmogenic corrected  $^4\text{He}$  in bulk Tieschitz is  $2269 \pm 294 \times 10^{-8} \text{ cm}^3\text{STP/g}$  similar to maximum expected radiogenic  $^4\text{He}$  ( $2047 \times 10^{-8} \text{ cm}^3\text{STP/g}$ , Table 3.1) in H chondrites. The depletion of  $^4\text{He}$  in chondrules compared to bulk is suggesting loss of He from chondrules.

It is observed that bulk of Tieschitz chondrite has  $2249 \times 10^{-8} \text{ cm}^3\text{STP/g}$  of  $^{40}\text{Ar}_r$ . Except chondrule TCZ-9, rest of the chondrules are found to have low  $^{40}\text{Ar}_r$  as seen in Fig. 3.14. Chondrule TCZ-2 shows amount of  $^{40}\text{Ar}_r$  which almost lower by factor of 2 compared to bulk. Similar depletion is observed in case  $^{38}\text{Ar}_c$  of this chondrule when compared to bulk. Based on concentrations of  $^4\text{He}$  and elemental ratios  $^4\text{He}/^{40}\text{Ar}$  of chondrules, chondrules do not show presence of trapped He. For three chondrules, we could detect the Xe and  $^{129}\text{Xe}_r$  is varying between 32 to  $462 \times 10^{-12} \text{ cm}^3\text{STP/g}$  compared to  $510 \times 10^{-12} \text{ cm}^3\text{STP/g}$  as observed in Tieschitz bulk (Table 3.2). This difference can be attributed to chemical differences between chondrules and bulk.

### **Chainpur (LL3.4):**

For Chainpur we have analyzed fine and coarse-grained matrix samples. The fine and coarse-grained matrix material are found similar when compared to maximum  ${}^4\text{He}_r$  ( $2181 \times 10^{-8} \text{ cm}^3\text{STP/g}$ , Table 3.1) expected in LL chondrites. It is observed that cosmogenic corrected  ${}^4\text{He}$  in chondrules is varying from 1390 to  $1992 \times 10^{-8} \text{ cm}^3\text{STP/g}$ . These amounts are lower than the maximum  ${}^4\text{He}_r$  as well as amount observed in both fine and coarse-grained matrix materials. In contrast to this, chondrules are found enriched in cosmogenic  ${}^3\text{He}_c$  when compared to matrix material. As mentioned earlier, cosmogenic gases are more retentive when compared to trapped and radiogenic gases. This discrepancy can only be explained by lower concentration of U and Th in chondrules compared to matrix. It is found that fine grained matrix ( $<100 \mu\text{m}$ ) is depleted in  ${}^4\text{He}$  compared to coarse grained matrix material ( $100\text{-}200 \mu\text{m}$ ) probably due to higher diffusion loss of He from fine grained matrix compared to coarse grained material.

Except chondrule CH-3, all chondrules analyzed from Chainpur chondrite show lower  ${}^{40}\text{Ar}_r$  compared to matrix material from Chainpur chondrite (Table 3.2, Fig. 3.14). For chondrule CH-3,  $3512 \times 10^{-8} \text{ cm}^3\text{STP/g}$  of  ${}^{40}\text{Ar}_r$  is observed compared to  $3009 \times 10^{-8} \text{ cm}^3\text{STP/g}$  of  ${}^{40}\text{Ar}_r$  observed in coarse-grained matrix. We found that fine grained matrix material is lower in  ${}^{40}\text{Ar}_r$  compared to coarse-grained as observed for  ${}^4\text{He}$  which yields similar values of  ${}^4\text{He}/{}^{40}\text{Ar}$  for both types of matrix materials (Fig. 3.14). Other chondrules show similar or lower abundances of  ${}^{40}\text{Ar}$  as compared to even fine-grained matrix material (values are listed in Table 3.2).

We could calculate  ${}^{129}\text{Xe}_r$  in all chondrules. The observed range is between 2 to  $1431 \times 10^{-12} \text{ cm}^3\text{STP/g}$  compared to  $\sim 250 \times 10^{-12} \text{ cm}^3\text{STP/g}$  observed in matrix material. Chondrule CH-2 shows highest  ${}^{129}\text{Xe}_r$  compared to other chondrules and higher by factor of  $\sim 7$  compared to matrix (Table 3.2). The observed differences can be explained by different initial Iodine contents.

### **Udaipur (H3):**

The cosmogenic corrected  ${}^4\text{He}$  in Udaipur bulk chondrite is  $1474 \times 10^{-8} \text{ cm}^3\text{STP/g}$  lower compared to expected maximum  ${}^4\text{He}_r$  ( $2047 \times 10^{-8} \text{ cm}^3\text{STP/g}$ , Table 3.1) suggesting loss of  ${}^4\text{He}$  from the bulk chondrite. It is observed that cosmogenic corrected  ${}^4\text{He}$  in chondrules is varying from 266 to  $862 \times 10^{-8} \text{ cm}^3\text{STP/g}$ .

It is observed that three chondrules are rich in  ${}^{40}\text{Ar}_r$  compared to bulk (Table 3.2, Fig. 3.14). Chondrules show a range from 3673 to  $43180 \times 10^{-8} \text{ cm}^3\text{STP/g}$  compared to

$3179 \times 10^{-8} \text{ cm}^3\text{STP/g}$  of  $^{40}\text{Ar}_r$  in bulk. In chondrule UD-2, highest  $^{40}\text{Ar}_r$  ( $43180 \pm 4340 \times 10^{-8} \text{ cm}^3\text{STP/g}$ ) is observed, which is higher by factor of 14 compared to bulk. For chondrule UD-3,  $^{40}\text{Ar}_r$  is also higher by factor of 3 compared to bulk. This can be due to either atmospheric contamination or presence of higher K content in these chondrules. For chondrule UD-2, if we consider that all trapped  $^{36}\text{Ar}$  (which is  $12.4 \times 10^{-8} \text{ cm}^3\text{STP/g}$ ) is of atmospheric origin and calculate  $^{40}\text{Ar}_r$  due to atmospheric contamination ( $^{40}\text{Ar}_{\text{air}} = 295.5 \times ^{36}\text{Ar}_t$ ) it is around  $370 \times 10^{-8} \text{ cm}^3\text{STP/g}$  accounting for only ~8% of the observed value. In this case, presence of higher K content is the possible reason for high abundance of  $^{40}\text{Ar}_r$  in these chondrules. All three chondrules show a range between 71 to  $200 \times 10^{-12} \text{ cm}^3\text{STP/g}$  of  $^{129}\text{Xe}_r$  whereas bulk is having  $159 \times 10^{-12} \text{ cm}^3\text{STP/g}$  of  $^{129}\text{Xe}_r$ .

#### **Saratov (L4):**

Saratov bulk shows lower cosmogenic corrected  $^4\text{He}$  compared to maximum  $^4\text{He}_r$  in Saratov ( $2181 \times 10^{-8} \text{ cm}^3\text{STP/g}$ , Table 3.1) indicating loss of  $^4\text{He}$  from Saratov chondrite. The calculated cosmogenic corrected  $^4\text{He}$  in chondrules ranges from 380 to  $1072 \times 10^{-8} \text{ cm}^3\text{STP/g}$  compared to  $1736 \times 10^{-8} \text{ cm}^3\text{STP/g}$  in bulk Saratov. Similar depletion of  $^3\text{He}_c$  is observed in these chondrules compared to bulk.

For Saratov bulk,  $^{40}\text{Ar}_r$  is  $\sim 6820 \times 10^{-8} \text{ cm}^3\text{STP/g}$ . All other chondrules, except chondrule STV-6 and STV-7, show higher amount of  $^{40}\text{Ar}_r$  compared to bulk Saratov (Table 3.2, Fig 3.14). Chondrules seem to have variable amount of  $^{40}\text{Ar}_r$ . The observed  $^{40}\text{Ar}_r$  in chondrules and bulk of Saratov are consistent with earlier reports as compiled by Schultz and Franck (2004). The  $^{129}\text{Xe}_r$  in chondrules varies from 56 to  $440 \times 10^{-12} \text{ cm}^3\text{STP/g}$  compared to  $115 \times 10^{-12} \text{ cm}^3\text{STP/g}$  in bulk (Table 3.2).

#### **3.3.3.2 Chondrules from enstatite chondrites**

##### **Parsa (EH3):**

The cosmogenic corrected  $^4\text{He}$  in bulk Parsa chondrite is  $2300 \times 10^{-8} \text{ cm}^3\text{STP/g}$ . Three chondrules analyzed show a narrow range of cosmogenic corrected  $^4\text{He}$  from 1141 to  $1371 \times 10^{-8} \text{ cm}^3\text{STP/g}$  lower compared to bulk and expected maximum radiogenic  $^4\text{He}$  ( $1700 \times 10^{-8} \text{ cm}^3\text{STP/g}$ , Table 3.1). This kind of depletion in  $^3\text{He}_c$  is not observed; instead, it is found that chondrules are rich in  $^3\text{He}_c$  as also observed in the case of chondrules from Chainpur chondrite. This kind of observation can be explained based on better retention of cosmogenic gases compared to radiogenic gases.

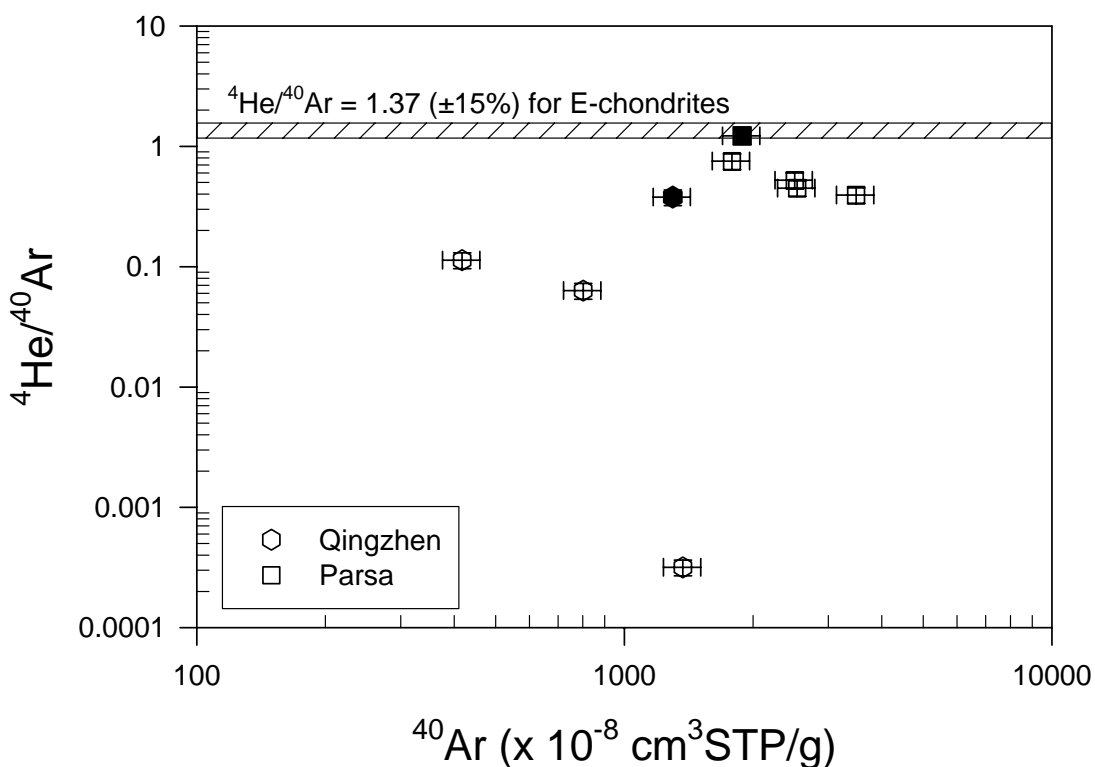


**Fig. 3.15** Elemental ratio  $^4\text{He}/^{40}\text{Ar}$  of chondrules from enstatite chondrites plotted with concentration of  $^{40}\text{Ar}$  in chondrules. The band gives the expected value of  $^4\text{He}/^{40}\text{Ar}$  for the enstatite chondrites (see Table 3.4, for details). In most chondrules, value of  $^4\text{He}/^{40}\text{Ar}$  is lower compared to expected chondritic value most possibly due to loss of radiogenic  $^4\text{He}$ . Symbol: open – chondrules, filled – bulk

It is observed that  $^{40}\text{Ar}_r$  in four chondrule samples of Parsa vary from 1785 to 3484 x  $10^{-8}$  cm $^3$ STP/g (as listed in Table 3.3 and shown in Fig. 3.15). The other two chondrules Parsa-1 and 2 show similar  $^{40}\text{Ar}_r$ . It is found that bulk of Parsa chondrite is depleted in  $^{40}\text{Ar}_r$ , compared to chondrules.

Chondrules show lower values of  $^4\text{He}/^{40}\text{Ar}$  compared to bulk. Parsa bulk shows value of  $^4\text{He}/^{40}\text{Ar}$  similar to expected value in enstatite chondrite (Fig. 3.15). Presence of solar type noble gases are reported earlier in Parsa chondrite (Murty 1992). Qingzhen show depleted value suggesting loss of  $^4\text{He}$  from this chondrite. In chondrules similar evidence of solar type gases are not observed.

It is observed that the radiogenic  $^{129}\text{Xe}$  in chondrules are similar to Parsa bulk within errors. Chondrules Parsa-1 and splits of Parsa-3 show lower concentration of  $^{129}\text{Xe}_r$  compared to 914 x  $10^{-12}$  cm $^3$ STP/g measured in bulk Parsa. Chondrule Parsa-2 shows similar (953 x  $10^{-12}$  cm $^3$ STP/g) concentration of  $^{129}\text{Xe}_r$  (values are listed in Table 3.3).

### **Qingzhen (EH3):**

Cosmogenic corrected  $^4\text{He}$  in Qingzhen bulk sample is  $490 \times 10^{-8} \text{ cm}^3\text{STP/g}$ . Chondrules show very low amount of cosmogenic corrected  $^4\text{He}$ . It is possible that He loss in chondrules is more severe as compared to bulk. In chondrules, cosmogenic corrected  $^4\text{He}$  varies from 0.43 to  $51 \times 10^{-8} \text{ cm}^3\text{STP/g}$  as listed in Table 3.3. As mentioned earlier, cosmogenic  $^3\text{He}$  is also depleted in chondrules compared to bulk chondrite. For smaller chondrules QZN-3 and QZN-5, we could not detect any He above blank concentration. For chondrule QZN-2, lowest concentration of cosmogenic corrected  $^4\text{He}$  is observed ( $0.43 \times 10^{-8} \text{ cm}^3\text{STP/g}$ , Table 3.3). The  $^4\text{He}/^{40}\text{Ar}$  value of this chondrule is also very low due to this lower value of  $^4\text{He}$  suggesting loss of  $^4\text{He}$  compared to  $^{40}\text{Ar}$ . The gas retention age based on  $^4\text{He}_r$  calculated for Qingzhen is  $\sim 1\text{Ga}$ . Patzer and Schultz (2001) reported 0.89 Ga of gas retention age for Qingzhen based on  $^4\text{He}_r$ . These ages are surely indicative of loss of  $^4\text{He}$  from chondrules as well as bulk.

Two chondrules QZN-3 and QZN-5 show higher  $^{40}\text{Ar}_r$  ( $2400\text{-}2800 \times 10^{-8} \text{ cm}^3\text{STP/g}$ , Table 3.3). For Qingzhen bulk,  $1300 \times 10^{-8} \text{ cm}^3\text{STP/g}$  of  $^{40}\text{Ar}_r$  is observed. Other three chondrules show  $^{40}\text{Ar}_r$  from 510 to  $1371 \times 10^{-8} \text{ cm}^3\text{STP/g}$ , which is lower or similar compared to bulk (Fig. 3.15). Usually chondrules show depletion of Ar (like trapped  $^{36}\text{Ar}$  or cosmogenic  $^{38}\text{Ar}$ , due to loss of Ar) and the lower concentration of radiogenic  $^{40}\text{Ar}$  compared to bulk is explainable. However, it is difficult to explain the higher concentration of  $^{40}\text{Ar}$  in chondrules QZN-3 and 5. The higher concentration of K is the only possibility for these two chondrules. Unfortunately, very small sizes of these chondrules have not allowed us to determine the chemical composition of these chondrules.

Unlike the case of other chondrites, chondrules from Qingzhen chondrite show higher concentration of radiogenic  $^{129}\text{Xe}$  compared to bulk. The range is between 474 to  $1221 \times 10^{-12} \text{ cm}^3\text{STP/g}$  compared to  $368 \times 10^{-12} \text{ cm}^3\text{STP/g}$  of  $^{129}\text{Xe}_r$  in bulk. This result is consistent with earlier work of Grossmann et al (1985), which has also indicated higher concentration of  $^{129}\text{Xe}$  in chondrules. As discussed in the results of cosmogenic  $^{38}\text{Ar}$ , we suspected that as chondrules were rich in Cl and I compared to bulk and consequently could have contribution from neutron produced  $^{36}\text{Ar}$ .

### 3.3.3.3 Chondrules from carbonaceous chondrites

#### Allende (CV3.2):

Concentration of cosmogenic corrected  $^4\text{He}$  in these chondrules is varying from 648 to  $2748 \times 10^{-8} \text{ cm}^3\text{STP/g}$  a large range. All chondrules are having concentration of cosmogenic corrected  $^4\text{He}$  lower than maximum radiogenic  $^4\text{He}$  ( $2907 \times 10^{-8} \text{ cm}^3\text{STP/g}$ , Table 3.1). Chondrule ALD-14 shows highest amount of cosmogenic corrected  $^4\text{He}$  compared to all Allende chondrules. ALD-16 on the other hand shows lowest amount of cosmogenic corrected  $^4\text{He}$ . This large variation of  $^4\text{He}$  concentration suggests variable loss of He from chondrules. Although in case of  $^3\text{He}_c$  concentrations, variation of this magnitude is not observed in these chondrules probably due to better retention of cosmogenic gases.

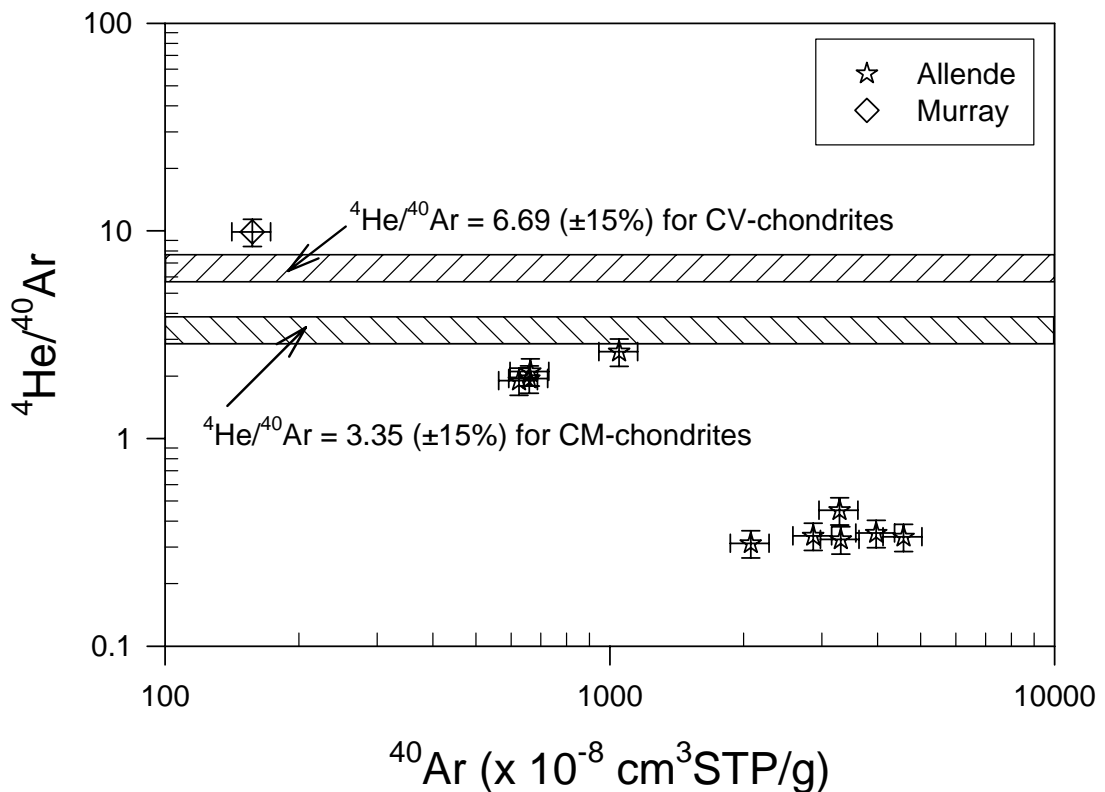


**Fig. 3.16** Elemental ratio  $^4\text{He}/^{40}\text{Ar}$  of chondrules from Allende and Murray chondrites plotted with concentration of  $^{40}\text{Ar}$  in chondrules. The band gives the expected value of  $^4\text{He}/^{40}\text{Ar}$  for the CV and CM chondrites (see Table 3.4, for details). In most chondrules, value of  $^4\text{He}/^{40}\text{Ar}$  is lower compared to expected chondritic value most possibly due to loss of radiogenic  $^4\text{He}$ . MRY-1 chondrule show higher  $^4\text{He}/^{40}\text{Ar}$  value.

As mentioned earlier, we could not analyze Ar in six chondrules due to problem in Ar analyses. For other eight chondrules, it is observed that concentration of radiogenic  $^{40}\text{Ar}$  varies from 663 to  $4576 \times 10^{-8} \text{ cm}^3\text{STP/g}$  (Fig. 3.16). The elemental ratio

$^4\text{He}/^{40}\text{Ar}$  for most of the chondrules are uniform and lower compared to expected value in CV3 bulk chondrites suggesting similar loss of He and Ar from chondrules.

We could not detect any radiogenic  $^{129}\text{Xe}$  in Allende chondrules.

### **Murray (CM2):**

It is observed that cosmogenic corrected  $^4\text{He}$  in Murray bulk sample is  $\sim 9320 \times 10^{-8} \text{ cm}^3\text{STP/g}$  highest concentration observed compared to all chondrites analyzed in this work. The amount of  $^4\text{He}$  observed in Murray bulk chondrite is higher by factor of 5 compared to maximum radiogenic  $^4\text{He}$  expected in Murray chondrite ( $1898 \times 10^{-8} \text{ cm}^3\text{STP/g}$ , Table 3.1). This can be explained by the presence of a trapped He component. Chondrules show concentration of cosmogenic corrected  $^4\text{He}$  varying from 329 to  $1554 \times 10^{-8} \text{ cm}^3\text{STP/g}$ . The highest concentration of  $^4\text{He}$  is observed for MRY-1 chondrule (Table 3.4). The values observed in chondrules are very low compared to the bulk chondrite could be due to differences in parent elements.

$^{40}\text{Ar}_r$  in bulk of Murray chondrite is  $176 \times 10^{-8} \text{ cm}^3\text{STP/g}$  (Table 3.4, Fig. 3.16). We could not measure Ar concentration in three chondrules of Murray except the large chondrule MRY-1B.  $^{40}\text{Ar}_r$  in this chondrule is depleted comparable to bulk ( $157 \times 10^{-8} \text{ cm}^3\text{STP/g}$ ). Probably difference in chemistry is responsible for such differences in amount of  $^{40}\text{Ar}$ . The elemental ratio of  $^4\text{He}/^{40}\text{Ar}$  is higher in this chondrule compared to expected value in CM2 chondrites (Fig. 3.16).

We could not detect any Kr or Xe concentrations in the chondrules from this chondrite.

### **3.3.4 Gas retention ages ( $T_4$ , $T_{40}$ ) of chondrules**

The calculated gas retention ages of chondrules and their chondrites are given in Tables 3.2, 3.3, and 3.4. The comparison between  $T_4$  (gas retention age based on radiogenic  $^4\text{He}$ ) and  $T_{40}$  (gas retention age based on radiogenic  $^{40}\text{Ar}$ ) is made in Fig. 3.17.

Gas retention ages are determined from the concentrations of U, Th, and K and their radiogenic products  $^4\text{He}$  and  $^{40}\text{Ar}$  (e.g., Faure, 1986). Ideally, the gas retention ages characterize the crystallization time of meteoritic matter. Generally, thermal events possibly initiated by impact events on the parent body led to loss of radiogenic gases. Hence, usually the calculated retention ages are lower than the actual crystallization ages and reflect the thermal history of the material. Since  $^4\text{He}$  is already mobilized at a few hundred degrees Celsius, the corresponding U, Th- $^4\text{He}_r$  age is more easily modified or reset than the K- $^{40}\text{Ar}$  age of the same sample (Anders, 1964).

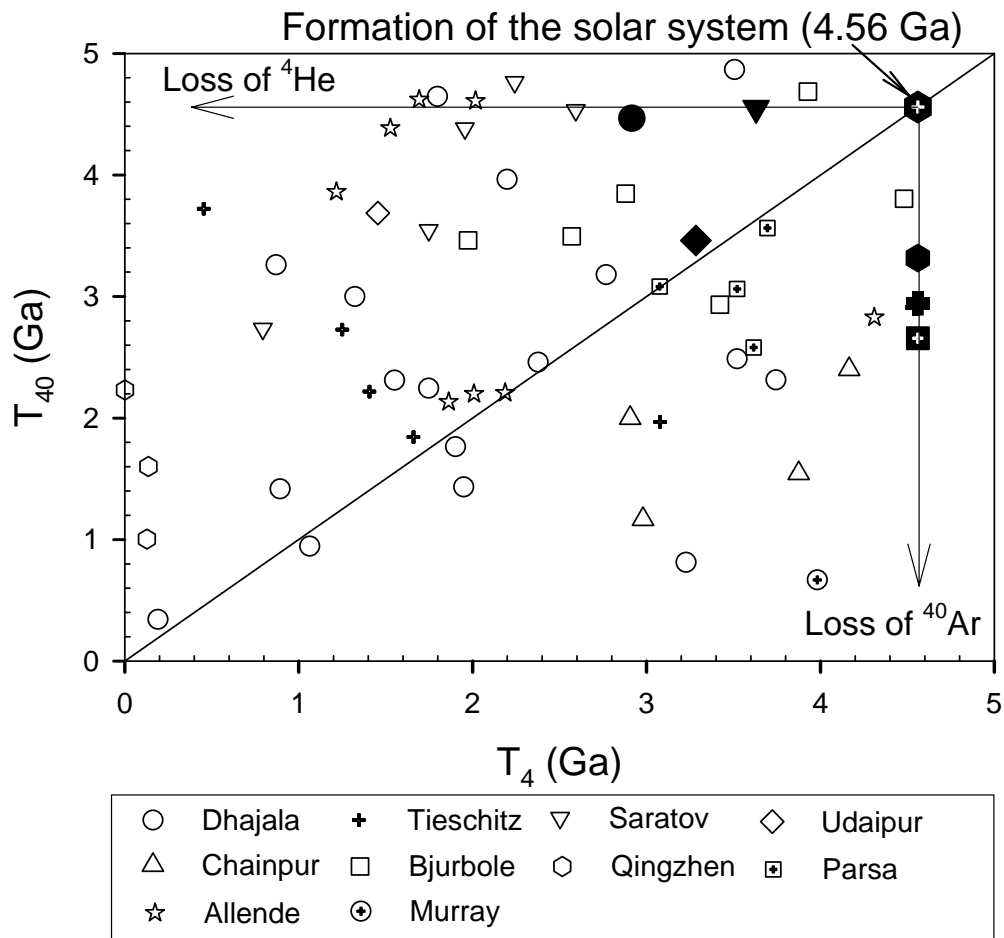


**Fig. 3.17**  $K\text{-}^{40}\text{Ar}$  and  $U/\text{Th}\text{-}^4\text{He}$  gas retention ages of all chondrules and their respective bulk (Open: chondrules, Filled: Bulk). Most of the chondrules show loss of He and Ar indicating the effect of secondary events on chondrules. Compared to  $^{40}\text{Ar}$  loss of  $^4\text{He}$  is higher.

As can be seen in Fig. 3.17, most chondrules show lower  $U, \text{Th}\text{-}^4\text{He}_r$  ages compared to  $K\text{-}^{40}\text{Ar}_r$  ages. Few chondrules also show higher values of  $K\text{-}^{40}\text{Ar}_r$ , suggesting that the assumed content of K is an under estimate. Above all, most chondrule samples show ages, which apparently reflect thermal processing. For L chondrites such age distribution show cluster at  $\sim 1\text{Ga}$  (e.g. Schultz, 1993, Lipschultz and Schultz, 1999). On the other hand, H chondrites exhibit cluster at 4- 4.5Ga. In case of chondrules, cluster at single value is not evident. It is possible that chondrules might have experienced different degree of secondary events and at the same time, heterogeneity in chondrule precursors for the content of U, Th and K cannot be ruled out.

### **3.4 Discussion**

#### **3.4.1 Loss of cosmogenic and radiogenic noble gases from chondrules**

As discussed in results for most chondrules, loss of cosmogenic and radiogenic gases is observed compared to bulk as well as maximum expected values for chondritic components. Variable losses of different gases (like cosmogenic, radiogenic as well as He, Ne and Ar) can be explained based on their retention against loss by diffusion. Based on production rates (which normalize abundances of cosmogenic noble gases based on chemical composition of chondrules) of cosmogenic noble gases, the variation observed in abundances of cosmogenic noble gases in chondrules is understood up to certain extent. Similarly, the variation observed for radiogenic gases can be attributed to difference in initial contents of parent nuclides. Another reason can be possible higher uncertainty with calculated production rates. As discussed in Chapter 2, section 2.7.2), due to possible limitations involve with EPMA method, the chemical composition (of the surface) used for calculation of production rates may not truly represent the actual (volume) composition of the chondrule. The uncertainty can also be high in abundances of cosmogenic isotopes due to uncertainty in weights of chondrules especially for smaller chondrules. However, the maximum uncertainty in the smallest samples (~60  $\mu\text{g}$ ) can be at best  $\leq 5\%$  only. In some cases, it is found that chondrules have lower cosmic ray exposure duration compared to bulk. In such case, loss of cosmogenic gases is the only possible explanation. In most cases, loss of cosmogenic noble gases is associated with loss of radiogenic gases especially in case of He. This suggests that loss of gases occurred during exposure duration, most probably due to solar heating on orbits with small perihelia (Schultz and Weber, 1995, 1997). In a few cases like DH-V38 chondrule, It is found that cosmogenic  $^3\text{He}$  is depleted by a factor 33 compared to Dhajala bulk. Though expected loss of radiogenic  $^4\text{He}$  is higher compared to the cosmogenic  $^3\text{He}$ , however the depletion of  $^4\text{He}_r$  is found lower compared to  $^3\text{He}_c$ . It is possible that chondrule DH-V38, may have some amount of trapped  $^4\text{He}$  making the apparent depletion factor of  $^4\text{He}$  less when compared with depletion of  $^3\text{He}_c$  in this chondrule compared to Dhajala bulk. Hence, presence of trapped He sometime can overshadow the partial loss of He from total He present in chondrules as well as chondrites. On the other hand, lower Argon exposure ages ( $T_{38}$ ) of enstatite chondrites indicates the loss of  $^{38}\text{Ar}_c$  from Ca-rich phases. The

results suggest that Ne is least affected by secondary process and up to certain extent able to preserve the primary signatures.

***Loss of cosmogenic gases: comparison between chondrules and their host chondrite***

As discussed earlier, loss of cosmogenic gases are evident in most chondrules. The CRE ages calculated based on these abundances yield lower ages compared to bulk. The expectation is that either chondrule can have similar or higher cosmic ray exposure duration compared to its host meteorite. In case of loss of gases, similar extent of loss is expected from chondrules and bulk. However, the observed lower CRE ages compared to bulk suggest loss of cosmogenic gases preferentially from chondrules. Similar is the case for radiogenic gases. For most chondrules, we found that abundances of  $^4\text{He}$  and  $^{40}\text{Ar}$  are lower compared to bulk. In case of radiogenic cases, assuming higher loss of gases from chondrules relative to bulk is not possible as lower content of initial parent elements can also result in lower radiogenic gases.

***Gas retention ages of chondrules and secondary thermal events***

As discussed in section 3.4.3, gas retention ages of chondrules based on  $^4\text{He}$  and  $^{40}\text{Ar}$  mostly suggest loss of gases mainly for He. This suggests the effect of secondary events on chondrules. These events can be in three stages: (1) after formation and before becoming part of parent body (nebular secondary alteration) (2) on parent body by any thermal event initiated by impact (3) during their journey to earth as meteoroid. In last two stages, the secondary events affect bulk chondrite and chondrules simultaneously unlike first stage when chondrules were freely floating in space. It is very difficult to decouple the effects of secondary events at various stages. However, due to such secondary event, finding signatures of precompaction exposure in chondrules is not easy. In contrast to this, Polnau et al. (1999) have reported evidence of precompaction exposure in single large chondrule (~ 4mm) found in H6 chondrite ALH76008. The other study, which has reported evidence of precompaction exposure of chondrules, was performed on powder of many chondrules (Polnau et al., 2001). Homogenized powders represent an average of many large chondrules (> 0.7 mm).

**3.4.2 Precompaction exposure of chondrules and duration of their formation**

As mentioned in introduction, for detection of precompaction exposure in chondrules chondrites with lower cosmic ray exposure ages will be ideal samples. As discussed earlier, most of our chondrites are of higher exposure ages except Dhajala (~ 5 Ma), Bjurböle (~ 8 Ma) Allende (~ 5 Ma) and Murray (2-6 Ma). However, gas retention

ages of chondrules based on  $^4\text{He}$  and  $^{40}\text{Ar}$  suggest loss of gases from these chondrules. Hence, to detect the signature of precompaction exposure, together with lower exposure age lower degree of secondary alteration event also is an important criterion for chondrite under study.

As discussed earlier, most chondrules seem to be affected by secondary event as well as belong to chondrites with higher cosmic ray exposure ages. However, for a few chondrules, higher concentrations of cosmogenic noble gases (mainly  $^{21}\text{Ne}$  and  $^{38}\text{Ar}$ ) compared to bulk, which cannot be explained based on different chemical compositions or preferential loss of cosmogenic noble gases from bulk.

In case of chondrule DH-5 from Dhajala chondrite, Helium exposure age ( $T_3$ ) is  $1.52 \pm 0.15$  Ma, less than that of bulk ( $3.83 \pm 0.38$  Ma). It is observed that radiogenic  $^4\text{He}$  is lower by factor 1.3 compared to bulk supporting loss of He from this chondrule. On the other hand, gas retention age of bulk based on radiogenic  $^4\text{He}$  is 2.97 Ga, which is also suggesting loss of He. For chondrule DH-5 still lower gas retention age (2.20 Ga) is calculated. Possibility of loss of He (more loss in chondrule compared to bulk) cannot be ruled out based on these results. However, CRE age calculated by  $^{21}\text{Ne}$  concentration of this chondrule is  $7.15 \pm 1.29$  Ma compared to  $5.71 \pm 1.03$  Ma CRE age of bulk. The CRE ages of chondrule and bulk overlap if we considering the lower limit of error for CRE age of chondrule and higher limit of error for that of bulk. However, chondrule seems to have 25% higher exposure age if we consider the main values. The CRE ages based on  $^{38}\text{Ar}$  are  $9.36 \pm 1.69$  Ma and  $5.42 \pm 0.98$  Ma for DH-5 and bulk Dhajala chondrite respectively. Clear excess of maximum 1.3 Ma of excess exposure is evident for chondrule DH-5. The gas retention age of Dhajala chondrite based on  $^{40}\text{Ar}$  radiogenic is 4.47 Ga. Within 10% error this is matching with solar system age (4.56 Ga) suggesting no loss of radiogenic Ar from this chondrite. Radiogenic  $^{40}\text{Ar}$  in chondrule DH-5 is comparable with bulk within errors and the gas retention age calculated based on  $^{40}\text{Ar}$  is 4.00 Ga. Based on CRE ages ( $T_{21}$  and  $T_{38}$ ) chondrule DH-5 clearly shows evidence of excess cosmic ray exposure duration ( $\sim 1$  Ma) compared to bulk.

In case of Bjurböle chondrules, it was found that chondrules show either lower or higher cosmic ray exposure ages compared to reported exposure duration for matrix. The Neon exposure ages ( $T_{21}$ ) of chondrules vary from 8 to 10 Ma. Polnau et al. (2001) have reported evidence of pre-compaction exposure for chondrules (analyzed as powder of chondrules  $> 0.7$  mm) compared to matrix in Bjurböle chondrite. To

explain the observed range of cosmic ray exposure duration for Bjurböle chondrules it is required that chondrules or precursors of chondrules experienced the cosmic ray exposure over extended period like 2 Ma before accreting to the parent body.

Argon ages ( $T_{38}$ ) of three Chainpur chondrules are also higher compared to matrix. Chondrules show 30 to 40 Ma of age compared to matrix (~23 Ma). The difference of exposure ages suggested by this observation is very large. As discussed earlier the high concentration of trapped Ar as well as partial loss of Ar from matrix also seems responsible for such large difference of exposure ages.

Although most chondrules from Allende seem severely affected by secondary processes based on their lower exposure ages, one of the chondrules shows higher Argon exposure duration. Chondrule ALD-14 shows excess of 3.4 Ma exposure compared to calculated-exposure age of Allende bulk based on literature data. The gas retention age of this chondrule is 4.31 Ga, which is higher compared to other chondrules suggesting that Ar from other chondrules is affected due to partial loss whereas ALD-14 chondrule, which seems least affected is indicating the excess duration of cosmic ray exposure compared to bulk.

For chondrule MRY-1 from Murray chondrite, CRE age based on  $^3\text{He}$  is  $3.22 \pm 0.32$  Ma higher compared to  $1.04 \pm 0.10$  Ma CRE age of bulk chondrite. The reported CRE age of Murray bulk is 6 Ma (based on cosmogenic noble gases, Hohenberg et al., 1990). However, Herzog et al. (1997) suggest 2 to 6 Ma of complex exposure for Murray due to range observed for CRE age based on activities of short-lived radionuclides ( $^{26}\text{Al}$ ,  $^{10}\text{Be}$  and  $^{53}\text{Mn}$ ). Loss of  $^3\text{He}_c$  from Murray bulk is evident based on low  $T_3$  age. The gas retention age of Murray bulk based on radiogenic  $^4\text{He}$  is 4.56 Ga (gas retention age of MRY-1 chondrule is 3.98 Ga). This can be explained in two ways: either no loss of He from bulk or presence of trapped  $^4\text{He}$  which is enough to overshadow the loss of radiogenic  $^4\text{He}$ . As shown in Fig. 3.5,  $(^3\text{He}/^{21}\text{Ne})_c$  of Murray bulk is lower compared to expected range in carbonaceous chondrites. It seems that CRE age of Murray bulk is affected due to loss of He. Hence, difference of exposure ages ( $T_3$ ) in chondrule and bulk can be explained by loss of  $^3\text{He}_c$  from bulk compared to chondrule.  $T_{21}$  of chondrule MRY-1 is  $3.66 \pm 0.66$  Ma, which is higher, compared to  $2.85 \pm 0.51$  Ma CRE age of bulk. Considering the lower limit of error for this CRE age of chondrule and higher limit of error for that of bulk, the CRE ages overlap however; the difference of main value is 0.8 Ma. For chondrule MRY-1, the CRE age based on  $^{38}\text{Ar}$  is  $8.08 \pm 1.21$  Ma. Unfortunately, due to some technical

problem, Ar measurement could not be performed for Murray bulk. However, based on higher CRE age ( $T_{21}$ ) of chondrule MRY-1, excess cosmic ray exposure for duration of  $\sim 0.8$  Ma is evident when compared to bulk. Hohenberg et al. (1990) observed that excesses of nuclear tracks in single grains of CM chondrites including Murray associated with variable but occasionally large excesses of cosmogenic neon in these grains. Authors explained this by an event of enhanced solar cosmic ray intensity (e.g. during the T-Tauri phase of the early sun). It is possible that chondrule MRY-1 or precursors of it have experienced such event before becoming part of parent body.

These above discussed cases show evidence for possible precompaction irradiation of the chondrules from ordinary and carbonaceous chondrites. Cosmic ray exposure history of three chondrules from Parsa chondrite is investigated and no chondrule shows any evidence of excess cosmic ray exposure.

### **3.4.3 Pre-compaction irradiation and exposure to solar cosmic rays:**

As discussed above, in a few chondrules, evidence of excess exposure in chondrules are observed compared to their bulk. As explained in Chapter 1 (Fig. 1.6), chondrule can possibly have this excess duration of exposure after their formation and before accreting into chondritic parent body. In the model proposed by Shu et al. (1996), the formation of chondrule is suggested near to the sun around 0.6 AU. In this case, it is expected that chondrule formed near the sun would have signatures of solar environment. Presence of solar type trapped noble gases is also reported (Okazaki et al., 2001a). In similar argument, it is expected that chondrules should show similar evidences of exposure to solar cosmic rays in case of precompaction exposure (Das and Murty, 2005). The SCR and GCR nuclides are produced in comparable abundances within a few mm of an exposure surface, and at depths of a few cm, the GCR component greatly dominates. Hence, in case of precompaction exposure, chondrules would have received both SCR and GCR as their sizes are in range of 1 mm. Based on comparison between abundances of SCR produced nuclides and GCR produced nuclides, SCR and GCR components can be decoupled.  $(^{22}\text{Ne}/^{21}\text{Ne})_c$  ratio can be used as an indicator for this purpose (e.g. Garrison et al., 1995) as SCR and GCR components are made by different suites of energetic particles, production mechanisms of cosmogenic  $^{22}\text{Ne}$  (favored by SCR) and  $^{21}\text{Ne}$  (favored by GCR) are not same. Hence,  $(^{22}\text{Ne}/^{21}\text{Ne})_c$  ratio can show characteristic difference for the presence of SCR component in chondrules in case of their precompaction history. The

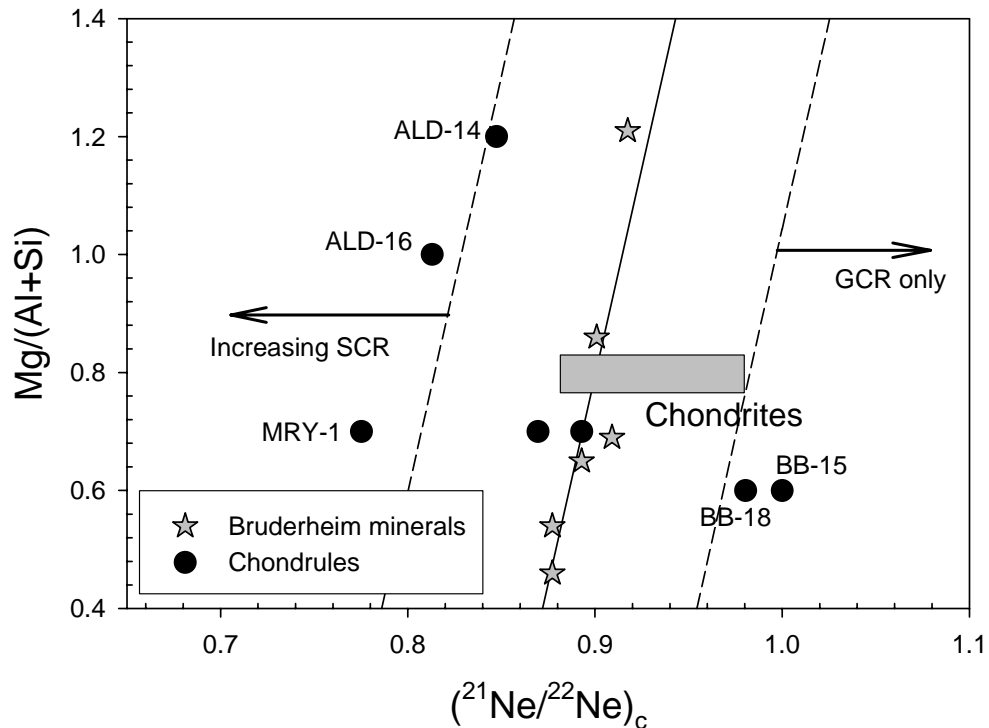


**Fig. 3.18** Plot of the Mg/(Al+Si) element concentration ratio against cosmogenic  $(^{22}\text{Ne}/^{21}\text{Ne})_c$  for the chondrules with precompaction exposure history. The regression line represents the variation of  $(^{22}\text{Ne}/^{21}\text{Ne})_c$  with Mg/(Al+Si) ratio as observed in mineral separates of Bruderheim meteorite (Bogard and Cressy, 1973). The box represents the ranges of  $^{21}\text{Ne}/^{22}\text{Ne}$  (Wieler, 2002) and Mg/(Al+Si) (Jarosewich, 1990) in chondrites. Chondrules MRY-1 and ALD-16 show possibility of SCR component acquired during precompaction exposure.

Chondrules where evidence of precompaction exposure is found generally show higher values of  $(^{22}\text{Ne}/^{21}\text{Ne})_c$  ratio as listed in Table 3.6. However, the ratio is also sensitive to the target chemical composition of the sample. As suggested by Garrison et al. (1995),  $(^{22}\text{Ne}/^{21}\text{Ne})_c$  ratio can increase with increase in Mg/(Al+Si) ratio in samples as Mg is the major target element for the production of cosmogenic  $^{21}\text{Ne}$ . To investigate the reason for higher values of  $(^{22}\text{Ne}/^{21}\text{Ne})_c$  ratio in these chondrules, in Fig. 3.18, the  $(^{22}\text{Ne}/^{21}\text{Ne})_c$  ratio of chondrules (with evidence of precompaction exposure history) are compared with their Mg/(Al+Si) ratios. The regression line (with  $\pm 10\%$  range) given in Fig. 3.18, represents the variation observed in the mineral separates of Bruderheim meteorite (data taken from Bogard and Cressy, 1973). The observed range for chondrites is also shown as box in this plot. Except chondrules ALD-16 and MRY-1, either fall within the range (shown by dotted lines) or towards GCR component. The plot suggests that the higher value of  $(^{22}\text{Ne}/^{21}\text{Ne})_c$  ratio in chondrules ALD-16 and MRY-1. Higher values of  $(^{22}\text{Ne}/^{21}\text{Ne})_c$  for these chondrules clearly suggest a two stage exposure for them: a normal exposure in parent body

along with the chondrules from the same depth, and a free space exposure prior to compaction. This precompaction irradiation is a combination of exposure to SCR (at possibly higher flux compared to present, as suggested by Caffee et al. 1987) and GCR. Precise portioning into SCR and GCR contribution is not possible. If flux of solar cosmic rays was several orders of magnitude higher during early stages of solar system formation then it is difficult to constrain the actual precompaction exposure duration of these chondrules. In case of very high intensity of solar cosmic rays, the precompaction exposure duration of chondrules would be correspondingly short. However, the presence of SCR component in at least two chondrules (ALD-16 and MRY-1) suggests that before accreting to chondritic parent body chondrules were irradiated by solar cosmic rays.

### **3.5 Summary**

1. Compared to bulk chondrites it is found that chondrules are depleted in  $^3\text{He}_c$  concentrations resulting in lower value of cosmic ray exposure ages of chondrules. For the case of Chainpur, Parsa and Murray it was found that, bulk/matrix-material is lower in  $^3\text{He}_c$  concentration compared to chondrules. Loss of  $^3\text{He}_c$  is also associated with lower cosmogenic corrected  $^4\text{He}$  in chondrules, which are mostly found lower compared to bulk. In addition, for such cases lower gas retention ages are observed.
2. Cosmic ray exposure ages based on  $^{21}\text{Ne}$  of chondrules are found more useful and consistent with bulk chondrites. For most cases, the cosmic ray exposure ages of chondrules match with bulk except few chondrules.
3. Chondrules DH-5, BB-29, BB-18, BB-15, ALD-14 and MRY-1 show evidence of precompaction exposure compared to their bulk. The precompaction exposure duration for these chondrules is from 0.8 to 3.4 Ma, suggesting extended duration of chondrule formation. These results support the nebular environment of chondrule formation. The presence of SCR component based on ( $^{22}\text{Ne}/^{21}\text{Ne}$ ) ratio in chondrules ALD-16 and MRY-1 suggests the chondrule formation possibly near the sun as suggested by X-wind model (Shu et al., 1996).
4. Higher variation of  $^{38}\text{Ar}$  concentration are observed in chondrules within their suits as well as compared to their host chondrites. Similar kind of variation is also observed for radiogenic  $^{40}\text{Ar}$  in chondrules. For the case of Qingzhen

chondrite, we found the evidence of neutron-capture produced  $^{36}\text{Ar}$  in chondrules. There is no evidence for the presence of such kind of Ar in bulk Qingzhen.

5. Gas retention ages of chondrules suggest effect of secondary events on noble gases. In presence of such secondary effects, it is not easy to detect any evidence of precompaction exposure of chondrules compared to bulk. For chondrites with higher exposure ages, finding such evidences is more complex.
6. Range of values observed for the  $^{129}\text{Xe}_r$  in chondrules compared to bulk suggesting existence of heterogeneous phases in chondrules.

Chapter 4  
Noble gases in chondrules  
-trapped components

## **4.1 Introduction**

Chemical inertness and high volatility make noble gases a useful tracer to understand the origin of chondrule precursors as well as effect of chondrule formation event on chondrule precursors. Earlier studies on chondrules showed very low noble gas concentrations of trapped origin (Kim and Marti 1994; Miura and Nagao 1996; Nakamura et al. 1999; Okazaki et al. 2001a; Smith et al. 1977, Swindle et al. 1991). This is generally attributed to extensive gas loss during chondrule formation from precursors. However, recently Okazaki et al. (2001b) and Vogel et al. (2004) reported that small abundance of primordial Ne and Ar exists in chondrules. Okazaki et al. (2001b) reported high noble gas concentrations (e.g. up to  $7 \times 10^{-6} \text{ cm}^3\text{STP/g } ^{36}\text{Ar}$ ) in chondrules (mainly with porphyritic texture) of the enstatite chondrite Yamato (Y)-791790. Matrix surrounding these chondrules has lower gas concentrations. The noble gas compositions of chondrules suggest presence of solar type noble gases. Authors argue that chondrules or phases of chondrules exposed to solar radiation possibly during chondrule formation as suggested by X-wind model (Shu et al., 1996). Authors suggest that as porphyritic texture suggests incomplete melting of chondrule precursors (Lofgren and Russell, 1986) there is a possibility that trapped solar type gases survived the chondrules melting event. However, recent work of Vogel et al. (2004) did not observe presence of solar type noble gases in chondrules from unequilibrated ordinary and carbonaceous chondrites and suggested that the small abundance of trapped  $^{36}\text{Ar}_t$  is better explained as due to phase Q that survived the metal silicate fractionation, possible during chondrule formation event. Based on earlier studies it is clear that trapped noble gases are present in chondrules and these gases can be contributed by various noble gas components. In this work, chondrules are analyzed from three major classes i.e. ordinary, enstatite and carbonaceous chondrites. The prime objective is to characterize trapped noble gases in chondrules and understanding their variation which could be related directly to the chondrule formation event. This chapter deals with the results of trapped Neon ( $^{20}\text{Ne}_t$ ), Argon ( $^{36}\text{Ar}_t$ ), and for few chondrules Krypton ( $^{84}\text{Kr}$ ) and Xenon ( $^{132}\text{Xe}$ ). On the basis of various trapped elemental and isotopic ratios, noble gas components are discussed. As for example, Neon and Argon are mainly carried by Presolar diamond (HL) and Phase-Q respectively. Hence, the elemental ratio  $^{36}\text{Ar}/^{20}\text{Ne}$  can be used to understand the setting of these components in chondrules. Together with  $^{36}\text{Ar}/^{20}\text{Ne}$  ratio, other

ratios like  $^{36}\text{Ar}/^{132}\text{Xe}$ ,  $^{84}\text{Kr}/^{132}\text{Xe}$ , and  $^4\text{He}/^{40}\text{Ar}$  are also used to understand the obtained results. Results are given in Tables 4.1, 4.2, 4.3 and 4.4.

## **4.2 Calculations of trapped noble gases**

Measured noble gases in chondrules and chondrites are mainly a mixture of trapped and in-situ components. Generally, due to substantial contribution of in-situ components and low abundance of trapped noble gases, the calculation for trapped noble gases is very critical. In the following sections (4.2.1, 4.2.2, 4.2.3), the methods used for calculation of various trapped gases are given.

### **4.2.1 Correction of the measured $^{20}\text{Ne}$ for cosmogenic contributions**

Neon in chondrites (as well as in chondrules) is significantly affected by cosmogenic contribution, which is a function of: (1) Cosmic ray exposure ages of chondrites (2) the target chemistry of the samples (chondrule and chondrites) and (3) Shielding of sample during cosmic ray exposure. Cosmogenic noble gases are discussed in details in chapter 3. To infer the abundance of trapped Neon, the measured Neon abundances have to be corrected for cosmogenic contribution. For typical chondritic material, the cosmogenic  $^{21}\text{Ne}/^{20}\text{Ne}$  ratio is in the range of 1.02-1.14, depending on the chemistry and the shielding depth of a given sample (Leya et al., 2000; Wieler 2002). This ratio indicates that the cosmogenic contribution is most visible in the  $^{21}\text{Ne}/^{20}\text{Ne}$  ratio, as the trapped ratio  $^{21}\text{Ne}/^{20}\text{Ne} \sim 0.003$ , is very low.

Details of the method used for the calculation of trapped Neon are given in *Appendix*.

In this method, the following values are required to be adopted for the calculation of e.g.  $(^{20}\text{Ne}/^{22}\text{Ne})_t$  and  $(^{20}\text{Ne}/^{22}\text{Ne})_c$ .

Values of  $(^{20}\text{Ne}/^{22}\text{Ne})_t$  are decided for each chondrule by following certain criteria (detailed description is given in section 3.2, chapter 3).  $(^{20}\text{Ne}/^{22}\text{Ne})_c = 0.8$  is taken for all the chondrules (Eugster 1988). A different way of deciding  $(^{20}\text{Ne}/^{22}\text{Ne})_c$  in chondrules is suggested by Vogel et al. (2004) on the bases of OCNL (ordinary chondrite cosmogenic Ne line). We found that for most of the chondrules the ratio  $(^{20}\text{Ne}/^{22}\text{Ne})_c$  is very close to  $(^{20}\text{Ne}/^{22}\text{Ne})_c = 0.8$ , considered by Eugster (1988) except in case of chondrules having very different chemical composition (see *appendix* for details).

### **4.2.2 Correction of the measured $^{36}\text{Ar}$ for cosmogenic contributions**

To calculate the trapped Ar ( $^{36}\text{Ar}$ ) for individual chondrules it is necessary to correct measured Ar for cosmogenic contribution. Unlike Ne where three isotopes are used

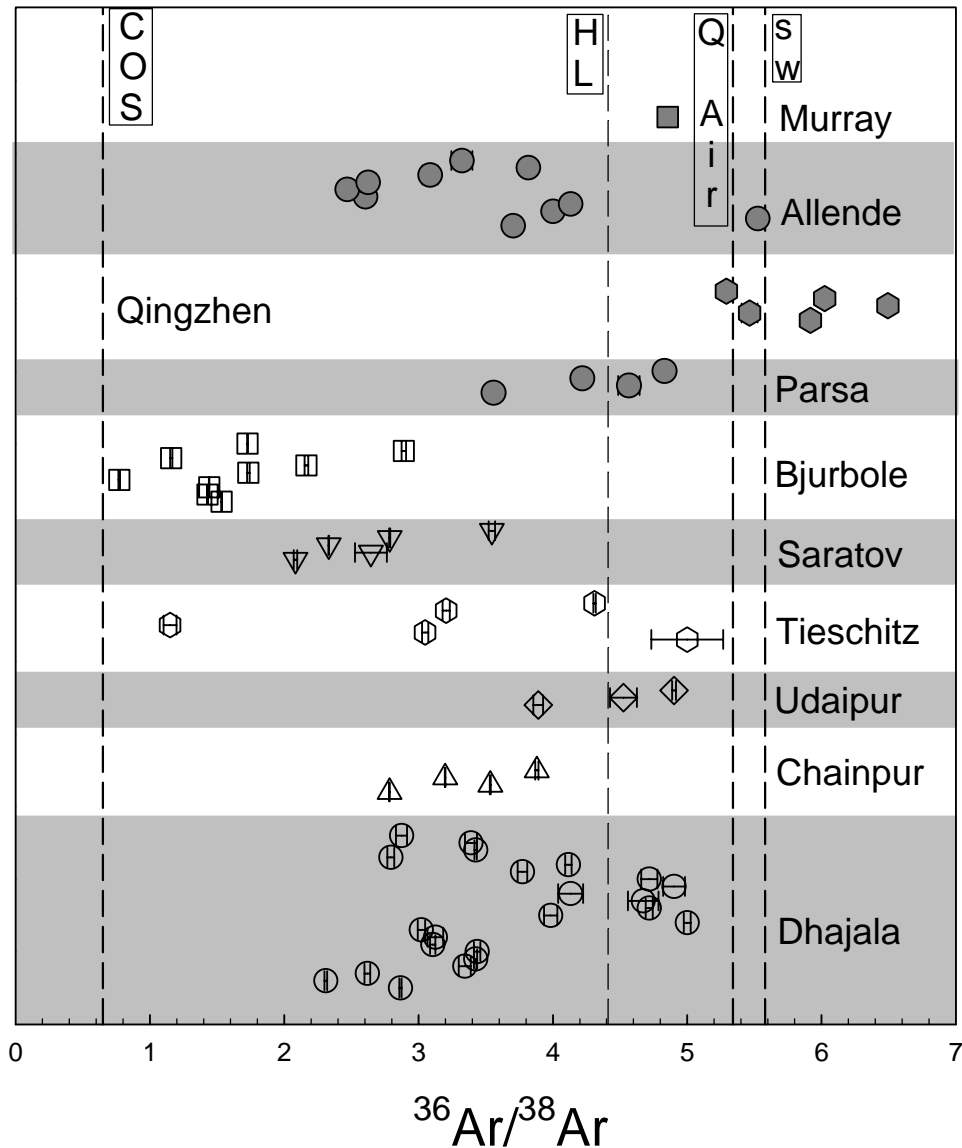


**Fig. 4.1** Plot of measured  $^{36}\text{Ar}/^{38}\text{Ar}$  values of all studied chondrules. All chondrules plot to the right side of the cosmogenic  $^{36}\text{Ar}/^{38}\text{Ar}$  ratio of  $0.65 \pm 0.03$ , indicating the presence of non-cosmogenic component of Ar. Most of the chondrules show values that scatter between cosmogenic and presolar diamonds. A few chondrules show value towards Phase Q components also. Presence of trapped Ar is evident in these measured ratios of chondrules. Values used for each component is listed in Tables 1.4 and 1.5, Chapter 1.

for cosmogenic correction, only two isotopes can be used for cosmogenic correction in case of Ar since  $^{40}\text{Ar}$  is mainly radiogenic. A uniform cosmogenic  $^{36}\text{Ar}/^{38}\text{Ar}$  ratio of  $0.65 \pm 0.03$  was adopted for all chondrules. Fig. 4.1 shows measured  $^{36}\text{Ar}/^{38}\text{Ar}$  ratios of the chondrules analyzed. Most of data are indicating the presence of non-cosmogenic  $^{36}\text{Ar}$ . All chondrules from Qingzhen chondrite are showing higher values of  $^{36}\text{Ar}/^{38}\text{Ar}$ . As discussed in detail in chapter 3 (section 3.4.1.3), independent evidences suggest the presence of higher Cl content in Qingzhen chondrite, which has

possibly affected the  $^{36}\text{Ar}/^{38}\text{Ar}$  ratio, due to contribution from  $^{35}\text{Cl} (n,\gamma) ^{36}\text{Cl} (\beta^-)$   $^{36}\text{Ar}_{\text{Cl}}$  reaction.

For a trapped (non-cosmogenic) contribution,  $^{36}\text{Ar}/^{38}\text{Ar}$  ratio of Phase-Q ( $5.34 \pm 0.02$ ), the major Ar-carrier phase in unequilibrated chondrites is adopted, to deduce trapped amount of  $^{36}\text{Ar}$  in all chondrules.

### **4.3 Results**

Results related to isotopic ratios of Neon and Argon for all the chondrules are discussed in section 3.3 (chapter 3). As mentioned there, Neon is dominated by cosmogenic component but some amount of trapped Neon is also present (discussed next). In Fig. 4.1, measured  $^{36}\text{Ar}/^{38}\text{Ar}$  ratio is plotted for all chondrules. Dotted lines show different possible components of Ar (values are listed in Tables 1.4 and 1.5). As evident in Fig. 4.1, Argon isotopic ratio shows presence of trapped Ar. Here in this section, results of trapped Ne and Ar concentrations as well as trapped  $^{36}\text{Ar}/^{20}\text{Ne}$  ratio are given, calculated based on above mentioned methods. The results of measured  $^{84}\text{Kr}$  and  $^{132}\text{Xe}$  are also presented.

#### **4.3.1 Trapped $^{20}\text{Ne}$**

The abundances of trapped  $^{20}\text{Ne}$  in individual chondrules and their respective bulk are listed in Tables 4.1, 4.2 and 4.3 respectively for ordinary, enstatite and carbonaceous chondrites. The calculated trapped  $^{20}\text{Ne}$  in chondrules and their respective chondrites are plotted in Fig. 4.2a. The concentrations of  $^{20}\text{Ne}_t$  in chondrules are generally low ( $< 10 \times 10^{-8}\text{cm}^3\text{STP/g}$ , Fig. 4.2) and some chondrules show higher value compared to bulk as well as range observed in chondrites. The hatched area in plot represents the range of abundances of trapped  $^{20}\text{Ne}$  and  $^{36}\text{Ar}$  in chondrites. There are few exceptions like DH-8 and DH-11 chondrules from Dhajala showing  $885 \times 10^{-8}\text{cm}^3\text{STP/g}$  and  $151 \times 10^{-8}\text{cm}^3\text{STP/g}$  of  $^{20}\text{Ne}_t$  respectively. The Ne isotopic composition of these chondrules suggests domination of trapped Ne in these chondrules over cosmogenic contribution (Fig. 4.6, discussed later). Other chondrules from Udaipur (UD-3), Allende (ALD-8, ALD-9) and very small chondrules from Murray (MRY-5, MRY-7 and MRY-8) also show relatively higher values for the trapped  $^{20}\text{Ne}$ .  $^{20}\text{Ne}_t$  values obtained are sensitive to two corrections, that of blank and  $^{40}\text{Ar}^{++}$  contribution. Due to small sample size ( $< 1\text{mg}$ ) and low gas amounts, the blank and  $^{40}\text{Ar}^{++}$  interference corrections are significant in certain cases, though such is not the case for  $^{21}\text{Ne}_c$ . Chondrules, where blank contribution (and or  $^{40}\text{Ar}^{++}$ ) is found to be more than 50%

**Table 4.1** He, Ne and Ar isotopic and elemental compositions,  $^{20}\text{Ne}_t$ ,  $^{36}\text{Ar}_t$  concentrations, and  $(^{36}\text{Ar}/^{20}\text{Ne})_t$  ratios of chondrules from Dhajala, Chainpur, Bjurböle, Saratov, Tieschitz and Udaipur chondrites. Also given are blank contributions to measured  $^{20}\text{Ne}$  and  $^{36}\text{Ar}$ .

Sample	$^4\text{He}^*$	$^3\text{He}/^4\text{He}$ ( $\times 10^4$ )	$^{22}\text{Ne}^*$	$^{20}\text{Ne}/^{22}\text{Ne}$	$^{21}\text{Ne}/^{22}\text{Ne}$	$^{36}\text{Ar}^*$	$^{38}\text{Ar}/^{36}\text{Ar}$	$^{40}\text{Ar}/^{36}\text{Ar}$	$^{20}\text{Ne}_t^*$	$^{36}\text{Ar}_t^*$	$(^{36}\text{Ar}/^{20}\text{Ne})_t$	Blank Contr. To $^{20}\text{Ne}$ (%)	Blank Contr. To $^{36}\text{Ar}$ (%)
<b>Dhajala (H3.8)</b>													
DH-2A	1266	35.6 $\pm 3.0$	1.70	3.85 $\pm 0.09$	0.79 $\pm 0.01$	2.04	0.25 $\pm 0.003$	332 $\pm 3$	5.71	2.00	0.35	5	8
DH-2B	1602	33.3 2.8	2.45	3.44 0.09	0.76 .004	2.78	.212 .001	700 7	7.13	2.73	0.38	4	5
DH-5 (nm)	1000	24.9 2.1	2.99	1.62 .33	0.80 .05	13.3	.242 .005	562 5	2.72	12.8	4.70	38	22
DH-8 (nm)	64632	0.77 .07	84.9	10.44 .01	0.05 .0003	2.88	.200 .001	1770 16	885	2.85	0.003	<1	8
Dh-9	1097	52.0 4.4	1.77	2.74 .19	1.07 .04	6.59	.214 .005	266 3	3.71	6.46	1.74	44	36
Dh-11 (nm)	14004	1.4 .1	13.0	11.66 .75	.148 .014	7.99	.204 .003	767 6	151	7.90	0.052	24	36
Dh-NO25 (nm)	485	30.7 2.6	1.82	2.48 .10	.869 .013	3.48	.348 .005	1527 10	3.38	0.30	-	25	63
Dh-S1	876	48.6 4.1	2.13	.89 .06	.610 .016	1.09	.291 .002	1173 8	0.76	1.00	-	70	55
Dh-S8	1760	36.3 3.1	4.40	1.57 .02	.764 .038	1.34	.349 .001	9627 73	3.96	1.17	-	52	77
Dh-S11	1610	35.2 3.0	1.86	.66 .03	.900 .069	0.96	.433 .002	2376 17	-	0.78	-	80	64
Dh-S18	2090	27.3 2.3	4.32	.95 .06	.572 .048	1.60	.382 .003	11940 94	1.94	1.41	-	65	83
Dh-S19	2530	5.37 .45	3.08	.93 .01	.789 .049	3.46	.299 .004	3996 28	0.71	3.17	-	68	48
Dh-S23	829	50.2 4.3	2.52	1.80 .04	.701 .015	1.69	.322 .002	5543 40	3.00	1.52	-	54	48

Sample	<sup>4</sup> He*	<sup>3</sup> He/ <sup>4</sup> He (x 10 <sup>4</sup> )	<sup>22</sup> Ne*	<sup>20</sup> Ne/ <sup>22</sup> Ne	<sup>21</sup> Ne/ <sup>22</sup> Ne	<sup>36</sup> Ar*	<sup>38</sup> Ar/ <sup>36</sup> Ar	<sup>40</sup> Ar/ <sup>36</sup> Ar	<sup>20</sup> Ne <sub>t</sub> *	<sup>36</sup> Ar <sub>t</sub> *	( <sup>36</sup> Ar/ <sup>20</sup> Ne) <sub>t</sub>	Blank Contr. To <sup>20</sup> Ne (%)	Blank Contr. To <sup>36</sup> Ar (%)
Dh-S24	710	37.0	2.52	4.55	.638	1.18	.292	1700	10.3	1.12	-	60	85
		3.1		.07	.062		.0002	13					
Dh-S27	895	42.4	4.89	2.55	0.605	1.79	0.320	522	9.89	1.66	0.17	31	48
		3.6		.07	.018		.006	4					
Dh-S28	1710	32.8	3.47	2.26	0.634	1.73	0.331	1162	5.92	1.54	0.26	42	49
		2.8		.04	.016		.003	8					
Dh-V7 (nm)	1462	17.7	2.58	2.85	0.779	2.01	0.244	218	5.83	2.00	0.34	12	31
		1.5		.16	.027		.001	22					
Dh-V11 (m)	400	37.7	2.36	0.98	0.847	0.65	0.295	6042	0.54	0.62	1.14	30	45
		3.2		.09	.029		.004	44					
Dh-V18 (nm)	603	29.5	1.35	1.26	0.860	0.26	0.358	12762	0.68	0.23	-	38	78
		2.5		.07	.025		.003	96					
Dh-V30 (nm)	795	26.0	2.08	0.96	0.914	1.49	0.265	1282	0.36	1.44	4.06	33	29
		2.2		.12	.031		.002	10					
Dh-V35 (nm)	408	33.7	1.70	4.51	0.509	1.29	0.212	712	6.97	1.27	0.18	25	34
		2.9		.30	.026		.003	6					
Dh-V38 (nm)	87	20.8	1.86	1.16	0.883	0.86	0.292	188	7.39	8.13	1.1	16	23
		1.8		.05	.042		.001	2					
T11	1341	45.1	2.28	1.91	0.810	16.7	0.198	422	2.72	16.5	6.06	20	2
Bulk		3.0		.02	.003		.001	4					
<b>Chainpur (LL3.4)</b>													
CH1A	1600	209	7.59	0.92	0.883	5.84	0.359	196	1.00	5.07	5.10	3	2
		17		0.01	0.004		0.0003	2					
CH1B	1564	214	8.25	0.96	0.896	21.20	0.283	121	1.48	19.7	13.3	3	1
		18		.01	.001		.003	1					
CH2	2012	151	9.60	0.88	0.876	11.00	0.313	156	1.00	10	10.0	6	3
		13		.01	.002		.0002	1					
CH3	2226	202	13.5	1.10	0.885	26.90	0.258	130	4.36	25.5	5.85	10	5
		17		.01	.009		.001	1					
CH-bulk Coarse	3035	57.8	10.7	1.88	0.793	54.8	0.204	55	8.35	46	5.51	53	<1
		4.9		.02	.005		.0002	.12					

Sample	<sup>4</sup> He*	<sup>3</sup> He/ <sup>4</sup> He (x 10 <sup>4</sup> )	<sup>22</sup> Ne*	<sup>20</sup> Ne/ <sup>22</sup> Ne	<sup>21</sup> Ne/ <sup>22</sup> Ne	<sup>36</sup> Ar*	<sup>38</sup> Ar/ <sup>36</sup> Ar	<sup>40</sup> Ar/ <sup>36</sup> Ar	<sup>20</sup> Ne <sub>t</sub> *	<sup>36</sup> Ar <sub>t</sub> *	( <sup>36</sup> Ar/ <sup>20</sup> Ne) <sub>t</sub>	Blank Contr. To <sup>20</sup> Ne (%)	Blank Contr. To <sup>36</sup> Ar (%)
CH-bulk	2592	81.0	10.3	1.53	0.797	46.5	.204	53	12.5	54.1	4.33	49	<1
Fine		6.8		.01	.002		.0001	.34					
<b>Bjurböle (L/LL4)</b>													
BB3	1378	48.1	2.65	1.75	0.866	0.31	1.296	13411	2.77	0.06	-	61	88
(nm)		4.1		0.18	0.036		0.001	117					
BB8	1478	59.0	2.86	1.87	0.839	0.80	0.625	4647	3.39	0.55	-	70	82
(nm)		5.0		.21	.032		.002	38					
BB10	1273	66.5	2.49	2.16	0.890	0.56	0.695	6145	3.74	0.36	-	76	92
(m)		5.6		.52	.054		.001	55					
BB15	1000	107	3.15	1.61	0.944	0.74	0.580	4561	2.81	0.54	-	63	78
(nm)		9		.12	.005		.096	36					
BB18	4896	18.1	3.77	2.17	0.882	0.65	0.863	3590	5.71	0.33	-	53	81
(nm)		1.5		.23	.045		.006	29					
BB25	1916	37.2	3.26	2.54	0.823	1.99	0.462	3646	6.27	1.63	-	58	77
(nm)		3.1		.15	.032		.003	28					
BB26	1432	72.8	3.22	1.18	0.874	0.71	0.577	6126	1.36	0.52	-	65	75
(m)		6.2		.13	.005		.003	47					
BB28	1074	86.7	3.03	1.21	0.777	1.87	0.346	1267	1.59	1.7	-	72	81
(nm)		7.0		.01	.021		.002	10					
BB29	658	148	4.40	1.56	0.822	1.40	0.700	9378	3.67	0.90	-	67	74
(nm)		12		.12	.017		.002	72					
<b>Saratov (L4)</b>													
STV2A	1000	121	2.79	0.88	0.866	1.51	0.430	5291	0.33	1.28	3.91	27	37
(nm)		11		±0.032	±0.015		± 0.004	± 53					
STV2B	1140	114	4.47	0.956	0.886	3.95	0.359	2543	0.77	3.43	-	34	52
(nm)		10		.031	.026		.001	26					
STV3	836	135	5.29	0.97	0.888	1.92	0.378	4558	1.00	1.70	-	31	64
(nm)		11		.03	.014		.017	53					
STV6	910	156	4.84	0.93	0.935	1.23	0.516	3858	0.70	0.96	-	33	79
(nm)		13		.04	.010		.003	46					

Sample	<sup>4</sup> He*	<sup>3</sup> He/ <sup>4</sup> He (x 10 <sup>4</sup> )	<sup>22</sup> Ne*	<sup>20</sup> Ne/ <sup>22</sup> Ne	<sup>21</sup> Ne/ <sup>22</sup> Ne	<sup>36</sup> Ar*	<sup>38</sup> Ar/ <sup>36</sup> Ar	<sup>40</sup> Ar/ <sup>36</sup> Ar	<sup>20</sup> Ne <sub>t</sub> *	<sup>36</sup> Ar <sub>t</sub> *	( <sup>36</sup> Ar/ <sup>20</sup> Ne) <sub>t</sub>	Blank Contr. To <sup>20</sup> Ne (%)	Blank Contr. To <sup>36</sup> Ar (%)
STV7	416	165	3.90	1.40	0.748	4.44	0.282	617	2.90	4.12	-	47	66
(m)		14		.17	.044		.002	6.4					
STV-bulk	1881	148	8.68	0.86	0.898	7.35	0.292	928	5.26	6.77	12.9	30	1
		13		.02	.010		<.002	8					
<b>Tieschitz (H3.6)</b>													
TCZ-1	630	210	3.44	1.14	0.806	73.9	0.200	26.2	1.46	75.4	51.6	34	3
(m)		18		.04	.010		.011	.4					
TCZ-2	1500	153	6.32	1.47	0.843	4.89	0.339	221	4.71	4.47	0.95	20	39
(nm)		13		.06	.023		.002	2					
TCZ-5	728	254	4.60	0.87	0.801	3.48	0.350	380	0.74	3.15	4.25	33	33
(m)		22		.04	.007		.003	4					
TCZ-8	839	215	6.52	1.61	0.680	4.04	0.313	241	6.61	3.77	-	51	62
(nm)		18		.09	.023		.003	2					
TCZ-9	281	526	4.67	2.26	0.495	17.6	0.233	214	8.56	17.5	-	59	67
(nm)		44		.18	.022		.001	2.5					
TCZ-BLK	2486	167	9.09	1.26	0.780	29.5	0.223	76.1	5.16	28.8	5.57	50	1
		14		.05	.003		<.001	.74					
<b>Udaipur (H3)</b>													
UD-1	752	253	3.91	0.85	0.884	19.6	0.223	187	0.26	19.1	74.8	67	17
(nm)		21		.03	.012		.005	2					
UD-2	956	190	4.92	.89	.804	13.1	0.257	3290	0.91	1.24	13.7	37	28
(nm)		16		.07	.031		.002	31					
UD-3	304	239	6.67	4.11	.626	51.4	0.204	158	24.37	50.7	2.08	40	32
(nm)		20		.20	.028		.001	2					
UD-bulk	1698	253	8.68	1.05	.792	54.9	0.197	57.9	2.34	54.5	23	20	2
		17		.005	.006		.001	.14					

\* Concentrations of <sup>4</sup>He, <sup>22</sup>Ne, <sup>36</sup>Ar, <sup>20</sup>Ne<sub>t</sub> and <sup>36</sup>Ar<sub>t</sub> are in unit of 10<sup>-8</sup> cm<sup>3</sup>STP/g. Errors in concentrations are ±10%; Errors in isotopic ratios represent 95% confidence limits. (m = magnetic sample, nm = nonmagnetic sample)

**Table 4.2** He, Ne and Ar isotopic and elemental compositions,  $^{20}\text{Ne}_t$ ,  $^{36}\text{Ar}_t$  concentrations, and  $(^{36}\text{Ar}/^{20}\text{Ne})_t$  ratios of chondrules from Parsa and Qingzhen chondrites. Also given are blank contributions to measured  $^{20}\text{Ne}$  and  $^{36}\text{Ar}$ .

Sample	$^4\text{He}^*$	$^3\text{He}/^4\text{He}$ ( $\times 10^4$ )	$^{22}\text{Ne}^*$	$^{20}\text{Ne}/^{22}\text{Ne}$	$^{21}\text{Ne}/^{22}\text{Ne}$	$^{36}\text{Ar}^*$	$^{38}\text{Ar}/^{36}\text{Ar}$	$^{40}\text{Ar}/^{36}\text{Ar}$	$^{20}\text{Ne}_t$	$^{36}\text{Ar}_t$	$(^{36}\text{Ar}/^{20}\text{Ne})_t$	Blank Contr. to $^{20}\text{Ne}$ (%)	Blank Contr. to $^{36}\text{Ar}$ (%)
<b>Parsa (EH3)</b>													
PR1	1348	296 $\pm 25$	10.4	0.862 $\pm 0.002$	0.878 $\pm 0.002$	3.34	0.281 $\pm 0.0004$	760 $\pm 7$	0.86	3.10	3.59	4	12
PR2	1516	266 22	7.52	1.28 .003	.849 .002	7.87	0.219 .004	324 3	4.00	7.69	1.92	3	3
PR3A	1538	246 21	6.50	1.01 .005	.871 .003	4.09	0.237 .001	436 4	1.55	3.94	2.54	5	4
PR3B	1575	250 21	6.62	1.35 .006	.850 .004	8.76	0.207 .001	398 4	4.04	8.64	2.14	3	2
PR	12852	35.8	10.4	3.02	0.72	14.6	0.233	242	24.7	14.1	0.57	5	5
BLK-1 <sup>#</sup>		1.6		.023	.01		.001	2					
PR	2448	118	8.15	1.85	0.77	6.46	0.264	292	8.65	6.10	0.70	5	5
BLK-3 <sup>#</sup>		9		.010	.003		.001	2					
<b>Qingzhen (EH3)</b>													
Q11 (nm)	516	158 13	2.15	0.911 .112	0.910 .029	27.9	0.169 .0003	183 2.2	0.26	2.83	10.8	42	46
Q12 (nm)	53	72.4 6.1	4.24	1.43 .044	0.797 .026	5.05	0.183 .002	156 2	3.07	5.07	1.65	34	33
Q2 (nm)	1.72	1438 122	3.69	2.81 .077	0.682 .013	4.52	0.154 .0006	303 3	8.18	4.77	-	26	59
Q3 (m)	-	-	4.33	3.22 .359	0.553 .029	9.87	0.166 .001	286 3	1.19	10.04	-	44	60
Q5 (nm)	-	-	0.82	3.74 .644	1.332 .096	9.58	0.189 .002	251 2	2.67	9.57	-	79	52
QNBLK	5415	3.67 0.31	3.42	1.45 .043	0.766 .008	5.09	0.205 .0004	254 2.46	2.63	5.03	-	70	7

\* Concentrations of  $^4\text{He}$ ,  $^{22}\text{Ne}$ ,  $^{36}\text{Ar}$ ,  $^{20}\text{Ne}_t$  and  $^{36}\text{Ar}_t$  are in unit of  $10^{-8} \text{ cm}^3\text{STP/g}$ . Errors in concentrations are  $\pm 10\%$ ; Errors in isotopic ratios represent 95% confidence limits. <sup>#</sup> Data taken from Murty (1992, 1993). (m = magnetic sample, nm = nonmagnetic sample)

**Table 4.3** He, Ne and Ar isotopic and elemental compositions,  $^{20}\text{Ne}_t$ ,  $^{36}\text{Ar}_t$  concentrations, and  $(^{36}\text{Ar}/^{20}\text{Ne})_t$  ratios of chondrules from Allende and Murray chondrites. Also given are blank contributions to measured  $^{20}\text{Ne}$  and  $^{36}\text{Ar}$ .

Sample	$^4\text{He}^*$	$^3\text{He}/^4\text{He}$ ( $\times 10^4$ )	$^{22}\text{Ne}^*$	$^{20}\text{Ne}/^{22}\text{Ne}$	$^{21}\text{Ne}/^{22}\text{Ne}$	$^{36}\text{Ar}^*$	$^{38}\text{Ar}/^{36}\text{Ar}$	$^{40}\text{Ar}/^{36}\text{Ar}$	$^{20}\text{Ne}_t$	$^{36}\text{Ar}_t$	$(^{36}\text{Ar}/^{20}\text{Ne})_t$	Blank Contr. to $^{20}\text{Ne}$ (%)	Blank Contr. to $^{36}\text{Ar}$ (%)
<b>Allende (CV3.2)</b>													
ALD1 (nm)	1648	20.9 $\pm 1.8$	1.74	3.09 $\pm 0.27$	0.779 $\pm 0.020$	-	-	-	4.28	-	-	84	-
ALD2 (m)	1852	25.2 2.1	1.66	4.98 .31	0.577 .008	-	-	-	7.48	-	-	83	-
ALD3 (nm)	2300	10.8 0.9	1.76	6.57 .07	0.587 .026	-	-	-	10.9	-	-	71	-
ALD4	1434	52.6 4.4	3.67	4.79 .40	0.365 .025	0.22	0.270 .0002	2986 14	1.62	0.21	-	45	84
ALD5 (nm)	690	20.4 1.7	1.62	5.78 .52	0.604 .108	-	-	-	8.88	-	-	86	-
ALD6 (nm)	1103	39.9 3.4	1.81	5.52 .31	0.746 .041	2.72	0.181 0.001	1322 10	9.43	2.73	-	47	77
ALD8 (nm)	720	51.4 4.4	2.64	8.94 .51	0.414 .026	-	-	-	23.7	-	-	65	-
ALD9 (m)	1318	59.2 3.8	5.86	7.74 .48	0.200 .022	-	-	-	44.9	-	-	34	-
ALD11 (nm)	995	41.0 3.5	1.41	4.55 .16	0.515 .019	1.48	0.250 .001	1938 14	5.81	1.45	-	45	65
ALD12 (nm)	1560	27.7 2.3	1.73	1.46 .05	0.756 .022	2.33	0.242 .001	1963 14	1.36	2.23	-	62	65
ALD13A (nm)	1208	33.1 2.8	1.41	2.01 .08	0.885 .102	0.61	0.384 .006	1032 2	1.82	0.52	0.29	20	25
ALD13C (nm)	1305	36.2 2.8	1.47	1.30 .15	0.934 .118	0.70	0.405 .005	936 2	7.83	0.61	0.08	33	37
ALD14 (m)	2771	16.4 1.4	1.70	1.15 .05	0.822 .067	1.50	0.381 .008	700 1	0.7	1.28	1.83	18	19
ALD15A (nm)	1503	29.0 2.5	1.71	1.26 .16	0.830 .058	1.16	0.324 .006	2824 3	0.83	1.07	1.29	20	15
ALD15B (nm)	1417	33.1 2.8	1.88	2.18 .14	0.810 .059	1.53	0.262 .002	2594 3	2.83	1.49	0.53	14	15

Sample	<sup>4</sup> He*	<sup>3</sup> He/ <sup>4</sup> He (x 10 <sup>4</sup> )	<sup>22</sup> Ne*	<sup>20</sup> Ne/ <sup>22</sup> Ne	<sup>21</sup> Ne/ <sup>22</sup> Ne	<sup>36</sup> Ar*	<sup>38</sup> Ar/ <sup>36</sup> Ar	<sup>40</sup> Ar/ <sup>36</sup> Ar	<sup>20</sup> Ne <sub>t</sub>	<sup>36</sup> Ar <sub>t</sub>	( <sup>36</sup> Ar/ <sup>20</sup> Ne) <sub>t</sub>	Blank Contr. to <sup>20</sup> Ne (%)	Blank Contr. to <sup>36</sup> Ar (%)
ALD16 (m)	665	48.3 4.1	1.47	1.25 .16	0.789 .087	0.74	0.301 .007	2797 8	0.7	0.7	1.0	29	47
<b>Murray (CM2)</b>													
MRY-1B (nm)	1583	35.4 3.0	2.81	3.33 0.09	0.527 .011	19.6	0.206 .0002	8.00 .10	8.13	19.35	2.38	43	26
MRY-5 (nm)	390	302 26	8.64	11.16 .39	0.069 .004	-	-	-	96	-	-	28	-
MRY-7 (nm)	1492	115 10	8.13	4.12 .39	0.127 .008	-	-	-	32.8	-	-	59	-
MRY-8 (nm)	638	269 23	3.93	7.41 .68	0.144 .004	-	-	-	28.7	-	-	71	-
MRY-BLK	9332	2.23 0.19	4.24	8.13 .08	0.199 .001	92.3	0.181 .0003	1.91 .01	33.8			79	

\* Concentrations of <sup>4</sup>He, <sup>22</sup>Ne, <sup>36</sup>Ar, <sup>20</sup>Ne<sub>t</sub> and <sup>36</sup>Ar<sub>t</sub> are in unit of 10<sup>-8</sup> cm<sup>3</sup> STP/g. Errors in concentrations are ±10%; Errors in isotopic ratios represent 95% confidence limits. (m = magnetic sample, nm = nonmagnetic sample)

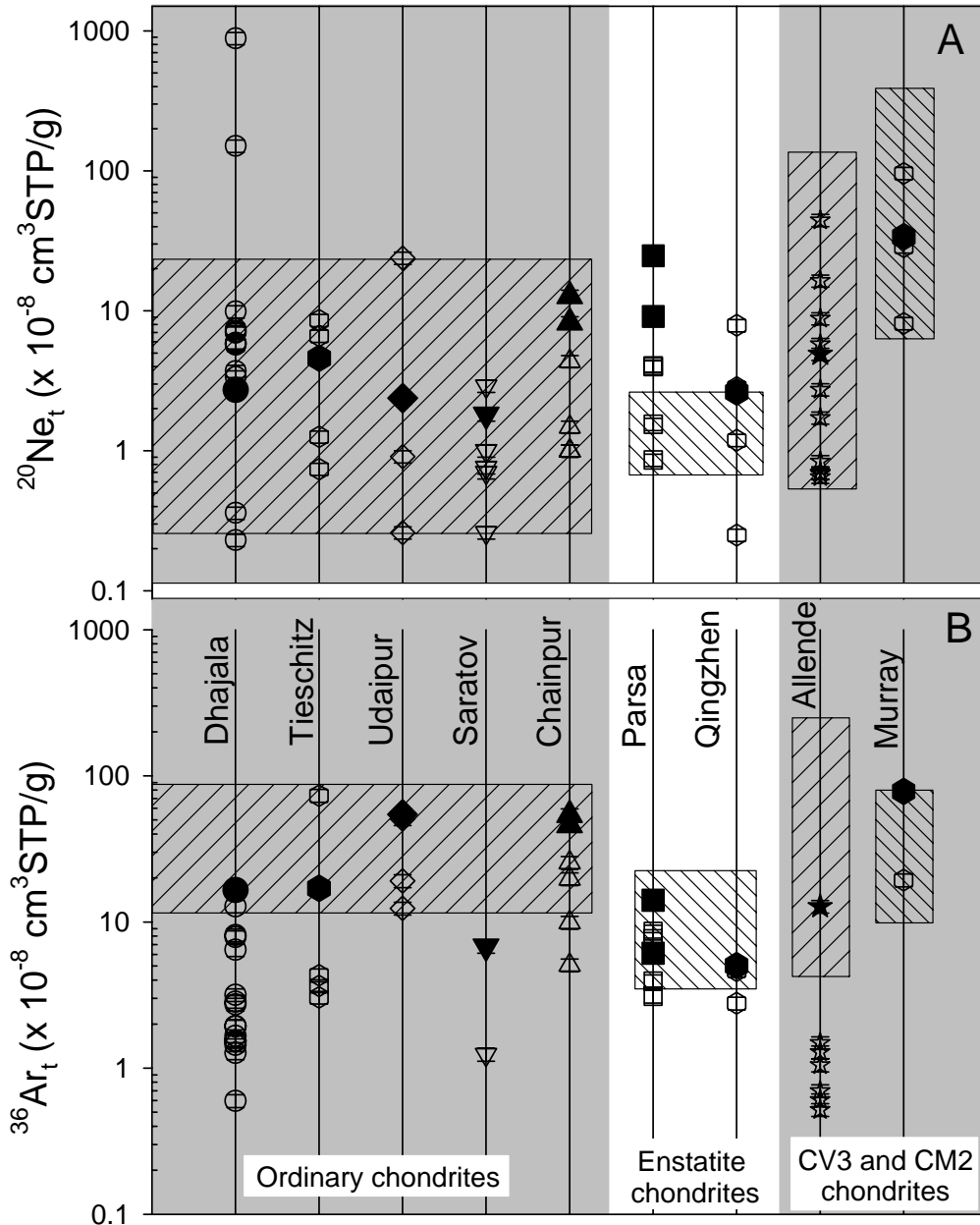


**Fig. 4.2** Abundances of trapped  $^{20}\text{Ne}$  and  $^{36}\text{Ar}$  in chondrules and their respective bulk. Hatched areas show range of trapped  $^{20}\text{Ne}$  and  $^{36}\text{Ar}$  in chondrites calculated from references: (OC: Schelhaas et al., 1991, EC: Patzer et al., 2001, 2002, CV: Scherer and Schultz 2000, CM: Mazor et al., 1970). It is clearly seen that most chondrules are depleted in trapped  $^{36}\text{Ar}$  compared to their bulk. In case of trapped  $^{20}\text{Ne}$  such depletion is not noticeable. *Symbol: open – Chondrule, filled – Bulk*

were not considered further in the discussion of  $(^{36}\text{Ar}/^{20}\text{Ne})_t$  ratio as well as excluded from Figs. 4.2 and 4.3.

54 out of 79 chondrules measured are found to be having blank contribution less than 50%. Generally, it is observed that bulk chondrites have higher concentrations of trapped  $^{20}\text{Ne}$ . The chondrules with unusually higher concentrations of trapped  $^{20}\text{Ne}$  can be due to presence of any  $^{20}\text{Ne}$  rich noble gas component in these chondrules.

However, it is also possible that precursors of these chondrules were originally rich in noble gases especially in Neon carriers. As seen in Fig. 4.2, loss of  $^{20}\text{Ne}_t$  in chondrules of enstatite chondrites seems more when compared loss of trapped  $^{36}\text{Ar}$ .

#### 4.3.2 Trapped $^{36}\text{Ar}$

The trapped  $^{36}\text{Ar}$  could be detected in almost all the chondrules. The results of  $^{36}\text{Ar}_t$  are listed in Tables 4.1, 4.2 and 4.3 for ordinary, enstatite and carbonaceous chondrites respectively. The comparison of  $^{36}\text{Ar}_t$  of chondrules and their respective bulk chondrites is drawn in Fig. 4.2b. The concentration of trapped  $^{36}\text{Ar}$  in chondrules ranges from 1 to  $10 \times 10^{-8} \text{ cm}^3\text{STP/g}$ . No chondrules show abundance of  $^{36}\text{Ar}_t$  as high as  $7 \times 10^{-6} \text{ cm}^3\text{STP/g}$ , as reported by Okazaki et al. (2001) in chondrules from Y-791790 enstatite chondrite. More recently, Vogel et al. (2004) reported  $^{36}\text{Ar}_t$  up to  $5 \times 10^{-8} \text{ cm}^3\text{STP/g}$ , which is within the range observed in this work. However, there are exceptions like chondrules in Chainpur (CH-1B, CH-3), Tieschitz (TCZ-1, TCZ-9 and Udaipur (UD-1, UD-3) with  $^{36}\text{Ar}_t$  concentrations as high as  $7 \times 10^{-7} \text{ cm}^3\text{STP/g}$  (but order of magnitude lower compared to reported values of Okazaki et al. 2001). Similar to the case of trapped  $^{20}\text{Ne}$ , trapped Ar data of 29 chondrules were abandoned as the blank contribution in these chondrules are found higher than 50% (as can be seen in Tables 4.1, 4.2 and 4.3). Therefore, these data are not considered any further. The ratio of  $(^{36}\text{Ar}/^{20}\text{Ne})_t$  in these chondrules is discussed with an aim to identify possible sources of these gases in chondrules. The amount of  $^{36}\text{Ar}_t$  is also calculated similarly for the bulk chondrites analyzed during this work. As can be seen in Tables 4.1, 4.2 and 4.3, most of the bulk chondrites have higher amount of  $^{36}\text{Ar}_t$  compared to chondrules. This may be due to the pristine matrix material present in bulk, which is expected to be rich in  $^{36}\text{Ar}_t$ . TCZ-1 chondrule is again an exception as it shows higher amount of  $^{36}\text{Ar}_t$  compared to bulk.

#### 4.3.3 The elemental ratio $^{36}\text{Ar}/^{20}\text{Ne}$ in chondrules

As mentioned in results section, 37 out of 79 chondrules clearly show presence of both trapped Ne and Ar ranging from  $(0.3 - 885) \times 10^{-8} \text{ cm}^3\text{STP/g}$  and  $(0.2-75) \times 10^{-8} \text{ cm}^3\text{STP/g}$  respectively. The ratio of  $(^{36}\text{Ar}/^{20}\text{Ne})_t$  for these chondrules (Tables 4.1, 4.2 and 4.3) are plotted in Fig. 4.3 as a function of  $^{36}\text{Ar}_t$  concentrations in chondrules. Data of bulk chondrites are also included in this plot for the comparison. Values of  $(^{36}\text{Ar}/^{20}\text{Ne})_t$  for noble gas components phase Q, HL (presolar diamonds), Solar wind (SW) and Air are shown by dotted lines in this plot. The values taken for these components are listed in Table 1.5 (Chapter 1). It is clearly seen that most of the

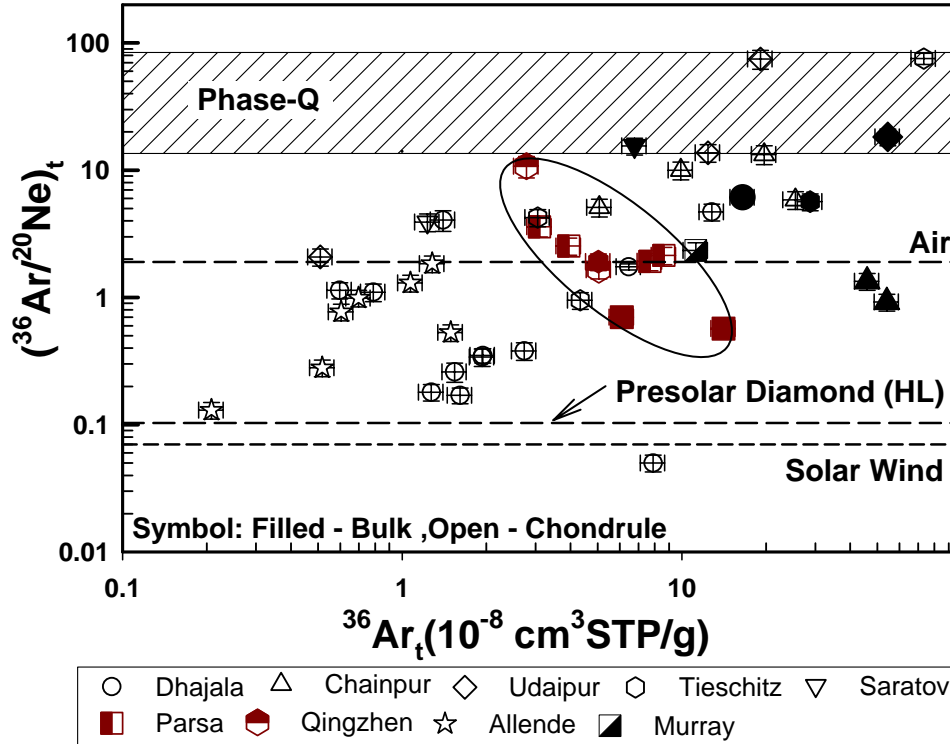


**Fig.4.3**  $(^{36}\text{Ar}/^{20}\text{Ne})_t$  of all chondrules and chondrites is plotted against  $^{36}\text{Ar}_t$ . The horizontal lines are showing the  $^{36}\text{Ar}/^{20}\text{Ne}$  values for different noble gas components. Values of  $^{36}\text{Ar}/^{20}\text{Ne}$  for these components are listed in Table 1.5 (chapter 1). Chondrules generally show lower  $(^{36}\text{Ar}/^{20}\text{Ne})_t$  ratios as well as lower  $^{36}\text{Ar}_t$  concentrations than the respective bulk chondrites. The encircled area highlights the trend observed for chondrules of enstatite chondrites (gray points). Unlike the case of ordinary and carbonaceous chondrites, chondrules from enstatite show relatively higher loss of  $^{20}\text{Ne}_t$  compared to  $^{36}\text{Ar}_t$  (marked with ellipse).

chondrules show values of  $(^{36}\text{Ar}/^{20}\text{Ne})_t$  falling between Q and HL components. Variation of  $(^{36}\text{Ar}/^{20}\text{Ne})_t$  in chondrules can be due to variation in either amount of trapped  $^{36}\text{Ar}$  or  $^{20}\text{Ne}$  or both. The encircled region in the Fig. 4.3 shows the trend observed in case of chondrules from enstatite chondrites. Generally, it is observed that chondrules from ordinary and carbonaceous chondrites are depleted more in amount of  $^{36}\text{Ar}_t$  relative to  $^{20}\text{Ne}_t$  based on their low  $(^{36}\text{Ar}/^{20}\text{Ne})_t$ . However, the trend shown for enstatite indicates that  $(^{36}\text{Ar}/^{20}\text{Ne})_t$  of chondrules is higher compared to bulk even with the lower abundances of  $^{36}\text{Ar}_t$ . Unlike the case of ordinary and carbonaceous chondrites, loss of  $^{20}\text{Ne}_t$  is higher relative to  $^{36}\text{Ar}_t$  in enstatite chondrules. This is also clearly indicated in Fig. 4.2. As indicated by  $\delta^{15}\text{N}$  and  $^{36}\text{Ar}/^{14}\text{N}$  values (discussed in Chapter 5), the narrow range of  $^{36}\text{Ar}_t$  and  $(^{36}\text{Ar}/^{20}\text{Ne})_t$  suggests more homogeneous precursor material for enstatite chondrules. Chondrules like DH-8 (not in plot, Table 4.1), DH-11 shows value of  $(^{36}\text{Ar}/^{20}\text{Ne})_t$  less than HL suggesting possibility of solar gases in these chondrules. For a few chondrules, splits are analyzed. It is observed

that splits of chondrules DH-2 and Parsa-3 show similar  $(^{36}\text{Ar}/^{20}\text{Ne})_t$  while splits of chondrules CH-1, QZN-1, ALD-13 and ALD-15 show different values of  $(^{36}\text{Ar}/^{20}\text{Ne})_t$ .

***Possibility of atmospheric contamination in chondrules:***

As can be seen in Fig. 4.3, Air is one of the noble gas reservoirs and its value is falling between HL and Q components. It is possible that some chondrules are affected by atmospheric contamination. However, we present arguments against it.  $(^{36}\text{Ar}/^{20}\text{Ne})$  value of Air reservoir is about 1.9 (Table 1.5, chapter 1). During contamination probability of  $^{36}\text{Ar}$  sticking with samples is greater compared to  $^{20}\text{Ne}$ . Hence the value of  $^{36}\text{Ar}/^{20}\text{Ne}$  in fractionated air would be higher than 1.9. From the Fig. 4.3, it can be seen that majority of chondrules are falling below the Air value (i.e. less than 1.9, Table 1.5, chapter 1). Few chondrules show higher values towards Q components and for these chondrules, other indicators like Ne and N isotopic composition do not show atmospheric like values ruling out the possibility of atmospheric contamination in chondrules.

It can be inferred that the observed variation in  $(^{36}\text{Ar}/^{20}\text{Ne})_t$  is due to variable presence of two noble gas components i.e. Q and HL as seen in Fig. 4.3., and the higher values of  $^{36}\text{Ar}/^{20}\text{Ne}$  in these chondrules are due to higher proportion of Q components in these chondrules.

**4.3.4  $^{84}\text{Kr}$  and  $^{132}\text{Xe}$  in chondrules**

The abundances of Krypton and Xenon in chondrules are usually observed extremely low, and in many cases are indistinguishable from the blank. Consequently, errors for  $^{84}\text{Kr}$  and  $^{132}\text{Xe}$  became large compared to those of  $^{20}\text{Ne}$  and  $^{36}\text{Ar}$ . Krypton and Xenon could be detected in 39 and 37 chondrules respectively (from five ordinary and two enstatite chondrites). Kr and Xe could not be detected in chondrules from Allende and Murray chondrites. The measured  $^{84}\text{Kr}$  and  $^{132}\text{Xe}$  are listed in Table 4.4, mostly corrected for blanks contribution.

**4.3.5 The elemental ratio  $^{84}\text{Kr}/^{132}\text{Xe}$  in chondrules**

The elemental ratio  $^{84}\text{Kr}/^{132}\text{Xe}$  of chondrules is listed in Table 4.4. In Fig 4.4, elemental ratio  $^{84}\text{Kr}/^{132}\text{Xe}$  is compared with  $^{36}\text{Ar}/^{132}\text{Xe}$  ratio (also listed in Table 4.4) of all the chondrules. For most chondrules, values of elemental ratios are clustering around Q component except for a few chondrules. According to Patzer et al. (2002),  $^{36}\text{Ar}/^{132}\text{Xe} > 220$  and  $^{84}\text{Kr}/^{132}\text{Xe} > 0.85$  characterize subsolar composition. Many chondrules fall above this limit suggesting the presence of subsolar gases in them.

Some chondrules like DH-9, DH-V35 (from Dhajala chondrite), QZN-2 (from Qingzhen chondrite) and UDP-3 (from Udaipur chondrite) show presence of sub-solar component as can be seen in Fig. 4.4A. The section of Fig. 4.4A, (shown as hatched area) is enlarged and given as Fig. 4.4B. Most chondrules show higher values for these elemental ratios compared to their bulk chondrites. All the measured bulk chondrites fall in the range observed for chondrites (shown as box, Fig. 4.3) and Q is the major component. Udaipur chondrite shows higher value of  $^{36}\text{Ar}/^{132}\text{Xe}$  and  $^{84}\text{Kr}/^{132}\text{Xe}$  compared to other chondrites. Above all, it is evident from the results that heavy trapped noble gas elemental composition in chondrules from ordinary and enstatite chondrites are contributed by three different reservoirs (Q, Subsolar and Air) and Q component is dominant contributor.

#### **4.4 Discussion**

##### **4.4.1 Presence of different noble gas components in chondrules**

As mentioned earlier, chondrules show  $(^{36}\text{Ar}/^{20}\text{Ne})_t$  ratio that falls between two noble gas components: Presolar diamond (HL) and Q (Fig. 4.3). On one hand, this suggests that precursors of chondrules were having carriers of HL and Q components in varying proportions and bulk chondrule is mixture of these two components. In support to this, different  $(^{36}\text{Ar}/^{20}\text{Ne})_t$  values in chondrule splits also indicate heterogeneity within chondrules as observed in a few chondrules (CH-1, QZN-1, ALD-13 and ALD-15). On the other hand it is also possible that during chondrule formation due to evaporative loss of trapped noble gases, fractionation occurred which resulted in range of  $(^{36}\text{Ar}/^{20}\text{Ne})_t$  based on different extent of loss and fractionation. In this case, the value of  $(^{36}\text{Ar}/^{20}\text{Ne})_t$  should be higher in chondrules as loss of  $^{20}\text{Ne}_t$  is favored during mass dependent fractionation. Compared to chondrules, matrix should have lower value of  $(^{36}\text{Ar}/^{20}\text{Ne})_t$  as matrix is less heated. As mentioned in result section, bulk chondrites generally have higher  $^{20}\text{Ne}_t$  (and as shown in Fig. 4.2). However, it is observed that values of  $(^{36}\text{Ar}/^{20}\text{Ne})_t$  in bulk are higher compared to chondrules. It seems that  $^{36}\text{Ar}$  was preferentially lost compared to  $^{20}\text{Ne}$  in chondrules (Fig. 4.2). Such observation cannot be explained by mass dependent fractionation.

Recently as suggested by Vogel et al. (2004), noble gases in metal/metal sulfide coatings (rims) in individual chondrules are found enriched in trapped  $^{36}\text{Ar}$  compared to chondrules and surrounding matrix. Authors argue that these coatings were formed

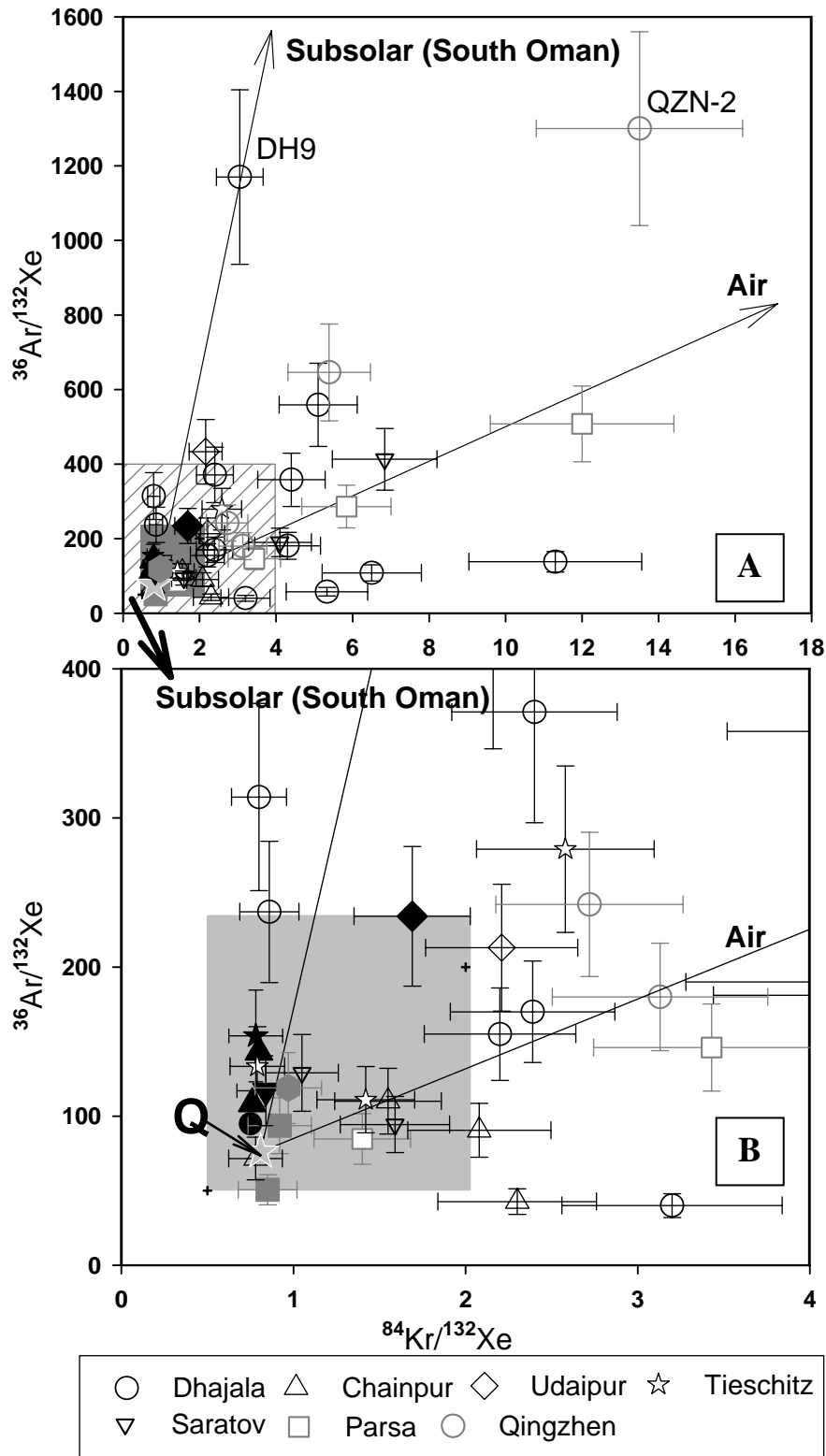


**Fig 4.4** Elemental ratios  $^{84}\text{Kr}/^{132}\text{Xe}$  and  $^{36}\text{Ar}/^{132}\text{Xe}$  of chondrules. **A:** Plot for all chondrules and their respective bulk chondrites. Yellow shaded box represents the range observed for chondrites. Arrows from Q value indicate towards subsolar (South Oman) and Air end members (values beyond the range of plot, see Table 4.4 for values). Chondrules from Dhajala and Qingzhen show values different from Q values. **B:** Gray box in plot A is enlarged. Most chondrules show values of elemental ratios higher than bulk chondrites. Symbol: open – chondrule, filled – bulk.

during chondrule formation because of metal silicate fractionation. They suggest that initially chondrule precursors were having metal and silicate phases and the physical separation of metal from the silicate during chondrule formation made the chondrule rich in silicate as metal is being expelled from chondrules. Some of the metal solidified while being expelled from the chondrules and formed compact metal sulfide rich coatings around the chondrules. Phase-Q is carbonaceous in nature (Ott et al., 1981) and it is possible that due to this carbonaceous nature it got associated with metal phase during chondrule melting (Vogel et al., 2004). This explains the depletion of trapped  $^{36}\text{Ar}$  relative to trapped  $^{20}\text{Ne}$  in chondrules and the enrichment of trapped  $^{36}\text{Ar}$  in metal/metal sulfide coatings of chondrules.

Based on this result of Vogel et al. (2004) it can be inferred that the amount of Ar in a given chondrule therefore depends on (a) initial heterogeneity in chondrule precursors and (b) the amount of metal remaining in chondrule after metal silicate fractionation. Another important controlling parameter would be the degree of metal silicate fractionation in a given chondrule. Initial heterogeneity in chondrule precursors refers to different amount of presolar diamonds (carrier of HL component) and phase Q (carrier of Q component). The amount of metal remaining in the chondrules depends on several conditions during chondrule formation. Fractionation or separation (physical) of metal and silicate from chondrule precursors is one of the important deciding factors. Degree of metal and silicate fractionation in turn depends on parameters like: (1) heating duration of chondrule precursors (2) peak temperature achieved during heating (3) cooling duration. Heating duration is expected to control the degree of separation between Q and HL, whereas cooling time decides the amount of metal expelled from chondrule. This suggest that chondrules with solidified metal sulfide rim were cooled relatively faster compared to chondrules without rim.

Hence, the abundances of trapped noble gas components in chondrules mainly depend on two parameters: (1) Initial abundances of various noble gas components in chondrule precursors (2) extent of rearrangement between these primary noble gas components during chondrule forming event and loss of noble gases carried by Phase Q. The lower abundance of trapped  $^{36}\text{Ar}$  in chondrules compared to their host chondrites (Fig. 4.2) supports the argument of Ar-loss through loss of metal from chondrule precursors during chondrule melting. Overall, these results also suggest that during chondrule formation, HL and Q were the major noble gas components present in the chondrule precursors before and during chondrule formation.

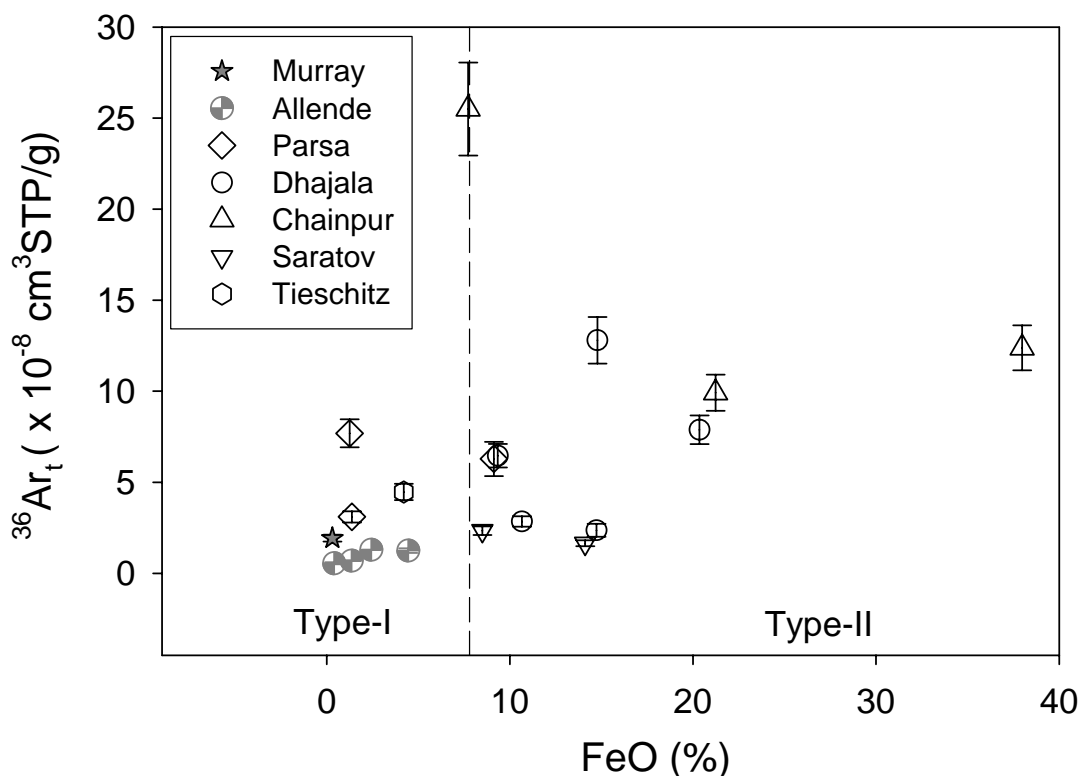


**Fig. 4.5** Concentrations of  $^{36}\text{Ar}_t$  in studied chondrules versus FeO content of the chondrules. Dotted line at FeO = 7.8% represents chondrules as Type-I and Type-II. A positive relation is noticeable between trapped Ar in chondrules and their FeO contents. FeO amount in chondrules indirectly represents the degree of silicate and metal fractionation during chondrule formation. The more FeO content indicates less amount of metal in chondrules as well as higher oxygen fugacity. Less metal in chondrules suggests less loss of Ar from the chondrules.

***Evidence of metal silicate fractionation from chemical composition of chondrules:***

The above suggested fractionation between metal and silicate in chondrule precursors in course of chondrule formation can also affect the chemical composition of these chondrules. As discussed in Chapter 1, chondrules can be classified into Type-I or Type-II based on their FeO content. There are evidences for genetic link between these two types of chondrules (Hewins, 1997). As for example, Sears et al. (1996) suggested that chondrule precursors were FeO rich (similar to Type-II) and subsequent heating in an environment with high oxygen fugacity resulted in less volatile loss or reduction forming Type-II chondrules. While same FeO rich precursor heated with lower oxygen fugacity, resulted in extensive volatile loss (e.g. Na, K) and FeO reduction to Fe metal, giving Type-I chondrules. It is commonly found that Type-I chondrules have higher metal and lower volatile abundance compared to Type-II (Lauretta et al., 2006) suggesting their formation in reduced environment. On the bases of these evidences, it can be argued that fractionation of metal and silicate

occurred more in Type-I chondrules as compared to Type-II chondrules. This further suggests that Type-II chondrules are more primary in nature and experienced lesser degree of metal and silicate fractionation relative to Type-I chondrules.

In Fig. 4.5, estimated FeO content of individual chondrules (based on EPMA, details given in section 2.9, chapter 2) and trapped  $^{36}\text{Ar}$  are plotted. Our results suggest that trapped  $^{36}\text{Ar}$  seems to be related with FeO content of the chondrules. The observed trend can be explained based on various degree of metal and silicate fractionation experienced by individual chondrules. As mentioned above, Type-II chondrules should have experienced less metal silicate fractionation resulting in lower loss of  $^{36}\text{Ar}$  carried by phase Q. This explains the higher amount of trapped  $^{36}\text{Ar}$  in Type-II chondrules compared to Type-I chondrules. One of the Chainpur chondrules (CH-3) shows higher amount of trapped  $^{36}\text{Ar}$  compared to other chondrules from ordinary chondrites. This chondrule has a thick rim of metal (~ 140 micron), which probably represents solidified coating of metal crystallized before it could escape (the detailed description about this chondrule texture and rim is given in chapter 2, section 2.9). However, based on noble gas results and trend observed between FeO and trapped  $^{36}\text{Ar}$  content, there is evidence that noble gas components in individual chondrules were redistributed into metal / metal sulfide phase(Q gases) while the HL component is mostly hosted by the silicates during the chondrule melting.

#### ***Is mixing between HL and Q components independent of the class of chondrites?***

We have analyzed chondrules from ordinary, enstatite and carbonaceous chondrites.  $(^{36}\text{Ar}/^{20}\text{Ne})_t$  values of all chondrules irrespective of which chondrite type they belong, fall between Q and HL components (Fig 4.3). As discussed above, this mixing can be due to initial variable amounts of silicate and metal in chondrules and later rearrangement due to fractionation between metal and silicate phases during chondrule formation. As discussed above, during chondrule formation, the fractionation between metal and silicate resulted in the loss of metal from the chondrules. This loss is also seen for the trapped Ar (mainly carried by phase Q). The trend of lower  $(^{36}\text{Ar}/^{20}\text{Ne})_t$  and  $^{36}\text{Ar}_t$  observed in chondrules from ordinary and carbonaceous chondrites can be explained by this later rearrangement expected to occur during chondrule formation. However, as mentioned earlier the trend observed for the chondrules of enstatite is opposite to this where instead of  $^{36}\text{Ar}_t$  loss,  $^{20}\text{Ne}_t$  loss seems to be responsible for the different  $(^{36}\text{Ar}/^{20}\text{Ne})_t$  ratio compared to bulk. In addition to this, loss of Ar from these chondrules is not as prominent as in the case of

chondrules from ordinary and carbonaceous chondrites (Fig. 4.2). This observation of enstatite chondrules indicates that these chondrules may not have experienced the later stage of fractionation between metal and silicate during their formation. This further implies different environment of formation for enstatite chondrules compared to chondrules from ordinary and carbonaceous chondrites.

The evidence of mixing between HL and Q in chondrules from ordinary and carbonaceous chondrites suggests that precursors of these chondrules were mainly having variable amount of silicate and metal irrespective of the meteorite class from which chondrules are analyzed. Additionally, this mixing also suggests that (a) the heterogeneity in chondrule precursors was widespread and (b) the mechanism responsible for fractionation between metal and silicate phases was common and similar for chondrules from ordinary and carbonaceous chondrites. In comparison to this, case of chondrules from enstatite chondrites seems different and suggests different environment and mechanism of chondrule formation.

#### **4.4.2 Solar type noble gases in chondrules**

As suggested by Okazaki et al. (2001b), chondrules do not show higher abundance of  $^{36}\text{Ar}_t$  (e.g. up to  $7 \times 10^{-6} \text{ cm}^3\text{STP/g } ^{36}\text{Ar}$ ) and as discussed in earlier section that most chondrules show  $(^{36}\text{Ar}/^{20}\text{Ne})_t$  composition which can be explained by mixing between Q and HL components. However, a few chondrules show clues of the solar type noble gases as discussed in next section. As evident in Fig. 4.4, elemental ratios  $^{36}\text{Ar}/^{132}\text{Xe}$  and  $^{84}\text{Kr}/^{132}\text{Xe}$  in individual chondrules suggests the presence of subsolar noble gas component together with Q and Air components. Chondrules DH-9 and QZN-2 show (Fig. 4.4). However,  $(^{36}\text{Ar}/^{20}\text{Ne})_t$  value of DH-9 is around 1.8 which is not indicative of contribution from solar gases. As discussed in trapped  $^{20}\text{Ne}$  results, two chondrules from Dhajala DH-8 and DH-11 show very high concentrations of trapped  $^{20}\text{Ne}$  (Fig. 4.2a). Such Ne-compositions are not observed for DH-9 and QZN-2 chondrules (see Tables 4.1, 4.2). On the other hand,  $^{84}\text{Kr}/^{132}\text{Xe}$  and  $^{36}\text{Ar}/^{132}\text{Xe}$  of DH-8 chondrule does not suggest solar/subsolar component as major noble gas component in this chondrule. We could not detect Kr and Xe in porphyritic DH-11 chondrule. Other chondrules from Udaipur (UD-3), Allende (ALD-8, ALD-9) and very small chondrules from Murray (MRY-5, MRY-7 and MRY-8) also show relatively higher values for the trapped  $^{20}\text{Ne}$ .

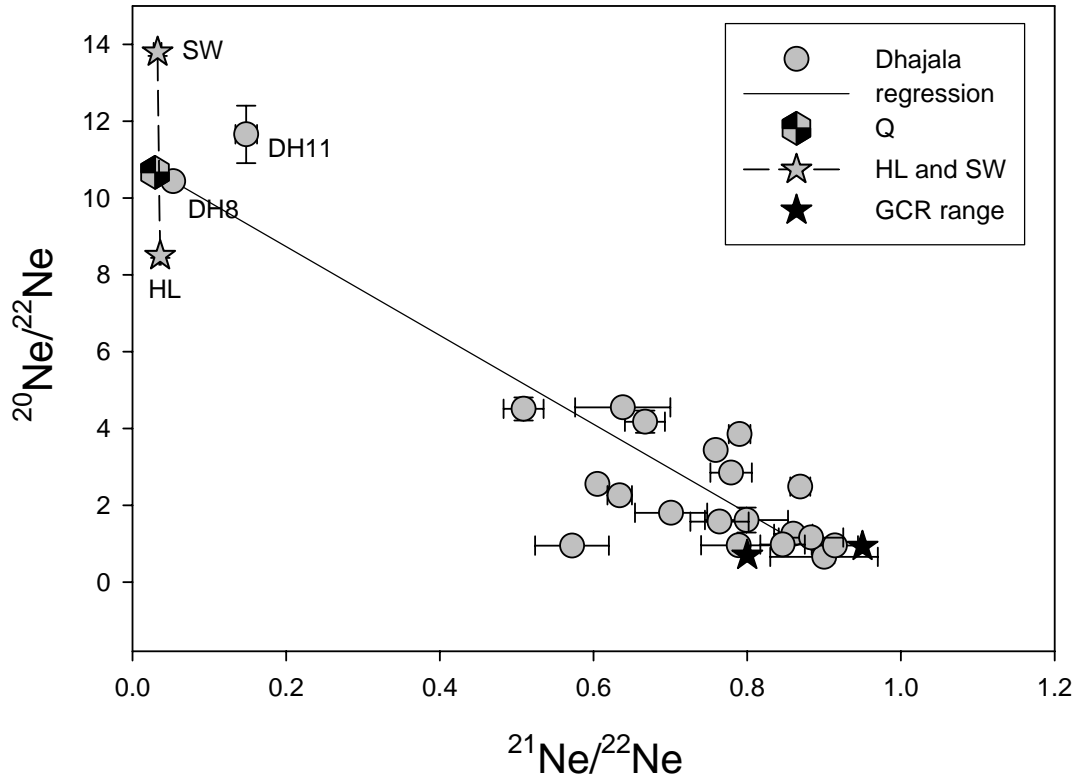


**Fig. 4.6**  $^{20}\text{Ne}/^{22}\text{Ne}$  vs.  $^{21}\text{Ne}/^{22}\text{Ne}$  of chondrules from Dhajala are plotted. As expected in chondritic components, most of the chondrules are showing presence of cosmogenic Ne and falling near the generally observed GCR range in chondrites. Together with this, trapped end-members of Ne like SW, Q and HL are also expected. However, as it can be clearly seen that two chondrules DH-8 and DH-11, are showing presence of trapped components dominating over cosmogenic contribution. This could be due to presence of solar type noble gases in these two chondrites.

Chondrule UD-3 is also found to have higher concentrations of trapped  $^{36}\text{Ar}$  compared to other chondrules (Table 4.1). The  $(^{36}\text{Ar}/^{20}\text{Ne})_t$  value of this chondrule is around 2.1 which is surely not indicating any solar component in it. Other elemental compositions ( $^{84}\text{Kr}/^{132}\text{Xe}$  and  $^{36}\text{Ar}/^{132}\text{Xe}$ ) of UD-3 suggest possibility of minor amount of subsolar component in this chondrule (Fig. 4.4B and Table 4.4). However, another chondrule from Udaipur chondrite (UD-1) show higher values for these elemental ratios compared to UD-3, which is mainly because of difference in  $^{132}\text{Xe}$  abundances in these chondrules. Such difference indicates the primary heterogeneity in chondrule precursors as affecting Xe abundances is difficult during chondrule melting or secondary processes.

Unfortunately, for other chondrules (ALD-8, ALD-9, MRY-5, MRY-7 and MRY-8), trapped  $^{36}\text{Ar}_t$ ,  $^{84}\text{Kr}$  and  $^{132}\text{Xe}$  data are not available and it is difficult to ascertain the reason for high concentrations of trapped  $^{20}\text{Ne}$  in these chondrules.

DH-8 and DH-11 show  $(^{36}\text{Ar}/^{20}\text{Ne})_t$  values towards solar composition (as listed in Table 4.1, not shown in Fig. 4.3) .

The Ne isotopic composition of these chondrules is very different compared to other chondrules. Generally chondrules show Ne composition which can be explained by mixing trapped end members like Q, HL and SW and average cosmogenic values observed for chondrites as can be seen in Fig. 4.6, where  $^{20}\text{Ne}/^{22}\text{Ne}$  vs.  $^{21}\text{Ne}/^{22}\text{Ne}$  of Dhajala chondrules are plotted. DH-8 and DH-11 show Ne composition dominated by trapped Ne. These chondrules also show large amount of trapped  $^{20}\text{Ne}$  as discussed earlier. While the rest of chondrules plot near the cosmogenic end member in the Ne three-isotope plot.

#### ***Excess of $^4\text{He}$ in DH-8 and DH-11***

Generally,  $^4\text{He}$  concentrations in chondrules are contributed by radiogenic  $^4\text{He}$  produced by U-Th decay and a trapped component of He. The concentrations are mostly dominated by radiogenic  $^4\text{He}$ . The expected radiogenic  $^4\text{He}$  in chondrules due to U and Th decay can be calculated, assuming complete retention during 4.56 Ga

#### ***Calculation of maximum radiogenic $^4\text{He}$ contributed by U, Th decay:***

The measured  $^4\text{He}$  in a give chondrule can be contributed by three components: cosmogenic, radiogenic and trapped. We considered that measured  $^3\text{He}$  in our samples are only due to cosmogenic contribution as trapped  $^3\text{He}$  concentrations are expected to be negligible due to  $(^3\text{He}/^4\text{He})_t \sim 10^{-4}$  We assumed  $(^4\text{He}/^3\text{He})_c = 5.2$  to correct for the cosmogenic  $^4\text{He}$  from the measured amount. Details of the calculation are already discussed in section 3.2, Chapter 3.

It is possible to calculate maximum radiogenic  $^4\text{He}$  contributed by U-decay series (produced as  $\alpha$ -particles from the radioactive decay of  $^{238}\text{U}$ ,  $^{235}\text{U}$  and  $^{232}\text{Th}$ ), provided the concentrations of U and Th are known for the samples. The amount of  $^4\text{He}$  produced in a closed system and over time t is given by:

$$^4\text{He}^* = ^{238}\text{U} [8(e^{\lambda_{238}t} - 1) + 0.0504(e^{\lambda_{235}t} - 1) + 6\{(Th/U) \times (e^{\lambda_{232}t} - 1)\}]$$

In this equation:  $^4\text{He}$  is expressed in units of  $10^{-6} \text{ cm}^3\text{STP/g}$  and U as well as Th concentrations are considered in atoms/g. By using this equation, maximum in time (t) = 4.56 Ga radiogenic  $^4\text{He}$  produced in Dhajala chondrite is  $\sim 1.31 \times 10^{-5} \text{ cm}^3\text{STP/g}$  (42 and 12 ppb adopted as concentration of U and Th respectively, as suggested for H chondrites by Wasson and Kallemeyn [1988]). In Fig. 4.7, this expected maximum

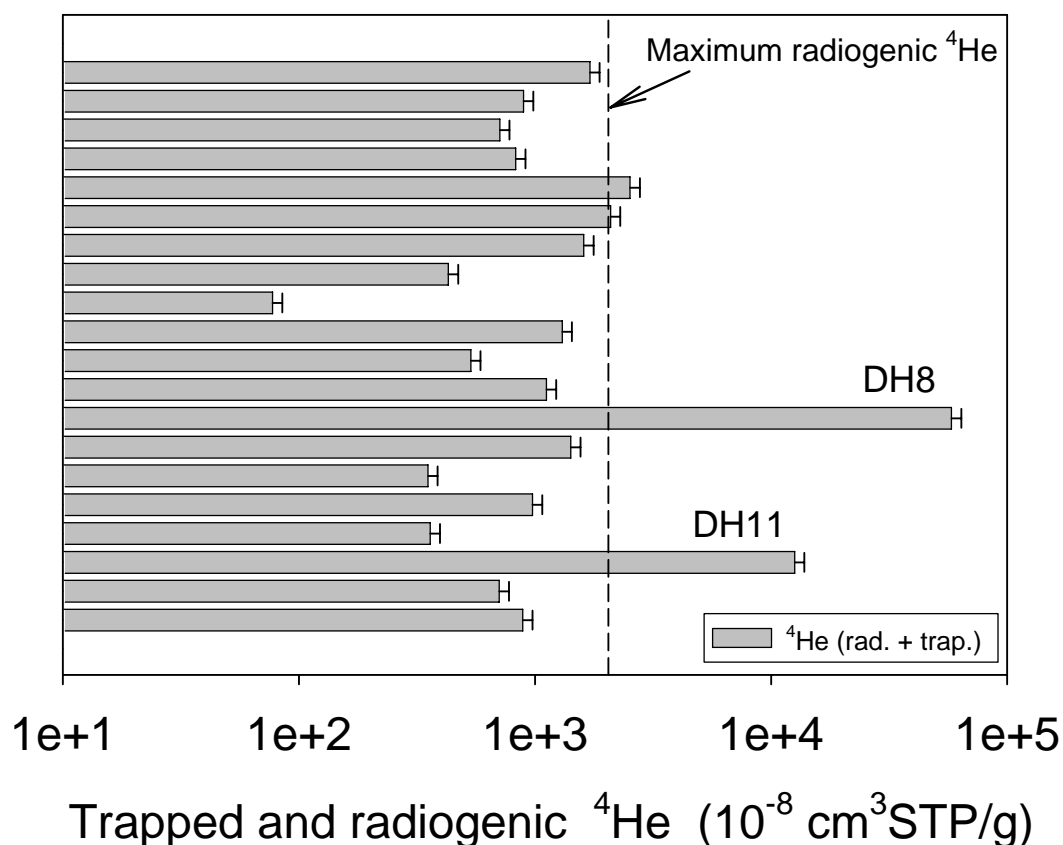


**Fig. 4.7**  ${}^4\text{He}$  in chondrules of Dhajala contributed by trapped and radiogenic components. These concentrations are corrected for cosmogenic contribution in  ${}^4\text{He}$ . Dotted line in plot gives the value ( $2047 \times 10^{-8} \text{ cm}^3\text{STP/g}$ ), of maximum radiogenic  ${}^4\text{He}$  produced in 4.56 Ga through U-decay series in H-chondrite (Table 3.1, chapter 1). In absence of any significant trapped  ${}^4\text{He}$ , concentration of  ${}^4\text{He}$  in chondrules should be less or equal to this maximum value. The less concentration of  ${}^4\text{He}$  in chondrules can be explained by loss of  ${}^4\text{He}$ . However, the excess observed for chondrules DH-8 and DH-11 requires the presence of trapped  ${}^4\text{He}$  in these chondrules, which could be contributed by solar component.

value is ( $2047 \times 10^{-8} \text{ cm}^3\text{STP/g}$ ) represented by dotted lines. The cosmogenic corrected  ${}^4\text{He}$  is plotted for all Dhajala chondrules in figure.

As can be seen in Fig. 4.7, most chondrules are showing lower amount of  ${}^4\text{He}$  which can be mainly due to partial loss of  ${}^4\text{He}$ . However as clearly seen, the DH-8 and DH-11 chondrules are showing  ${}^4\text{He}$  concentrations higher than expected maximum contribution by U-decay series. For example, the concentration of  ${}^4\text{He}$  in DH-11 is higher by factor of 7 compared to maximum radiogenic  ${}^4\text{He}$  expected in H-chondrite. Such high increase in  ${}^4\text{He}$  clearly suggests the presence of excess  ${}^4\text{He}$  possibly of trapped origin.

Porphyritic chondrules are the chondrules with large phenocrysts ( $> 100 \mu\text{m}$ ) with interstitial fine mesostasis. It is suggested that to form chondrules with porphyritic

textures some grains should survive during chondrule melting to provide nucleation site to generate larger phenocrysts during chondrule cooling (Lauretta et al., 2006). Survival of grains in these chondrules suggests incomplete melting of their precursors which subsequently suggest incomplete removal of trapped gases from precursors. Okazaki et al. (2001a) have reported higher concentrations of  $^{36}\text{Ar}_t$  in porphyritic chondrules from the enstatite chondrite Yamato (Y)-791790. They argue that this high concentration is due to solar type noble gases trapped during chondrule formation as suggested by X-wind model. Their porphyritic texture is suggesting incomplete removal of these solar gases.

We found that DH-11 chondrule is a porphyritic chondrule whereas DH-8 shows radial texture. The detailed description of textures as well as back scattered electron (BSE) images of these chondrules is discussed in Chapter 2. However, DH-11 and DH-8 chondrule do not show higher concentrations of  $^{36}\text{Ar}_t$  like Okazaki et al. (2001a) reported for porphyritic chondrules of Yamato (Y)-791790.

Based on these arguments, we propose that DH-8 and DH-11 chondrules from Dhajala chondrite are having signatures of solar type noble gases, as suggested by  $(^{36}\text{Ar}/^{20}\text{Ne})_t$ , Ne-isotopic compositions and excess of  $^4\text{He}$ .

#### **4.5 Summary**

1. Detectable amounts of trapped  $^{20}\text{Ne}$  and  $^{36}\text{Ar}_t$  are present in chondrules.
2.  $(^{36}\text{Ar}/^{20}\text{Ne})_t$  and its relation with abundance  $^{36}\text{Ar}_t$  of chondrules (from ordinary and carbonaceous chondrites) suggests mixing between HL and Q components, the proportions of which are determined by: (1) Initial abundances of various noble gas components in chondrule precursors (2) extent of rearrangement between these primary noble gas components during chondrule forming event and loss of noble gases carried by Phase Q. In addition to this, it can be inferred that HL and Q were the major components in chondrule precursors before and during chondrule formation.
3. Compared to host chondrites, chondrules from ordinary and carbonaceous chondrites are found depleted in abundances of  $^{36}\text{Ar}_t$  suggesting loss most probably during chondrule formation. Such depletion is not observed in case of  $^{20}\text{Ne}_t$ . This observation overrules the possibility of evaporative loss of noble gases during chondrule formation and instead suggests the loss of certain phase (carrier of  $^{36}\text{Ar}_t$ ).

4. Based on relation between concentrations of trapped  $^{36}\text{Ar}$  and FeO, it can be argued that the relative amount of HL and Q components is related with the degree of metal and silicate fractionation that occurred during chondrule formation.
5. Different observation in case of chondrules from enstatite chondrites indicates different environment and/or mechanism for their formation compared to chondrules from ordinary and carbonaceous chondrites.
6. DH-8 and DH-11 chondrules from Dhajala chondrites show presence of solar type noble gases. The presence of solar component is reflected by  $(^{36}\text{Ar}/^{20}\text{Ne})_t$  values, Ne-compositions and presence of excess  $^4\text{He}$ . For other chondrules, although some evidences of high abundances in gases are observed, it cannot be surely attributed to solar type noble gases.
7. The elemental ratios  $^{84}\text{Kr}/^{132}\text{Xe}$  and  $^{36}\text{Ar}/^{132}\text{Xe}$  indicate the presence of subsolar components in chondrules, which seems minor compared to contribution from Q component.

Chapter 5

## Trapped Nitrogen in chondrules

## 5.1 Introduction

Studies of nitrogen in individual chondrules are scarce. This work is the first systematic approach to investigate different N-components possibly present in an individual chondrule. This chapter gives the results of nitrogen measured in individual chondrules from ordinary, enstatite and carbonaceous chondrites as well as discusses the possible implications in light of these results. Nitrogen in individual chondrules essentially has two components, namely trapped and cosmogenic components. The trapped component represents the source region from where the sample has acquired its gases, while the cosmogenic component is that produced in the sample after its crystallization. Hence, study of trapped gases is relevant for evaluation of various processes recorded by chondrule precursors and subsequently in course of chondrule formation. As the isotopic ratio of  $^{15}\text{N}/^{14}\text{N}$  of cosmogenic nitrogen is  $\geq 1$ , the cosmogenic component significantly contributes to the measured  $\delta^{15}\text{N}$ , though negligibly contributes to the concentration of N. To obtain the  $\delta^{15}\text{N}$  of trapped component, the measured  $\delta^{15}\text{N}$  needs to be corrected for cosmogenic contribution. Silicate materials comprise ~45% oxygen and hence the production of  $^{15}\text{N}$  in a given sample, which is mainly silicate, is significant. It is difficult to decipher cosmogenic N-component in samples because of the presence of large primary N-components, which are found to be heterogeneous in these primitive samples. To overcome this difficulty a different approach has been adopted. In this indirect method, by using the cosmogenic  $^{21}\text{Ne}$ , cosmogenic  $^{15}\text{N}$  is derived. Following are the details.

## 5.2 Corrections of the measured $\delta^{15}\text{N}$ for cosmogenic contribution

The principal targets for the production of cosmogenic  $^{15}\text{N}$  and  $^{21}\text{Ne}$  respectively are O and Mg, Si, Al. For the average bulk compositions (and average shielding depth) of the ordinary, enstatite and carbonaceous chondrites, one can derive the relation  $(^{15}\text{N}/^{21}\text{Ne})_c = 4.5 \pm 0.5$  (Mathew and Murty, 1993). For individual chondrules, the chemical composition has been used to derive the  $(^{15}\text{N}/^{21}\text{Ne})_c$  ratio (example is given in *Appendix*) and for those chondrules where no chemical data is available, the average chondrule composition for that class has been used. Using the measured  $^{21}\text{Ne}_c$  and the appropriate  $(^{15}\text{N}/^{21}\text{Ne})_c$  ratio, the measured  $\delta^{15}\text{N}$  has been corrected for the cosmogenic contribution by using the following relation (derivation of this relation is given in *Appendix*).

$$\delta^{15}\text{N}_t = \delta^{15}\text{N}_m - (^{15}\text{N}/^{21}\text{Ne})_c \times (^{21}\text{Ne}_c \times 1.7) / \text{N (ppm)}$$

Where  $^{21}\text{Ne}_c$  is to be inserted in units of  $10^{-8}\text{cm}^3\text{STP/g}$ . N-compositions corrected for cosmogenic contribution represents trapped N-compositions of chondrules. Subscripts 't' and 'm' indicate, *trapped* and *measured* respectively.

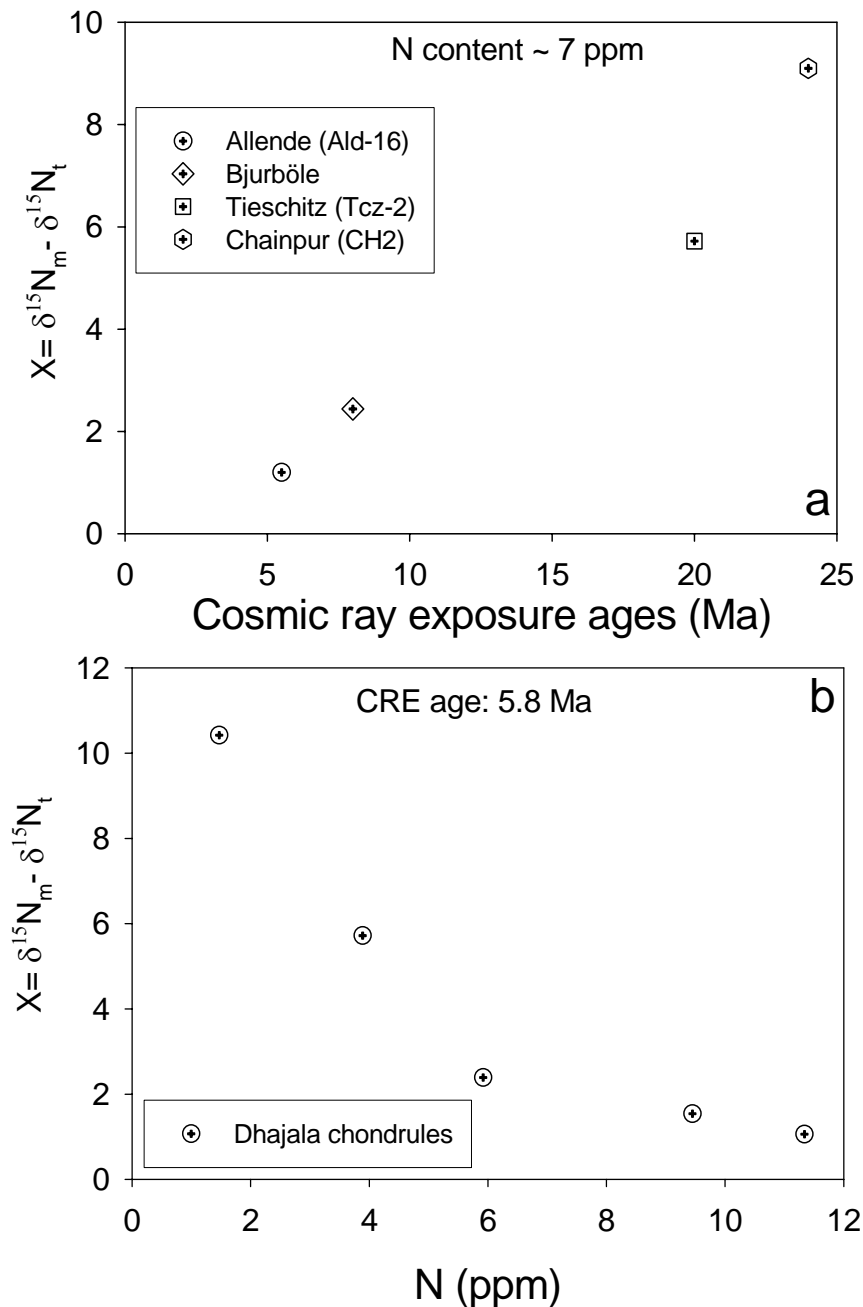


**Fig. 5.1** Correction in nitrogen composition for cosmogenic contribution (defined as  $X$ ) compared for (a) chondrites of different cosmic ray exposure ages (with similar N content) and (b) from Dhajala (CRE age = 5.8Ma) with different N concentrations. It is clearly seen that, the correction  $X$ , defined as  $\delta^{15}\text{N}_m - \delta^{15}\text{N}_t$ , is increasing with higher cosmic ray exposure ages. The correction  $X$  reduces with higher concentration of N for a given chondrite.

The reduction in  $\delta^{15}\text{N}$  values due to correction by cosmogenic contribution (defined as  $X = \delta^{15}\text{N}_m - \delta^{15}\text{N}_t$ ) is listed for all the chondrules in Tables 5.1, 5.2 and 5.3. The

amount of correction depends on the amount of cosmogenic  $^{21}\text{Ne}$  (function of cosmic ray exposure (CRE) age of the sample) as well as the amount of nitrogen in a given sample. In Fig. 5.1a, Correction in measured  $\delta^{15}\text{N}$  due to cosmogenic contribution is plotted against the CRE ages of four chondrites with different cosmic ray exposure ages and similar N-content. It is clearly seen that the amount of correction 'X' increases with increase CRE ages. On the other hand as shown in Fig. 5.1b, the correction 'X' decreases with increase N abundances in chondrules (from Dhajala with  $\sim 5.7$  Ma of exposure age).

### **5.3 Results**

*Earlier studies:* Systematic study of nitrogen abundance and composition has been attempted for the first time by the present study. However, in addition to earlier work on some Dhajala chondrules (Mahajan and Murty, 2003) and a halogen rich Allende chondrules (Murty, 1998) in our lab, there have been only two studies in literature; measurement of 4 individual Bjurböle chondrules (Fredriksson et al., 1985) and an ensemble of chondrules from Soko-Banja (LL4) chondrite (Kung and Clayton, 1978). The earlier attempts were random and mainly tried on large and specific chondrules. These earlier attempts indicated that chondrules have different N-compositions compared to their bulk as well as there is no apparent trend between composition and content of N.

N-compositions corrected for cosmogenic contribution, in individual chondrules from ordinary, enstatite and carbonaceous chondrites are given in Tables 5.2, 5.3 and 5.4. These compositions of chondrules are plotted against their N-abundances in Figs. 5.2, 5.3, 5.4 and 5.5 for chondrules of Dhajala chondrite, ordinary chondrites, enstatite chondrites and carbonaceous chondrites respectively.

#### **5.3.1 N-compositions of chondrules from ordinary chondrites**

A total 46 chondrules from six different chondrites are analyzed for nitrogen together with noble gases. In the following sections, N results for chondrules and their respective bulk sample of each chondrite are described. Results are listed in Table 5.1, for chondrules from ordinary chondrites.

##### **Dhajala (H3.8)**

A total 22 chondrules have been analyzed from Dhajala chondrite. In Fig. 5.2, composition of trapped nitrogen is plotted against N-abundances of chondrules from Dhajala chondrite. Also shown by hatched box is the range of N-composition and

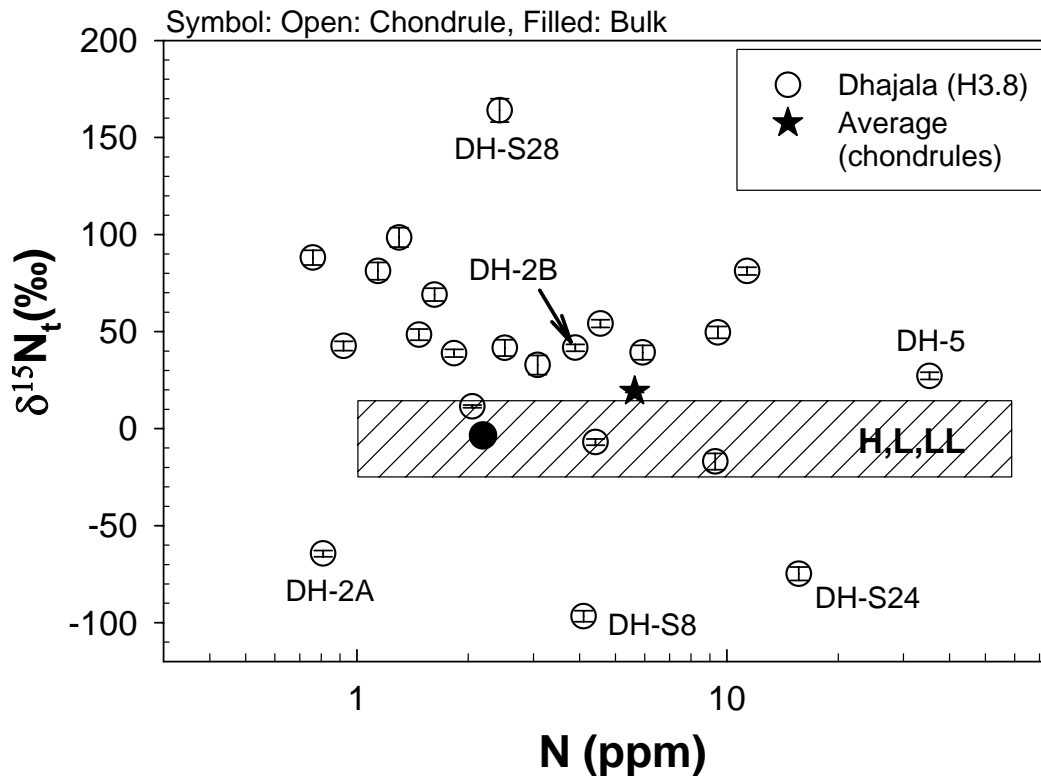


**Fig. 5.2** Nitrogen composition corrected for cosmogenic contribution ( $\delta^{15}\text{N}_t$ ) vs. nitrogen concentration is plotted for Dhajala chondrules and bulk. Hatched Box represents the average values observed for ordinary chondrites (Grady and Wright 2002). Average N-composition is calculated from n-compositions of chondrule weighted by their nitrogen concentrations, which is similar to bulk ordinary chondrites suggesting that although individual chondrules may be heterogeneous in N-compositions, their average is similar to bulk ordinary chondrites.

abundances observed for bulk. The N-composition of chondrules is ranging from -100‰ to 164‰ whereas bulk N composition of Dhajala is -3.6‰ (Murty, 1996). Most chondrules show  $^{15}\text{N}$ -rich compositions compared to bulk Dhajala. DH-S28 shows high value of  $\delta^{15}\text{N}$  (+164 ‰). In contrast to this, three chondrules are found depleted in  $^{15}\text{N}$  with respect to bulk as well as ordinary chondrites. Two splits of chondrule DH-2 show large difference in N-composition. As shown in Fig. 5.2, DH-2A shows  $\delta^{15}\text{N} = -64\text{‰}$  with ~0.8 ppm nitrogen whereas another split DH-2B is  $^{15}\text{N}$  rich ( $\delta^{15}\text{N} = 40\text{‰}$ ) with higher abundance of nitrogen (~6 ppm). This result clearly indicates the presence of at least two different N-components within a single chondrule and their heterogeneous distribution. N-concentrations of chondrules are within 1 – 40 ppm. As described in section 2.7.2, Chapter 2, the split of this chondrule has Fe, S and Ca rich wave like lines within pyroxenes. It is possible that the difference observed in nitrogen results are due to heterogeneous distribution of such phases, carrying different N components.

It can be seen in Fig. 5.2 that there is no apparent relationship between N-compositions of individual chondrules and their N-concentrations. If the variation in  $\delta^{15}\text{N}$  is a consequence of partial nitrogen loss from individual chondrules (all of them initially having identical N and  $\delta^{15}\text{N}$ ) and the associated isotopic fractionation (enrichment of  $^{15}\text{N}$  in the residual reservoir) then a trend of increased  $\delta^{15}\text{N}$  with lower N content is expected. Such trend is not evident in Fig. 5.2, ruling out, this possibility as the principal reason for the spread in  $\delta^{15}\text{N}$  values. The relation of nitrogen composition and concentration with size (can be represented by weight of chondrule) of individual chondrule has also been surveyed which is discussed separately in section 5.4.2. As shown in Fig. 5.2, average N-composition calculated from N-compositions of individual chondrules weighted by nitrogen concentrations in these chondrules is in the observed range of N-composition for ordinary chondrites.

### Tieschitz (H3.6)

Five chondrules have been analyzed from this chondrite. In Fig. 5.3, N-compositions of chondrules from ordinary chondrites are compared to their N-abundances. Values observed in bulk are also plotted. Nitrogen composition of Tieschitz chondrules varies from  $-4\%$  to  $99\%$ . These values are different compared to N-composition of Tieschitz bulk ( $10.2\%$ , Table 5.1, Fig. 5.3). Concentration of N ranges from 2 to 16 ppm in chondrules where as N-concentration of Tieschitz bulk is 10 ppm. The variation of N-composition among individual chondrules as compared to bulk is clear from the five chondrules analyzed.

**Table 5.1** Nitrogen results for the individual chondrules of ordinary chondrites. Measured and corrected (for cosmogenic contribution) N-compositions are given with trapped  $^{36}\text{Ar}$  in chondrules.

Sample	Mass (mg)	N (ppm)	$\delta^{15}\text{N}_m$	$\delta^{15}\text{N}_t$	X	$^{36}\text{Ar}_t$	$(^{14}\text{N}/^{36}\text{Ar})_t$ ( $10^5$ )	
			(‰)					
<b>Dhajala (H3.8)</b>								
DH-S1	0.985	1.30	106 5	98.5 5.1	7.52	1.0	2.08	
DH-S8	0.605	4.10	-90.4 2.8	-96.7 2.8	6.2	1.18	5.59	
DH-S11	0.665	2.05	17.8 0.4	11.4 .7	6.3	0.78	4.12	
DH-S18	0.348	9.3	-14.9 4.2	-16.9 4.2	2	1.36	10.9	
DH-S19	0.359	4.55	58.2 1.9	54.1 2.0	4.1	3.17	2.3	

Sample	Mass (mg)	N (ppm)	$\delta^{15}\text{N}_m$	$\delta^{15}\text{N}_t$	X	$^{36}\text{Ar}_t$	$(^{14}\text{N}/^{36}\text{Ar})_t$ ( $10^5$ )
			(‰)				
DH-S23	0.845	3.08	37.1 5.0	32.8 5.0	4.3	1.52	3.25
DH-S24	0.172	15.6	-74.0 3.5	-74.8 3.5	0.8	1.09	23
DH-S27	0.805	3.89	47.4 1.7	41.7 1.8	5.7	1.61	3.87
DH-S28	0.797	2.43	171 6	164 6	8.7	1.54	2.52
DH-2A	3.659	0.81	-51.9 1.0	-64.4 1.6	12.5	1.94	0.67
DH-2B	3.926	5.92	41.6 3.7	39.2 3.7	2.4	2.73	3.47
DH-5	0.253	35.3	27.7 1.9	27.2 1.9	0.5	11.0	5.18
DH-8	1.721	4.41	-3.9 1.5	-6.9 1.5	2.6	2.85	2.48
DH-9	0.386	9.45	51.1 3.1	49.5 3.1	1.5	6.46	2.34
DH-11	0.213	11.3	82.3 1.9	81.2 1.9	1	7.89	2.3
DH- V7	3.258	1.47	58.8 2.7	48.4 2.9	10.4	1.93	1.22
DH-V11	4.073	1.83	47.2 1.7	38.9 1.9	8.3	0.6	4.90
DH-V18	3.782	0.92	52.2 2.1	42.5 2.4	9.7	0.23	6.51
DH-V30	3.158	0.76	107 3	88.1 3.8	19.2	1.40	0.86
DH-V35	2.158	1.62	73.0 3.3	69.0 3.3	4	1.27	2.04
DH-V38	5.737	1.14	92.2 4.4	81.2 4.5	11	0.79	2.32
DH-No25	3.677	2.51	46.4 4.2	41.6 4.2	4.8	0.30	13.1
DH-Bulk	205.0	2.19	2.9 1.4	-3.56 1.55	6.42	16.5	0.21
<b>Chainpur (LL3.4)</b>							
CH-1A	6.602	24.7	5.59 .13	3.52 .26	2.1	5.09	7.8
CH-1B	5.898	60.7	5.66 .69	4.73 0.70	0.9	19.7	4.93
CH-2	2.356	7.07	17.23 .67	8.13 1.13	9.1	9.94	1.14
CH-3	0.798	28.8	-6.43 .53	-9.60 .62	3.2	25.5	1.81

Sample	Mass (mg)	N (ppm)	$\delta^{15}\text{N}_m$	$\delta^{15}\text{N}_t$	X	$^{36}\text{Ar}_t$	$(^{14}\text{N}/^{36}\text{Ar})_t$ ( $10^5$ )
			(‰)				
Matrix (fine)	58.04	38.6	3.72 0.17	2.11 .24	1.6	46.0	1.34
Matrix (coarse)	18.45	31.3	-0.50 .38	-2.55 .43	2.1	54.1	0.92
<b>Udaipur (H3.6)</b>							
UDP-1	1.418	4.5	28.6 .7	22.7 .9	5.9	19.1	0.38
UDP-2	0.801	8.03	19.3 1.3	15.5 1.3	3.8	12.4	1.03
UDP-3	0.247	5.01	68.9 4.1	62.7 4.1	6.2	50.7	0.16
UDP (Bulk)	216.0	6.05	-14.2 1.4	-22.8 1.6	8.7	54.5	0.18
<b>Saratov (L4)</b>							
STV-2A	2.257	1.9	23.0 5.0	13.3 5.1	9.7	1.24	2.45
STV-2B	0.948	7.2	21.7 3.2	17.5 3.2	4.2	3.45	3.35
STV-3	1.812	1.12	69.2 4.8	37.2 5.8	32	1.65	1.09
STV-6	1.195	1.31	129 2	103 3	26.5	0.93	2.27
STV-7	0.238	-	-	-	-	4.12	-
STV (bulk)	214	1.95	21.8 1.1	-8.76 3.24	30.6	6.77	0.46
<b>Tieschitz (H3.6)</b>							
TCZ-1	2.142	15.8	-4.25 .71	-5.59 .72	1.3	73.3	0.34
TCZ-2	1.814	7.11	14.5 .7	8.78 .92	5.7	4.34	2.62
TCZ-5	1.168	1.90	23.0 5.0	8.24 5.25	14.8	3.05	1.00
TCZ-8	0.303	14.3	82.9 4.7	80.6 4.7	2.3	3.65	6.26
TCZ-9	0.169	7.15	99.4 6.9	97.0 6.9	2.4	17	0.67
TCZ (bulk)	58.04	10.2	-4.9 .4	-10.2 .6	5.3	28.8	0.57
<b>Bjurböle (LL4)</b>							
BB-3	0.89	3.75	-4.01 .75	-8.69 .88	4.7	0.06	106

Sample	Mass (mg)	N (ppm)	$\delta^{15}\text{N}_m$	$\delta^{15}\text{N}_t$	X	$^{36}\text{Ar}_t$	$(^{14}\text{N}/^{36}\text{Ar})_t$
			(‰)				( $10^5$ )
BB-8	0.72	12.0	-38.8 1.5	-40.3 1.5	1.5	0.55	34.7
BB-10	0.39	5.32	-34.3 2.8	-37.5 2.8	3.18	0.35	24.2
BB-15	0.756	2.57	-25.9 7.1	-34.8 7.2	8.9	0.53	7.80
BB-18	0.721	4.07	-33.3 1.1	-39.6 1.2	6.2	0.33	19.6
BB-25	0.583	7.52	-131 6	-134 6	2.7	1.63	7.39
BB-28	0.719	7.39	-51.9 6.1	-54.3 6.1	2.4	1.70	7.14
BB-29	0.655	5.39	-85.4 2.1	-90.6 2.1	5.1	0.9	10.0

X is Decrease in measured  $\delta^{15}\text{N}$  due to cosmogenic correction (defined as  $X = \delta^{15}\text{N}_m - \delta^{15}\text{N}_t$ ),  $^{36}\text{Ar}_t$  concentrations are given in units of  $10^{-8} \text{ cm}^3\text{STP/g}$  (error  $\pm 10\%$ ). For,  $\delta^{15}\text{N}$ , the errors are  $2\sigma$ .

### Udaipur (H3.6)

N-composition of three chondrules analyzed from Udaipur chondrite, ranges from 16 to 63‰ whereas nitrogen concentration is 5 to 8 ppm. As evident in Fig. 5.3, similar to chondrules from other OC chondrites, chondrules from Udaipur are also different from the bulk Udaipur ( $\delta^{15}\text{N} = -22.8\%$ , 6 ppm of N).

### Saratov (L4)

The N-composition of four Saratov chondrules ranges from 22‰ to 129‰, which is different from that of bulk Saratov chondrite (-8.8‰). Concentration of nitrogen is between 1 to 7 ppm compared to 2 ppm in bulk. Large variation of N-compositions is evident among the five chondrules. This variation of N-composition in chondrules is not related with their N-concentration similar to Dhajala and Bjurböle chondrules. N-composition of STV-2A and STV-2B (splits of a chondrule STV-2) is different as observed for the case of chondrule DH-2 from Dhajala chondrite (Table 5.1). The texture of this chondrule (as describe in section 2.7.2, Chapter 2) suggests the presence of metal sulfide blebs at the edges (not in the form of rims). As mentioned above, unequal distribution of such phases in chondrules can be a reason for different N-compositions for the splits of this chondrule. Such results are indicative of heterogeneity within chondrules, suggesting that precursors of chondrules were heterogeneous in N-composition.

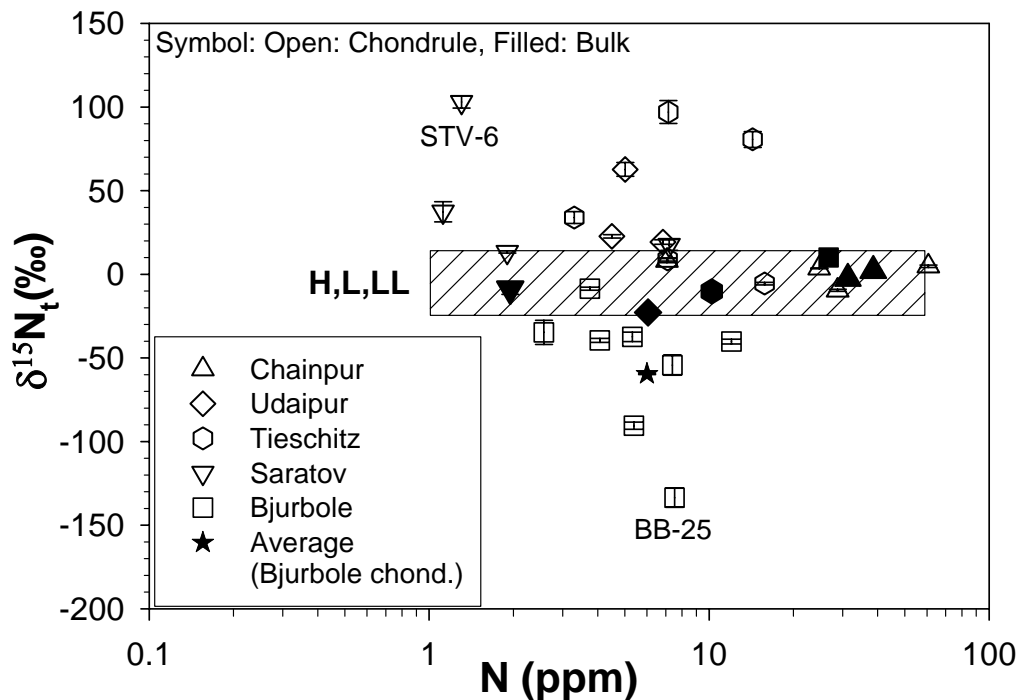


**Fig. 5.3** Nitrogen composition corrected for cosmogenic contribution ( $\delta^{15}\text{N}_i$ ) vs. nitrogen concentration is plotted for chondrules and bulk sample of five ordinary chondrites. Hatched Box represents the average values observed for ordinary chondrites (Grady and Wright 2002). Average N-composition is also plotted, calculated from n-compositions of chondrule weighted by their nitrogen concentrations for Bjurböle chondrites.

#### **Chainpur (LL3.4)**

Three chondrules have been analyzed from this LL3.4 chondrite. Weights of these chondrules are from 0.8 to 6.6 mg. In case of CH-1 chondrule, two splits (CH-1A and CH-1B) have been analyzed separately. N-composition varies from  $-10\text{‰}$  to  $8\text{‰}$  whereas 7 to 60 ppm N-concentration is observed in these chondrules (Fig. 5.3). Highest amount of nitrogen (60 ppm) is found in one of the Chainpur chondrules, among all chondrules analyzed from ordinary chondrites. Different N-compositions as well as N-contents for the splits of CH-1 chondrule has been observed, similar to the cases of DH-2 (Dhajala) and STV-2 (Saratov) chondrules. As discussed in Chapter 2 (section 2.7.2), the split of this chondrule have  $\sim 700\mu\text{m}$  size metal bleb inclusion. The presence of heterogeneously distributed phases is the possible reason for different N-compositions and contents.

#### **Bjurböle (L/LL4)**

Nine chondrules have been analyzed for nitrogen and noble gases from Bjurböle chondrite. In Bjurböle chondrules, large depletion of  $^{15}\text{N}$  is observed and  $\delta^{15}\text{N}$  varies from  $-9\text{‰}$  to  $-134\text{‰}$  (Table 5.1, Fig. 5.3). This is the highest depletion observed among all chondrules studied from ordinary chondrites. Nitrogen concentration in

chondrules varied from 2.5 to 12 ppm well within the range, observed for ordinary chondrites. N-compositions of chondrules are depleted compared to bulk ( $\delta^{15}\text{N}=10.1\%$ , Fredriksson et al., 1985) as well as average ordinary chondrites. Like Dhajala chondrules, these chondrules also do not show any relation between N-composition and amount of N. In Fig. 5.2, average value of  $\delta^{15}\text{N}$  and N-abundance calculated for Bjurböle chondrules are also plotted. The value is different compared to bulk and the range observed for ordinary chondrites. All chondrules of Bjurböle show  $\delta^{15}\text{N}$  values depleted in  $^{15}\text{N}$ .

Fredriksson et al. (1985) have also analyzed nitrogen and noble gases in individual chondrules from Bjurböle chondrite (range of results are listed in Table 5.1). One of the chondrules, BJU-20 was found to have N-composition with  $\delta^{15}\text{N} \sim -17\%$  and  $\sim 4$  ppm of N. In another chondrule BJU-50, which was a fragment of troilite, nitrogen was found  $^{15}\text{N}$  rich ( $\delta^{15}\text{N} = +6.4\%$ ) with higher N-content ( $\sim 11$  ppm). Nitrogen was lower and different in chondrules compared to Bjurböle matrix ( $\delta^{15}\text{N} \sim 10\%$ , N  $\sim 27$  ppm). These Authors suggested the presence of at least two different N components (lighter component carried by silicates, heavier carried by sulfides). Back scattered electron (BSE) images of five Bjurböle chondrule splits analyzed in the present study suggest porphyritic texture of chondrules with absence of any significant amount of metal/metal sulfide phases in these chondrules and chondrules are dominated by silicate phases. As all Bjurböle chondrules show lighter values of  $\delta^{15}\text{N}$ , our result agrees to the conclusion drawn by Fredriksson et al. (1985) that silicates carry mainly lighter N. Above all, the range observed for chondrules in this work is surely very large compared to this earlier report (Fredriksson et al., 1985).

### **5.3.2 N-compositions of chondrules from enstatite chondrites**

Chondrules from two enstatite chondrites, Parsa and Qingzhen are analyzed for nitrogen with noble gases. The results are listed in Table 5.2. In Fig. 5.4, N-compositions of chondrules and their bulk are compared with concentration of N in these samples.

#### **Parsa (EH3)**

Four chondrules have been analyzed from this chondrite. The N-composition of chondrules and bulk Parsa is similar ( $\delta^{15}\text{N} \sim -23\%$ , Fig.5.4). As described before, all chondrules from ordinary chondrites show different N-composition compared to their respective bulk. In contrast to this, in case of Parsa results clearly show similar N-

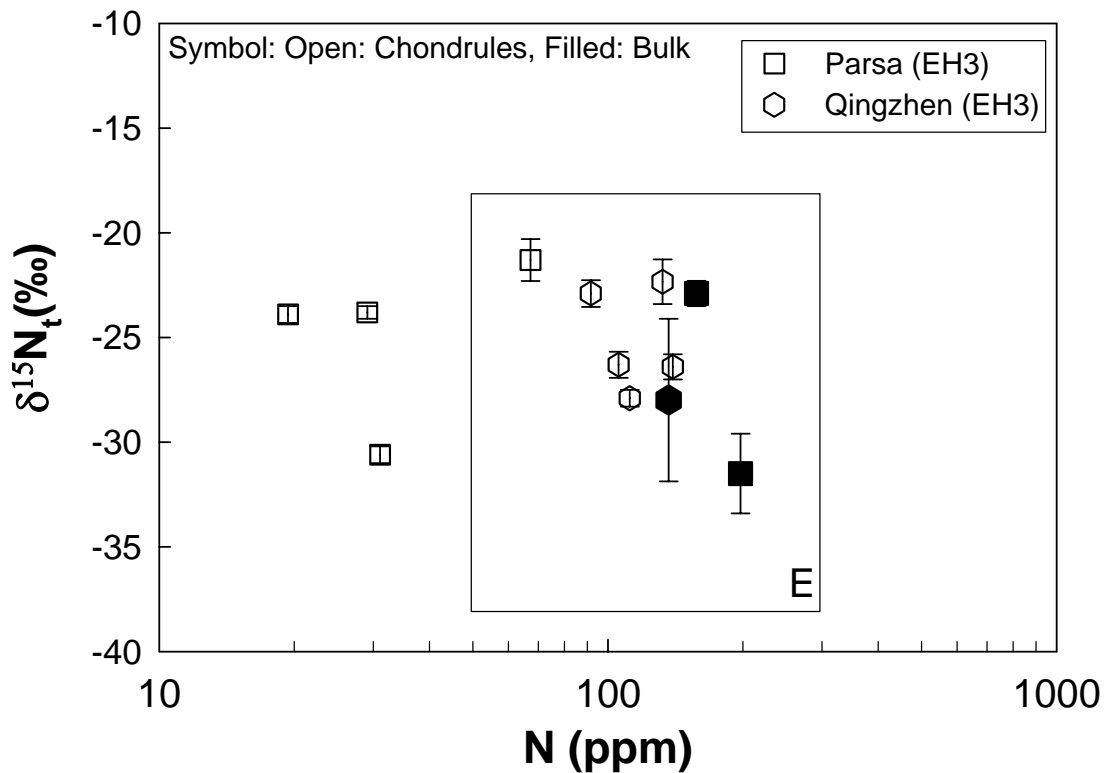


**Fig. 5.4** Nitrogen composition corrected for cosmogenic contribution ( $\delta^{15}\text{N}_t$ ) vs. nitrogen concentration is plotted for chondrules and bulk sample of Parsa and Qingzhen chondrites. Box represents the average values observed for enstatite chondrites (Grady and Wright 2002). Unlike OC chondrules, chondrules from enstatite chondrites show N-compositions similar to enstatite chondrites

compositions for chondrules and bulk Parsa (Fig. 5.4). Splits of chondrule Parsa-3 have been analyzed. These splits also show similar N-composition and content (Table 5.2). This is in contrast to the cases observed in chondrule splits from ordinary chondrites. As described in Chapter 2, texture of the split of Parsa-3 chondrule is uniform and does not show any presence of metal/metal sulfide bleb unlike the cases of chondrules from ordinary chondrites. This indicates homogeneous distribution of precursor phases in Parsa-3 chondrule. Chondrule Parsa-2 shows lighter N-composition compared to Parsa bulk however within the range observed for enstatite chondrites. Nitrogen amount in chondrules varies from 20 to 70 ppm compared to 160 ppm detected in Parsa bulk. Lower content of nitrogen can be due to partial loss of nitrogen during chondrule formation. On the other hand, it is also possible that precursors of chondrules were originally depleted in nitrogen. In addition to this, variation in N contents and  $\delta^{15}\text{N}$  (the range is smaller compared to ordinary and carbonaceous chondrites) for Parsa chondrite (Murty, 1993) as well as for other

enstatite chondrites (Grady et al., 1986) has been reported. This difference was attributed to heterogeneous distribution of N-bearing minerals in enstatite chondrites.

**Table 5.2** Nitrogen results for the individual chondrules of Parsa and Qingzhen chondrites. Measured and corrected (for cosmogenic contribution) N-compositions are given with trapped  $^{36}\text{Ar}$  in chondrules.

Sample	Mass (mg)	N (ppm)	$\delta^{15}\text{N}$	$\delta^{15}\text{N}_t$ (‰)	X	$^{36}\text{Ar}_t$	$(^{14}\text{N}/^{36}\text{Ar})_t$ ( $10^5$ )
<b>Parsa (EH3)</b>							
Parsa-1	1.827	19.4	-21.0 .1	-23.9 .4	3.61	3.11	10.0
Parsa-2	4.022	31.1	-29.0 .3	-30.6 .4	1.57	7.65	6.50
Parsa-3a	4.402	67.2	-20.6 .9	-21.3 .9	0.64	3.94	27.3
Parsa-3b	4.856	29.2	-22.4 .3	-23.8 .3	1.47	8.64	5.41
Parsa <sup>#</sup> (bulk-1)	52.91	197	-31.2 1.9	-31.5 1.9	0.3	14.1	22.4
Parsa <sup>#</sup> (bulk-3)	138.12	157	-22.6 .6	-22.9 .6	0.3	6.1	41.4
<b>Qingzhen (EH3)</b>							
QZN-11	3.433	112	-27.8 .4	-27.9 .3	0.13	2.23	80.1
QZN-12	3.322	140	-26.2 .6	-26.4 .6	0.18	5.1	44.0
QZN-2	0.949	106	-26.1 .6	-26.3 .6	0.18	4.77	35.6
QZN-3	0.409	92	-22.7 .6	-22.9 .6	0.19	10.0	14.6
QZN-5	0.192	132	-22.3 1.1	-22.4 1.1	0.06	9.57	22.1
QZN (bulk)	55.362	137	-27.6 .3	-27.7 .3	0.15	5.03	43.6

X is Decrease in measured  $\delta^{15}\text{N}$  due to cosmogenic correction (defined as  $X = \delta^{15}\text{N}_m - \delta^{15}\text{N}_t$ ),  $^{36}\text{Ar}_t$  concentrations are given in units of  $10^{-8} \text{ cm}^3\text{STP/g}$  (error  $\pm 10\%$ ). For,  $\delta^{15}\text{N}$ , the errors are  $2\sigma$ .<sup>#</sup> Data taken from Murty (1992, 1993)

### Qingzhen (EH3)

As observed in case of Parsa chondrite, N-compositions of chondrules are comparable to Qingzhen bulk. In addition, N-concentrations of chondrules vary from 92 to 142 ppm; similar/lower compared to bulk. Splits of chondrule QZN-1 shows similar N-

composition (Table 5.2) as similarly observed for the case of chondrule splits from Parsa. This suggests homogeneous distribution of N-carrying phases in QZN-1 chondrule. It is also clear from the Fig. 5.4 that chondrules of both Parsa and Qingzhen chondrite show similar values of  $\delta^{15}\text{N}$  within the range observed for bulk enstatite chondrites. However, larger variation in N-contents is observed. As mentioned above, unlike the case of chondrules from ordinary chondrites, it seems that chondrules from enstatite chondrites have similar composition of N when compared to their respective bulk.

### 5.3.3 N-compositions of chondrules from carbonaceous chondrites

20 chondrules were analyzed for nitrogen and noble gases from two carbonaceous chondrites, Allende and Murray. Results of nitrogen are listed in Table 5.4. N-composition of chondrules and their respective bulk are plotted against N-contents in Fig. 5.5.

**Table 5.3** Nitrogen results for the individual chondrules of Allende and Murray chondrites. Measured and corrected (for cosmogenic contribution) N-compositions are given with trapped  $^{36}\text{Ar}$  in chondrules.

Sample	Mass (mg)	N (ppm)	$\delta^{15}\text{N}$	$\delta^{15}\text{N}_t$ (‰)	X	$^{36}\text{Ar}_t$	$(^{14}\text{N}/^{36}\text{Ar})_t$ ( $10^5$ )
<b>Allende (CV3.2)</b>							
ALD-1	3.038	8.25	16.9 $\pm 0.3$	15.7 $\pm 0.3$	1.25	-	-
ALD-2	2.991	4.32	-1.67 .67	-3.32 .69	1.66	-	-
ALD-3	1.216	4.19	-32.5 .1	-34.4 .2	1.84	-	-
ALD-4	0.422	2.44	54.4 1.8	51.0 1.9	3.40	0.21	21.8
ALD-5	0.699	1.77	-6.38 3.27	-9.95 3.29	3.57	-	-
ALD-6	0.545	10.7	-25.6 3.5	-26.5 3.5	0.96	2.73	6.26
ALD-8	0.711	8.57	-58.8 1.5	-59.6 1.5	0.71	-	-
ALD-9	0.384	9.74	5.44 1.20	4.64 1.24	0.79	-	-
ALD-11	1.818	3.75	4.32 1.28	3.09 1.28	1.23	1.43	4.94
ALD-12	1.153	8.26	15.7 .7	14.5 .7	1.15	2.24	5.91

Sample	Mass (mg)	N (ppm)	$\delta^{15}\text{N}$	$\delta^{15}\text{N}_t$ (‰)	X	$^{36}\text{Ar}_t$	$(^{14}\text{N}/^{36}\text{Ar})_t$ ( $10^5$ )
ALD-13A	2.202	3.83	61.1 2.2	58.7 2.2	2.5	0.52	11.8
ALD-13C	1.587	4.25	84.1 3.5	81.6 3.52	2.5	0.60	11.2
ALD-14	1.837	4.19	75.1 6.0	72.6 6.0	2.54	1.29	5.22
ALD-15A	4.485	6.57	20.0 1.8	18.2 1.8	1.65	1.07	9.79
ALD-15B	2.420	2.31	103 4	98.1 3.7	5	1.45	2.56
ALD-16	1.029	7.18	45.7 3.1	44.5 3.1	1.23	0.70	16.9
<b>Murray (CM2)</b>							
MRY-1	0.839	47.4	60.13 .54	59.90 .54	-	19.4	3.9
MRY-5	0.082	46.3	78.13 1.16	78.08 1.16	-	-	-
MRY-7	0.062	77.5	116.0 4.8	115.94 4.82	-	-	-
MRY-8	0.062	67.7	87.10 3.28	87.05 3.28	-	-	-

X is Decrease in measured  $\delta^{15}\text{N}$  due to cosmogenic correction (defined as  $X = \delta^{15}\text{N}_m - \delta^{15}\text{N}_t$ ),  $^{36}\text{Ar}_t$  concentrations are given in units of  $10^{-8}$   $\text{cm}^3\text{STP/g}$  (error  $\pm 10\%$ ). For,  $\delta^{15}\text{N}$ , the errors are  $2\sigma$ .

### Allende (CV3.2)

16 chondrules have been analyzed from Allende chondrite. N-composition of chondrules is rich in  $^{15}\text{N}$  (ranging from -40 to 95 ‰) compared to bulk Allende (Murty, 1998) and average of values reported for CV bulk chondrites (Kerridge et al., 1985, Pearson et al., 2006). The amount of nitrogen is lower (maximum  $\sim 10$  ppm) in chondrules compared to bulk CV chondrites suggesting possible loss of nitrogen in chondrules if chondrule precursors are presumed similar to Allende bulk. As nitrogen is highly volatile, loss of nitrogen is expected from chondrule precursors during chondrule formation event.

### Murray (CM2)

Four chondrules have been analyzed from Murray chondrites. One of chondrules (MRY-1) is large compared to average size ( $\sim 0.3$  mm, Table 1.1) observed for the CM type of chondrites. Split has been taken for this chondrule. Other three chondrules are very small, weight ranging from 0.065mg to 0.085mg. The exceptionally large

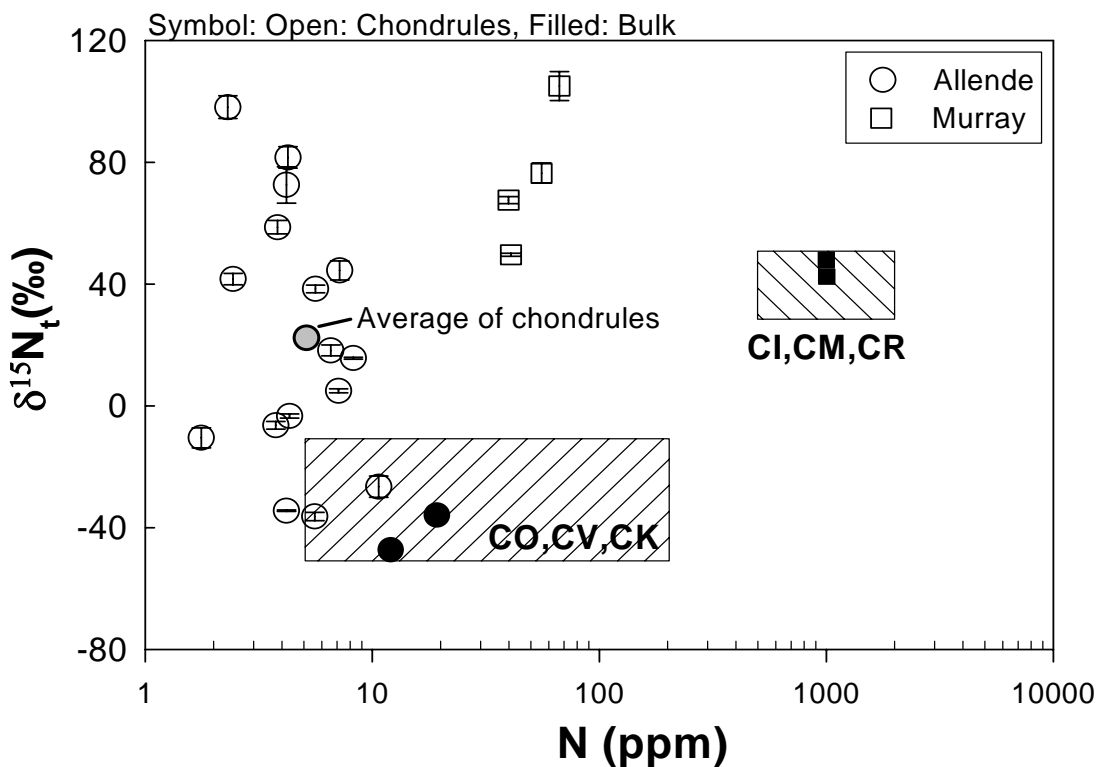


**Fig. 5.5** Nitrogen composition corrected for cosmogenic contribution ( $\delta^{15}\text{N}_t$ ) vs. nitrogen concentration is plotted for chondrules and bulk sample of Allende and Murray chondrites. Hatched box represents the average values observed for carbonaceous chondrites (Grady and Wright 2002). Values for Allende bulk are taken from Murty (1998). Values for Murray bulk are taken from Kerridge (1985) and Pearson et al. (2006). Chondrules are enriched in  $^{15}\text{N}$  as well as have lower N abundances compared to bulk and range observed in carbonaceous chondrites. Average of Allende chondrules is also given.

chondrule (MRY-1) is found to be a barred chondrule with rim (description is given in section 2.9.1, Chapter 2). Around 0.8mg of this chondrule has been analyzed for the nitrogen and noble gases. In case of N-composition, it is found that these chondrules are enriched in  $^{15}\text{N}$  compared to the average of values reported for CM chondrites. The MRY-1 chondrule is less enriched in  $^{15}\text{N}$  compared to other three chondrites. Similar to chondrules from Allende, these chondrules also show less nitrogen compared to average CM chondrite value, but the difference is large (few hundred ppm) compared to the case of Allende chondrules. It will be important to understand the effect of secondary alteration on nitrogen of chondrules especially in case of carbonaceous chondrites.

#### 5.4 Discussion

Large variation of N-composition in chondrules of ordinary and carbonaceous chondrites is observed compared to their host chondrites whereas chondrules from

enstatite chondrites show N-composition similar to their host chondrites. The reasons for the large variation of N-compositions in chondrules of ordinary and carbonaceous chondrites could be either primary or secondary. Heterogeneous precursors can be one of the primary reasons. On the other hand, as chondrule formation is high temperature event, extensive loss and rearrangement of volatiles like nitrogen and noble gases are highly expected. At the same time if chondrule formation was an open system event then exchange of gases with surrounding environment is also expected. Later, it is also possible that chondrules could have experienced secondary alterations after their accretion on the chondrite parent bodies. However, extent of such processes is expected minimum in case of chondrules from low petrographic grade chondrites. In contrast to this, similarity in N-composition for chondrules and their bulk chondrite as observed for enstatite chondrites, may suggests similar environment for chondrule formation and/or similar precursors for both. This inference implies different formation mechanism for chondrules from enstatite chondrites (Das and Murty, 2004; 2006).

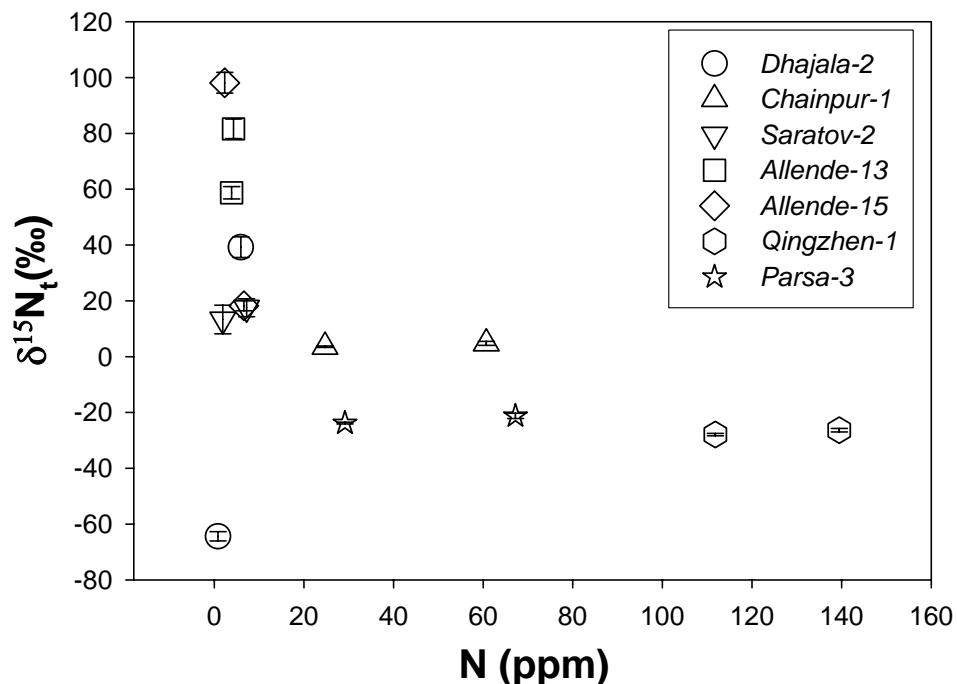


**Fig. 5.6**  $\delta^{15}\text{N}$  vs. N content of splits analyzed from same chondrules. Splits of DH-2, ALD-13 and ALD-15 show large variation in  $\delta^{15}\text{N}$  values whereas other chondrules show similar  $\delta^{15}\text{N}$  values with different N-content.

***N-composition within a single chondrule:***

As discussed already, splits of the same chondrule have been analyzed from Dhajala, Saratov, Chainpur (OC), Parsa, Qingzhen (EC) and Allende (CC). As shown in Fig.

5.6, heterogeneous distribution of N components is clearly indicated within three chondrules for OC and CC whereas uniform  $\delta^{15}\text{N}$  are found for two OC chondrules and EC chondrules. This finding reiterates the fact that some chondrules retain their precursor heterogeneity especially from OC and CC while a homogenization took place for some chondrule precursors especially EC chondrules, as their composition is also similar to their parent chondrites. This has a significant implication towards the chondrule forming process/environment for EC and other (OC, CC) chondrites.

#### **5.4.1 Did the chondrule-forming event affect the N-composition of chondrules?**

N in molecular form behaves similar to noble gases and is highly volatile. Precursors of chondrules were heated for short periods (probably tens of seconds or less, Rubin, 2000) at temperature  $\sim 1750\text{-}2150\text{K}$  (Sears et al., 1996). As observed by earlier studies for noble gases (Kim and Marti 1994; Miura and Nagao 1996; Nakamura et al. 1999; Okazaki et al. 2001a; Smith et al. 1977, Swindle et al. 1991), it is expected that most of the nitrogen (together with noble gases) is lost during chondrule forming event. The loss of any gases from chondrule/chondrule precursors mainly depends on size of the grain experiencing heating, duration of heating, ambient pressure and peak temperature achieved during heating. Mass dependent isotopic fractionation is also possible during an event of gas loss. Of course, the extent of fractionation is a function of several parameters. For example, for Rayleigh fractionation to occur, the evaporating residue must remain isotopically uniform as well as evaporation must be unidirectional (as back reaction can result in less or no fractionation). The other parameter is rate of evaporation. During evaporation, if diffusion and convection occurs in the evaporating material on the timescales that are much slower than evaporation then also evaporation may result in only mass loss without any isotopic fractionation. On the other hand, ambient gas pressures can suppress isotopic fractionation and absolute evaporation rates (e.g. Richter et al., 2002). However, in favorable conditions for isotopic fractionation, it is expected that the remaining nitrogen in chondrule become rich in  $^{15}\text{N}$ , in case of nitrogen loss from chondrules (chondrule precursors) during their formation. Enrichment of  $^{15}\text{N}$  can increase with higher loss of N. Naturally, this requires an assumption that the precursors of chondrules were homogeneous in N-composition and abundance of nitrogen in chondrules represents the remaining nitrogen after loss.

As mentioned in results of Dhajala chondrules and evident in Fig. 5.2, relation expected between nitrogen abundances and compositions based on mass dependent

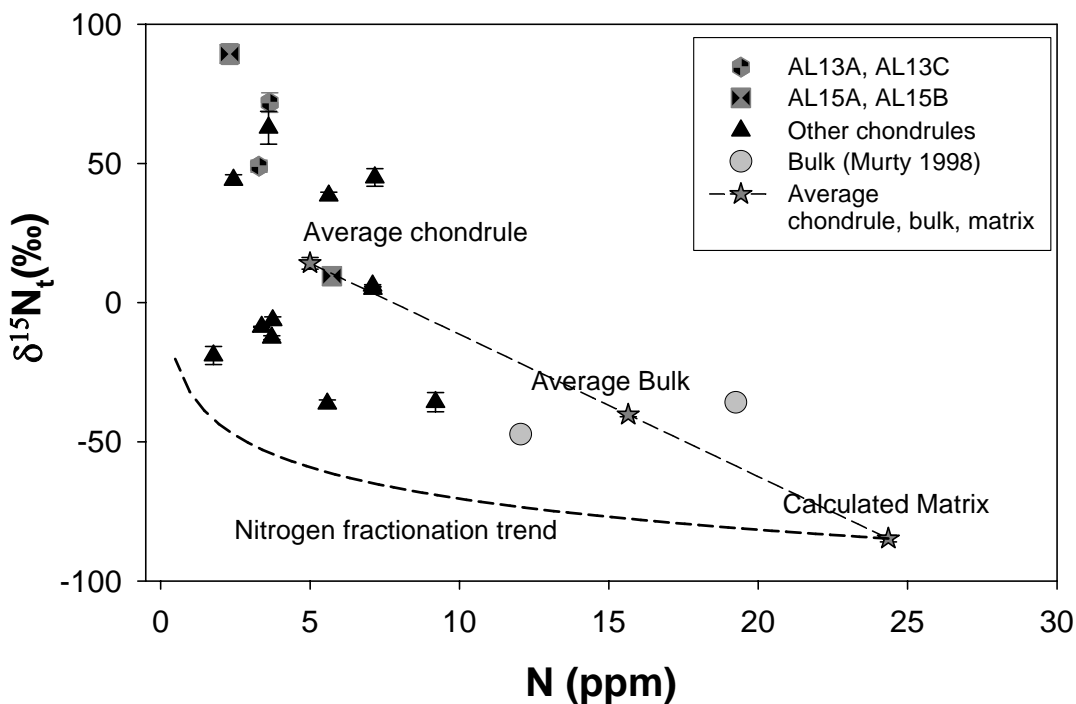


**Fig. 5.7**  $\delta^{15}\text{N}$  vs. N content of Allende chondrules Nitrogen fractionation trend represents evolution of N-composition based on Rayleigh loss of molecular nitrogen during chondrule formation. Based on average values of chondrules and bulk, N-composition and content of matrix calculated. These values are taken for chondrule precursors. The trend could not explain the observed  $\delta^{15}\text{N}$  values of chondrules and suggests requirement of  $^{15}\text{N}$  rich component ( $\delta^{15}\text{N} > 100 \text{ ‰}$ ) to explain the data.

fractionation is not observed. Similar is the case with chondrules from other ordinary chondrites. However, in case of Allende chondrules, there is a hint of a relation between  $\delta^{15}\text{N}$  and N-abundances (as seen in Fig. 5.5). In Fig. 5.7,  $\delta^{15}\text{N}$  vs. N content of only Allende chondrules are plotted. To investigate the effect of isotopic fractionation in chondrules of Allende, we calculated the possible enrichment of  $^{15}\text{N}$  in chondrules by Rayleigh fractionation. In carbonaceous chondrites, matrix is the most primitive component. By assuming matrix like material as primary precursors for chondrules, the initial composition and concentration of nitrogen in chondrule precursors are taken similar to matrix. N-composition and content of matrix are calculated based on average chondrule and average bulk values and considering bulk as 45% of matrix and 55% of chondrules. To calculate the final isotopic composition of N after loss during chondrule forming event, the fractionation factor ( $\alpha$ ) is taken as square root of the ratio of light to heavy isotope mass. Molecular nitrogen is the most abundant species so we assumed that nitrogen was lost in molecular form. Dashed curve in Fig. 5.7 represents enrichment of  $^{15}\text{N}$  (N-composition becoming heavier) in residue (chondrule) with loss of nitrogen. This simple minded calculation suggests

that after loss of even maximum (> 90%) nitrogen from chondrule precursors the enrichment in the residual isotopic composition of nitrogen is still insufficient to explain the observed  $\delta^{15}\text{N}_i$  in chondrules. This implies that fractionation of nitrogen during chondrule formation is not enough to account for the large positive  $\delta^{15}\text{N}$  values found in the chondrules. There is also scope of changes in the assumptions made in this calculation. As for example, in chondrule precursors, initial N-composition and content could be different compared to matrix values assumed for calculation. As observed for chondrule ALD-15 and ALD-13, splits show different N-compositions suggesting presence of heterogeneous phases in these chondrules. Based on these observations, presence of heterogeneous precursors during chondrule formation cannot be ruled out.

On the other hand, it is widely observed that chondrules are depleted in volatile elements but not isotopically fractionated. As suggested by Lauretta et al., (2006), decoupling between chemical and isotopic fractionations is a major constraint during explaining chondrule formation. To account for these two observed features, these authors have suggested (1) moderately volatile components from chondrule precursors were lost during heating due to evaporation. The degree of evaporative loss depended on melt composition, evaporative loss, rate of heating, total heating time and the physical conditions such as pressure and temperature (2) Evaporated gas was not lost from the system and significant amount of it condensed back during cooling (crystallization of chondrules) (3) During early stage of evaporation, isotopic fractionation should have been significant. However, isotopic re-equilibration occurred later during cooling, which resulted in little isotopic fractionation being preserved in chondrules.

Based on this discussion it is possible that the trend observed in Allende chondrules is not really due to evaporative loss of nitrogen with fractionation. At least it can be inferred that fractionation during loss of nitrogen in course of chondrule formation is not the principle reason for the observed large range of N-compositions in chondrules.

#### **5.4.2 Did Chondrules act as open systems during their formation?**

As discussed above, effect of fractionation process can be overshadowed by the interaction between chondrules and surrounding nebula during their formation even in case of evaporative loss. Sears et al. (1996) suggested, based on major chondrule properties like range of oxygen fugacity, fugacity related mineralogy, difference in

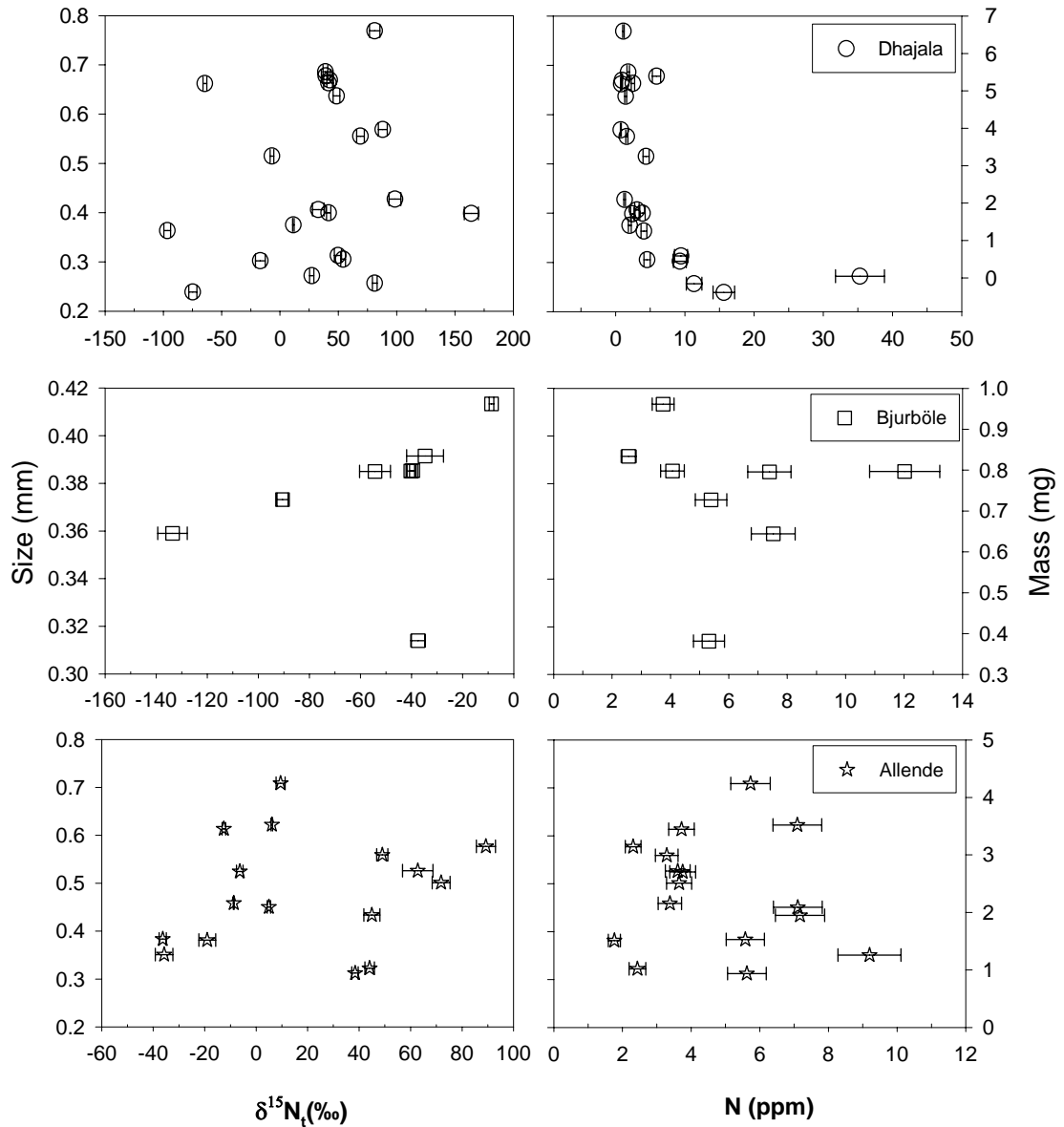


**Fig. 5.8** Relation of size with  $\delta^{15}\text{N}$  and N-content of chondrules from Dhajala, Bjurböle and Allende, No apparent relation of  $\delta^{15}\text{N}$  and N-content is observed with size of chondrules. On the right side of the plot scale for the mass of chondrules are also given.

chondrular sizes, O isotope trends and volatiles in chondrules, that open system behavior of chondrular is preferred instead of closed system. As for example, the observed systematic  $^{16}\text{O}$ -enrichment in smaller chondrules from ordinary chondrites is interpreted in terms of exchange with nebular gas by Clayton et al. (1991). This supports the open system behavior of chondrules during their formation. Similar kind of observation is also expected in case of N-composition of chondrules. In that case, final N-composition of a chondrular depends on the N-compositions of its chondrular precursors and surrounding environment where its formation took place.

Independently, as suggested in nebular shock wave model for chondrule formation (Connolly and Love 1998), the bigger sized precursors were heated for longer duration compared to smaller chondrules. It is expected that bigger chondrules were heated for longer duration resulting in higher loss of volatiles compared to smaller chondrules. This could establish a relation between size and abundances of volatiles in chondrules.

To investigate these aspects, in Fig. 5.8,  $\delta^{15}\text{N}$  and N contents of individual chondrules from Dhajala, Bjurböle and Allende (for which larger number of chondrules has been studied) are plotted against their weights. Weight of chondrule is an indirect measure of its size. As seen in Fig. 5.8, large spread in N-composition is present with no apparent relation with chondrule sizes. Similar is the observation for N-content. There could be several reasons for obscuring a possible trend of N-compositions and abundances with size of the chondrules. Large-scale heterogeneity, which is intrinsic for the case of N in most solar system bodies, can be one of the reasons. It is possible that the expected relation of  $\delta^{15}\text{N}$  and N-content with size of chondrules is overshadowed by heterogeneous precursors.

As for example, even though nitrogen loss from chondrules might have been related with their sizes, possible different initial content of N is enough to obscure the trend. On the other hand, it is also possible that during formation, chondrules really behaved as closed systems, preserving the initial heterogeneity of the precursors. Chondrules might have only lost their volatiles to the surrounding without any significant fractionation.

#### **5.4.3 N-components in chondrules/ chondrule precursors**

From above discussions, it is clear that neither fractionation during evaporative loss of nitrogen nor effects of possible nebular interactions can explain the large variation of N-compositions observed in chondrules from ordinary and carbonaceous chondrites. The discussion signifies the importance of intrinsic heterogeneity involved with N. As discussed in results, splits of chondrules from ordinary and carbonaceous chondrites generally show different N-compositions. This clearly suggests the presence of heterogeneous distribution of different carrier phases of N-components in chondrule precursors. On the other hand, splits of chondrules from enstatite chondrites show uniform N-compositions suggesting homogeneous precursor phases for these chondrules. As discussed in Chapter 4, chondrules from enstatite also show uniform

$(^{36}\text{Ar}/^{20}\text{Ne})_t$  unlike OC and CC chondrules suggesting different mechanism and environment for their formation.

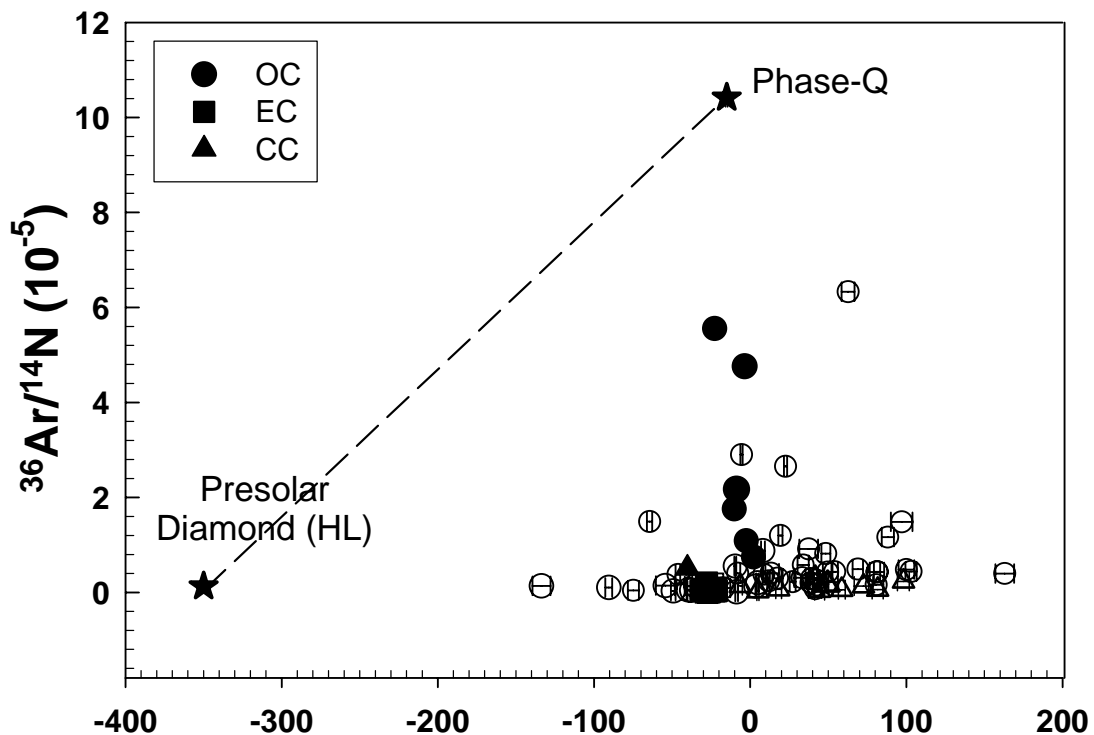


**Fig. 5.9** Elemental ratio  $^{36}\text{Ar}/^{14}\text{N}$  vs.  $\delta^{15}\text{N}$  of individual chondrules and their respective bulk plotted for all chondrites. Two components HL and Q cannot explain data of most chondrules from OC and CC whereas as discussed in chapter 4, trapped noble gases can explain by mixing of HL and Q.

As discussed in Chapter-4, noble gas results of chondrules suggest the presence of HL and Q components in chondrules/chondrule precursors. In addition to this, metal silicate fractionation during chondrule formation is also apparent as suggested by Vogel et al. (2004). In the nebular environment, and under oxidizing conditions, the behavior of trapped molecular N and Ar are expected to behave similarly. This similarity envisages similar trend of mixing between HL and Q components for N-compositions in chondrules (Das and Murty, 2004). However, as evident in Fig. 5.9, N-compositions of chondrules indicates very different trend, which cannot be explained by mixing of only HL and Q components as expected based on results observed for trapped noble gases. An additional N component not linked with trapped noble gases as well as having  $\delta^{15}\text{N} > 100\text{‰}$  is required to explain the observed N-compositions of chondrules from ordinary chondrites.

As discussed earlier in this chapter, chondrules from Allende and Murray chondrite also show very different N-compositions compared to their bulk as well as average N-

compositions observed for that class of chondrites. Although this observation is similar to the case of chondrules from ordinary chondrites, amount of nitrogen in chondrules are found to be lower compared to their bulk chondrites, which is not observed in case of ordinary chondrites.

#### **5.4.4 Nature of N-component required for chondrules of ordinary and carbonaceous chondrites in addition to HL and Q components**

As discussed above, chondrules from ordinary and carbonaceous chondrites require a nitrogen component with  $\delta^{15}\text{N}$  higher than 100‰ as well as not linked with trapped noble gases (having low  $^{36}\text{Ar}/^{14}\text{N}$  ratio). As discussed earlier, molecular form is the expected form of trapped nitrogen in meteoritic samples, which behaves similar to trapped Ar in nebular environment. Thus, the required nitrogen component with  $\delta^{15}\text{N} > 100\text{‰}$  cannot be of molecular nature. Under reducing conditions, N can be chemically active and enter into organic species and can be decoupled from noble gases (especially Ar).

This N-component should satisfy the following observations and organic speciation of N fits these criteria.

1.  $\delta^{15}\text{N}$  should be greater than 100 ‰.
2. It should not be associated with trapped noble gases.
3. It is most likely in chemically bound form.

Nitrogen shows wide range of composition in meteorites as discussed earlier. Recently, Wieler et al. (2006) have reviewed the trapped nitrogen in meteorites. Authors suggest that insoluble organic matter (IOM) in meteorites can contribute nitrogen with up to  $\delta^{15}\text{N} \sim 250\text{‰}$  ( $\delta^{15}\text{N}$  ranges from -25‰ to 250‰). According to them, if the solar  $\delta^{15}\text{N}$  value of -374‰ (adopted the Jupiter value:  $\delta^{15}\text{N} = -374 \pm 82$  ‰, measured by the Galileo probe mass spectrometer (Atreya et al., 2003) as the isotopic composition of protosolar N) is taken as representative of the local ISM value at the time of solar system formation, then admixture with another N-component with  $\delta^{15}\text{N}$  values as high as 250‰ can explain most meteorites which contain N with isotopic compositions between these two values. Mixing of these two components therefore could generate much of the wide range of  $\delta^{15}\text{N}$  values observed in solar system objects (Grady and Wright, 2003). The required N-component based on our result can also be supplied or carried by IOM where nitrogen is chemically bound and mainly associated with carbon. As shown in Fig. 5.10 (similar to Fig. 5.9), with the

help of IOM as a third component, the range observed for  $\delta^{15}\text{N}$  in chondrules from ordinary and carbonaceous chondrites can be explained. As evident in Fig. 5.10b,

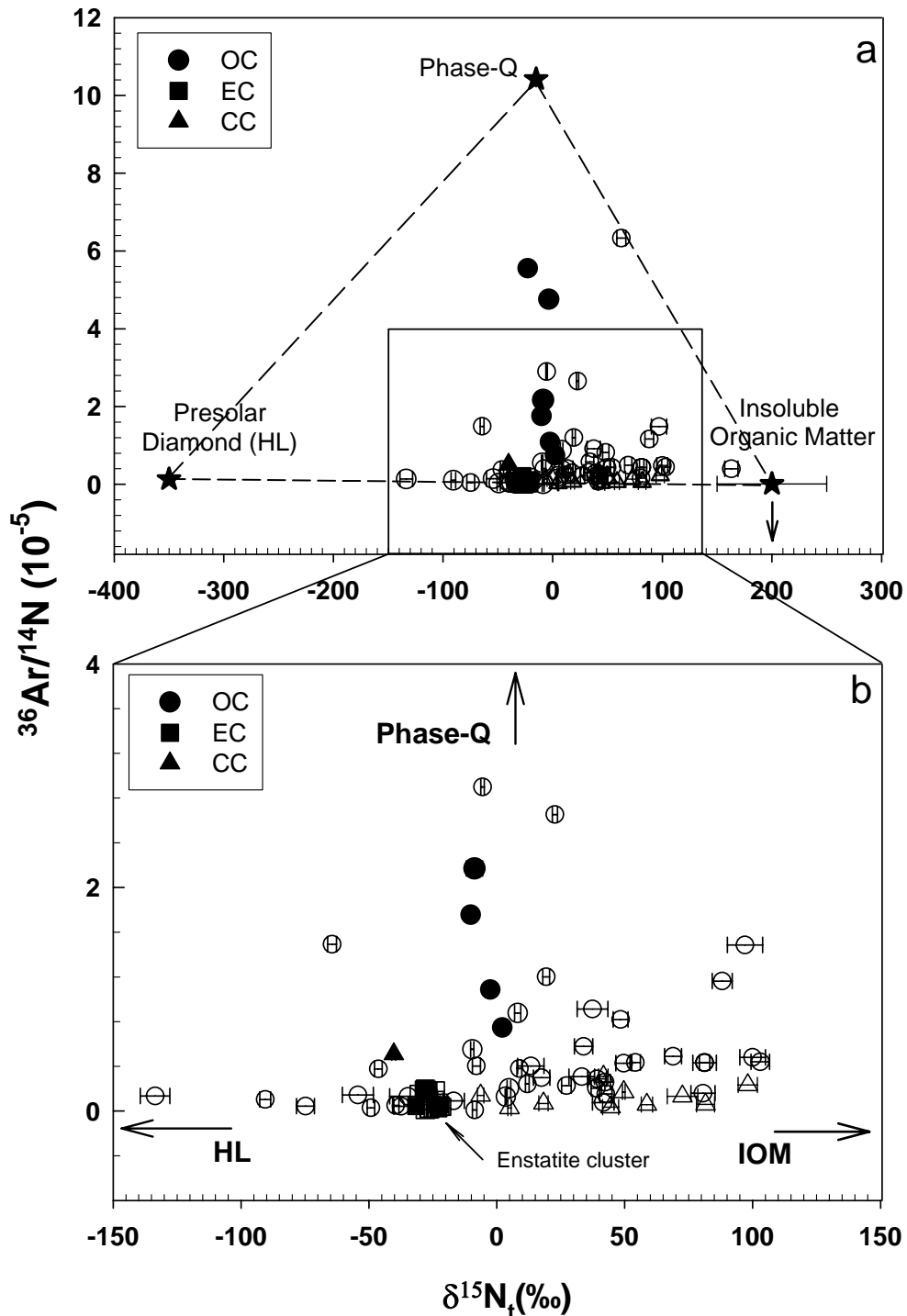


**Fig. 5.10** (a) Elemental ratio  $^{36}\text{Ar}/^{14}\text{N}$  vs.  $\delta^{15}\text{N}$  of individual chondrules and their respective bulk plotted for all chondrites. Three components HL, Q and component carried by IOM can explain data of most chondrules from OC and CC. (b) similar to (a) with selected range of data. Chondrules and bulk samples of enstatite chondrites mostly overlap and show very narrow cluster related to chondrules from OC and CC chondrites.

chondrules and bulk samples of enstatite chondrite form a cluster indicating a homogeneous  $\delta^{15}\text{N}$  in both chondrules and the bulk. However, IOM is required as one of the components to explain  $\delta^{15}\text{N}$  of these samples.

To explain the observed  $\delta^{15}\text{N}$  of chondrules, three components of nitrogen are required to be present. The first two components HL and Q are associated with trapped noble gases whereas the third nitrogen component carried by insoluble organic matter is not associated with any trapped noble gas component (rather carries only nitrogen) (Murty and Das, 2006). As evident in Fig. 5.10, plot of  $^{36}\text{Ar}/^{14}\text{N}$  vs.  $\delta^{15}\text{N}_t$  suggests that compared to chondrules, higher contribution from Q components is observed in bulk chondrites, probably due to higher amount of metal (as discussed in chapter 4, Q component has tendency to go with metal phases) present in chondrites compared to chondrules.

#### **5.4.5 Heterogeneity in chondrule precursors and survival of various N-components**

The observed  $\delta^{15}\text{N}$  of chondrules from ordinary and carbonaceous chondrites can be explained by the mixing between HL, Q and IOM components. Admixture of these components in various fractions can explain the observed N-composition of chondrules. Based on Fig. 5.10, it can be estimated that IOM should be the major component of total N inventory in chondrules. As discussed in chapter 4, the mixing between Q and HL components were present in chondrule precursors and there are evidences of fractionation between Q and HL during chondrule formation as suggested by Vogel et al. (2004). In similar way especially to explain N-compositions of chondrules, it is possible that three components (Q, HL and IOM) were present in chondrule precursors. On the other hand, later addition of IOM during chondrule formation is also possible. However, as discussed, interaction with surrounding nebula is not favored by N-results.

In Fig. 5.11, the N content of individual chondrules analyzed from different chondrites is compared. It is observed that chondrules from Murray (CM2) have N-concentrations up to 80 ppm higher compared to OC chondrules (few ppm in most chondrules). It is known that carbonaceous chondrites contain higher nitrogen amount (500-2000 ppm) as compared to ordinary chondrites (1-25 ppm) mainly due to the presence of organic matter in carbonaceous chondrites carrying nitrogen (Grady and Wright, 2003). Depletion of N-content in chondrules of Murray compared to bulk is

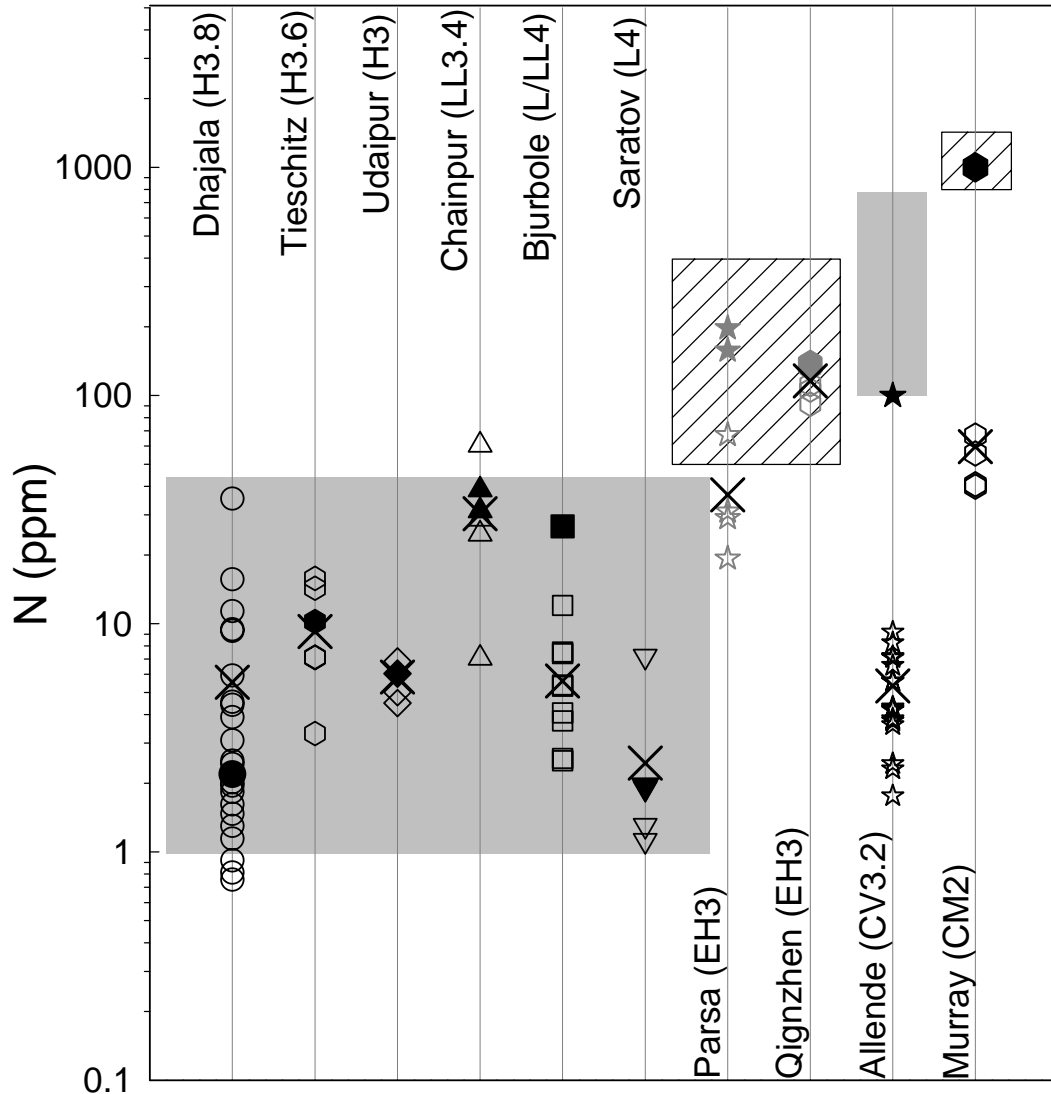


**Fig. 5.11** Concentrations of N in chondrules (open symbols) and their respective bulk (filled symbols) from various chondrites, chondrules from OC show concentrations within the range observed for O chondrites whereas chondrules from CC show large depletion compared to their bulk and range observed for C chondrites. Cross (X) represents the average of N-contents of chondrules.

around factor of 10 whereas chondrules of ordinary chondrites show similar range as seen in ordinary chondrites (Fig. 5.11). Higher amount of nitrogen in Murray chondrules is probably indicative of contribution from organic matter even if 90% of initial N-content (~1000 ppm) is lost from precursors during chondrule formation. This supports the possibility of nitrogen component contributed from insoluble organic matter in these chondrules. On the other hand, contribution up to 50 ppm of N is considered by IOM in ordinary chondrites (Grady and Wright, 2003). Obviously compared to carbonaceous chondrites, amount of organic matter in ordinary chondrites is lower. If chondrules of ordinary chondrite formed by precursors similar

to ordinary chondrites then N-content is expected to be lower in chondrules compared to bulk as seen in case of chondrules from carbonaceous chondrites. However, as mentioned, it is observed that the range of N-content in OC chondrules and ordinary chondrites is similar. This suggests different precursors for OC chondrules with higher amount of N compared to bulk.

On the bases of these arguments, it can be proposed that chondrule precursors were having different phases like silicates, metal and Insoluble organic matter in varying proportions. Hence, the N-compositions of chondrules were governed mainly by these phases. Fig 5.10 suggests that most of the chondrules require IOM as major component. However, we found that chondrules do not contain higher N concentrations as expected in case of presence of IOM component, which can be mainly because of loss of nitrogen during chondrule formation. Based on N-compositions of individual chondrules, heterogeneous precursors are required for chondrules as well as this heterogeneity survived even during the high temperature chondrule formation event. Later, these heterogeneities in form of chondrules became the part of parent body during accretion with fine matrix material, which was homogeneous in nature. Hence, chondrites made up of chondrules and matrix; represent average compositions whereas chondrules as individuals indicate the heterogeneous precursors.

A high range of elevated temperatures is required to form chondrules (Lauretta et al., 2006, Jones et al., 2005 and some recent reviews on chondrules). It is highly expected that organic matter would not have survived under chondrule forming conditions.

As suggested by Kong et al. (2001), during chondrule melting, organic material has possibly decomposed, dissolved into the metal, and later released to form thin layers around metal grains. It is possible that nitrogen composition of metal in chondrules is actually a contribution of nitrogen components carried by phase Q and IOM. If this was true, then similar to noble gas results, variation of N-composition of chondrules can also be explained as due to fractionation between metal and silicate during chondrule formation. The knowledge of N-composition of metal in chondrules is important to support this idea. However, if nitrogen carried by IOM became part of metal in chondrules it would dominate the N-composition as the proportion of nitrogen due to IOM is expected to be more as compared to that carried by phase Q. As shown in Fig 5.12, N-compositions of chondrules show a trend with FeO content of chondrules. Content of FeO in chondrules can be considered as the measure of the

extent of oxidation. Based on FeO content type of chondrule is also defined. Lower FeO content, in a given chondrule suggests more reducing environment during chondrule formation, which further implies higher amount of metal in chondrules. We found that chondrules with expected higher amount of metal show IOM as major component while those with lower metal (higher FeO) show HL as dominating

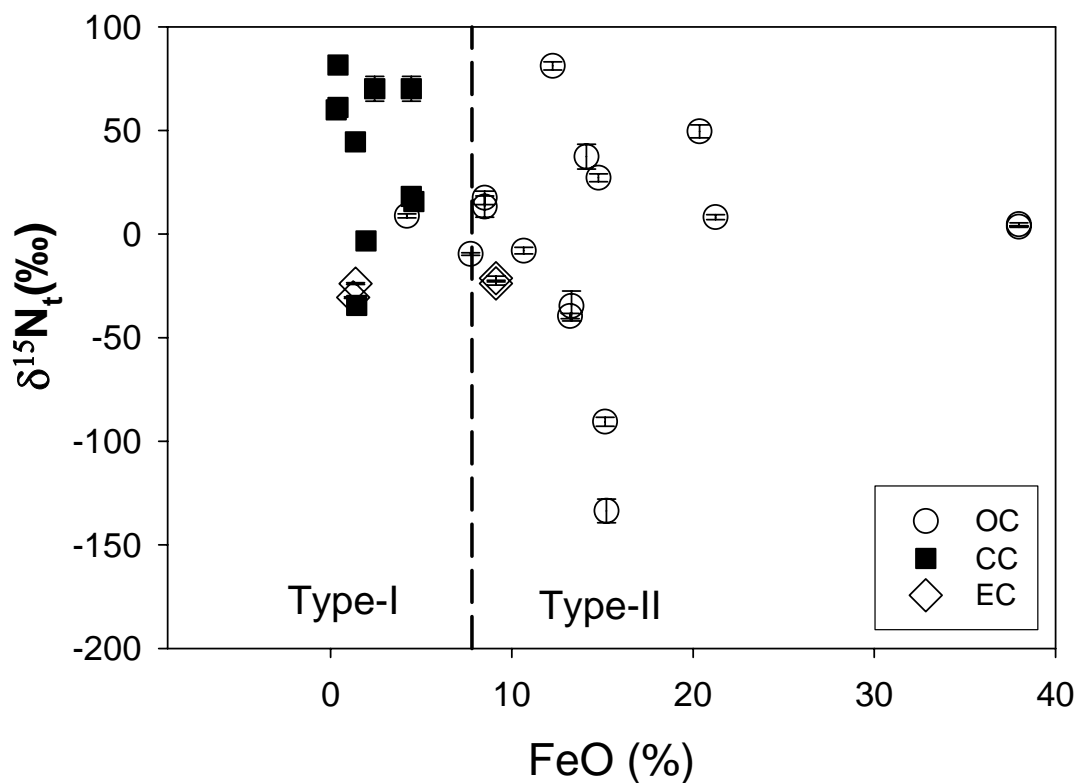


**Fig. 5.12** N-composition of Type-I ( $\text{FeO} < 7.8\%$ ) and II ( $\text{FeO} > 7.8\%$ ) chondrules plotted against content of FeO in chondrules. Type-II seems more heterogeneous compared to Type-I. Dotted line demarcates the two types of chondrules. On the other hand it is also possible that Type-I chondrules interacted more with nebula ( $\delta^{15}\text{N} > 100\text{‰}$ ) compared to Type-II chondrules.

nitrogen component. We suggest that like noble gas results, fractionation between silicate and metal can also explain the variation observed for N-compositions of chondrules provided the IOM dissolved into metal during chondrule forming event. The amount of IOM present in chondrule precursors decided the final N-composition of metal. It is hence possible that metal in chondrules can have wide range of N-compositions depending on how much IOM in chondrule dissolved in metal and how much is lost during chondrule formation. This further decides the N-compositions of bulk chondrules.

#### 5.4.6 Uniform N-composition of EC chondrules

As discussed earlier in results section, N-composition of enstatite chondrules is similar to their parent chondrites unlike the case of ordinary and carbonaceous chondrites (Fig 5.4). Similar N-compositions of chondrules and their parent chondrites suggest that chondrules formed from material similar to their parent chondrites further implying same environment of formation for chondrules and their parent E-chondrites. Formation of chondrules together with accretion of enstatite parent bodies or after accretion of parent bodies (using parent bodies themselves as precursors) is required to satisfy this condition. However, chondrules formation after accretion of parent bodies seems more viable. Processes like impact or volcanic activity on parent planetesimals can form chondrules.

According to Shukolyukov and Lugmair (2004), enstatite chondrites accreted at about 1.4 AU or somewhat closer to the Sun (i.e. > 1.0 -1.4 AU) as compared to OC and CC. This argument is based on excess of  $^{53}\text{Cr}$  and observed gradient of  $^{53}\text{Cr}$  as function of heliocentric distance from Sun. This result strengthens the idea that enstatite chondrites formed at a different place compared to ordinary and carbonaceous chondrites. Mineralogy and chemistry of enstatite chondrites also suggest their formation in the inner most part of the solar nebula (Sears, 1980; Kellemeyn & Wasson, 1986) a location different from OC and CC chondrites. This is also supported by distinct oxygen and nitrogen compositions of enstatite chondrites compared to ordinary and carbonaceous chondrites (Clayton et al., 1984, Grady and Wright 2003).

In addition, I-Xe ages and petrology of EC chondrules suggest existence of enstatite parent bodies during chondrule formation (Whitby et al., 2002, Schneider et al., 2002). These studies suggest that enstatite chondrites have formed in different location compared to ordinary and carbonaceous chondrites as well as there are evidence that EC chondrules might have formed on parent bodies similar to EC chondrites.

Based on similar  $\delta^{15}\text{N}$  of enstatite chondrules and several above discussed results, we propose that the formation of EC chondrules occurred on enstatite parent bodies. Enstatite chondrites and the aubrites (enstatite achondrite) have similar oxygen isotopic compositions (Clayton et al., 1984) and therefore it is believed that they might have formed from a reservoir of similar composition, presumably in the same region of the solar system. The plausible formation scenario for the chondrules of

enstatite chondrites could be as follows: The accretion of the parent bodies of aubrites and their melting and differentiation has preceded the accretion of enstatite chondrite parent bodies (Whitby et al., 2002). Volcanic eruptions on the molten (still cooling) aubrite parent bodies (probably aided by impacts) could have resulted in the formation of silicate spherules (chondrules) that have been thrown into the neighborhood. These chondrules must have become part of the enstatite chondrite parent bodies that subsequently accreted in the same region (based on similar oxygen and nitrogen isotopic compositions of enstatite chondrites and aubrites). This process of chondrule formation is quite different from the one involved for the formation of chondrules from ordinary and carbonaceous chondrites.

### **5.5 Summary**

1. OC and CC chondrules have large range of N-compositions compared to their parent chondrites suggesting that chondrules are different compared to their host.
2. During chondrule formation, loss of nitrogen from the chondrules is possible. In case of simple Rayleigh fractionation during this loss, the enrichment of  $^{15}\text{N}$  in chondrules is expected. However, the enrichment of  $^{15}\text{N}$  observed in chondrules is much above the shift caused by simple Rayleigh loss.
3. There is no apparent relation of  $\delta^{15}\text{N}$  and N-content of chondrules and their sizes either suggesting chondrules behaved as closed system during their formation or the expected relation is overshadowed by heterogeneous distribution of N components in chondrule precursors.
4. Heterogeneous precursors are required to explain the large range of N-composition observed in OC and CC chondrules. This is also evident in splits of three chondrules. These results indicate the survival of heterogeneous phases in some chondrules even after experiencing high temperature chondrule forming event.
5. N-compositions of OC and CC chondrules cannot be explained by mixing the two components Q and HL like trapped noble gases.
6. A third component with  $\delta^{15}\text{N} > 100 \text{ ‰}$  and very low  $^{36}\text{Ar}/^{14}\text{N}$  is required for chondrules of ordinary and carbonaceous chondrites. Insoluble organic matter (IOM) is the most appropriate candidate that fits this requirement.

7. Higher amount of N in chondrules from Murray chondrite is probably due to contribution of IOM.
8. The observed range of  $\delta^{15}\text{N}$  in chondrules from ordinary and carbonaceous chondrites can be explained by three components: Q, HL and component carried by IOM.
9. To overcome the problem of survival of IOM during chondrule formation (also lower amount of nitrogen in chondrules) the alternative explanation is that IOM dissolved in metal during chondrule formation. Hence, N-composition of metal may be governed by nitrogen carried by IOM and phase Q. Based on this argument, N-compositions of OC and CC chondrules can be explained by metal and silicate fractionation during chondrule formation. This argument is supported by observed trend between  $\delta^{15}\text{N}$  and FeO content of the chondrules.
10. EC chondrules are similar to their parent chondrites and suggest parent body formation, as similar environment is necessary to explain similar N-compositions between them.

## Chapter 6

# Implications to the chondrule formation process and Future Directions

## ***6.1 Introduction***

Isotopic signatures of trapped nitrogen and noble gases will tell us about the precursors of chondrules, the environment(s) and process(es) of chondrule formation, while cosmogenic noble gas isotopes might reveal precompaction irradiation records attesting to nebular formation of chondrules. In this thesis, 76 individual chondrules from 6 ordinary, 2 enstatite and 2 carbonaceous chondrites have been studied for nitrogen (for the first time) and noble gases in an effort to understand the types of chondrule precursors and the environment and process of chondrule formation. The results are discussed in Chapters 3, 4 and 5 and herein, the implications to the stated objectives are discussed.

## ***6.2 Cosmogenic noble gases and precompaction irradiation records in chondrules:***

As discussed in Chapter 3, generally chondrules are found depleted in  $^3\text{He}_c$  concentrations, associated with lower cosmogenic corrected  $^4\text{He}$  in chondrules, which are mostly found lower compared to bulk. Gas retention age ( $T_4$ ) of chondrules also suggest effect of secondary events on chondrules. On the other hand, cosmic ray exposure ages based on  $^{21}\text{Ne}$  of chondrules mostly consistent with bulk chondrites. For most cases, the cosmic ray exposure ages of chondrules match with that of bulk except in a few chondrules. These chondrules show evidence of excess exposure compared to their host chondrites. The precompaction exposure duration for these chondrules is from 0.8 to 4.2 Ma, suggesting extended duration of chondrule formation. The presence of SCR component is suggestive, based on  $(^{22}\text{Ne}/^{21}\text{Ne})_c$  ratio in chondrules ALD-16 and MRY-1. Chondrule formation during intense solar activity is one of the possibilities as suggested by X-wind model (Shu et al., 1996). Overall, these results support the nebular environment of chondrule formation.

## ***6.3 Evidence of fractionation between metal and silicate phases during chondrule formation***

Based on trapped noble gas results we found the evidence of fractionation between metal and silicate phases during formation of chondrules.

Recently, Vogel et al., (2004) have found that chondrules containing primordial trapped noble gases show presolar-diamond-like ( $^{36}\text{Ar}/^{20}\text{Ne}$ ) ratios whereas the metal-sulfide-rich coatings generally show Q like ( $^{36}\text{Ar}/^{20}\text{Ne}$ ) ratios and higher concentrations of trapped  $^{36}\text{Ar}$ . According to Vogel et al., (2004), during chondrule

formation, due to fractionation between metal and silicate, the Ar-carrying phase Q became enriched in the metal-sulfide-rich coatings whereas the silicate interior of chondrules became rich in the most stable Ne-carrying presolar diamonds. The findings of the present work are in agreement with Vogel et al., (2004). We conclude that the process of metal and silicate fractionation during chondrule formation seems to play a crucial role in deciding the final ( $^{36}\text{Ar}/^{20}\text{Ne}$ ) ratio in the chondrule.

Sears et al. (1996) have proposed that initially chondrule precursors were FeO-rich, similar to Type-II chondrules. Subsequent heating in high oxygen fugacity environment formed Type-II chondrules; while heating in low oxygen fugacity caused higher degree of reduction forming Type-I chondrules. Type-I chondrules are hence more reduced compared to Type-II chondrules (Lauretta et al., 2006 and references therein). Usually this is reflected in olivine of these chondrules, as olivine in Type-I chondrules shows presence of metal blebs whereas metal blebs can be rarely found in olivine of Type-II chondrules (Hanon et al., 1998). If Type-I chondrules are formed from Type-II kind of precursors in reducing environment then fractionation between metal and silicate is expected more in case of Type-I chondrules.

As concluded in Chapter 4, chondrules from ordinary and carbonaceous chondrites suggest mixing between HL and Q components based on ( $^{36}\text{Ar}/^{20}\text{Ne}$ )<sub>t</sub> values. Proportion of these two components generally depends on: (1) Initial abundances of various noble gas components in chondrule precursors (2) extent of rearrangement between these primary noble gas components during chondrule forming event and loss of noble gases carried by Phase Q. Compared to host chondrites, chondrules from ordinary and carbonaceous chondrites are found depleted in abundances of  $^{36}\text{Ar}_t$  suggesting loss most probably during chondrule formation. The relation observed between concentrations of  $^{36}\text{Ar}_t$  and FeO content in chondrules (from OC and CC) supports this argument. As discussed in Chapter 4, as Type-II (FeO-rich) chondrules have experienced less metal and silicate fractionation it is resulting in lower loss of  $^{36}\text{Ar}$  from these chondrules whereas higher loss of  $^{36}\text{Ar}$  is expected in case of Type-I (FeO-poor) as they formed in reducing environment resulting in higher degree of metal and silicate fractionation.

Our results indicate different trend in case of chondrules from enstatite chondrites. As discussed in Chapter 4, the variation observed in ( $^{36}\text{Ar}/^{20}\text{Ne}$ )<sub>t</sub> values in chondrules of enstatite chondrites is smaller compared to that of in chondrules from ordinary and carbonaceous chondrites. In addition, this smaller variation can be explained by loss

of  $^{20}\text{Ne}_t$  rather than loss of  $^{36}\text{Ar}_t$ . This different observation in case of chondrules from enstatite chondrites indicates different environment and/or mechanism for their formation compared to chondrules from ordinary and carbonaceous chondrites.

#### ***6.4 Solar type noble gases in chondrules***

As discussed above, trapped noble gases in chondrules can be explained mostly by mixing between HL and Q components. However, we found evidences of solar type noble gases for some chondrules. As discussed in Chapter 4, cosmogenic corrected  $^4\text{He}$  concentrations are higher in two of Dhajala chondrules (DH-8 and DH-11) compared to maximum expected radiogenic  $^4\text{He}$  produced during the presumed age of 4.56 Ga. This suggests the presence of trapped  $^4\text{He}$  in these chondrules. For DH-8 and DH-11 chondrules, presence of solar type gases is also observed based on their Ne-isotopic compositions as well as  $(^{36}\text{Ar}/^{20}\text{Ne})_t$  values. This indicates that chondrules or at least some mineral phases within the chondrules might have experienced solar irradiation before/during chondrule formation. This result is consistent with the predictions of the X-wind model for the chondrule formation (Shu et al., 1996).

#### ***6.5 Trapped components of nitrogen in chondrules: presence of Insoluble organic matter in chondrules***

In chondrules, presence of two noble gas components Q and HL (presolar diamonds) are suggested based on observation of trapped noble gases in chondrules. To explain the relative abundance of these components fractionation between metal and silicate during chondrule formation is considered especially for the chondrules from ordinary and carbonaceous chondrites. The important results from this thesis are listed in Table 6.1. As shown in Fig. 6.1, in case of N-composition of chondrules, large range is observed for  $\delta^{15}\text{N}$  of the chondrules from ordinary and carbonaceous chondrites which are different compared to bulk chondrite values whereas uniform composition is observed for chondrules and their host chondrites in case of enstatite chondrites. This observation indicates that the precursors of chondrules and their parent chondrites are different for ordinary and carbonaceous chondrites. In case of enstatite chondrites, similar precursors are expected for chondrules and their host chondrites. The large variation of  $\delta^{15}\text{N}$ , observed in chondrules from ordinary and carbonaceous chondrites is not related to effect of chondrule formation process on primary phases of

**Table 6.1** Important results of this thesis

	OC		CC		EC	
	chondrules	chondrite	chondrules	chondrite	chondrules	chondrite
N (ppm)	0.8 – 60	2 – 40	2 – 80	10 – 1000	19 – 140	140 – 200
$\delta^{15}\text{N}_i(\text{‰})$	164 to -134	-10 to 2	-60 to 115	-20 to 40	-21 to -31	-22 to -31
$(^{14}\text{N}/^{36}\text{Ar})_t^*$	0.2 – 110	0.2 – 1.3	4 – 21	~2.5	6 – 80	22 – 44
$(^{36}\text{Ar}/^{20}\text{Ne})_t$	0.003 – 75	4 – 23	0.08 – 1.8	~10	1.6 – 11	~0.7

\*in units of  $10^5$

chondrule precursors, as it cannot be explained as the effect of fractionation during loss of nitrogen as well as interaction with nebular gases. Our results clearly indicate the presence of heterogeneous precursors for the chondrules of ordinary and carbonaceous chondrites. This is well supported by observation of different N-compositions in splits of chondrules mainly from ordinary and carbonaceous chondrites. Hence, presence of different N-components in chondrule precursors is expected. In nebular environment, behavior of trapped nitrogen (in molecular form) is expected to be similar to trapped Ar. However, trapped nitrogen in chondrules cannot be explained as a two component mixture of Q and HL components as in the case of Ne and Ar. Hence, it is possible that the trapped nitrogen in chondrules is not completely associated with trapped  $^{36}\text{Ar}$  and can have another component which is not related with noble gas components. Our results clearly indicate the presence of an N-component with  $\delta^{15}\text{N}$  higher than 100‰, which is not related to trapped Ar. As we have discussed in Chapter 5, insoluble organic matter (IOM) is the appropriate component, as N-composition of IOM ranges from 150 to 250‰ (Sephton et al., 2004, Grady and Wright 2002) as well as it is not carrying any significant amount of trapped noble gases.

However, presence of any IOM (in its pristine form) in chondrules seems unlikely (e.g. Alexander et al., 1998). It was suggested that organic material was possibly decomposed and partially dissolved into the metal during chondrule melting (Kong et al., 1999, and references therein). The resultant N-composition of metal with dissolved organic matter hence should be dominated by IOM component, the other

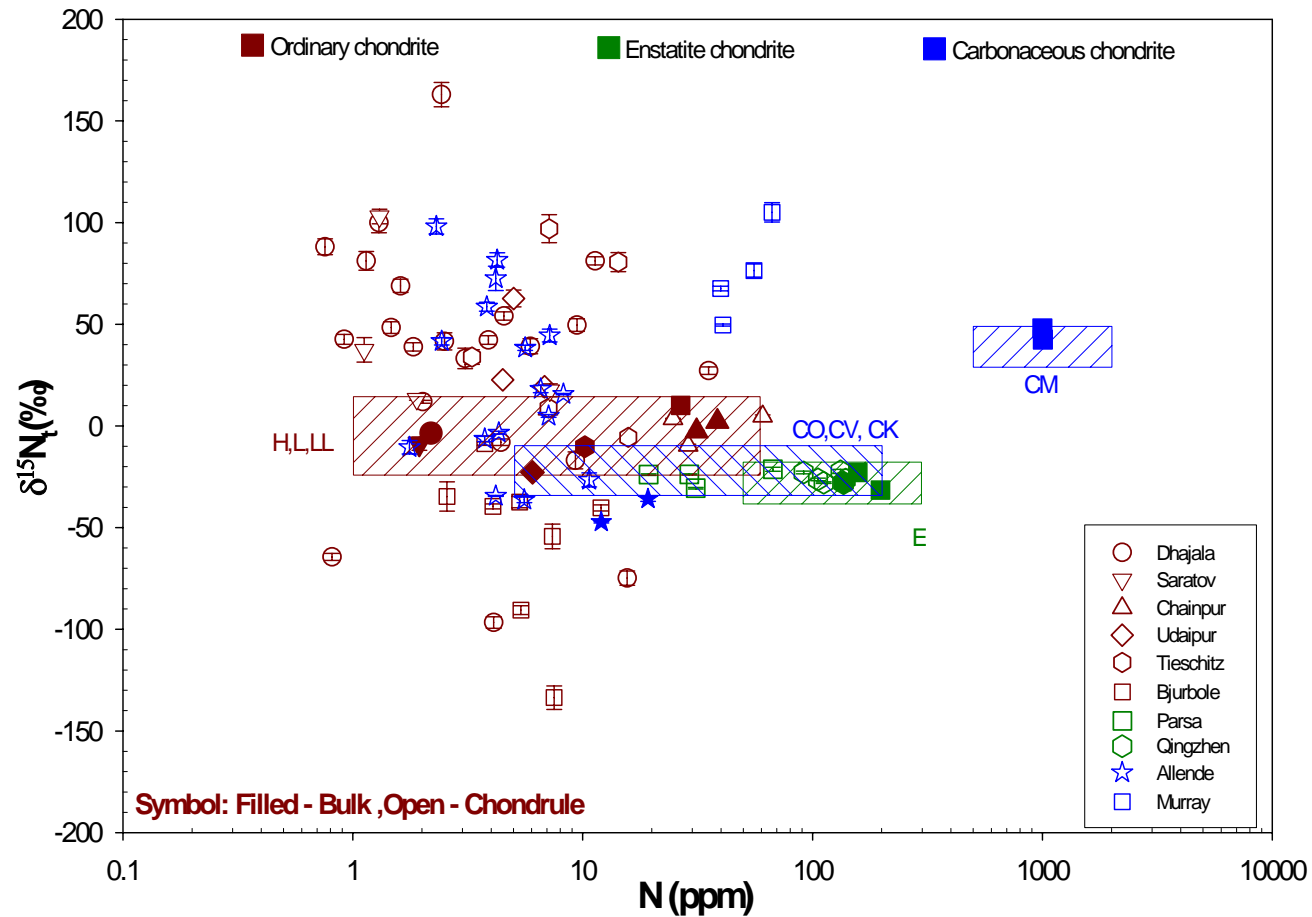


**Fig. 6.1** N-compositions of for all chondrules from OC, EC and CC are plotted against the content of N. Respective host chondrites are also plotted for comparison. Box represents the range of values observed for three classes of chondrites. Chondrules from OC and CC are different compared to their host chondrites whereas chondrules from EC show similar N-composition within the observed range for enstatite chondrites. OC chondrules show large range of  $\delta^{15}\text{N}$  and either depleted or enriched in  $^{15}\text{N}$  compared to bulk. CC-chondrules show heavy  $\delta^{15}\text{N}$  values as well as lower in N-content compared to host chondrites. Chondrules do not show any apparent relation with N-content.

component being Q-nitrogen. Unfortunately, there is no measurement of N-composition in metal grains of chondrules to confirm this hypothesis.

Based on these arguments, we suggest that composition of trapped noble gases in chondrules can be explained by fractionation between metal and silicate during chondrule formation. For the case of noble gases, metal phase of chondrule is associated with Q component. However, nitrogen does not follow similar trend as the N-composition of metal might be changed due to dissolution of organic matter in the metal during chondrule forming event. The final composition of trapped nitrogen in chondrules depends on several parameters like (1) the amount of organic matter present in chondrule precursors (2) degree of dissolution of organic matter in metal and (3) degree of metal and silicate fractionation as well as loss of metal from chondrule system during this fractionation.

Hence, for the case of trapped noble gases, metal shows Q-composition whereas for the case of trapped nitrogen, a composition reflecting the admixture of IOM component with Q should be observed.

### ***6.6 Possible scenario to account for trapped N and noble gas compositions***

Based on nitrogen and noble gas results it is evident that:

- (1) Mixing between HL, Q and IOM components in case of trapped nitrogen are required for OC and CC chondrules to explain the large variation.
- (2) The fractionation of metal and silicate during chondrule formation seems a possible reason for the observed values of trapped noble gases. In addition, it is observed that in a given chondrite, based on noble gases only a few (if at all) show signatures of solar component and/or precompaction irradiation.

Based on these results, following scenario is expected during chondrule formation.

- Demonstration of heterogeneity in precursors of chondrules is one of the main outcomes of this present study. Hence, heterogeneous distribution of different phases like silicate, metal and organic matter (suggested by this study) in chondrule precursors can result in the observed spread in  $\delta^{15}\text{N}$  among chondrules.
- These precursors received solar radiation before the event of chondrule formation. It is also likely that instead all precursors, only a subset may have experienced such irradiation.

- During the chondrule formation event, initially organic matter might have decomposed and dissolved in metal phases present in chondrule precursors (as suggested for different components of Renazzo chondrite by Kong et al., 1999). It is possible that the resultant N-composition of metal hence represents the mixing of organic matter and metal. The contribution of noble gases due to mixing of organic matter to metal phases is not significant and hence, noble gas composition of metal remains similar to Q-composition.
- After this initial relatively low temperature setting, the fractionation between silicate and metal takes place subsequently. The further rearrangement of trapped nitrogen and noble gas compositions takes place during this fractionation.
- It is likely that these rearrangements (between organic matter, metal and silicate phases) erased earlier records of possible solar radiation in chondrule precursors completely or partly. However, during chondrule formation event different phases could not have achieved the equilibration fully, resulting in heterogeneous distribution. This is well supported by different  $\delta^{15}\text{N}$  values in splits of same chondrule.
- The final composition of trapped noble gases can be explained by the rearrangement of different phases (mainly metal and silicate) whereas for nitrogen results presence of organic matter is also required. However, results of nitrogen and noble gases together can be explained by fractionation between metal and silicate phases if before this fractionation, IOM dissolved in metal phases.
- As discussed in Chapter 5, Type-II chondrules show mainly  $^{15}\text{N}$  depleted composition towards HL-composition of trapped nitrogen whereas Type-I chondrules show  $\delta^{15}\text{N}$  values towards the IOM component ( $\sim 100\%$ ). Type-I chondrules are mainly from carbonaceous chondrites and the initial amount of organic matter in these chondrule precursors are expected to be higher compared to chondrules from other class of chondrites. This is the possible reason for having N-composition of all the type-I chondrules towards IOM component of trapped nitrogen.

### ***6.7 Uniform N-composition of EC chondrules: are chondrules formed in planetary environment?***

As discussed in Chapter 5, N-composition of enstatite chondrules is found similar to their parent chondrites unlike the case of ordinary and carbonaceous chondrites (Fig.

6.1). In addition, splits of EC chondrules also show similar  $\delta^{15}\text{N}$ . These observations suggest: **(a)** enstatite chondrules as well as chondrites are different from ordinary and carbonaceous chondrites, **(b)** EC chondrules and their parent bodies possibly formed from similar material and imply same environment for their formation.

**Evidences in support of (a):** Trapped noble gas results (as discussed above) clearly indicate different trend for enstatite chondrites (and chondrules) when compared with ordinary and carbonaceous chondrites supporting (a). Distinct oxygen and nitrogen compositions of enstatite chondrites compared to ordinary and carbonaceous chondrites (Clayton et al., 1984, Grady and Wright 2003) also support argument (a). As discussed in Chapter 5, independent study on mineralogy, chemistry and  $\varepsilon^{53}\text{Cr}$  of enstatite chondrites suggested their formation closer to Sun (~1.4 AU) (Sears, 1980; Kellemeyn & Wasson, 1986; Shukolyukov & Lugmair, 2004), a location different from OC and CC chondrites.

**Evidences in support of (b):** Formation of chondrules together with accretion of enstatite parent bodies or after accretion of parent bodies (using parent bodies themselves as precursors) can explain similar  $\delta^{15}\text{N}$  values of EC chondrules and their host chondrites. This is also supported by I-Xe ages and petrology of EC chondrules that suggest existence of enstatite parent bodies during chondrule formation (Whitby et al., 2002, Schneider et al., 2002).

Enstatite chondrites and the aubrites (enstatite achondrite) have similar oxygen and nitrogen isotopic compositions (Clayton et al., 1984). Therefore, it is believed that they might have formed from a reservoir of similar composition, presumably in the same region of the solar system. Based on similar  $\delta^{15}\text{N}$  of enstatite chondrules and results of independent studies, we propose that the formation of EC chondrules occurred from aubritic parent bodies. Processes like impact or volcanic activity on parent planetesimals seem more viable for the formation of chondrules. The plausible formation scenario for the chondrules of enstatite chondrites could be as follows: The accretion of the parent bodies of aubrites and their melting and differentiation has preceded the accretion of enstatite chondrite parent bodies (Whitby et al., 2002). Volcanic eruptions on the molten (still cooling) aubrite parent bodies (probably aided by impacts) could have resulted in the formation of silicate spherules (chondrules) that have been thrown into the neighborhood. These chondrules must have become part of the enstatite parent bodies that subsequently accreted in the same region (based

on similar oxygen and nitrogen isotopic compositions of enstatite chondrites and aubrites). This process of chondrule formation is quite different from the one involved for the formation of chondrules from ordinary and carbonaceous chondrites possibly due to different location of their formation as suggested in argument (a).

### ***6.8 Future Directions***

- This study suggests the importance of different phases like silicates and metal in chondrules as these phases seem to carry crucial information related to chondrule formation process and its effect on Nitrogen and Noble gas compositions of chondrules. This thesis highlights the presence of various components of noble gases and nitrogen related to chondrule phases hence study of Noble gas and Nitrogen composition in different phases of chondrule will help in confirming several suggestions made in this thesis based on results obtained from individual bulk chondrule analysis.
- Our results suggest the presence of nitrogen component in chondrules contributed by organic matter based on observed N-composition of these chondrules. Earlier work of Hanon et al., (1998) suggested that Type-I chondrules have higher (quantify) amount of carbon content compared to Type-II. Our N-compositions of Type-I chondrules tend more towards organic matter component whereas type-II chondrules show towards HL component. Study of carbon in chondrules together with nitrogen will be very diagnostic.
- Furthermore, analyses from core to rim of chondrule will also help in understanding noble gas evolution during chondrule formation. Similarly, noble gases analyses of different phases especially metal and silicates in individual chondrules will help in understanding noble gas partitioning in this process.
- To search for evidence of pre-compaction of exposure in chondrules, studies should be focused on chondrites with lower cosmic ray exposure ages (< 3 Ma).

***A1 Calculations of  $^{21}\text{Ne}_c$  and  $^{20}\text{Ne}_t$***

Measured isotopes of Neon generally have two components:

$$\text{Measured} = \text{Trapped} + \text{Cosmogenic}$$

It is necessary to calculate fraction of trapped Ne component to derive the cosmogenic  $^{21}\text{Ne}_c$  and  $(^{21}\text{Ne}/^{22}\text{Ne})_c$ . If **X** is the fraction of trapped component of Neon then based on two component mixing, measured Ne composition can be expressed in form of trapped and cosmogenic components as follows:

$$\begin{aligned} X\left(\frac{^{20}\text{Ne}}{^{22}\text{Ne}}\right)_t + (1 - X)\left(\frac{^{20}\text{Ne}}{^{22}\text{Ne}}\right)_c &= \left(\frac{^{20}\text{Ne}}{^{22}\text{Ne}}\right)_m \\ X\left[\left(\frac{^{20}\text{Ne}}{^{22}\text{Ne}}\right)_t - \left(\frac{^{20}\text{Ne}}{^{22}\text{Ne}}\right)_c\right] &= \left(\frac{^{20}\text{Ne}}{^{22}\text{Ne}}\right)_m - \left(\frac{^{20}\text{Ne}}{^{22}\text{Ne}}\right)_c \\ X &= \frac{\left(\frac{^{20}\text{Ne}}{^{22}\text{Ne}}\right)_m - \left(\frac{^{20}\text{Ne}}{^{22}\text{Ne}}\right)_c}{\left(\frac{^{20}\text{Ne}}{^{22}\text{Ne}}\right)_t - \left(\frac{^{20}\text{Ne}}{^{22}\text{Ne}}\right)_c} \dots\dots\dots(1) \end{aligned}$$

Where X represents the trapped fraction of Neon and to calculate it, values of  $(^{20}\text{Ne}/^{22}\text{Ne})_t$  and  $(^{20}\text{Ne}/^{22}\text{Ne})_c$  are required to be assumed (with certain criterion, as discussed in section 3.2, Chapter 3).

**Based on X (fraction of trapped Neon), ratio  $(^{21}\text{Ne}/^{22}\text{Ne})_c$  can be calculated the following way:**

$$\begin{aligned} X\left(\frac{^{21}\text{Ne}}{^{22}\text{Ne}}\right)_t + (1 - X)\left(\frac{^{21}\text{Ne}}{^{22}\text{Ne}}\right)_c &= \left(\frac{^{21}\text{Ne}}{^{22}\text{Ne}}\right)_m \\ \left(\frac{^{21}\text{Ne}}{^{22}\text{Ne}}\right)_c &= \frac{\left(\frac{^{21}\text{Ne}}{^{22}\text{Ne}}\right)_m - X\left(\frac{^{21}\text{Ne}}{^{22}\text{Ne}}\right)_t}{(1 - X)} \dots\dots\dots(2) \end{aligned}$$

Where, X is calculated using equation (1).

The concentration of  $^{21}\text{Ne}_c$  can be calculated now as follows:

$$\begin{aligned}
^{21}\text{Ne}_c &= ^{21}\text{Ne}_m - ^{21}\text{Ne}_t \\
&= \left( \frac{^{21}\text{Ne}}{^{22}\text{Ne}} \right)_m ^{22}\text{Ne}_m - \left( \frac{^{21}\text{Ne}}{^{22}\text{Ne}} \right)_t ^{22}\text{Ne}_t \\
&= \left( \frac{^{21}\text{Ne}}{^{22}\text{Ne}} \right)_m ^{22}\text{Ne}_m - \left( \frac{^{21}\text{Ne}}{^{22}\text{Ne}} \right)_t (^{22}\text{Ne}_m - ^{22}\text{Ne}_c) \\
&= ^{22}\text{Ne}_m \left[ \left( \frac{^{21}\text{Ne}}{^{22}\text{Ne}} \right)_m - \left( \frac{^{21}\text{Ne}}{^{22}\text{Ne}} \right)_t \right] + \left( \frac{^{21}\text{Ne}}{^{22}\text{Ne}} \right)_t ^{22}\text{Ne}_c \\
^{21}\text{Ne}_c - \left( \frac{^{21}\text{Ne}}{^{22}\text{Ne}} \right)_t ^{22}\text{Ne}_c &= ^{22}\text{Ne}_m \left[ \left( \frac{^{21}\text{Ne}}{^{22}\text{Ne}} \right)_m - \left( \frac{^{21}\text{Ne}}{^{22}\text{Ne}} \right)_t \right] \\
^{21}\text{Ne}_c - \left( \frac{^{21}\text{Ne}}{^{22}\text{Ne}} \right)_t \left( \frac{^{22}\text{Ne}}{^{21}\text{Ne}} \right)_c ^{21}\text{Ne}_c &= ^{22}\text{Ne}_m \left[ \left( \frac{^{21}\text{Ne}}{^{22}\text{Ne}} \right)_m - \left( \frac{^{21}\text{Ne}}{^{22}\text{Ne}} \right)_t \right] \\
^{21}\text{Ne}_c &= \frac{^{22}\text{Ne}_m \left[ \left( \frac{^{21}\text{Ne}}{^{22}\text{Ne}} \right)_m - \left( \frac{^{21}\text{Ne}}{^{22}\text{Ne}} \right)_t \right]}{1 - \left( \frac{^{21}\text{Ne}}{^{22}\text{Ne}} \right)_t \left( \frac{^{22}\text{Ne}}{^{21}\text{Ne}} \right)_c}
\end{aligned}$$

Where, value of  $(^{21}\text{Ne}/^{22}\text{Ne})_t$  is required to be assumed, whereas value of  $(^{22}\text{Ne}/^{21}\text{Ne})_c$  should be taken as calculated based on equation (2).

To calculate  $^{20}\text{Ne}_t$  following equation is used:

$$^{20}\text{Ne}_t = ^{20}\text{Ne}_m - ^{20}\text{Ne}_c = ^{20}\text{Ne}_m - ^{21}\text{Ne}_c \left( \frac{^{22}\text{Ne}}{^{21}\text{Ne}} \right)_c \left( \frac{^{20}\text{Ne}}{^{22}\text{Ne}} \right)_c$$

## A2 Calculations of $^{38}\text{Ar}_c$ and $^{36}\text{Ar}_t$

Following are the assumptions for the calculation:

- $^{36}\text{Ar}_m = ^{36}\text{Ar}_t + ^{36}\text{Ar}_c$
- $^{38}\text{Ar}_m = ^{38}\text{Ar}_t + ^{38}\text{Ar}_c$
- $^{40}\text{Ar}_m = ^{40}\text{Ar}_r$

**To Calculate  $^{38}\text{Ar}_c$ :**

$$\begin{aligned}
^{38}\text{Ar}_c &= ^{38}\text{Ar}_m - ^{38}\text{Ar}_t \\
&= \left(\frac{^{38}\text{Ar}}{^{36}\text{Ar}}\right)_m ^{36}\text{Ar}_m - \left(\frac{^{38}\text{Ar}}{^{36}\text{Ar}}\right)_t ^{36}\text{Ar}_t \\
&= \left(\frac{^{38}\text{Ar}}{^{36}\text{Ar}}\right)_m ^{36}\text{Ar}_m - \left(\frac{^{38}\text{Ar}}{^{36}\text{Ar}}\right)_t (^{36}\text{Ar}_m - ^{36}\text{Ar}_c) \\
&= \left[ \left(\frac{^{38}\text{Ar}}{^{36}\text{Ar}}\right)_m - \left(\frac{^{38}\text{Ar}}{^{36}\text{Ar}}\right)_t \right] ^{36}\text{Ar}_m + \left(\frac{^{38}\text{Ar}}{^{36}\text{Ar}}\right)_t ^{36}\text{Ar}_c \\
^{38}\text{Ar}_c - \left(\frac{^{38}\text{Ar}}{^{36}\text{Ar}}\right)_t ^{36}\text{Ar}_c &= ^{36}\text{Ar}_m \left[ \left(\frac{^{38}\text{Ar}}{^{36}\text{Ar}}\right)_m - \left(\frac{^{38}\text{Ar}}{^{36}\text{Ar}}\right)_t \right] \\
^{38}\text{Ar}_c - \left(\frac{^{38}\text{Ar}}{^{36}\text{Ar}}\right)_t \left(\frac{^{36}\text{Ar}}{^{38}\text{Ar}}\right)_c ^{38}\text{Ar}_c &= ^{36}\text{Ar}_m \left[ \left(\frac{^{38}\text{Ar}}{^{36}\text{Ar}}\right)_m - \left(\frac{^{38}\text{Ar}}{^{36}\text{Ar}}\right)_t \right] \\
^{38}\text{Ar}_c &= \frac{^{36}\text{Ar}_m \left[ \left(\frac{^{38}\text{Ar}}{^{36}\text{Ar}}\right)_m - \left(\frac{^{38}\text{Ar}}{^{36}\text{Ar}}\right)_t \right]}{1 - \left(\frac{^{38}\text{Ar}}{^{36}\text{Ar}}\right)_t \left(\frac{^{36}\text{Ar}}{^{38}\text{Ar}}\right)_c}
\end{aligned}$$

**To calculate  $^{36}\text{Ar}_t$ :**

$$\begin{aligned}
^{36}\text{Ar}_t &= ^{36}\text{Ar}_m - ^{36}\text{Ar}_c \\
&= ^{36}\text{Ar}_m - \left(\frac{^{36}\text{Ar}}{^{38}\text{Ar}}\right)_c ^{38}\text{Ar}_c
\end{aligned}$$

### ***A3 Production rates of $^3\text{He}_c$ , $^{21}\text{Ne}_c$ and $^{38}\text{Ar}_c$***

Production rates of  $^3\text{He}_c$ ,  $^{21}\text{Ne}_c$  and  $^{38}\text{Ar}_c$  of *chondrules* are calculated based on their chemical composition. Following are the formulas used:

$$P_3 = 1.15 \cdot (\text{Ti} + \text{Cr} + \text{Fe} + \text{Ni}) + 1.75 \cdot [100 - (\text{Ti} + \text{Cr} + \text{Fe} + \text{Ni})]$$

*(Eugster and Michel, 1995)*

$$P_{21} = 1.63 [\text{Mg}] + 0.6[\text{Al}] + 0.32[\text{Si}] + 0.22[\text{S}] + 0.07[\text{Ca}] + 0.021[\text{Fe} + \text{Ni}]$$

*(Schultz and Freundel, 1985)*

$$P_{38} = 1.58[\text{Ca}] + 0.086[\text{Fe} + \text{Ni}] + 0.33[\text{Ti} + \text{Cr} + \text{Mn}] + 11 [\text{K}]$$

*Freundel et al., (1986)*

In all formulas, concentrations of elements are in weight %.

Calculation of elemental correction factor  $F = P_i / P_L$ , where  $P_i$  is the production rate of given noble gas isotope based on chemical composition of chondrules and  $P_L$

represents the production rate of the same noble gas isotope for average shielding and L-chondrite composition.

The values of  $P_L$  for  $^3\text{He}_c$ ,  $^{21}\text{Ne}_c$  and  $^{38}\text{Ar}_c$  are as follows:

$$P_L^3 = 1.61 \times 10^{-8} \text{ cm}^3\text{STP/g per Ma}$$

$$P_L^{21} = 0.332 \times 10^{-8} \text{ cm}^3\text{STP/g per Ma}$$

$$P_L^{38} = 0.0462 \times 10^{-8} \text{ cm}^3\text{STP/g per Ma} \quad (\text{Eugster 1988})$$

Final production rates as a function of shielding dependent cosmogenic ratio ( $^{22}\text{Ne}/^{21}\text{Ne}_c$ ) and chemical composition:

$$\left. \begin{aligned} P'_3 &= F \cdot [2.09 - 0.43(^{22}\text{Ne}/^{21}\text{Ne}_c)] \\ P'_{21} &= 1.61 \cdot F \cdot [21.77(^{22}\text{Ne}/^{21}\text{Ne}_c) - 19.32]^{-1} \end{aligned} \right\} \quad (\text{Eugster 1988})$$

$$P'_{38} = F \cdot [0.125 - 0.071(^{22}\text{Ne}/^{21}\text{Ne}_c)] \quad (\text{Marti and Graf, 1992})$$

( $^{22}\text{Ne}/^{21}\text{Ne}_c$ ) is calculated for each chondrule. For most chondrules, values are found similar to bulk. Possibly due to differences in Mg/(Al+Si) ratios, which have been shown to cause significant increase in ( $^{22}\text{Ne}/^{21}\text{Ne}_c$ ) values (Garrison et al., 1995), chondrule can show different (higher) ( $^{22}\text{Ne}/^{21}\text{Ne}_c$ ) value compared to bulk. In that case, ( $^{22}\text{Ne}/^{21}\text{Ne}_c$ ) of bulk is adopted for chondrule.  $P'_3$ ,  $P'_{21}$ ,  $P'_{38}$  are used for bulk samples and elemental corrections factors are taken according to the class of bulk meteorite as suggested by Eugster (1988) and Marti and Graf, (1992). Final production rates of  $^{21}\text{Ne}_c$  and  $^{38}\text{Ar}_c$  carry error  $\pm 15\%$  whereas error in  $P'_3$  is  $\pm 3\%$ . These uncertainties include uncertainties involved in chemical composition of chondrules.

#### ***A4 Nitrogen isotopes: the $\delta$ notation***

Nitrogen has two stable isotopes,  $^{14}\text{N}$  and  $^{15}\text{N}$ , of which  $^{14}\text{N}$  is far more abundant. The terrestrial atmosphere, with a uniform  $^{15}\text{N}/^{14}\text{N}$  ratio of 0.003676, serves as the standard for the nitrogen isotopic measurements. The N isotopic composition of a sample is expressed as the deviation of the  $^{15}\text{N}/^{14}\text{N}$  ratio from that in the terrestrial atmosphere (air). Symbolically it is represented as  $\delta$ , defined as

$$\delta^{15}\text{N} = \left[ \frac{\left( \frac{^{15}\text{N}}{^{14}\text{N}} \right)_{\text{sample}}}{\left( \frac{^{15}\text{N}}{^{14}\text{N}} \right)_{\text{std.}}} - 1 \right] \times 10^3 \text{ (‰)}$$

## A5 Corrections of the measured $\delta^{15}\text{N}$ for cosmogenic contribution

$$\begin{aligned}
 {}^{15}\text{N} &= {}^{15}\text{N}_c + {}^{15}\text{N}_t \\
 \frac{{}^{15}\text{N}}{{}^{14}\text{N}} &= {}^{15}\text{N}_c/{}^{14}\text{N} + {}^{15}\text{N}_t/{}^{14}\text{N} \\
 \frac{{}^{15}\text{N}}{{}^{14}\text{N}} &= \left(\frac{{}^{15}\text{N}}{{}^{21}\text{Ne}}\right)_c \left(\frac{{}^{21}\text{Ne}_c}{{}^{14}\text{N}}\right) + \left(\frac{{}^{15}\text{N}_t}{{}^{14}\text{N}}\right) \\
 \frac{{}^{15}\text{N}_t}{{}^{14}\text{N}} &= \left(\frac{{}^{15}\text{N}}{{}^{14}\text{N}}\right) - \left(\frac{{}^{15}\text{N}}{{}^{21}\text{Ne}}\right)_c \left(\frac{{}^{21}\text{Ne}_c}{{}^{14}\text{N}}\right)
 \end{aligned}$$

Value of N ( ${}^{14}\text{N}$ ) is available in units of parts per million (ppm), so required to be convert into units of  $\text{cm}^3\text{STP/g}$ . 14 gm of N = 22414  $\text{cm}^3\text{STP}$ , hence 1  $\mu\text{g}$  of  ${}^{14}\text{N}$  =  $1.6 \times 10^{-3} \text{cm}^3\text{STP}$

$$\frac{{}^{15}\text{N}_t}{{}^{14}\text{N}} = \left(\frac{{}^{15}\text{N}}{{}^{14}\text{N}}\right) - \left(\frac{{}^{15}\text{N}}{{}^{21}\text{Ne}}\right)_c \left(\frac{{}^{21}\text{Ne}_c}{N_{ppm}}\right) (0.62 \times 10^3)$$

Defining  $R_t = \left(\frac{{}^{15}\text{N}}{{}^{14}\text{N}}\right)_t \approx \frac{{}^{15}\text{N}_t}{{}^{14}\text{N}_m}$ , as  ${}^{14}\text{N}_c$  is negligible compared to  ${}^{14}\text{N}$ , we take

$${}^{14}\text{N}_t = {}^{14}\text{N}_m - {}^{14}\text{N}_c \sim {}^{14}\text{N}_m$$

$$R = \frac{{}^{15}\text{N}}{{}^{14}\text{N}} \text{ and } R_{std} = \left(\frac{{}^{15}\text{N}}{{}^{14}\text{N}}\right)_{std} = \left(\frac{{}^{15}\text{N}}{{}^{14}\text{N}}\right)_{air} = 0.003676$$

$$\frac{R_t}{R_{std}} = \frac{R}{R_{std}} - \left(\frac{{}^{15}\text{N}}{{}^{21}\text{Ne}}\right)_c \left(\frac{{}^{21}\text{Ne}_c}{N_{ppm}}\right) (1.7 \times 10^5)$$

$$\left(\frac{R_t}{R_{std}} - 1\right) = \left(\frac{R}{R_{std}} - 1\right) - \left(\frac{{}^{15}\text{N}}{{}^{21}\text{Ne}}\right)_c \left(\frac{{}^{21}\text{Ne}_c}{N_{ppm}}\right) (1.7 \times 10^5)$$

$$\left(\frac{R_t}{R_{std}} - 1\right) \times 10^3 = \left(\frac{R}{R_{std}} - 1\right) \times 10^3 - \left(\frac{{}^{15}\text{N}}{{}^{21}\text{Ne}}\right)_c \left(\frac{{}^{21}\text{Ne}_c}{N_{ppm}}\right) (1.7 \times 10^8)$$

$$\delta^{15}\text{N}_t = \delta^{15}\text{N}_t - \left(\frac{{}^{15}\text{N}}{{}^{21}\text{Ne}}\right)_c \left(\frac{{}^{21}\text{Ne}_c}{N_{ppm}}\right) (1.7 \times 10^8)$$

$$\therefore \delta^{15}\text{N}_t = \delta^{15}\text{N}_t - \left(\frac{{}^{15}\text{N}}{{}^{21}\text{Ne}}\right)_c \left(\frac{{}^{21}\text{Ne}_c \text{ (in } 10^{-8} \text{ cm}^3\text{STP)}}{N_{ppm}}\right) (1.7)$$

Where  ${}^{21}\text{Ne}_c$  is to be inserted in units of  $10^{-8} \text{cm}^3\text{STP/g}$ .  $({}^{15}\text{N}/{}^{21}\text{Ne})_c$  is derived for each chondrule using their chemical composition and production rates as suggested by Mathew and Murty (1993) for average shielding depth.

**Example for derivation of  $(^{15}\text{N}/^{21}\text{Ne})_c$  in DH-2 chondrule:**

	Mg	Al	Si	Na
DH-2 (wt%)	16.0	0.5	26.0	0.85*
$^{21}\text{Ne}_c$ # atoms/min/kg	768	290	158	302

\* Rubin (1986), # production rates at  $10 \text{ g/cm}^2$  shielding depth and  $4\pi$  radiation, taken from Mathew and Murty, (1993)

$^{21}\text{Ne}_c$  production rate of DH-2 chondrule can be obtained by from mentioned elemental production rates by multiplying them with the target element abundances and summing over all the targets.

Hence, production rate of  $^{21}\text{Ne}_c$  for DH-2 chondrule: *168 atoms/min/kg*

Production rate of  $^{15}\text{N}_c$ : *818 atoms/min/kg* (Mathew and Murty, 1993)

The ratio  $(^{15}\text{N}/^{21}\text{Ne})_c$  for DH-2 chondrule: *4.9*, which is similar to the value  $4.5 \pm 0.5$  suggested for average bulk compositions and average shielding depth by Mathew and Murty (1993).

## References

- Alexander C. M. O. D. (1989) Origin of chondrule rims and interchondrule matrices in unequilibrated ordinary chondrites. *Earth. Planet. Sci. Lett.* **95**, 187-207.
- Alexander C.M.O.D., Grossmann J. N., Wang J, Zanda B, Bourot-denise M and Hewins R H. (2000) The lack of potassium isotopic fractionations in Bishunpur chondrules. *Meteorit. Planet. Sci.* **35**, 859-868.
- Alexander C.M.O.D., Russell S. S., Arden J.W., Ash R.D., Grady M.M., and Pillinger C.T. (1998) The origin of chondritic macromolecular organic matter: A carbon and nitrogen isotope study. *Meteorit. Planet. Sci.* **33**, 603-622.
- Allen J. S., Nozette S. and Wilkening L. L. (1980) A study of chondrule rims and chondrule irradiation records in unequilibrated ordinary chondrites. *Geochim. Cosmochim. Acta.* **44**, 1161-1175.
- Anders E and Grevesse N (1989) Abundances of elements: Meteoritic and Solar. *Geochim. Cosmochim. Acta.* **53**, 197-214.
- Anders E. (1964) origin, age and composition of meteorites. *Space. Sci. Rev.* **3**, 583-714.
- Atreya S. K., Mahaffy P. R., Niemann H. B., Wong M. H., and Owen T. C. (2003) Composition and origin of the atmosphere of Jupiter — an update, and implications for the extrasolar giant planets. *Planet. Space Sci.*, **51**, 105–112.
- Begemann F., Weber H. W., Vilcsek E. and Hinterberger H. (1976) Rare gases and  $^{36}\text{Cl}$  in Stony-iron Meteorites: cosmogenic elemental production rates, exposure ages, diffusion losses and thermal histories. *Geochim. Cosmochim. Acta.* **40**, 353-368.
- Benkert J.-P., Baur H., Signer P. and Wieler R. (1993) He, Ne, and Ar from the solar wind and solar energetic particles in lunar ilmenites and pyroxenes. *J. Geophys. Res.* **98(E7)**, 13147-13162.
- Bland P A, Alard O, Benedix G K, Kearley A T, Menzies, Watt L. E and Rogers N. W (2005) Volatile fractionation in the early solar system and chondrule/matrix complementarity, Proc. Nat. Acad. Sci. 102,39, 13755-13760.
- Bogard D. D. and Cressy P. J. (1973) Spallation production of  $^3\text{He}$ ,  $^{21}\text{Ne}$ , and  $^{38}\text{Ar}$  from target elements in the Bruderheim chondrite. *Geochim. Cosmochim. Acta.* **37** 527-546.
- Brearley A. J. and Jones R. H. (1998) Chondritic meteorites. In Planetary materials, edited by Papike J. J. Washington D.C.: Mineralogical Society of America. 3.1-3.398.
- Busemann H. (1998) Primordial noble gases in “Phase Q” in carbonaceous and ordinary chondrites studied by closed system stepped etching. PhD-Thesi., Swiss Federal Institute of Technology Zurich, Zurich.
- Busemann H., Baur H. and Wieler R. (2000) Primordial noble gases in “phase Q” in carbonaceous and ordinary chondrites studied by closed-system stepped etching. *Meteorit. Planet. Sci.* **35** 949-973.
- Caffee M. W., Hohenberg C. M., Swindle T. D. (1982) I-Xe ages of individual Bjurble chondrules. *J. Geophys. Res.* **87** (Suppl.), A303-A317.
- Caffee M. W., Hohenberg C. M., Swindle T. D., and Goswami J. N. (1987) Evidence in meteorites for an active early sun. *Astrophys. J.* **313**, L31–L35.

- Carr L. P., Wright I. P. and Pillinger C. T. (1985) Nitrogen content and isotopic composition of lunar breccia 79135: A high resolution study. *Meteoritics* **20** 622-623.
- Chen J., Papanastassiou D. A., Wasserberg G. J. (1998) Re-Os systematics in chondrites and the fractionation of the platinum group elements in the early solar system. *Geochim. Cosmochim. Acta.* **62** 3379-3392.
- Clayton R. N. (1993) Oxygen isotopes in meteorites. *Ann. Rev. Earth Planet. Sci.* **21**, 114-149.
- Clayton R. N. and Mayeda T. K. (1985) Oxygen isotopes in chondrules from enstatite chondrites: possible identification of a major nebular reservoir (abstract). *Lunar Planet. Sci.* **XVI** 142-143.
- Clayton R. N. and Mayeda T. K. (1999) Links among CI and CM chondrites. *Lunar Planet. Sci.* **XXX**, abstract no. 1795
- Clayton R. N. and Thiemens M. H. (1980) Lunar nitrogen: Evidence for secular change in the solar wind. In *Proceedings of the Conference on the Ancient Sun* (R. O. Pepin et al., eds.), pp. 463–473. Pergamon, New York.
- Clayton R. N., Mayeda T. K. and Rubin A. E. (1984) Oxygen isotopic composition of enstatite chondrites and aubrites. *Proc. Lunar Planet. Sci. Conf.* **15th**, C245-C249
- Clayton R. N., Mayeda T. K., Goswami J. N., and Olsen E. J. (1991) Oxygen isotope studies of ordinary chondrites. *Geochim. Cosmochim. Acta.* **55** 2317–2337.
- Clayton R. N., Onuma N., Ikeda Y., et al., (1983) Oxygen isotopic compositions of chondrules in Allende and ordinary chondrites. In *Chondrules and Their Origins* (E. A. King, ed.), Lunar and Planetary Institute, Houston. pp. 37–43
- Connolly H. C. Jr, Hewins R. H., Ash R. D., Zanda B., Lofgren G. E., and Bourot-Denise M. (1994) Carbon and the formation of reduced chondrules. *Nature* **371**, 136–139.
- Connolly Jr. H. C. and Desch S. J. (2004) On the origin of the “kleine kügelchen” called chondrules. *Chemie der Erde* **64**, 95-125.
- Connolly Jr. H. C. and Love S. (1998) The formation of chondrules: petrologic tests of the shock wave model. *Science* **280**, 62-67.
- Connolly Jr. H. C., Huss G. R. and Dealney J. S. (2001) Reduction, metal loss, mixing: the origin of Fe-Mg chondrule compositions. *Meteorit. Planet. Sci.* **36**, A44.
- Crabb J. and Anders E. (1982) On the sitting of noble gases in E-chondrites. *Geochim. Cosmochim. Acta* **46** 2351-2361.
- Das J. P. and Murty S. V. S. (2004) Nitrogen in individual chondrules of unequilibrated ordinary and enstatite chondrites. *Meteorit. Planet. Sci.* **39**, A28.
- Das J.P. and Murty S.V.S. (2005) Search for solar cosmic ray records of early Sun in primitive meteorite phases 29th International Cosmic Ray Conference Pune **1**, 75-78
- Das J.P. and Murty S.V.S. (2006) Formation of chondrules: clues from nitrogen isotopes. 10<sup>th</sup> triennial Int. symp. On mass spect, Munnar EPS-9, 103.
- DeHart J. M., Lofgren G. E., Jie L., Benoit P. H., and Sears D. W. G. (1992) Chemical and physical studies of chondrites 10: Cathodoluminescence and phase-composition studies of metamorphism and nebular processes in chondrules of type-3 ordinary chondrites. *Geochim. Cosmochim. Acta.* **56**, 3791–3807.

- Desch S.J. and Connolly H.C. Jr. (2002) A model for the thermal processing of particles in solar nebula shocks: application to cooling rates of chondrules, *Meteorit. Planet. Sci.* **37**, 183-208.
- Eberhardt P., Eugster O. and Marti K. (1965) A redetermination of the isotopic composition of atmospheric neon. *Z. Naturforschung* **20a**, 623-624.
- El Gorse A., Zinner E., and Marti K. (1995) Survival of isotopically heterogeneous graphite in differentiated meteorite. *Nature* **373**, 496-499.
- Eugster O. (1988) Cosmic ray production rates for  $^3\text{He}$ ,  $^{21}\text{Ne}$ ,  $^{38}\text{Ar}$ , and  $^{126}\text{Xe}$  in chondrites based on  $^{81}\text{Kr}$ -Kr exposure ages *Geochim. Cosmochim. Acta.* **49**, 925-939.
- Faure G. (1986) Principles of Isotope Geology. 2<sup>nd</sup> ed. John Wiley & Sons, New York, USA. Pp 589.
- Franchi I. A., Wright I. P., and Pillinger C. T. (1986) Heavy nitrogen in Bencubbin — a light-element isotopic anomaly in a stony-iron meteorite. *Nature*, **323**, 138–140.
- Franchi I. A., Wright I. P., and Pillinger C. T. (1993) Constraints on the formation conditions of iron meteorites based on concentrations and isotopic compositions of nitrogen. *Geochim. Cosmochim. Acta.* **57**, 3105–3121.
- Fredriksson K., Murty S. V. S. and Marti K. (1985) Some chemical and isotopic observations in chondrules *Meteoritics* **20**, 347-357.
- Garrison D. H., Rao M. N. and Bogard D. D. (1995) Solar-proton-produced neon in shergottite meteorites and implications for their origin. *Meteoritics*, 30, 738-747.
- Geiss J. and Reeves H. (1972) Cosmic and solar system abundances of Deuterium and Helium-3. *Astron. & Astrophys.* **18**, 126-132.
- Gooding J. L. and Keil K. (1981) Relative abundances of chondrule primary textural types in ordinary chondrites and their bearing on conditions of chondrule formation. *Meteoritics*, **16**, 17–43.
- Grady M. M. and Pillinger C. T. (1990) ALH 85085: Nitrogen Isotope Analysis of a highly unusual chondrite. *Earth Planet. Sci. Lett.* **97**, 29-40.
- Grady M. M. and Wright I. P. (2003) Elemental and isotopic abundances of carbon and nitrogen in meteorites *Space Science Reviews* **106**, 231-248.
- Grady M. M., Wright I.P., Carr L. P. and Pillinger C. T. (1986) Compositional differences in enstatite chondrites based on carbon and nitrogen isotope measurements. *Geochim. Cosmochim. Acta.* **50**, 2799–2813.
- Grossman J. N. and Wasson J. T. (1983) The composition of chondrules in unequilibrated chondrites: An evaluation of models for the formation of chondrules and their precursor materials. In *Chondrules and Their Origins* (E. A. King, ed.), pp. 88–121. Lunar and Planetary Institute, Houston.
- Grossman J. N., Rubin A. E., Nagahara H. and King E. A. (1988) Properties of chondrules. In *Meteorites and the early solar system.* (Ed. J. F. Kerridge and M. S. Mathews) University of Arizona press, pp. 619-659.
- Grossmann J. N., Rubin A. E., Rambaldi E. R., Rajan R. S. and Wasson J. T. (1985) Chondrules in the Qingzhen type-3 enstatite chondrites: possible precursor components and comparison to ordinary chondrite chondrules. *Geochim. Cosmochim. Acta.* **49**, 1781-1795.

- Hanon P., Robert F. and Chaussidon M. (1998) High carbon concentrations in meteoritic chondrules: A record of metal-silicate differentiation *Geochim. Cosmochim. Acta.* **62**, 903-913.
- Hashizume K. and Nakaoka Y. T. (1998) Q nitrogen in CO<sub>3</sub> chondrites (abstract). *Meteorit. Planet. Sci.*, **33**, A65–A66.
- Hashizume K. and Sugiura N. (1995) Nitrogen isotopes in bulk ordinary chondrites. *Geochim. Cosmochim. Acta* **59**, 4057- 4069
- Hayatsu R. and Anders E (1981) Organic compounds in meteorites and their origins. In *Topics of Current Chemistry*, pp 1-37. Springer-verlag, Berlin, Germany.
- Hewins R. H. (1997) Chondrules. *Ann. Rev. Earth. Planet. Sci.* **25**, 61-83.
- Hewins R. H. and Connolly Jr. H. C. (1996) Peak temperatures of flash melted chondrules. In *chondrules and the Protoplanetary disk*.(eds. R. H. Hewins, R. H. Jones and E. R. D. Scott). Cambridge University Press, Cambridge U.K. pp 197-204.
- Hewins R. H. and Radomsky P. M. (1990) Temperature conditions of chondrule formation. *Meteoritics* **25**, 309-318.
- Horányi M., Morfill G., Goertz C. K. and Levy E.H. (1995) Chondrule formation in lightning discharges. *Icarus* **114**, 174-185.
- Humayun M. and Clayton R. N. (1995) Potassium isotope cosmochemistry — Genetic-implications of volatile element depletion. *Geochim. Cosmochim. Acta.* **59** 2131–2148.
- Huss G. R. and Alexander Jr. E. C. (1987) On the presolar origin of the "planetary" noble gas component in meteorites. *Proc. 7th Lunar Planet. Sci. Conf., J. Geophys. Res.* **92** (B4), E710-E716.
- Huss G. R. and Lewis R. S. (1994) Noble gases in presolar diamonds I: Three distinct components and their implications for diamond origins. *Meteoritics* **29**, 791-810.
- Hutchison R., Bridges J. C. and Gilmour J. D. (2005) Chondrules: chemical, petrographic and chronologic clues to their origin by impact. *Chondrites and the Protoplanetary Disk* ASP Conference Series, (eds.A. N. Krot, E. R. D. Scott, & B. Reipurth) **341**, 933-953.
- Jarosewich E. (1990) Chemical analyses of meteorites: A compilation of stony and iron meteorite analyses. *Meteoritics*, **25**, 323-337
- Jones R H., Grossman J. N. and Rubin A. E. (2005) Chemical, Mineralogical and Isotopic Properties of Chondrules: Clues to Their Origin. *Chondrites and the Protoplanetary Disk* ASP Conference Series, **341**, (eds.A. N. Krot, E. R. D. Scott, & B. Reipurth) 251-285.
- Jones R. H. (1990) Petrology and mineralogy of type-II, FeO-rich chondrules in Semarkona (LL3.0) — Origin by closed-system fractional crystallization, with evidence for supercooling. *Geochim. Cosmochim. Acta.* **54**, 1785–1802.
- Jones R. H. (1994) Petrology of FeO-poor, porphyritic pyroxene chondrules in the Semarkona chondrite. *Geochim. Cosmochim. Acta.* **58**, 5325–5340.
- Jones R. H. (1996) FeO-rich, porphyritic pyroxene chondrules in unequilibrated ordinary chondrites. *Geochim. Cosmochim. Acta.* **60**, 3115–3138.
- Jones R. H. and Scott E. R. D. (1989) Petrology and thermal history of type-IA chondrules in the Semarkona (LL3.0) chondrite. *Proc. Lunar Planet. Sci. Conf. 19th*, pp. 523–536.

- Kerr R. A. (2001) A Meteoriticist Speaks Out, His Rocks Remain Mute. *Science*, **293**, 1581-1583.
- Kerridge J. F. (1985) Carbon, Hydrogen and Nitrogen in Carbonaceous chondrites: Abundances and isotopic compositions of bulk samples. *Geochim. Cosmochim. Acta.* **49**, 1707-1714.
- Kieffer S. W. (1975), Droplet chondrules. *Science* **189**, 333-340.
- Kim Y. and Marti K. (1994) Isotopic evolution of nitrogen and trapped xenon in the Acapulco parent body. *Meteoritics*, **29**, 482-483.
- Kong P. and Ebihara M (1997) The origin and nebular history of the metal phase of ordinary chondrites. *Geochim. Cosmochim. Acta.* **61**, 2317-2329.
- Kong P. and Palme H. (1999) Compositional and genetic relationship between chondrules, chondrule rims, metal, and matrix in the Renazzo chondrite. *Geochim. Cosmochim. Acta.* **63**, 3673-3682.
- Kung C. C. and Clayton R. N. (1978) Nitrogen abundance and isotopic compositions in stony meteorites *Earth Planet. Sci. Lett.* **38**, 421-435.
- Kuramoto, K. & Yurimoto, H. (2005) Oxygen Isotopic Heterogeneity in the Solar System: The Molecular Cloud Origin Hypothesis and its Implications for Meteorites and the Planets. In *Chondrites and the Protoplanetary Disk*, eds A. N. Krot, E. R. D. Scott, and B. Reipurth **341**, 181-192.
- La Blue A. R. and Lauretta D. S. (2004) Metallic chondrules in NWA 1390 (H3-6): Clues to their history from metallic Cu (abstract). In *Lunar and Planetary Science XXXV*, Abstract #1939. Lunar and Planetary Institute, Houston (CD-ROM).
- Lauretta D. S. and Killgore M. (2005) *A Color Atlas of Meteorites in Thin Section*. Golden Retriever Publications/Southwest Meteorite Press.
- Lewis R. S., Anders E., and Draine B. T. (1989) Properties, detectability and origin of interstellar diamonds in meteorites. *Nature*, **339**, 117-121.
- Lewis R. S., Ming T., Wacker J. F., Anders E. and Steel E. (1987) Interstellar diamonds in meteorites. *Nature* **326**, 160-162.
- Lewis R. S., Srinivasan B. and Anders E. (1975) Host phase of a strange xenon component in Allende. *Science* **190**, 1251-1262.
- Lewis R.S., Anders E., Wright I. P., Norris S.J. and Pillinger C.T. (1983) Isotopically anomalous nitrogen in primitive meteorites *Nature* **305**, 767-771.
- Leya I., Lange H. J., Neumann S., Wieler R., and Michel R. (2000) The production of cosmogenic nuclides in stony meteoroids by galactic cosmic-ray particles. *Meteoritics* **35**, 259-286.
- Lipschultz M.E. and Schultz L. (1999) Meteorites. In encyclopedia of the solar system (Eds. P. R. Weissman, L-A McFadden and T. V. Johnson), pp. 629-671. Academic press, San Diego, California, USA.
- Lofgren G. (1989) Dynamic crystallization of chondrule melts of porphyritic olivine composition — Textures experimental and natural. *Geochim. Cosmochim. Acta.* **53**, 461-470.
- Lofgren G. and Lanier A. B. (1990) Dynamic crystallization study of barred olivine chondrules. *Geochim. Cosmochim. Acta.* **54**, 3537-3551.

- Lofgren G. and Russell W. J. (1986) Dynamic crystallization of chondrule melts of porphyritic and radial pyroxene composition. *Geochim. Cosmochim. Acta.* **50**, 1715–1726.
- Lofgren G. E. (1996) A dynamic crystallization model for chondrule melts. In *Chondrules and the Protoplanetary Disk* (R. H. Hewins et al., eds.), pp. 187–196. Cambridge Univ., New York.
- Lugmair G. W. and Sukolyukov A (2001) Early solar system events and time scales. *Meteorit. Planet. Sci.*, **36**, 1017–1026.
- Mahajan R. R. and Murty S. V. S. (2003) Laser microprobe for the study of noble gases and nitrogen in single grains: A case study of individual chondrules from the Dhajala meteorite. *Proc. Indian Acad. Sci. (Earth Planet. Sci.)* **112(1)**, 113-127
- Mason B. (1979) Cosmochemistry Part 1. Meteorites. In data of Geochemistry (ed. F Fleischer), Geological Survey Professional Paper 440-B-1, Washington, D.C: U.S. Government Printing Office. pp, B1-B132.
- Mathew K. J. and Murty S. V. S. (1993) Cosmic ray produced nitrogen in extra terrestrial matter. *Proc. Indian Acad. Sci. (Earth Planet. Sci.)* **102(3)**, 415-437.
- Mathew K. J., Palma R. L., Marti K., and Lavielle B. (2000) Isotopic signatures and origin of Nitrogen in IIE and IVA iron meteorites. *Geochim. Cosmochim. Acta.* **53**, 2377–2386.
- Matrajt G, Brownlee D, Sadilek M and Kruse L (2006) Survival of organic phases in porous IDPs during atmospheric entry: A pulse-heating study. *Meteorit. Planet. Sci.* **41**, 903-911.
- Mazor E., Heymann D. and Anders E. (1970) Noble Gases in Carbonaceous Chondrites. *Geochim. Cosmochim. Acta* **34**, 781-824.
- McSween H. Y. (1977) Chemical and petrographic constraints on origin of chondrules and inclusions in carbonaceous chondrites. *Geochim. Cosmochim. Acta.* **41**, 1843–1860.
- Merrill G. P. (1920) On chondrules and chondritic structure in meteorites. *Proc. Natl. Acad. Sci.* **6**, 449-472.
- Mewaldt R. A., Ogliore R. C., Gloeckler G. and Mason G. M. (2001) A new look at Neon-C and SEP-Neon. In *Solar and Galactic Composition* (ed. R. F. Wimmer-Schweingruber), pp. 423. American Institute of Physics, Melville, New York.
- Miura Y. N. and Nagao K. (1996) Noble gases in chondrules of the Allende CV3 chondrite (abstract). *Meteorit. Planet. Sci.* **31**, A91.
- Murty S. V. S. (1993) Nitrogen and light noble gases in Parsa enstatite chondrite. *Lunar and Planet. Science* **XXIV**, 1037-1038.
- Murty S. V. S. (1997) Noble gases and nitrogen in Muong Nong tektites. *Meteorit. Planet. Sci.* **32**, 687-691.
- Murty S. V. S. and Marti K. (1985) Nitrogen isotopic abundances in individual chondrules. *Lunar and Planet. Science* **XVI**, 605-606
- Murty S. V. S. and Marti K. (1994) Nitrogen isotopic signatures in Cape York: Implications for formation of Group III-A irons. *Geochim. Cosmochim. Acta.* **58**, 1841–1848.
- Murty S. V. S., Rai V. K., Shukla A.D., Srinivasan G., Shukla P. N., Suthar K. M., Bhandari N., and Bischoff A. (2004) Devgaon (H3) chondrite: Classification and complex cosmic ray exposure history. *Meteorit. Planet. Sci.* **39**, 387-399.

- Murty S.V.S. (1996) Isotopic composition of nitrogen in 'Phase Q' *Earth Planet. Sci. Lett.* **141**, 307-313
- Murty S.V.S. (1998) Nitrogen components in CV3 chondrites. *Lunar and Planet. Science* **XXIX**, 1139-1140.
- Nagahara H. and Ozawa K. (2000) Isotopic fractionation as a probe of heating processes in the solar nebula. *Chem. Geol.* **169**, 45-68.
- Nakamura T., Nagao K., and Takaoka N. (1999) Microdistribution of primordial noble gases in CM chondrites determined by in situ laser microprobe analysis: Decipherment of nebular processes. *Geochim. Cosmochim. Acta.* **63**, 241-255.
- Nichols Jr. R. H., Hohenberg C. M., Alexander C. M. O. D., Olinger C. T. and Arden J. W. (1991) Xenon and neon from acid-resistant residues of Inman and Tieschitz. *Geochim. Cosmochim. Acta* **55**, 2921-2936.
- Nier A. O. (1950a) A redetermination of the relative abundances of the isotopes of carbon, nitrogen, oxygen, argon and potassium. *Phys. Rev.* **77**, 789-793.
- Norris S. J., Swart P. K., Wright I. P., Grady M. M. and Pillinger C. T. (1983) A search for correlatable, isotopically light carbon and nitrogen components in lunar soils and breccias. *J. Geophys. Res.* **88**, B200-B210.
- Okazaki R., Nagao K., Takaoka N. and Nakamura T. (2001b) Studies of trapped noble gases in enstatite chondrites by laser microprobe techniques. *Meteorit. Planet. Sci.* **36**, A152-A153.
- Okazaki R., Takaoka N., Nagao K., Sekiya M., and Nakamura T. (2001a) Noble-gas-rich chondrules in an enstatite meteorite *Nature* **412**, 795-798.
- Ott (2002), Noble gases in meteorites. In Noble gases in geochemistry and cosmochemistry, edited by Porcelli D., Ballentine C. J. and Wieler R. Washington D.C.: Mineralogical Society of America. **47**, 71-100.
- Ott U., Mack R., and Chang S. (1981) Noble-gas-rich separates from the Allende meteorite. *Geochim. Cosmochim. Acta.* **45**, 1751-1788.
- Owen T., Mahaffy P. R., Niemann H. B., Atreya S. K., and Wong M. (2001) Protosolar nitrogen. *Astrophys. J. Lett.* **553**, L77-L79.
- Ozawa K., and Nagahara H. (2001) Chemical and isotopic fractionations by evaporation and their cosmochemical implications. *Geochim. et Cosmochim. Acta.* **65**, 2171-2199.
- Ozima M. and Podosek F. M. (2002) Noble gas geochemistry. Cambridge: Cambridge University Press.
- Patzer A. and Schultz L. (2001) Noble gases in enstatite chondrites I: Exposure ages, pairing, and weathering effects. *Meteorit. Planet. Sci.* **36**, 947-961.
- Patzer A. and Schultz L. (2002) Noble gases in enstatite chondrites II: the trapped component. *Meteorit. Planet. Sci.* **37**, 601-612.
- Pearson V. K., Sephton M. A., Franchi I. A., Gibson J. M. and Gilmour I. (2006) Carbon and nitrogen in carbonaceous chondrites: Elemental abundances and stable isotopic compositions. *Meteorit. Planet. Sci.* **41**, 1899-1918.

- Pellas P., Poupeau G., Lorin J. C., Reeves H., and Audouze J. (1969) Primitive low-energy particle irradiation of meteoritic crystals. *Nature* **223**, 272-274.
- Polanu E., Eugster O., Krahenbuhl U., and Marti K. (1999) Evidence for a precompaction exposure to cosmic rays in a chondrule from the H6 chondrite ALH76008. *Geochim. et Cosmochim. Acta.* **63**, 925-933
- Polnau E., Eugster O., Burger M., Krahenbuhl U., and Marti K (2001) Precompaction exposure of chondrules and implications. *Geochim. Cosmochim. Acta.* **65**, 1849–1866.
- Prombo C. A. and Clayton R. N. (1985) A striking nitrogen isotope anomaly in the Bencubbin and Weatherford meteorites. *Science* **230**, 935–937.
- Prombo C. A. and Clayton R. N. (1993) Nitrogen isotopic compositions of iron meteorites. *Geochim. Cosmochim. Acta.* **57**, 3749–3761
- Radomsky L. M. and Hewins R. H. (1990) Formation conditions of pyroxene-olivine and magnesian olivine chondrules. *Geochim. Cosmochim. Acta.* **65**, 1849–1866
- Rai V. K., Murty S. V. S., and Ott U. (2003) Nitrogen components in ureilites. *Geochim. et Cosmochim. Acta.* **67**, 2213-2237
- Richter F. M., Davis A. M., Ebel D. S., and Hashimoto A. (2002) Elemental and isotopic fractionation of Type B calcium-aluminum-rich inclusions: Experiments, theoretical considerations, and constraints on their thermal evolution. *Geochim. Cosmochim. Acta.* **66**, 521–540.
- Rowe M. W., Clayton R. N., Mayeda T. K. (1994) Oxygen isotopes in separated components of CI and CM meteorites. *Geochim. Cosmochim. Acta.* **58**, 5341–5347.
- Rubin A. E. (1986) Elemental compositions of major silicic phases in chondrules of unequilibrated chondritic meteorites. *Meteorit. Planet. Sci.* **28**, 283-293.
- Rubin A. E., Wasson J. T., Clayton R. N. and Mayeda T. K. (1990) Oxygen isotopes in chondrules and coarse-grained chondrule rims from the Allende meteorite. *Earth Planet. Sci. Lett.* **96**, 247-255
- Rubin A.E. (2000) Petrologic, geochemical and experimental constraints on models of chondrule formation. *Earth Sci. Rev.* **50**, 3-27
- Russell S. S., Arden J. W. and Pillinger C. T. (1991) Evidence for multiple sources of diamond from primitive chondrites. *Science*, **254**, 1188-1191.
- Russell S. S., Arden J.W. and Pillinger C.T. (1996). A carbon and nitrogen isotope study of diamond from primitive chondrites. *Meteorit. Planet. Sci.* **31**, 343-355.
- Ruzmaikina T. V. and Ip W. H. (1996) Chondrule formation in the accretional shock. In chondrules and the Protoplanetary disk. (Ed. R. H. Hewins, R. H. Jones and E. R. D. Scott.) Cambridge University Press. 277-284.
- Sanders I. S. (1996) A chondrule forming scenario involving molten planetesimals. In chondrules and the Protoplanetary disk. (Ed. R. H. Hewins, R. H. Jones and E. R. D. Scott.) Cambridge University Press. 327-334.
- Schelhaas N., Ott U and Begemann F. (1990) Trapped noble gases in unequilibrated ordinary chondrites. *Geochim. Cosmochim. Acta.* **54**, 2869–2882.

- Scherer P. and L. Schultz (1999) Noble gas record, collisional history and pairing of CV, CO, CK and other carbonaceous chondrites. *Meteorit. Planet. Sci.* **35**, 145-154.
- Schultz and Franke (2004) Helium, neon, and argon in meteorites: A data collection. *Meteorit. Planet. Sci.* **39**, 1889-1890.
- Schultz L. and Franke L. (2000) Helium, neon, and argon in meteorites. A data collection. Update 2000. MPI-Chemie, Mainz, Germany.
- Schultz L. and Weber H. (1995) Exposure ages of H-chondrites with Helium loss. *Meteoritics* **30**, 575-576.
- Schultz L. and Weber H. (1997) Exposure age distribution of H-chondrites with and without Helium loss (abstract). In isotopes in the solar system (Eds. J. N. Goswami, S. Sahijpal, P Chakravarti) pp. 34-35. Physical Research Lab., Ahmedabad, India.
- Schultz L., and Freundel M. (1985) On the production rate of  $^{21}\text{Ne}$  in ordinary chondrites. In *Isotopic Ratios in the Solar System* (ed. Centre National d'Etudes Spatiales), Cepadues-Editions, Toulouse, pp 27-33.
- Scott E. R. D. and Taylor G. J. (1983) Chondrules and other components in C-chondrite, O-chondrite, and E-chondrite — Similarities in their properties and origins. *Proc. Lunar Planet. Sci. Conf. 14th*, in *J. Geophys. Res.*, **88**, B275–B286.
- Sears D. W. (1980). Formation of *E* chondrites and aubrites—A thermodynamic model. *Icarus* **43**, 184-202.
- Sears D. W. G., Huang S., and Benoit P. H. (1996) Open-system behavior during chondrule formation. In *Chondrules and the Protoplanetary Disk* (R. H. Hewins et al., eds.), pp. 221–232. Cambridge Univ., New York.
- Sears et al., (1992) Sears D. W. G., Lu J., Benoit P. H., Dehart J. M., and Lofgren G. E. (1992) A compositional classification scheme for meteoritic chondrules. *Nature*, **357**, 207–210.
- Sephton M. A., Verchovsky A. B., Bland P. A., Gilmour I., Grady M. M., and Wright I. P. (2003) Investigating the variations in carbon and nitrogen isotopes in carbonaceous chondrites. *Geochim. Cosmochim. Acta.* **67**, 2093–2108.
- Sephton M A, Verchovsky A B and Wright P (2004) Carbon and nitrogen isotope ratios in meteoritic organic matter: indicators of alteration processes on the parent asteroid. *Int. jour. of astrob.* **3**, 221-227.
- Shu F. H., Shang H. and Lee T. (1996) Toward an astrophysical theory of chondrites. *Science* **271**, 1545-1552.
- Shu F., Shang H., Glassgold A. E., and Lee T. (1997) X-rays and fluctuating x-winds from protostars. *Science* **277**, 1475-1479.
- Shukolyukov A. and Lugmair G. W. (2004) Manganese-chromium isotope systematics of enstatite meteorites. *Geochim. Cosmochim. Acta.* **68**, 2875-2888.
- Smith P. S., Huneke J. C., Rajan R. S., and Wasserburg G. J. (1977) Neon and argon in the Allende meteorite. *Geochim. Cosmochim. Acta.* **41**, 627–647.
- Sugiura N. and Hashizume K. (1992) Nitrogen isotope anomalies in primitive ordinary chondrites, *Earth Planet. Sci. Lett.* **111**, 441-454.

- Swindle T. D., Caffee M., Hohenburg C. M., Lindstrom M. M., and Taylor G. J. (1991a). Iodine-xenon studies of petrographically and chemically characterized Chainpur chondrules. *Geochimica. Geochim. Cosmochim. Acta.* **55**:861-880.
- Swindle T. D., Grossman J. N., Olinger C. T. and Garrison D. H. (1991b). Iodine-xenon, chemical, and petrographic studies of Semarkona chondrules: Evidence for the timing of aqueous alteration. *Geochim. Cosmochim. Acta.* **55**, 3723-3734.
- Symes S. J. K. (1997) Problems with arguments against a planetary formation for chondrules (abstract). *Meteorit. Planet. Sci.* **32**, A127.
- Tang M. and Anders E. (1988) Isotopic anomalies of Ne, Xe and C in meteorites. II: Interstellar diamond and SiC carbide carriers of exotic noble gases. *Geochim. Cosmochim. Acta.* **52**, 1235-1244.
- Theimens M. H. and Clayton R. N. (1981) Nitrogen isotopes in the Allende meteorite. *Earth Planet. Sci. Lett.* **55**, 363-369.
- Thiemens M. H. (1996) Mass-independent isotopic effects in chondrites: The role of chemical processes. In *Chondrules and the Protoplanetary Disk* (R. H. Hewins et al., eds.), pp. 107–118. Cambridge Univ., New York.
- Tsuchiyama A., Osada Y., Nakano T., and Uesugi K. (2004) Experimental reproduction of classic barred olivine chondrules: Open-system behavior of chondrule formation. *Geochim. Cosmochim. Acta.* **68**, 653–672.
- Urey H. C. (1967) Parent bodies of meteorites and the origin of chondrules. *Icarus* **7**, 350-359.
- Verchovsky A. B., Sephton M. A., Wright I. P., and Pillinger C. T. (2002) Separation of planetary noble gas carrier from bulk carbon in enstatite chondrites during stepped combustion. *Earth Planet. Sci. Lett.* **199**, 243–255.
- Vogel N., Leya I., Bischoff A., Baur H. and Wieler R (2004) Noble gases in chondrules and associated metal-sulfide-rich samples: Clues on chondrule formation and the behavior of noble gas carrier phases. *Meteorit. Planet. Sci.* **39**, 117-135.
- Wasson J. T. and Kallemeyn G. W. (1988) Compositions of chondrites. *Philos. Tr. R. S.* **A325**, 535-544.
- Weisberg M. K., Prinz M., Clayton R. N. and Mayeda T. K. (1993) The CR (Renazzo-type) carbonaceous chondrite group and its implications. *Geochim. Cosmochim. Acta.* **57**, 1567-1586.
- Weisberg M. K., Prinz M., Cozima H., et al., (1991) The Carlisle Lake-type chondrites: a new grouplet with high  $\delta^{17}\text{O}$  and evidence for nebular oxidation. *Geochim. Cosmochim. Acta.* **55**, 2657-2669.
- Whipple F. L. (1966) Chondrules: Suggestions concerning their origin. *Science* **153**, 54-56.
- Whitby J. A., Gilmour J. D., Turner G., Prinz M. and Ash R. D. (2002) Iodine-Xenon dating of chondrule from the Qingzhen and Kota Kota enstatite chondrites. *Geochim. Cosmochim. Acta.* **66**, 347-359.

- Wieler R. (2002) Cosmic ray-produced noble gases in meteorites. In Noble gases in geochemistry and cosmochemistry, edited by Porcelli D., Ballentine C. J. and Wieler R. Washington D.C.: Mineralogical Society of America. **47**, 125-170.
- Wieler R., Busemann H and Franchi I A (2006) Trapping and Modification processes of Noble gases and Nitrogen in meteorites and their parent bodies, In *Meteorites and the Early Solar System II* (D. S. Lauretta and H. Y. McSween Jr., eds.), Univ. of Arizona, Tucson.
- Wood J. A. (1984) On the formation of meteoritic chondrules by aerodynamic drag heating in the solar nebula. *Earth Planet. Sci. Lett.* **70**, 11-26.
- Young E. D., Ash R. D., Galy A., and Belshaw N. S. (2002) Mg isotope heterogeneity in the Allende meteorite measured by UV laser ablation-MC-ICPMS and comparisons with O isotopes. *Geochim. Cosmochim. Acta.* **66**, 683–698.
- Zook H. A. (1980) A new impact theory for the generation of ordinary chondrites. *Meteoritics* **15**, 390-391.